

AD-A246 305



2



DTIC
ELECTE
S FEB 19 1992 D

Compiled 1991

This document has been approved
for public release and sale; if
distribution is unlimited.

92 2 17 014

92-04069





Ocean Engineering Studies

Compiled 1991

Volume VIII: Pressure Hulls— Cellular Sandwich Construction

J. D. Stachiw

Accession For	
NTIS GRA&I	✓
DTIC TAB	
Unannounced	
Justification	
By	
Report number	
Contract number	
Project number	
Task number	
Work number	
Other number	
Notes	
A-1	

PUBLISHED BY

**NAVAL OCEAN SYSTEMS CENTER
SAN DIEGO, CALIFORNIA**

Approved for public release; distribution is unlimited.

Foreword

To perform their missions, manned and unmanned underwater vehicles require external pressure housings that provide the payload inside the housings with an environment of one atmosphere. In unmanned vehicles, like Remotely Operated Vehicles (ROVs) and Autonomous Underwater Vehicles (AUVs), the payload generally consists of electronic or electrical equipment that radiates significant amounts of heat. This heat must be transferred through the housing walls to the seawater in which the housing is immersed.

Some equipment, like propulsion units that use chemical energy to generate power by turbines or reciprocating engines, require water-cooled heat exchangers, since air convection alone to the housing wall is inadequate for handling the added heat output. In such cases, weight and fabrication savings can be achieved by incorporating the water-cooled heat exchanger into the housing shell, if it is fabricated from material tolerant to high temperatures and if it can transfer high heat.

Many other pieces of equipment could be integrated into the pressure housing structure to save weight and conserve usable space inside the pressure housing envelope. Examples of such equipment are hydraulic accumulators, ballast tanks, fuel tanks, and compressed-gas storage vessels. The extent to which this can be accomplished depends on (1) the material and design chosen for constructing the pressure housing and (2) the imagination of the designer.

Plastic matrix composites do not lend themselves to construction of multifunction pressure housings, because of their poor heat-transfer capability and their inability to tolerate high temperatures without significantly degrading structural properties. Conversely, metals, ceramics, and ceramic composites are well suited for this purpose, because they can transfer high heat and tolerate high temperatures. Metals, in particular, are well suited for multifunction pressure housings, since, in addition to their good heat-transfer capabilities and high-temperature tolerances, they possess high-tensile strength, toughness, and the ability to be joined by welding or brazing. The only drawback metals have is low specific compressive strength, which limits their practical application to pressure housings with operational depths less than 20,000 feet.

Of the many external pressure housing types that have evolved, the sandwich wall housing, supported by annular ring stiffeners, is optimally suited for incorporating the following equipment: integral heat exchangers, hydraulic accumulators, gas or fuel storage tanks, and hard-ballast tanks. This type of sandwich shell construction has been named cellular sandwich to distinguish it from honeycomb and foam sandwich constructions. The cellular type of sandwich shell design was conceived in 1961 by Dr. Stachiw at the Pennsylvania State University Ordnance Research Laboratory. The analytical foundations for understanding the structural performance of the design were developed jointly with Dr. J. G. Pulos of David Taylor Model Basin and Dr. G. Oppel and Mr. P. K. Reddy of the Engineering Mechanics Department at Pennsylvania State University.

The uniqueness of the cellular sandwich structure for cylinders is based on two factors: it represents not only the best design for utilizing the pressure housing shell as a heat exchanger, hydraulic accumulator, or variable hard-ballast tank; but it also has the optimum design for maximizing the elastic stability of a cylinder with a minimum weight penalty. Because of its optimized structure for external pressure loading, properly designed cellular sandwich shells always fail due to plastic deformation of material (i.e., yielding), rather than general elastic instability of the cylinder (i.e., buckling). Utilizing this fundamental design feature of cellular sandwich shells, weight-to-displacement curves can be

generated, based on the materials compressive strength. The curves represent the minimum weight-to-displacement ratio that can be achieved by infinitely long cylindrical housings with cellular sandwich walls. These curves define the lower boundary for weight-to-displacement ratios of cylindrical housings from any given material. The upper upper boundary is defined by curves generated on the basis of elastic instability of infinitely long monocoque cylinders from the same material.

These curves are very useful, since they provide the designer with information about the magnitude of potential weight savings achievable by using cellular sandwich shells instead of monocoque cylinders. For every material, there is a range of depths where the reduction in structural weight (i.e., increase in positive buoyancy) generated by cellular sandwich shell construction can be very significant, offsetting the high fabrication costs associated with this design. Conversely, for every material, there is a depth range where additional buoyancy cannot be achieved by cellular sandwich shell construction. For such a depth range, the monocoque construction is not only the least expensive, but also the most cost effective; i.e., it provides the same buoyancy as a cellular sandwich shell, but at a much lower cost. In general, for weldable or castable corrosion-resistant aluminum alloys with compressive strength less than or equal to 45,000 psi, the cellular sandwich shell construction seems to provide significant weight savings only to about a design depth of 5,000 feet. However, by using titanium or steel alloys, significant weight savings can be achieved to design depths in excess of 20,000 feet.

Since information on the design of cellular sandwich shells is not readily accessible to most designers of external pressure housings, the technical publications dealing with this unique design approach have been collected and are presented in Volume VIII of the NOSC Engineering Series. The compilation of technical reports in Volume VIII is unique, because it provides not only the structural rationale for this design configuration of cylindrical external pressure housings, but also its experimental validation and experimental stress analysis. Thus, this volume is a valuable resource for the engineer faced with designing a multifunction cylindrical housing. In addition, it is a very helpful reference for serious investigators of external pressure housing structures—or for stress analysts seeking experimental confirmation of computer programs used in the structural modeling of cellular sandwich shell cylinders.

J. D. Stachiw
Marine Materials Office
Ocean Engineering
Division

TABLE OF CONTENTS: VOLUME VIII

ORL TR	Shells for Underwater Vehicles
ORL TR	General Instability of Circumferentially Stiffened Sandwich Shells Subjected to Uniform External Pressure
ORL TR	The Effects of Shell Joints and Bonding on the Stability of Acrylic Resin Cellular Shells
International Journal of Mechanical Sciences	Stress Analysis of Ring-Stiffened Sandwich Shells Subjected to Uniform External Pressure
FOUNDRY	Casting Cylinders—Subjected to External Pressure
DTMB TR	Axisymmetric Elastic Deformations and Stresses in a Web-Stiffened Sandwich Cylinder under External Hydrostatic Pressure



THE PENNSYLVANIA STATE UNIVERSITY
UNIVERSITY PARK, PENNSYLVANIA

Shells for Underwater Vehicles

September 28, 1962

SERIAL NO. NOrd 16597-89

Copy No.

NAVY DEPARTMENT • BUREAU OF NAVAL WEAPONS • CONTRACT NORD 16597

Shells for Underwater Vehicles

By J. D. Stachiw

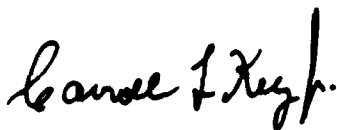
ORDNANCE RESEARCH LABORATORY

The Pennsylvania State University

University Park, Pennsylvania

September 28, 1962

APPROVED FOR DISTRIBUTION



ASSISTANT DIRECTOR

APPROVED FOR DISTRIBUTION



DIRECTOR

SERIAL NO. NOd 16597-89

Distribution List

Chief, Bureau of Naval Weapons (RU-2) Department of the Navy Washington 25, D. C.	1 copy	Chief, Bureau of Ships Department of the Navy Washington 25, D. C.	3 copies
Chief, Bureau of Naval Weapons (RUTO-33) Department of the Navy Washington 25, D. C.	2 copies	Commander U. S. Naval Ordnance Laboratory White Oak Silver Spring 19, Maryland	2 copies
Chief, Bureau of Naval Weapons (RUDC) Department of the Navy Washington 25, D. C.	1 copy	Commander U. S. Naval Ordnance Test Station 3202 East Foothill Boulevard Pasadena Annex Pasadena 8, California	2 copies
Chief, Bureau of Naval Weapons (RUSD) Department of the Navy Washington 25, D. C.	1 copy	Commanding Officer U. S. Naval Underwater Ordnance Station Newport, Rhode Island	2 copies
Chief, Bureau of Naval Weapons (DLI-3) Department of the Navy Washington 25, D. C.	2 copies	Commanding Officer U. S. Naval Torpedo Station Keyport, Washington	1 copy
Chief, Naval Operations (OP 721) Department of the Navy Washington 25, D. C.	5 copies	Commanding Officer U. S. Naval Torpedo Station Quality Evaluation Technical Library Keyport, Washington	1 copy
Chief, Naval Operations (OP 31) Department of the Navy Washington 25, D. C.	1 copy	Officer in Charge U. S. Navy Central Torpedo Office Newport, Rhode Island	1 copy
Chief, Naval Operations (OP 312) Department of the Navy Washington 25, D. C.	1 copy	Director (Code 2021) U. S. Naval Research Laboratory Washington 25, D. C.	3 copies
Chief, Naval Operations (OP 71) Department of the Navy Washington 25, D. C.	1 copy	Director (Code 2027) U. S. Naval Research Laboratory Washington 25, D. C.	1 copy
Chief, Naval Operations (OPO7TC) Technical Analysis and Advisory Group Rm5E813, Pentagon Washington 25, D. C.	1 copy	Commanding Officer and Director U. S. Navy Electronics Laboratory San Diego 52, California	1 copy
Commander Armed Services Technical Information Agency Attention TIPDR Arlington Hall Station Arlington 12, Virginia	10 copies	Commanding Officer and Director David Taylor Model Basin Washington 7, D. C.	1 copy
Commander U. S. Naval Ordnance Laboratory White Oak Silver Spring 19, Maryland Attn: Dr. S. J. Raff	1 copy	Commanding Officer U. S. Navy Mine Defense Laboratory Panama City, Florida	1 copy
		Commanding Officer and Director U. S. Navy Underwater Sound Laboratory Fort Trumbull New London, Connecticut	1 copy

Abstract

*T*HE DESIGN criteria for underwater shells are discussed, and the basic shell designs are evaluated on the basis of these criteria. Internally pressurized shells and shell-pressurization methods are also discussed.

At present, the sandwich-shell design offers the highest pressure-to-weight ratio consistent with the shell-design criteria. The honeycomb or microballoon fiber glass sandwich shells could be best used in the lower pressure ranges and cellular sandwich shells, for a large band of intermediate pressure ranges; the cellular or solid sandwich shells would be better used at the high pressure ranges.

It is recommended that research be directed toward development of higher-strength materials and improved fabrication methods. It is also recommended that fluids of lower compressibility and density be developed for shell pressurization.

Table of Contents

Shells for Underwater Vehicles	1
Design Criteria	1
Modes of Shell Failure	4
Selection of Parameters for High-Pressure Shells	5
Efficiency of Shell Designs	5
Ring-Stiffened Shells	10
Origin of Ring-Stiffened Shells	10
Structural Components of Ring-Stiffened Shells	11
Fabrication of Ring-Stiffened Shells	11
Sandwich Shells	12
Origin of Sandwich Shells	12
Sandwich-Shell Structure	13
Critical Comparison of Sandwich-Shell Designs	15
Internal Pressurization of Shells	20
Pressurization Methods	20
Comparison of Pressurization-System Weights	22
Summary and Evaluation of Shell Designs	25
Classification of Shell Designs	25
Present State of Shell Design	25
Future Research	26
Recommended Shell Designs	26
Appendix	27
Bibliography	49
Cylindrical Ring-Stiffened Shells	49
Sandwich Plates	50
Cylindrical Sandwich Shells	52
General	55

Acknowledgment

*T*HE AUTHOR is indebted to P. C. Sweetland, Associate Professor of Engineering Research at ORL, for his help in the calculation and plotting of curves used in this report.

List of Illustrations

Fig. 1.	Cylindrical Ring-Stiffened Shell	2
Fig. 2.	Cylindrical Sandwich Shells	3
Fig. 3.	Area of Possible Improvements in Cylindrical Shell Design	6
Fig. 4.	Method of Determining Shell-Design Efficiency	7
Fig. 5A.	Utilization of Shell Volume in Underwater Shells	8
Fig. 5B.	Internal Volumes of Cylindrical Shells	8
Fig. 5C.	Internal Useful Volumes of Cylindrical Shells	9
Fig. 6.	Methods of Separating Sandwich Facings	14
Fig. 7.	Buoyancy and Maximum Pressure Limits of Cylindrical Sandwich Shells	16
Fig. 8.	Internal Volumes of Cylindrical Sandwich Shells	16
Fig. 9.	Internal Useful Volumes of Cylindrical Sandwich Shells	17
Fig. 10.	Buoyancies of Cylindrical Sandwich Shells Fabricated from 6061-T6 Aluminum	18
Fig. 11.	Shell Volume Utilization in 6061-T6 Aluminum Sandwich Shells	19
Fig. 12.	Methods of Pressurizing Underwater Vessels	21
Fig. 13.	Buoyancies of Vessels Pressurized with Gas	23
Fig. 14.	Buoyancies of Vessels Pressurized with Liquids	24
Fig. 15.	Equations for Volume-Utilization and Buoyancy Curves	28
Fig. 16.	Limits of Theoretically Attainable Buoyancies for Cylindrical Shells Fabricated from Premium Materials	29
Fig. 17.	Actually Attainable Buoyancies for Cylindrical Shells Fabricated from Premium Materials	30
Fig. 18.	Internal and Useful Internal Volumes for Cylindrical Shells Fabricated from Premium Magnesium	31
Fig. 19.	Internal and Useful Internal Volumes for Cylindrical Shells Fabricated from Premium Glass Fiber Plastic Laminate	32

Fig. 20.	Internal and Useful Internal Volumes for Cylindrical Shells Fabricated from Premium Aluminum	33
Fig. 21.	Internal and Useful Internal Volumes for Cylindrical Shells Fabricated from Premium Titanium	34
Fig. 22.	Internal and Useful Internal Volumes for Cylindrical Shells Fabricated from Premium Steel	35
Fig. 23.	Internal and Useful Internal Volumes for Cylindrical Shells Fabricated from Premium Alumina Ceramic.	36
Fig. 24.	Buoyancies of Magnesium Cylindrical Shells	37
Fig. 25.	Buoyancies of Glass Fiber Plastic Laminate Cylindrical Shells	38
Fig. 26.	Buoyancies of Aluminum Cylindrical Shells	39
Fig. 27.	Buoyancies of Titanium Cylindrical Shells	40
Fig. 28.	Buoyancies of Steel Cylindrical Shells	41
Fig. 29.	Buoyancies of Alumina Ceramic Cylindrical Shells.	42
Fig. 30.	Internal Volumes of Cylindrical Shells Fabricated from Magnesium	43
Fig. 31.	Internal Volumes of Cylindrical Shells Fabricated from Glass Fiber Plastic Laminate	44
Fig. 32.	Internal Volumes of Cylindrical Shells Fabricated from Aluminum	45
Fig. 33.	Internal Volumes of Cylindrical Shells Fabricated from Titanium	46
Fig. 34.	Internal Volumes of Cylindrical Shells Fabricated from Steel	47
Fig. 35.	Internal Volumes of Cylindrical Shells Fabricated from Alumina Ceramic	48

Shells for Underwater Vehicles

*A*LL UNDERWATER vehicles require a shell structure primarily to prevent flooding of the vehicle cavity and to provide a skeleton on which the functional components are mounted. It also may provide the vehicle with a hydrodynamic shape. The basic shells for many underwater vehicles are the cylindrical ring-stiffened shell (Fig. 1) and the cylindrical sandwich shell (Fig. 2). The ring-stiffened shell consists of a smooth cylinder stiffened with rings; the sandwich shell consists of concentric cylinders separated by a spacer. There are several variations of the sandwich-shell design and each has its advantages, depending on the operating requirements of the shell. Despite the complexity of modern underwater vehicles, the basic criteria for shell design continue to be the same.

Design Criteria

There are four basic criteria that must be considered in the design of a successful shell. Listed in the order of their importance, they are:

1. resistance to collapse under external pressure;
2. rigidity of shell structure for mounting of propulsor and guidance components;
3. resistance to corrosion; and
4. fulfillment of all the above requirements with the least weight and the most internal space.

A shell should fulfill all these requirements. In addition, the shell may contribute to the reduction of drag forces and may provide some acoustic damping by using proper fabrication and design techniques. So far, no shell design satisfying all the basic requirements in one design has been found. As long as the fourth criterion is important, every shell design represents, at best, only a clever compromise.

Continuous demands for increased payload and increased speed will require that underwater vehicles shall continue to be weight-limited. There is no likelihood that this requirement will

diminish; therefore, it is postulated that shell weight must be kept to an absolute minimum compatible with the other criteria.

RESISTANCE TO COLLAPSE

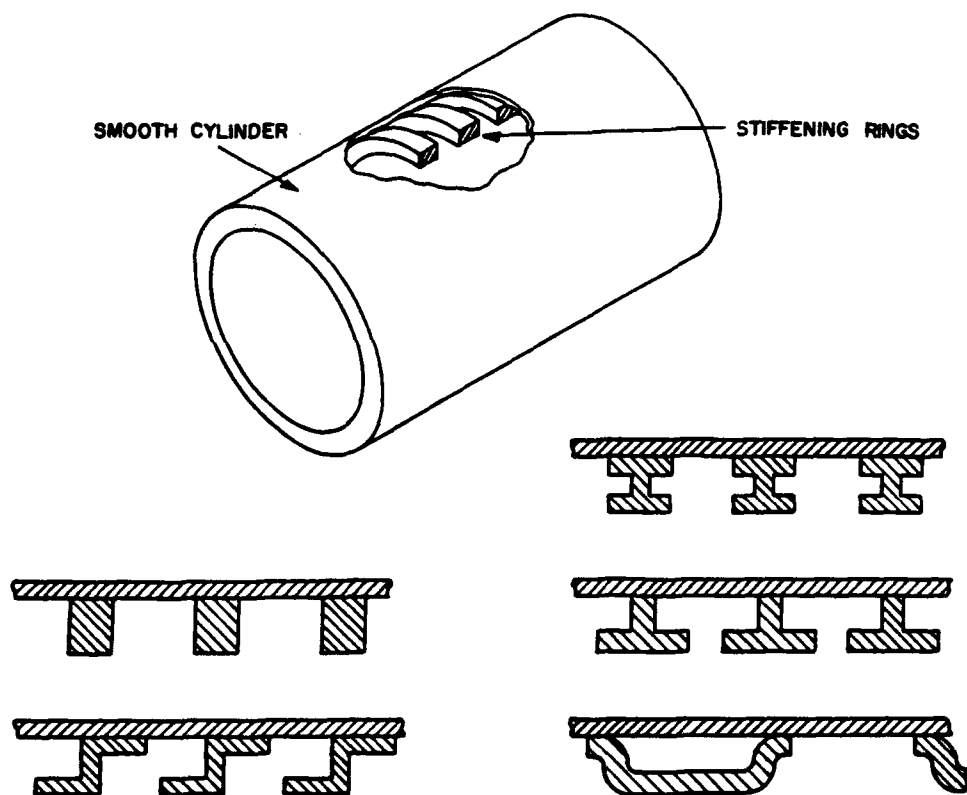
There are only three methods (discussed below) for providing the shell with sufficient strength and stability to operate under external hydrostatic pressure. Two of the methods have been used extensively; a third may find use in the future.

(1) The hydrostatic pressure acting on the outside of the shell must be counteracted by the compressive strength of shell material. To fully utilize the strength of the shell material, the shell must be built so that it will not fail because of elastic instability - a lower-energy-level failure.

(2) The external pressure can be neutralized by pressurizing the vessel cavity with gases or liquids so that the pressurized fluids, instead of the shell structure, carry the external load.

(3) The advantages of (1) and (2) can be judiciously combined, resulting in a superior shell design.

Resistance to collapse can be improved by designing a shell structure for external pressure having a spherical or double-curvature shape. However, many considerations preclude the use of a more implosion-resistant shape (such as the sphere) even though the strength of a spherical shell is considerably higher than that of a cylindrical shell of equal wall thickness. A spherical shell can be given a streamlined shape by means of fairings; but, when the weight of the fairing is included in the over-all vessel weight, the pressure-to-weight ratio of the vessel could equal or exceed that of a cylindrical vessel. It is possible to retain some of the implosion resistance of a sphere by means of a double-curvature pressure vessel. The strength advantages of double-curvature vessels decrease rapidly with an increase in length-to-



ALL WALL CROSS SECTIONS HAVE THE
SAME AREA AND DEPTH BUT DIFFER IN RIGIDITY

STIFFENERS FOR SHELLS

Fig. 1 - Cylindrical Ring-Stiffened Shell

diameter (L/D) ratio of the vessel, but some slight strength increase is present even in elliptical shells with an L/D ratio of 6. In any event these noncylindrical shapes are a special case to be used when the many considerations allow the necessary compromises.

SHELL RIGIDITY

The rigidity of an underwater vehicle is of great importance in the mounting of propulsor and guidance components inside the vehicle. When the shell is very rigid (less than 0.010-in. radial deflection under maximum operational pressure), most of the internal vehicle components can be rigidly mounted to the vehicle shell. Since the deflection is so minute, stresses induced in the equipment and structures secured directly to the inside surface are not likely to

be excessively high. It may even be possible to mount such sensitive guidance system components as gyro platforms and yet not experience enough deflection to substantially affect the course stability of the vehicle.

As the rigidity of the shell decreases, the shell deflections become greater, and a completely different approach to the mounting of internal vehicle components must be devised. Elastic mountings must be provided to absorb the shell deflections rather than transmit them as a high compressive load to the internally mounted components.

Although the internal mounting problem may be solved by the use of proper mounting, further problems could arise since the perfect cylindrical shell assumes a different shape under high hydrostatic pressure. Because of unevenness in contraction the cylinder may become elliptical in cross section and have local un-

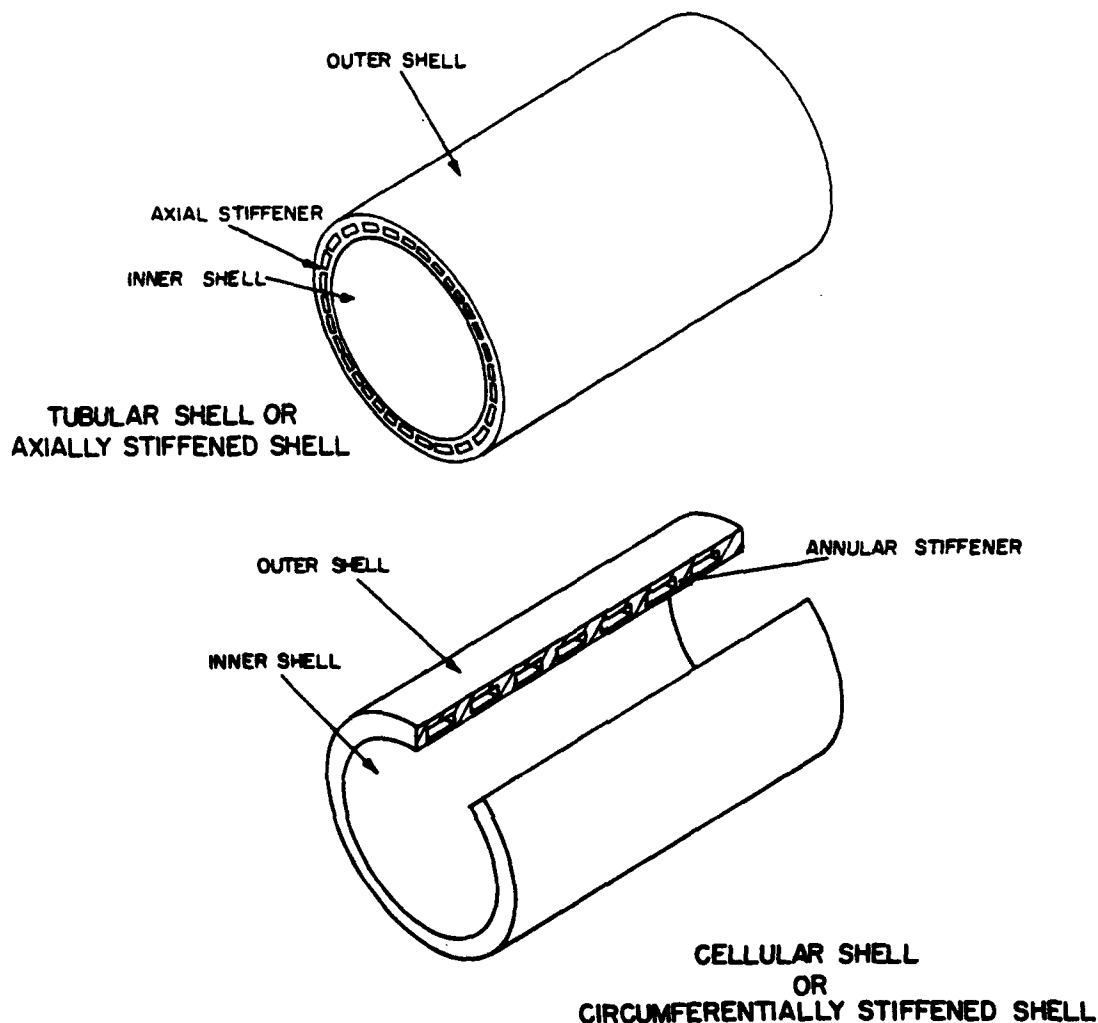


Fig. 2 - Cylindrical Sandwich Shells

evenness in the external shell surface, the inside and outside diameters varying from point to point along the length of the vessel.

The varying outside diameter is produced by the uneven rigidity of the shell. The shell-section joints, bulkheads, and hand-hole openings act like local stiffeners, increasing the rigidity of the shell. Since radial shell deflections are directly proportional to the rigidity of the shell, it follows that the deflections at stiffened shell-surface points will be less than those at points that do not have stiffeners. Because of the difference in radial deflections at various points on the shell, the originally smooth vehicle envelope develops a dimpled "toothpaste-tube" appearance. It is felt that this occurrence is undesirable for vehicles where hydrodynamic flow over the surface is critical.

The formation of local flat spots and local changes of outside diameter under external pressure can be minimized if the rigidity of the shell is kept constant along the entire length of the vessel. This can be accomplished by elimination of bulkheads, stiff shell joints, and hand-hole openings and covers. Considerable thought has been devoted to this subject, but not much has been done about it. However, as underwater vehicles descend to greater depths and attain greater speeds, the principles of uniform shell rigidity will become a prerequisite for successful shell design. Very rigid shells will need some internal pressurization to be successful under the weight limitation necessary. Unless some persuasive arguments are found for pressurization, the problems created by large shell deflections must be alleviated by uniformly rigid

shells and by elastic mounting of components inside the shell.

RESISTANCE TO CORROSION

Sea-water corrosion tends to decrease the compressive strength of underwater vehicle shells in proportion to the length of time they are exposed to the salt water. The term corrosion, as used in this report, means the decrease of the compressive strength of the material - not just the discoloration of its surface. This distinction is important, for there are many materials that lose varying amounts of their strength without any detectable sign of surface corrosion. Conversely, some materials suffer surface damage, but their over-all strength diminishes very little, the corrosion being limited to only the surface layer of the material.

At this point, it may be helpful to classify all underwater vehicles arbitrarily according to their length of continuous submergence:

1. momentary immersion - 1 hr or less;
2. temporary immersion - 1 to 1000 hr; and
3. permanent immersion - 1000 hr or more.

It is difficult to find a structural material whose mechanical properties will not change at all under the corrosive action of salt water. It is often more practical to use a material that will lose only a specified amount of tensile and compressive strength when exposed to sea water for a given period of time.

An arbitrary material-corrosiveness scale is listed below. The corrosion resistance is based on the decrease of tensile strength in a 1/16-in. sheet-metal sample subjected to tidewater exposure for one year:

1. for corrosion-resistant materials, tensile-strength decrease 11 per cent or less;
2. for corrosion-retardant materials, tensile-strength decrease 11 to 45 per cent;
3. for corrosion-prone materials, tensile-strength decrease 45 to 90 per cent; and
4. for reactive materials, tensile-strength decrease 90 to 100 per cent.

Only corrosion-resistant materials are recommended for permanent immersion; those that are either corrosion-resistant or corrosion-retardant are recommended for temporary immersion. Materials that are either corrosion-resistant, corrosion-retardant, or corrosion-prone are recommended for momentary immersion. Reactive materials should not be used for momentary immersion unless a severe shortage of other materials exists.

The use of paint or other protective finishes is highly recommended, but it cannot be substituted for the corrosion-resistant properties of the material itself; protective finishes are often scratched in launching or handling.

WEIGHT AND SPACE LIMITATIONS

All the requirements for a successful shell could be fulfilled easily if it were not for weight and space limitations. The utopian dreams of the design engineer cannot be satisfied because underwater vehicles must meet maximum density requirements and provide sufficient internal space for fuel, propulsor machinery, and guidance equipment. Since weight and space are primary shell requirements that must be satisfied at the expense of other shell requirements, the achievement of a well designed shell becomes mostly a matter of judicious compromise between all the shell parameters.

Modes of Shell Failure

The collapse resistance of any shell depends basically on two parameters: the compressive strength of the material, and the elastic stability of the structure. The compressive strength of the vessel is maintained by sufficient facing and ring cross sections; the elastic stability depends on the moments of inertia of the facings and the stiffener rings. The collapse may be general or local, but both are disastrous to the structural integrity of the vessel.

The difference between a local and a general failure is primarily one of degree. General collapse is caused by the failure of the whole shell structure between bulkheads. It may be initiated by the failure of only one structural component, but the end result is a mass of twisted wreckage. Local failure is not as severe; the shell retains its cylindrical outline.

General collapse occurs when both the shell facings and the ring stiffeners collapse simultaneously because of insufficient compressive strength or elastic stability. Since the facings and the ring stiffeners form a unique structure, the stability of the structure is not the sum of the stabilities of its components but is the result of interaction between each shell component. For each diameter, external pressure, and bulkhead spacing, there exists an optimum combination of facing thicknesses, ring size, and ring spacing. This combination represents

a shell that weighs less than any other shell made of the same material.

Selection of Parameters for High-Pressure Shells

Obtaining the optimum parameters involves a long process in which each parameter is varied while the others are held constant. (It is preferable to have these calculations performed by a computer.) Nevertheless some simplified generalizations can be made.

(1) The facings must be thick enough to carry compressive circumferential stresses and resultant longitudinal stresses between the rings.

(2) The spacing between the rings must stiffen the facings sufficiently to avoid buckling between stiffeners.

(3) The ring stiffeners must possess a sufficient moment of inertia to supplement the elastic stability of the facings between the stiffeners.

(4) The elastic stability of the facings and of the stiffeners must be achieved with a minimum of material.

To achieve high elastic stability with a minimum of material, designers have employed various stiffener shapes, some of which are shown in Fig. 1. Since the elastic stability of the ring is directly proportional to its moment of inertia, ring shapes that provide a large moment of inertia must be selected. This explains the wide use of T-rings, Z-rings, and Box-rings, all of which give a higher moment of inertia than a simple ring with a square or rectangular cross section.

In order to obtain lightweight collapse-resistant shells, optimum component proportions and premium materials with high strength-to-weight ratios must be selected. The selection of materials is limited to commercially available materials, but any acceptable design may be used. The use of premium materials and optimized parameters gives very attractive pressure-to-weight ratios.

To clarify some of the advantages gained from optimization of shell parameters, it is necessary to determine theoretical limits that no shell design, however well optimized, can exceed. To make the theoretical limits applicable to all shell designs, the limits must be made general. Such general limits are inherent in the compressive strength of the material and the elastic stability of a long smooth shell.

The compressive strength of a material is one of the limits that cannot be improved by

shell design. The compressive strength of a long shell, when plotted against external pressure, can be used to illustrate the maximum buoyancy of the vessel for any given design pressure. Since the bulkheads of a long shell do not influence the collapse pressure of the shell between bulkheads, the designer can determine easily the lightest shell that will survive failure by compressive yielding. If close bulkhead spacing is a part of a given shell design, then the bulkhead weight must be included in the shell weight to put the shell comparison on a sound basis.

The compressive strength of the material provides the lower weight limit of the shell; that is, the lowest shell weight that will survive failure by compressive yielding. The elastic stability of a long smooth tube provides the upper weight limit of the shell. This upper limit is based on the premise that no shell design need be heavier than a long smooth shell, which possesses less elastic stability than any ring-stiffened or sandwich shell of the same diameter, weight, and pressure rating.

The strength-of-materials equation describing the lower weight limit of shells, when plotted on linear graph paper, is almost a straight line. The expression for the elastic stability of smooth tubes is a third-degree equation that, when plotted on the same coordinates as the strength-of-materials graph, takes the shape of a sharp curve intersecting the strength-of-materials line. The area between the two curves shows the possible weight savings and potential buoyancy gain for the shell with optimum parameters. The point at which these curves intersect gives the external pressure limit for the material - the limit beyond which no weight and, therefore, no buoyancy improvements over a smooth shell are possible (Fig. 3). The gain in buoyancy of a shell design over the buoyancy of a smooth tube made of the same material, having the same dimensions, and made for the same collapse pressure, is defined here as efficiency of shell design when it is compared to the maximum gain possible at that pressure.

Efficiency of Shell Designs

The efficiency of a shell design can now be described in terms of the two equations that serve as the upper and lower boundaries of shell-design efficiency. Since no design will surpass the strength-of-materials requirement represented by the almost straight line, it will

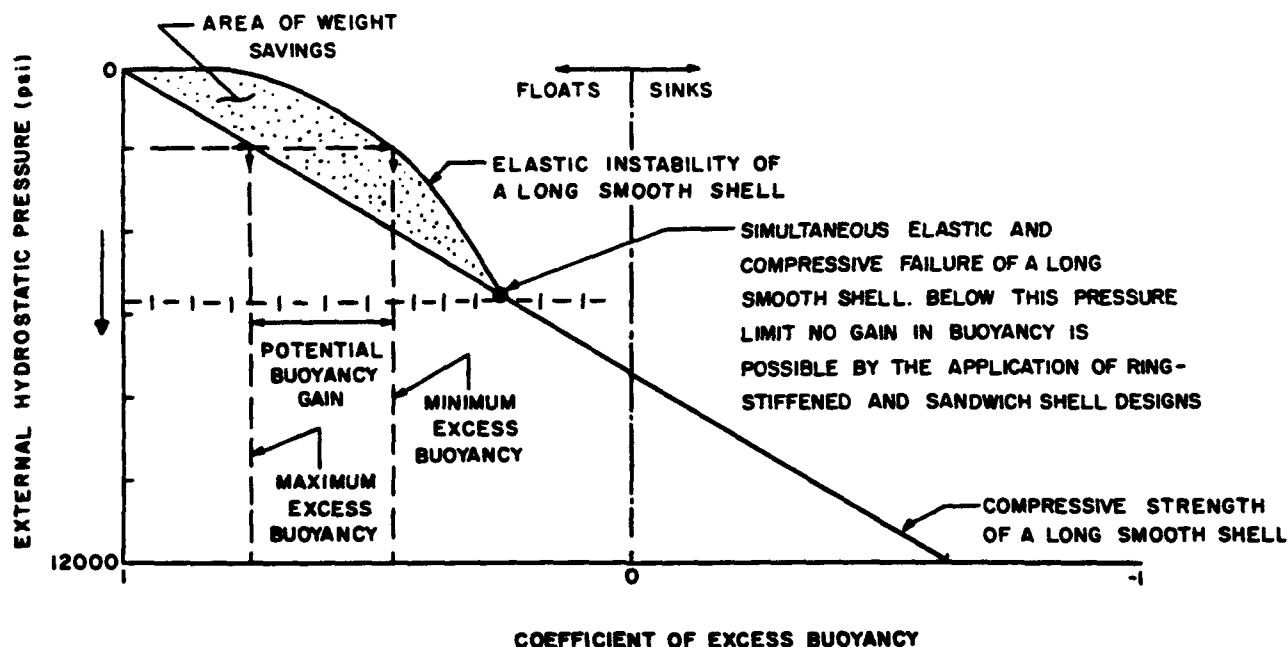


Fig. 3 - Area of Possible Improvements in Cylindrical Shell Design

be used as the upper buoyancy parameter (Fig. 4). The smooth-tube stability curve, describing the least efficient type of shell design, will be used as the lower buoyancy parameter. But a smooth infinitely long tube that fails by simultaneously buckling and yielding is given no rating since it represents the intersection point between the strength-of-materials and the elastic-stability curves where no gain in buoyancy is possible by better shell design. At pressures larger than the cross-over-point pressure, no advantages can be found for any other shell design but a smooth tube, because yielding of the material is the only mode of failure possible, and thus no design efficiency rating can be given to it.

Once upper and lower buoyancy parameter curves have been plotted, it is easy to determine the efficiency of any shell design provided the experimental data for the collapse of a long shell of this design are available. The efficiency is calculated in the following manner:

(1) Experimentally determine the collapse pressure of a long shell (short-shell collapse data may be used if the reinforcing action of the bulkheads or bulkhead weight is taken into consideration).

(2) Calculate and plot the strength-of-materials and elastic-stability curves for the construction material.

(3) Using the experimental collapse pressure as the starting point, draw a horizontal line to intersect both the strength-of-materials and elastic-stability curves (Fig. 4).

(4) Determine the coefficients of excess buoyancy (Fig. 3) for the intersection points and for the experimental shell. Excess buoyancy is defined as

$$E.B. = 1 - \frac{W}{VA}$$

where

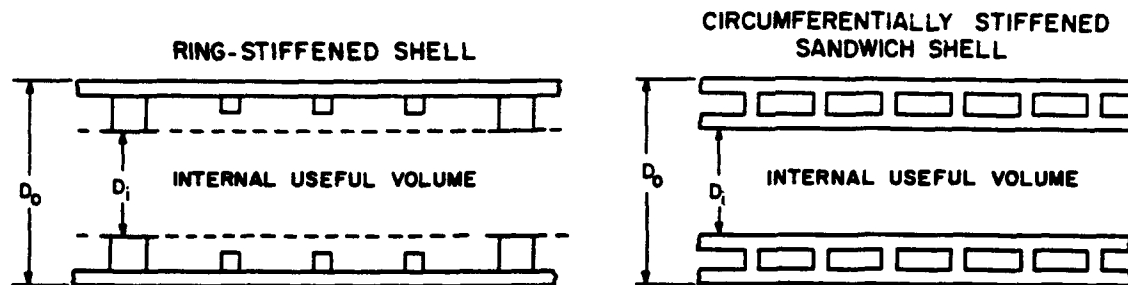
W = weight of the shell structure

and

VA = weight of the sea water displaced by the enclosed shell.

The coefficients of excess buoyancy are then substituted in the design efficiency formula:

$$\text{Design efficiency} = \frac{E.B._2 - E.B._1}{E.B._2 - E.B._1} \times 100,$$



LEGEND:

VOLUMES:

DISPLACEMENT VOLUME = $\pi D_o^2/4$

INTERNAL VOLUME = DISPLACEMENT - VOLUME OF SHELL MATERIAL

INTERNAL USEFUL VOLUME = $\pi D_i^2/4$

*ANNULAR VOLUME = $(\pi D_o^2/4 - \pi D_i^2/4) - \text{VOLUME OF SHELL MATERIAL}$

COEFFICIENTS:

COEFFICIENT OF INTERNAL VOLUME = INTERNAL VOLUME/DISPLACEMENT VOLUME

COEFFICIENT OF INTERNAL USEFUL VOLUME = INTERNAL USEFUL VOLUME/DISPLACEMENT VOLUME

*APPLIES ONLY TO CIRCUMFERENTIALLY AND AXIALLY STIFFENED SANDWICH SHELLS

Fig. 5A - Utilization of Shell Volume in Underwater Shells

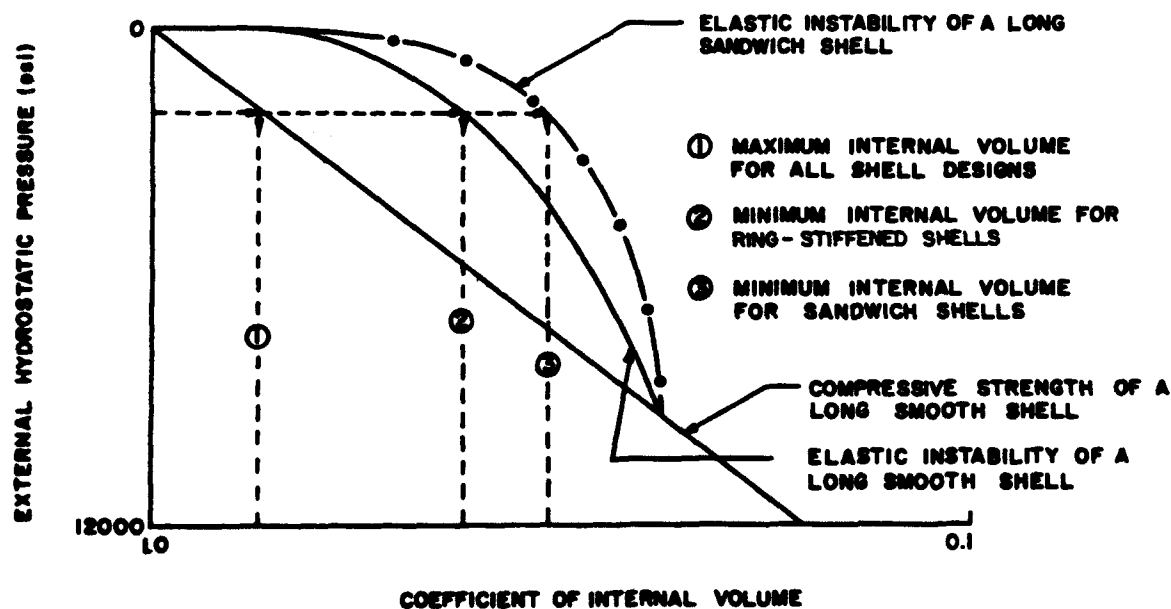


Fig. 5B - Internal Volumes of Cylindrical Shells

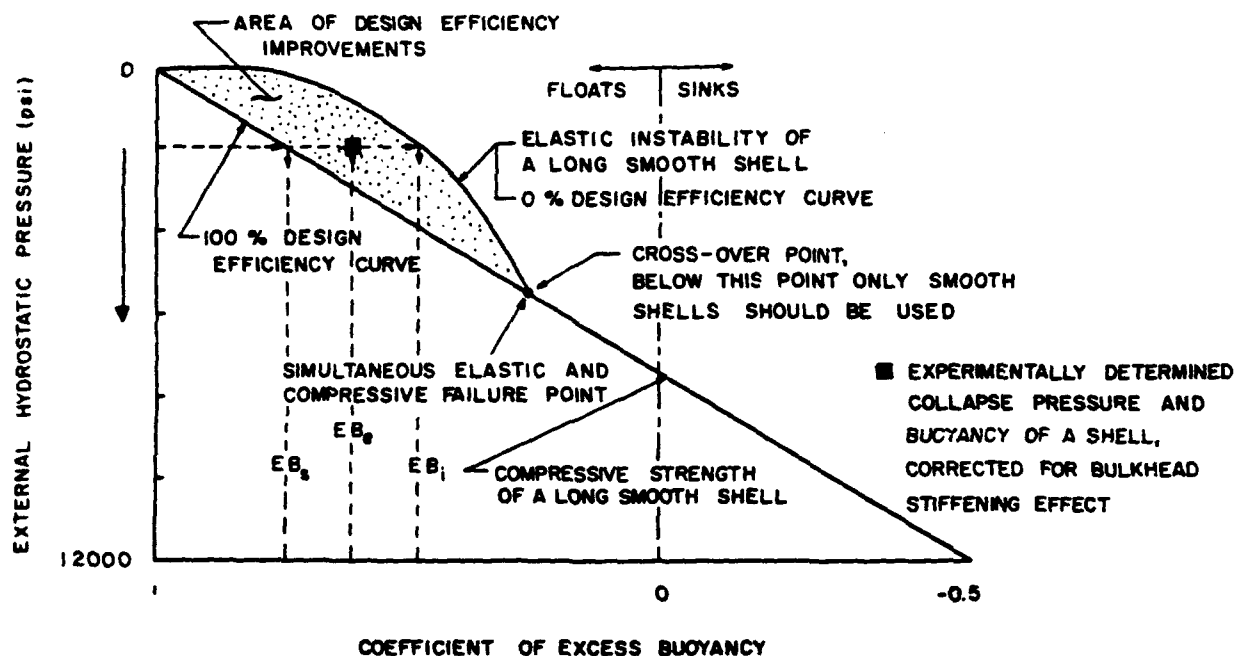


Fig. 4 - Method of Determining Shell-Design Efficiency

where

$E.B_e$ = coefficient of excess buoyancy of the shell at the experimentally determined collapse pressure, corrected for the bulkhead stiffening effect;

$E.B_s$ = coefficient of excess buoyancy of a 100 per cent efficient shell, shown on the graph by the intersection point between the experimental pressure line and the strength-of-materials curve;

and

$E.B_i$ = coefficient of excess buoyancy of a 0 per cent efficient shell, shown on the graph by the intersection point between the experimental pressure line and the elastic-stability curve of a long smooth shell.

For example, the design efficiency of ORL

cellular shell models A and A', calculated by this formula, was 100 per cent:

$$\text{Design efficiency} = \frac{0.92 - 0.54}{0.92 - 0.54} \times 100 = 100 \text{ per cent.}$$

The graphical representation of the strength-of-materials and elastic-stability equations permits comparison of the weight saving possible with other shell designs over the smooth shell in a given pressure range. Inspection of the curves shows that, for a given material, there is a limited pressure band in which it is advantageous to use shell designs other than a smooth tube. Not only that, it shows the relative and absolute magnitudes of the weight savings.

The design efficiency of ring-stiffened shells varies considerably as the position of the experimental collapse pressure of the shell varies with respect to the position of the material's cross-over pressure. Considerable data concerning the implosion testing of ring-stiffened shells have been collected, but unfortunately

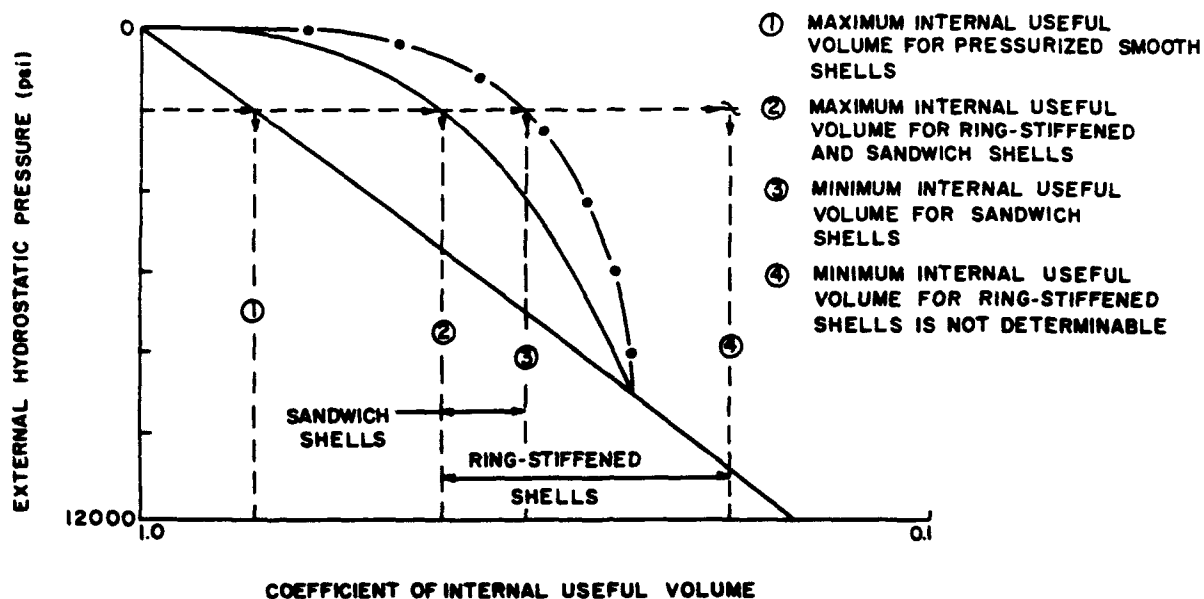


Fig. 5C - Internal Useful Volumes of Cylindrical Shells

most of the tests were conducted with shells having short bulkhead spacing. Failure to take into account the effect of the bulkheads, the elastic stability of which contributes considerably towards the over-all collapse resistance of the assembly, makes most of the plotted collapse data of dubious value for shell-efficiency evaluation purposes. Therefore, before comparisons of design efficiencies are made, the data must be carefully checked to ensure that they pertain either to long shells or to short shells whose bulkhead weights or reinforcing action have been taken into consideration.

A very useful yardstick for the comparison of shells is also the pressure-to-weight ratio:

Pressure-to-weight ratio =

$$\text{collapse pressure} \times \frac{\text{displacement}}{\text{shell weight}}$$

The pressure-to-weight ratio has been used for some time, and there are many references to it in the literature. This rating, in a brief expression, conveys the relationship between the weight of the shell, its displacement, and its experimentally determined ability to withstand pressure. However, it does not show the contributing factors, such as material strength, modulus of elasticity, or density, but gives the sum of all these properties as applied to a particular shell design. Briefly, this rating of the shell design

concerns itself only with the over-all properties of the shell and not with the appropriateness of the shell design, the real measure of engineering achievement.

UTILIZATION OF INTERNAL SPACE

Ring-stiffened shells provide considerable internal volume, but the height and close spacing of the ribs reduce the useful volume (Figs. 5A to 5C). Since increasing the rib height increases the elastic stability of the shell without adding much weight, ring-stiffened shells are usually designed with high ribs. However, this severely restricts the size of any package that is to be inserted in the shell. To obtain more shell space, low ribs spaced at shorter intervals may be substituted, but the net result is an increase in the weight of the shell. Sandwich shells have the possibility of providing more internal space for the same weight and pressure because of the inherently higher moment of inertia of this sandwich wall structure. Although the weight of any rib is directly proportional to the height of the rib, the moment of inertia of the rib varies with the cube of the height. The use of T- and Z-shaped ribs (Fig. 1) has alleviated this problem somewhat, but the space limitation continues to be serious.

Ring-Stiffened Shells

Origin of Ring-Stiffened Shells

PRESSURE vessels subjected to external pressure received little attention in engineering circles until the late eighteen hundreds. It was felt that the smooth cylindrical tube provided a cheap and yet very satisfactory type of structure for vessels subjected to external pressure. The construction materials, mostly cast iron or steel, were of inferior quality; and relatively thick-walled shells were always used for underwater vessels. The thick walls prevented stressing of the tubes to their elastic-stability limits and presented no stimulus for research and experimentation in this area.

It was not until 1880 that Bresse derived an expression for the buckling of rings. In 1888 Bryan developed an accurate expression for the elastic buckling of infinitely long shells subjected to uniform external pressure; and Engesser extended this formula to include materials that do not follow Hooke's law, and to include the plastic region of materials that do follow Hooke's law. Until the outbreak of World War I, this simple formula satisfied the needs of the engineering profession.

World War I saw the development of the submarine as an instrument of war. The early submarines did not present structural problems because they were limited to shallow dives; but, near the end of the war, they had obtained depths of 250 ft and hull collapse caused by elastic buckling became prevalent. Although the reasons for these failures are obvious today, they were unknown to early investigators, who did not understand the complicated relationship between frame stiffness, plating thickness, and frame spacing. The stock remedy for hull collapse - that of increasing the design safety factor - could no longer be applied because the new submarines needed every pound of positive buoyancy. Spurred on by this crisis in submarine design, Von Mises developed a theory for

the buckling of shells between stiffeners. Von Sanden and Gunther then developed a formula for the calculation of stresses in the shell at the stiffeners and midway between them. The size of the stiffeners and the collapse pressure of the shell caused by general elastic instability were not determined then, and it took another world war before these questions were answered.

In the lull between the two world wars, previously postulated theories were tested and information concerning ring-stiffened shells was gradually acquired. Trilling, Windenburg, Donnell, and Tokugawa performed many experiments in which shells were subjected to bending, and to compressive and implosive loading. The theories postulated by Von Mises and Von Sanden were found to predict the experimental results well, although they were not satisfactory in all areas. The theory of Von Mises, in particular, was found to accurately predict the number of lobes formed during buckling of tubes; but, according to Batdorf, it differed significantly from experimental collapse pressures in the low-curvature region (for $L^2/R_0 \sqrt{1-\mu^2} < 100$, the theoretical values are up to 50 per cent higher than the experimental values).

Since World War II, the collapse of ring-stiffened cylinders has become more fully understood. The general elastic instability of ring-stiffened shells was explained by Kendrick; and the distribution of stresses in the shell and stiffeners, by Salerno and Pulos. With the contribution of Lunck's theory on plastic failure, the failure of ring-stiffened cylinders, both in the elastic- and plastic-stress regions, became well understood. Ring-stiffened shells can now be designed to withstand a given pressure with a minimum of weight.

A selected bibliography of publications on ring-stiffened shells is given at the end of this report. This bibliography gives the primary sources listed here, as well as general information on ring-stiffened shells.

Structural Components of Ring-Stiffened Shells

The ring-stiffened shell is made up of three structural elements: the facing, the ring stiffeners, and the bulkheads.

The most important element is the facing, which serves as a barrier against the water outside the vessel. Although the facing contributes a large share of elastic stability and compressive strength to the vehicle, it must be stiffened by rings at close intervals to retain its cylindrical shape under pressure.

The ring stiffeners, or ribs, supply both elastic stability and compressive strength. The cross section and moment of inertia of the rings depend on the diameter of the vessel, maximum external pressure, spacing between the rings, and thickness of the facing - variables that thoroughly interact one with the other. Generally, the ring dimensions are such that, even when that part of the cylinder between the rings has been deformed and all load-carrying ability has been lost, the rings still retain their circular shape and prevent a general shell collapse.

The bulkheads, either solid discs or circular frames of at least twice the rigidity and strength of ordinary rings, divide the vessel structure into independent sections. All strength and stability calculations are based on the shell length

between bulkheads, the bulkheads being considered perfectly rigid and uncollapsible.

The spacing of the bulkheads and rings gives the shell two independent parameters with which all other parameters must vary. To give calculations and figures a more nondimensional and general character, the ring and bulkhead spacings are given in terms of L/D and L_b/D , where L indicates ring spacing; L_b , bulkhead spacing; and D , the diameter of the smooth cylinder. The ring stiffeners come in a variety of forms, the form of the stiffener depending on the space and weight limitations.

Fabrication of Ring-Stiffened Shells

Ring-stiffened shells can be easily fabricated from almost any material. They can be cast, welded, or even machined from a single billet. Since most of the high-strength materials are either unweldable or require expensive post-heat treatment, the ability to machine the shell from one billet is very important. The quality of the ring-stiffened shell can be easily controlled during manufacture, since both the external and internal shell surfaces are accessible. Because of these advantages, ring-stiffened shells are widely employed, except for a few applications where the pressure-to-weight ratio needed is extremely high.

Sandwich Shells

Origin of Sandwich Shells

THE pressure-to-weight ratio of the ring-stiffened smooth shell leaves much to be desired, even when all the shell parameters are optimized. The study of ring-stiffened smooth shells made it more and more apparent that the ability of the shell to withstand external pressure was dependent on two physical parameters: the strength of the construction material, and the stability of the stiffened wall. There is no shortage of high-strength materials; the problem is to find the proper shell structure with which to utilize these high-strength materials to maximum advantage. The talents of many engineers produced a number of ideas, but the high rigidity of the sandwich-wall design promised to significantly improve the pressure-to-weight ratio of shells subjected to external pressure. Although the idea for sandwich walls did not appear until the late nineteen forties, it has already become accepted as the optimum shell design for underwater vessels.

The idea for the sandwich-wall shell grew out of previous work with sandwich panels. Although sandwich panels were proposed a long time ago, they were not widely used until bonding and brazing techniques were perfected.

As engineers began to use the sandwich-type structure for different applications, it became imperative to derive, both on theoretical and experimental bases, stress-strain and stress-load relationships for sandwich structures of various configurations. In the short span of time from 1940 to 1960, the theory for flat sandwich plates became established and well supported by experimental data. However, the sandwich shell has not developed as rapidly. There are only a few researchers working on sandwich shells, and experimental data supporting the available theories are lacking. Most of the research in this field has been conducted at the Forest Products Laboratory, New York University, and at Soviet research institutions.

The earliest work in the sandwich-shell field was done by Leggett and Hopkins in England, Reissner in the United States, and Panov in the USSR. The major contribution was made by Reissner, who developed a nonbuckling theory for small deflections and strains in sandwich shells. His theory accounted for deflections resulting from compression of the sandwich core normal to the facings, as well as those caused by shear.

Following studies by Reissner, Stein and Mayers developed a linear small-deflection theory that does not consider core compression but includes average shear strains. Their theory, in terms of shears and deflections normal to the median surface, is expressed in three general equations with ten independent physical constants. If the simplification is introduced that the sandwich core is isotropic and does not carry the stresses directly, these equations can be reduced to Donnell's equation. Other workers in the field applied the equations of Stein and Mayers to various sandwich-shell configurations under different types of loadings.

The research group at New York University produced some outstanding results. They conducted many theoretical and experimental studies of sandwich shells. Their greatest contribution is a theory for the symmetrical buckling of sandwich shells under compressive end loads. Gerard and Wang derived a generalized nonlinear buckling theory, which is based on the principles of equilibrium and conservation of energy and includes shear effects. This theory neglects the rigidity of the facings, the basic assumptions being that the core behaves as a three-dimensional elastic medium in which stresses parallel to the facings are negligible when compared to the normal and transverse shear stresses.

The New York University group, using experimental data, compared their theoretical solutions with the Donnell equation as modified by Stein and Mayers. It can be stated that the modified Donnell equation predicts the axial

bending load of weak-core cylinders well, but that the correlation between bending and torsional loads and the experimental data is not as good. However, until better theories are postulated, it must be stated that the linear buckling theory is acceptable for sandwich cylinders with soft cores under bending and torsional loading.

The Forest Products Laboratory, although primarily interested in the structural applications of wood-fiber board and plywood, has consistently contributed to analytical and experimental work on sandwich panels and cylinders. Raville, extending the work performed at the Forest Products Laboratory, concluded that when the sandwich facings are relatively thin an analysis in which the facings are treated as membranes is sufficiently accurate. However, he found that when the thickness of the facings is greater than one quarter of the core thickness the stiffness of the facings must be considered. The analytical work of Raville and others was mainly concerned with cylinders subjected to axial and lateral loads.

Soviet scientists, realizing the potential of sandwich structures, have spent considerable effort on sandwich-shell theory, as evidenced by the work of Prusakov, Vlasov, Grigolyuk, Korolev, Kurshin, Ambartsumian, and others. The work of Grigolyuk has produced the most generalized set of equations, and also provides for some plastic effects.

Bibliographies of publications on sandwich plates and sandwich shells are given at the end of this report. These bibliographies give the primary sources listed here, and are followed by a general shell bibliography. A review of the work done on sandwich shells will reveal how little is actually known about the detailed stress distribution in the sandwich cylinders and the various mechanisms of plastic and elastic collapse. Even when generalized sets of equations are available, like those of Grigolyuk and Donnell, it is quite difficult for the designer to use them for solutions of actual engineering problems. The one exception is Fulton's work, which graphically presents some of the equations for steel shells. Although there is an acute need for generalized stress-strain and deflection equations for orthotropic unsymmetric sandwich cylinders, there is also a very pressing need for special equations applicable to specific engineering applications.

Some experimentation has been conducted at the Ordnance Research Laboratory of The Pennsylvania State University toward development of a semiempirical expression for the general

instability collapse of a sandwich shell. On the basis of theoretical considerations and the implosion data from four circumferentially stiffened cellular sandwich shells, the ring-buckling equation of Bresse has been modified to predict the general instability collapse of sandwich shells within ± 5 per cent. The modified Bresse equation has been used at ORL exclusively and has produced good results.* Most of the general elastic instability curves for sandwich shells have been plotted on the basis of this equation.

Sandwich-Shell Structure

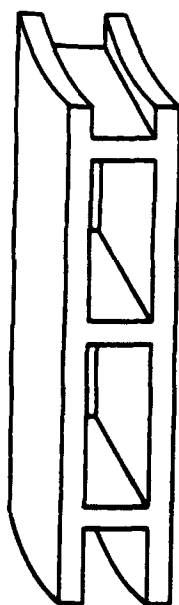
The sandwich-shell structure satisfies two of the basic requirements for shell strength: it permits the use of high-strength materials, and it provides structural stability. The use of high-strength sandwich facings provides the desired compressive strength; the large moment of inertia of the widely separated facings supplies the required elastic stability. In the sandwich shell, the elastic stability is supplied by the wall itself, and not by rings and bulkheads, as in the ring-stiffened smooth shell. Since it is the wall itself that maintains the circular shape of the shell under load, it is quite easy to design the shell once the dimensions of the wall are determined. The shell becomes more homogeneous because of the uniformity of structure.

Although all sandwich shells are based on the same principle, the method of separating the sandwich facing differs considerably. The five basic methods for separating the sandwich facing are shown in Fig. 6. These are:

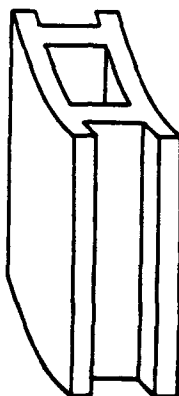
1. honeycomb matrix;
2. microballoon plastic matrix;
3. cellular matrix;
4. solid filler; and
5. tubular matrix.

Prototype shells employing these separation methods have been built. The David Taylor Model Basin and the Ordnance Research Laboratory have devoted most of their efforts to the cellular sandwich shell. Westinghouse has experimented with microballoon plastic sandwiches, and both ORL and the Hexcel Company have performed some exploratory work with honeycomb sandwich shells. So far, the microballoon, honey-

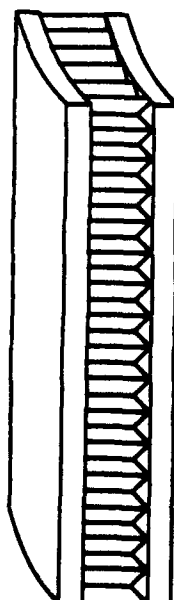
*Jaroslaw D. Stachiw, General Instability of Circumferentially Stiffened Sandwich Shells Subjected to Uniform External Pressure, Master's Thesis, The Pennsylvania State University, 1961, p. 96.



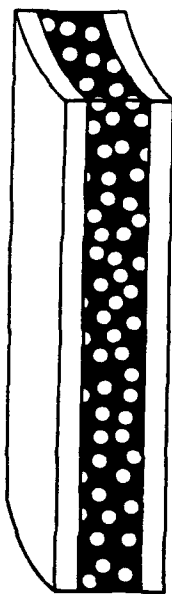
CELLULAR SANDWICH



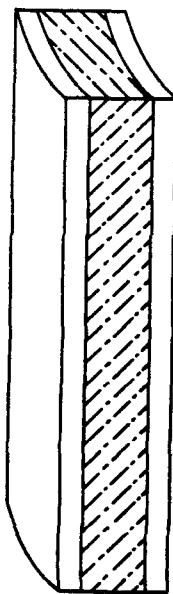
TUBULAR SANDWICH



HONEYCOMB SANDWICH



MICROBALLOON SANDWICH



SOLID SANDWICH

ALL WALL CROSS SECTIONS ABOVE
HAVE THE SAME FACING THICKNESS AND OVER-ALL DEPTH
BUT DIFFER IN RIGIDITY

Fig. 6 - Methods of Separating Sandwich Facings

comb, tubular, and cellular sandwich shells have been subjected to external hydrostatic pressure. Of these, only the cellular sandwich type has been designed and tested for external pressures greater than 1500 psi.

Each of the sandwich-shell designs has its merits, and no one design is distinctly superior to the others. The honeycomb matrices have been made of fiber glass materials, and are available in a variety of thicknesses and compressive strengths. However, they are limited to a compressive strength of 1500 psi, and they present difficulties when formed into small cylinders or when used in cylinders having metal facings. The space between the facings is completely filled, and the shell wall cannot be used for heat-transfer purposes because of its heat-isolation properties. Nevertheless, honeycomb matrices faced with glass fiber laminations are inexpensive and can be used to construct lightweight, pressure-resistant vehicles (less than 1500 psi) with the possibility of an excellent structure.

Microballoon shell construction is a new development, but it has been tested experimentally and found to be satisfactory. The microballoon sandwich shell has a core of lightweight porous plastic, the porosity of which can be varied to meet the compressive strength requirements of the shell. The microballoon matrix is a visco-elastic material that may be useful for damping the shell wall. The space between the facings, however, cannot be utilized for storage of fluids or heat exchange. The latter limitation prohibits its use around propulsors that radiate appreciable heat.

The cellular sandwich shell relies on annular stiffeners for separating the shell facings. These stiffeners must be sufficiently thick and so spaced as to avoid local instability or yielding of the facings. This sandwich construction creates a convenient annular space that can be used for fluid storage (gases under pressure, or liquids), heat exchange functions, or other purposes. However, such construction creates problems in fabrication; but it is felt that they are amenable to solution by good product engineering practices. Adhesives, which are so admirably suited for honeycomb and microballoon sandwich shells, are unsuited for the cellular sandwich shell, which requires narrow joints and puts great strains on adhesives. It appears that only welded, cast, or laminate constructions are suitable for cellular sandwich shells. The annular stiffeners are designed to carry a considerable share of circumferential load, giving

the cellular sandwich shell an inherently higher pressure-to-weight ratio than that of other types of sandwich shells, except for the solid sandwich. The only serious disadvantage of cellular construction is the difficulty involved in fabricating shell components of foil thickness. Although it is theoretically possible to construct very light cellular shells for low external pressures, there is a limit on the minimum thickness of the shell components.

The tubular shell has a lower pressure-to-weight ratio because the stiffeners are arranged axially instead of circumferentially. This type of construction will result in a shell having less stability than that of a cellular sandwich shell having the same weight. There may be some conditions regarding the use of the annular space in which tubular shells can have a distinct advantage and the extra weight can be absorbed. Fabrication problems for tubular shells appear to be similar to those for cellular type shells.

The solid sandwich shell utilizes either a metallic or nonmetallic spacer material of lower density than that of the facings. This design is particularly applicable to shells subjected to high external pressures. The high compressive strength of the spacer material eliminates the possibility of local failure. The use of a solid metallic spacer may make it easier to attach propulsor machinery and other heavy shell components to the wall. The fabrication of metal sandwich shells does not present any special difficulties. The solid spacer, however, eliminates the possibility of using the sandwich wall for storage of fluids or heat exchange.

Critical Comparison of Sandwich-Shell Designs

The five types of sandwich-shell designs - for small-diameter (10- to 30-in.) shells - can be grouped arbitrarily as follows:

1. designs applicable to low external pressure vehicles (0 to 1500 psi) - honeycomb, microballoon;
2. designs applicable to intermediate external pressure vehicles (1500 to 4000 psi) - cellular, solid, tubular; and
3. designs applicable to high external pressure vehicles (>4000 psi) - solid, cellular.

The honeycomb and microballoon sandwiches give very high pressure-to-weight ratios at low pressures. The extremely light honeycomb and microballoon spacers assure uniform support

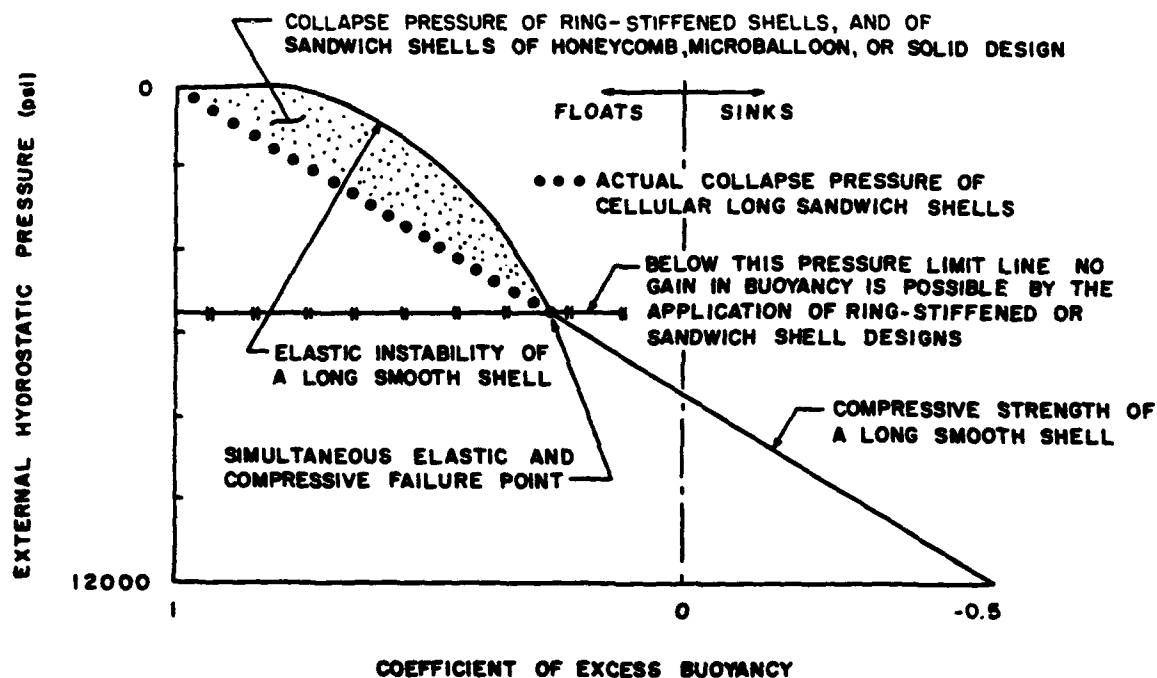


Fig. 7 - Buoyancy and Maximum Pressure Limits of Cylindrical Sandwich Shells

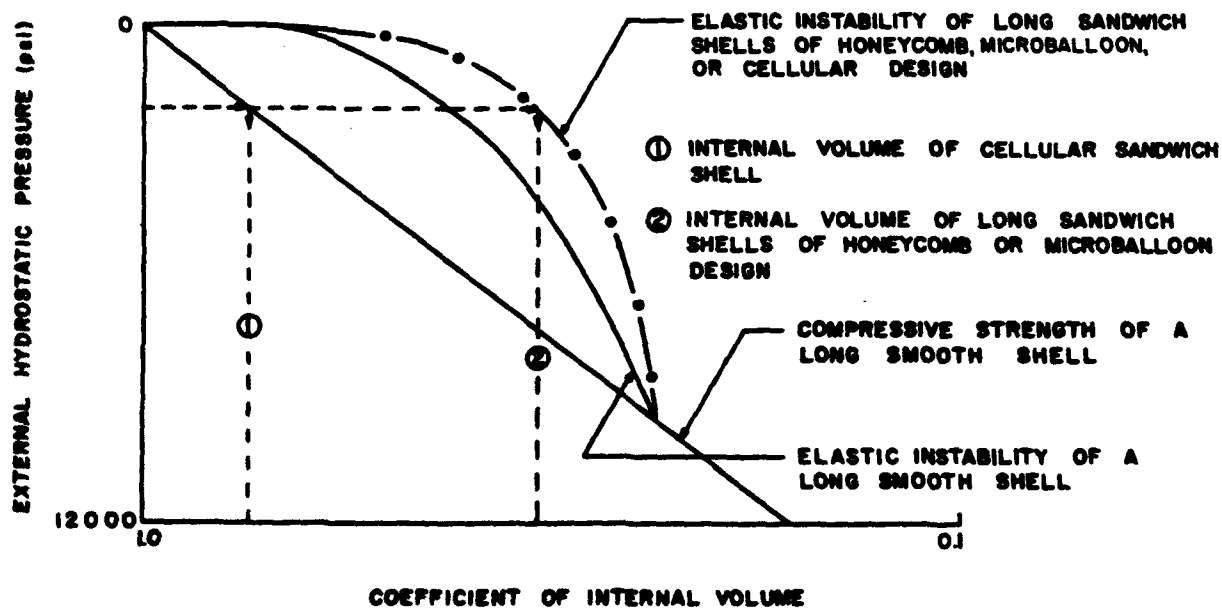


Fig. 8 - Internal Volumes of Cylindrical Sandwich Shells

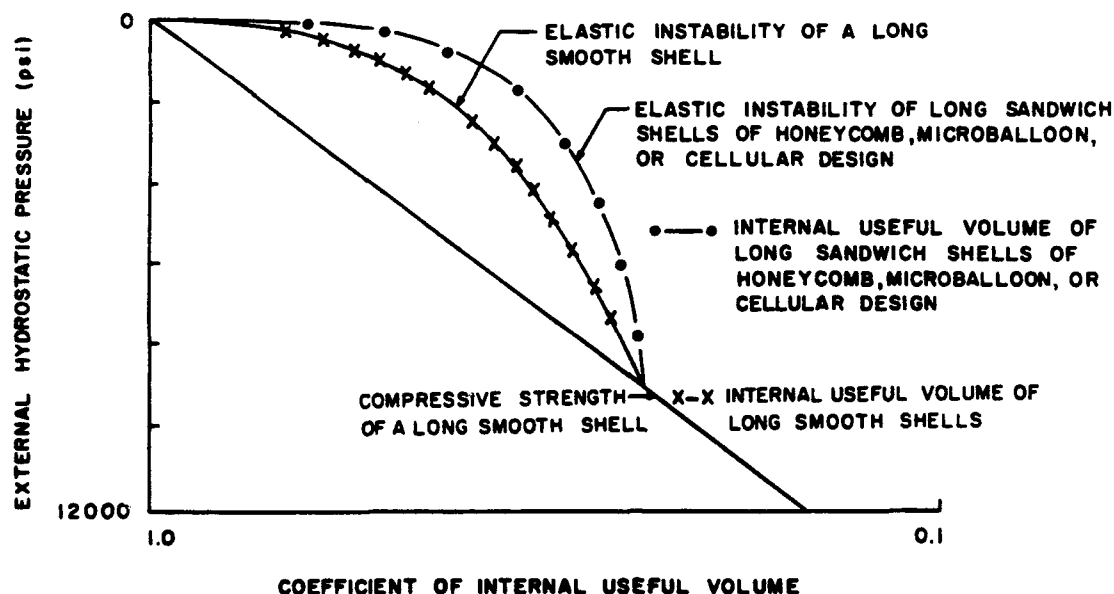


Fig. 9 - Internal Useful Volumes of Cylindrical Sandwich Shells

for the high-strength facings and make difficult the fabrication of small shells with an excess buoyancy factor of 0.9 below 1500 psi. It is impossible to fabricate a cellular sandwich shell with an excess buoyancy factor of 0.9 below 1500 psi because the thin facings cannot withstand the pressure. The solid sandwich, even when constructed of extremely light metal and strengthened with solid nonmetallic spacers, cannot meet the 0.9 excess buoyancy criterion that is so easily met by the honeycomb or microballoon sandwiches.

At intermediate pressures, the cellular and solid sandwiches are recommended because of their ability to withstand high compressive loading. Also, the extra fluid-storage capacity in the walls of the cellular sandwich makes this design applicable to vessels that require an efficient heat exchange for the gases or liquids used or produced by the various subsystems making up the complete vehicle. At intermediate and high pressures, the facings and annular stiffeners are substantial, and cellular sandwich shells with excess buoyancy coefficients of 0.9 and 0.8 can be fabricated without difficulty.

The tubular sandwich shell has a relatively low pressure-to-weight ratio, but the axial passages between its stiffeners may provide a unique solution for certain problems involving heat exchange, fluid transfer, or even conduit passages. Coefficients of excess buoyancy in general will be less than those for the cellular sandwich shell.

If heat exchange and boundary-layer control are not required, the solid sandwich shell offers the best design for vessels subjected to high external pressures. This design assures elastic stability, good pressure-to-weight ratio, and resistance to local failure. However, design criteria and fabrication methods for this type of shell have not been explored. The cellular shell is also an attractive solution to the high external pressure requirement.

At present, underwater vehicles are limited to intermediate external pressures. The cellular sandwich design offers a very attractive answer to all the shell requirements in this pressure range, including a high coefficient of excess buoyancy, and fair utilization of internal vessel space. The cellular sandwich shell can be fabricated from a variety of structural materials and by existing fabrication methods. In addition to providing a good practical shell structure, the cellular sandwich shell can be used for fluid storage and heat transfer.

Figure 7 shows the buoyancies and maximum pressure limits for cylindrical sandwich shells; Figs. 8 and 9 show internal volumes and internal useful volumes, respectively, for cylindrical sandwich shells. Figures 10 and 11 give the same information as Figs. 7 to 9 for 6061-T6 aluminum sandwich shells, the collapse pressures of which have been adjusted for the stiffening action of bulkheads and shell joints. Volume-utilization and buoyancy curves for other shell materials are given in the Appendix.

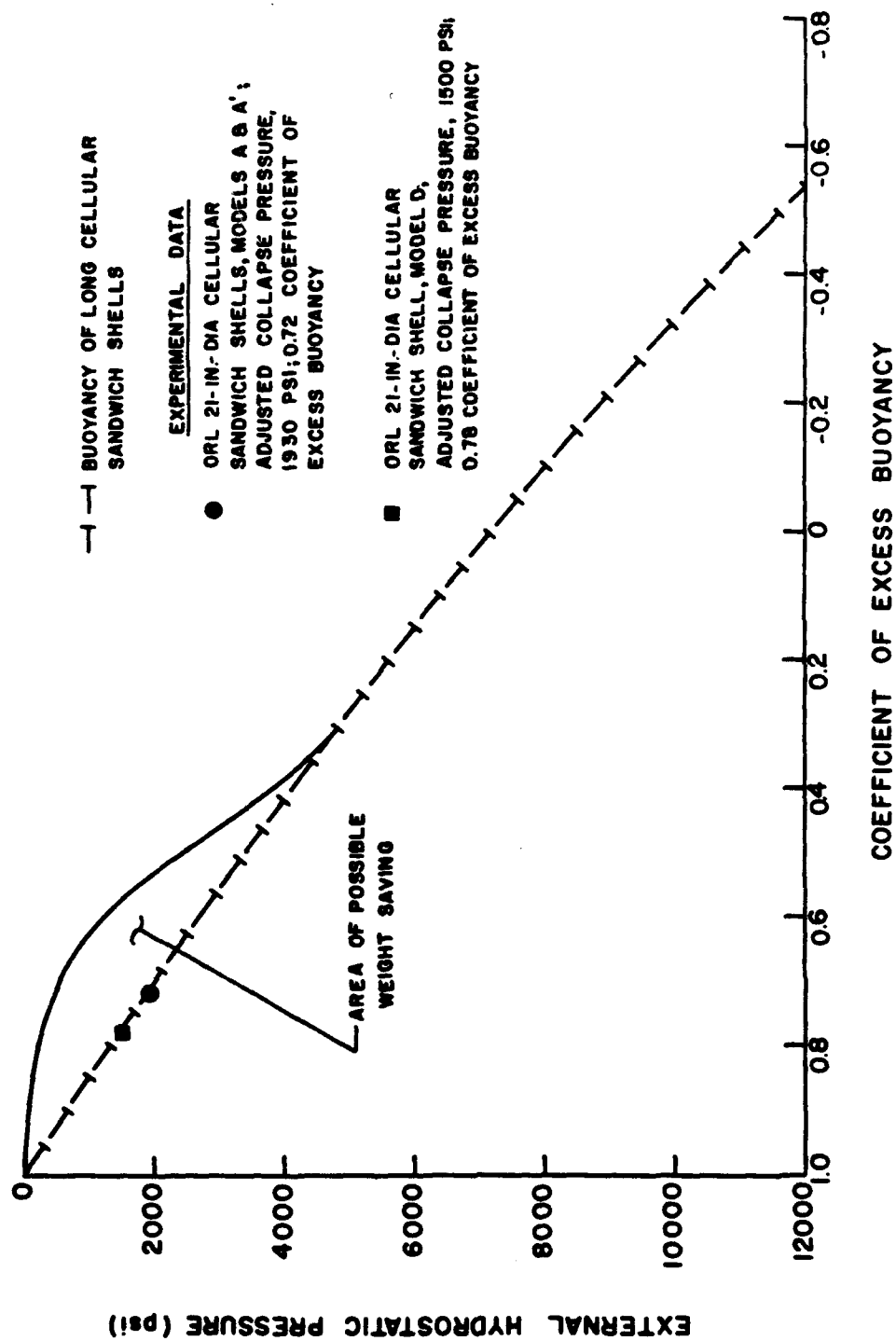


Fig. 10 - Buoyancies of Cylindrical Sandwich Shells Fabricated from 6061-T6 Aluminum

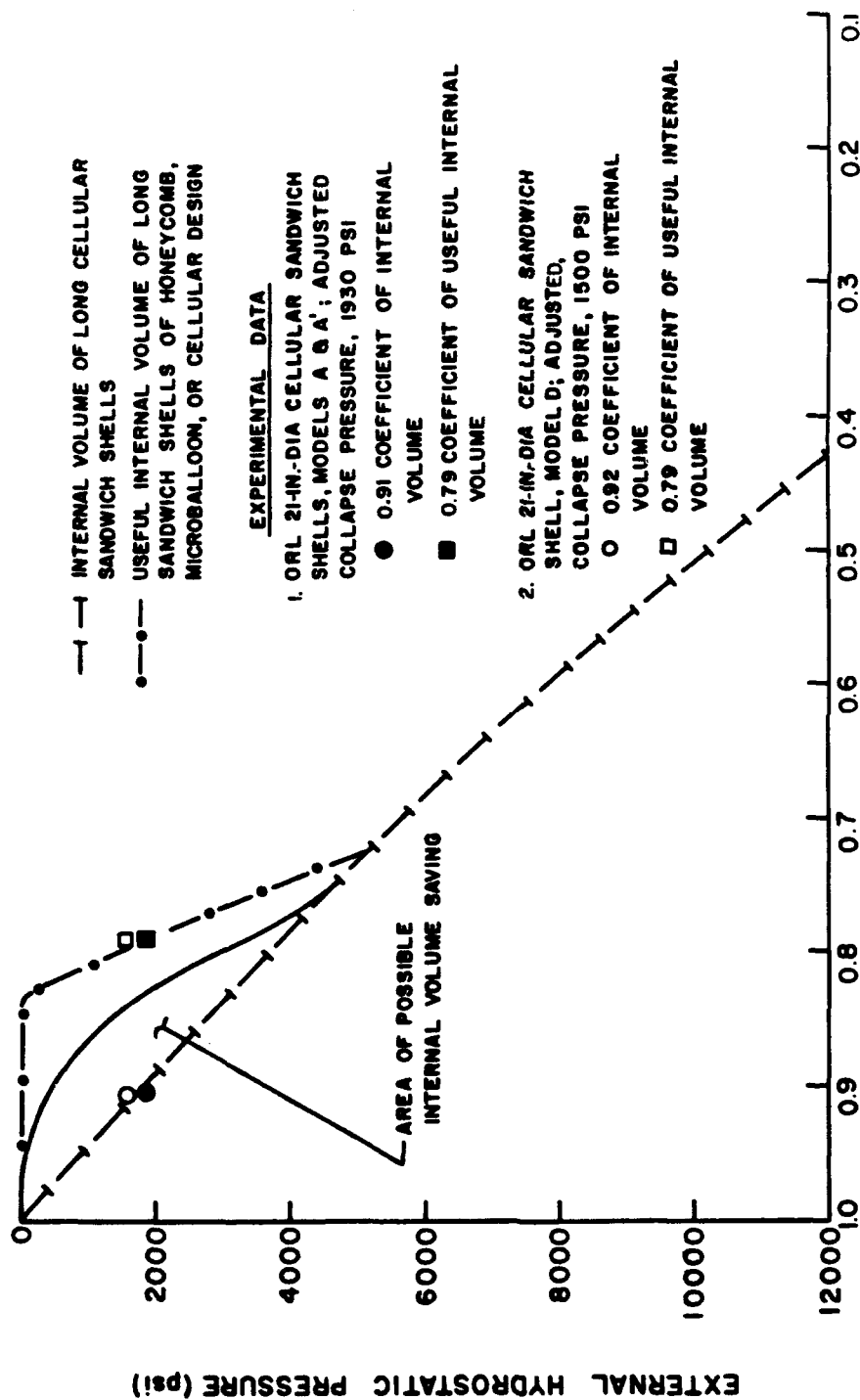


Fig. 11 - Shell Volume Utilization in 6061-T6 Aluminum Sandwich Shells

Internal Pressurization of Shells

INTERNAL pressurization is one method of increasing the implosion resistance of a shell without adding material to the shell structure. This method utilizes compressed gases or liquids to counteract the hydrostatic pressure acting on the outside of the shell (Fig. 12). Pressurizing the internal volume of the vessel makes it possible to design a vehicle shell that could operate at almost any external pressure. Internal pressurization for external pressure vessels has not been used to any great extent, but extension of pressure capability may require its use for future applications.

Pressurization Methods

Pressurization systems can be classified according to: (1) the pressurizing fluid, (2) the method by which the pressurized fluid carries the external load, and (3) the method by which the fluid is pressurized.

Pressurization systems may employ either liquid or gas as the pressurizing fluid. Gas-pressurization systems would be likely to use the low-density, inert gases as a pressurizing fluid. Liquid-pressurization systems would be apt to utilize a liquid that has a specific gravity lower than that of water, although water itself as a pressurizing fluid is a simple solution involving only free flooding of the cavity. The lower the specific gravity of the gas or liquid used, the higher will be the strength-to-weight ratio of the shell since pressurizing fluid weight must be charged to the shell weight.

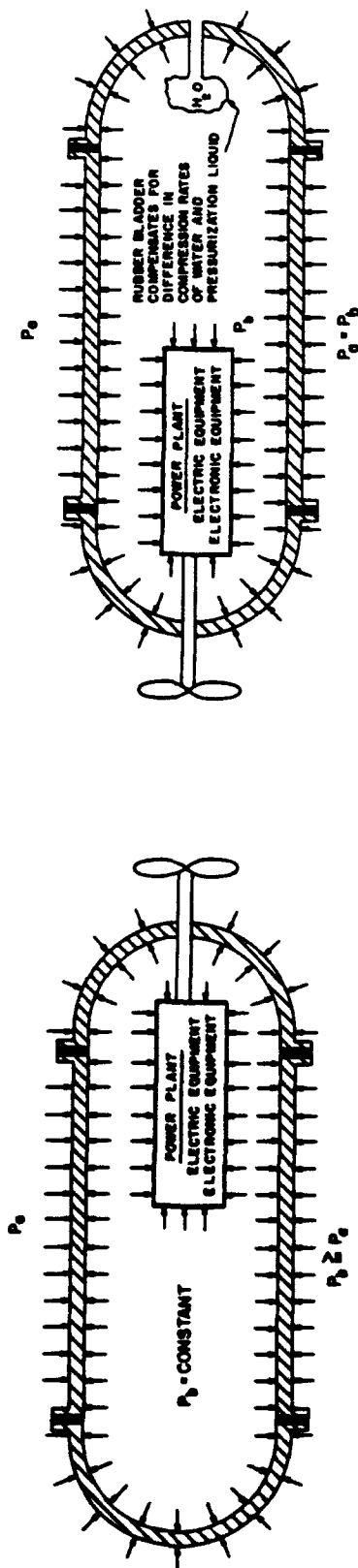
Pressurization systems can also be classified according to the load-carrying methods employed. There are two basic systems: the first relies completely upon the internal fluid pressure to counteract the external pressure; the second is a hybrid system that uses both fluid pressure and shell structure to share the external load. In the first system, the shell serves as a membrane only, separating the sea water from the fluid inside the shell. The shell does

not carry any external pressure, its compressive strength and elastic stability being completely disregarded in the internal-pressure calculations. The only strength requirement is that the shell withstand flexural loads imposed during use, handling, and storage. The hybrid system takes into consideration the compressive strength and elastic stability of the shell, as well as the forces exerted by the compressed fluid. This system is more economical, for it requires a lower internal fluid pressure and thus a smaller mass of pressurizing fluid.

The method by which the fluid is pressurized provides the third means of classifying pressurization systems. There are three ways of pressurizing the fluid: (1) pressurizing the shell cavity before launch; (2) pressurizing the vehicle by means of a pressure tank located within the vehicle; and (3) pressurizing the vehicle by means of the external pressure itself, which uses the external fluid for flooding or exerts pressure across a membrane. Each of these methods places special demands on the shell structure and the pressure-regulating system.

If the shell cavity is charged with a gas from some separate source, the shell must be capable of holding the high internal pressure. Since compressed gases are dangerous to operating personnel, a high safety factor must be used in the design of the shell. The absence of pressure regulators makes this type of pressurization system very reliable, but the shell becomes an internal pressure vessel that may be prohibitively heavy because of the thick shell walls.

When the vehicle uses gas from a pressure tank inside the shell, the only requirement is that the vehicle shell withstand those stresses caused by use, handling, or storage. As the external pressure varies with the operational depth of the vehicle, the pressure-regulator mechanism meters out the gas accordingly so that a set pressure differential is always maintained between the outside and the inside of the vehicle. The disadvantage of this system is the

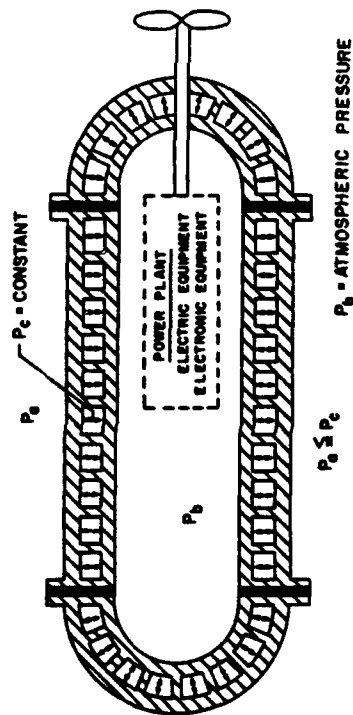


VESSEL PRECHARGED WITH COMPRESSED GAS

EQUIPMENT MUST BE ENCAPSULATED TO PROTECT IT FROM THE HIGH PRESSURE GAS ATMOSPHERE

VESSEL FILLED WITH LIQUID

EQUIPMENT MUST BE ENCAPSULATED TO PROTECT IT FROM COMING IN CONTACT WITH THE HIGH PRESSURE LIQUID



DOUBLE WALLED VESSEL WITH PRESSURIZED ANNULAR SPACE

EQUIPMENT DOES NOT NEED ANY SPECIAL PROTECTION FROM THE AIR AT ATMOSPHERIC PRESSURE

Fig. 12 - Methods of Pressurizing Underwater Vessels

necessity for venting the excess gas pressure so that it will not rupture the vehicle. The alternating pressurization and venting operations may deplete the compressed gas in the tank rapidly, limiting the depth variations of the vehicle.

In vehicles pressurized with liquid, the pressure of the liquid can be adjusted to the external pressure by means of flexible diaphragms that transmit the external pressure to the pressurizing liquid. Such an arrangement is very simple and yet very effective. There are no moving parts, and the vehicle shell serves as a membrane only. However, the shell must withstand the flexural stresses during prelaunch handling.

Comparison of Pressurization-System Weights

The weight of a pressurized underwater vehicle is the sum of the weights of the shell, shell components, component encapsulations, and pressurizing fluid. Once the pressurization system has been selected, the only way to lighten the vehicle is to obtain a gas or liquid having a lower specific gravity. Figures 13 and 14 show the excess buoyancy coefficients of shells pressurized with various gases and liquids under the conditions stated thereon.

It is easy to determine the best gas- or liquid-pressurization system for a given pressure. The weight of the gas-type system varies with the maximum operational depth for which it is designed; the weight of the liquid-type system is almost independent of the maximum operational depth. When the buoyancies of both systems are plotted as a function of external hydrostatic pressure, they intersect at some external-pressure coordinate. At any pressure less than that of the intersection point, a certain gas system is preferred because it possesses better pressure-to-weight characteristics than the liquid system. At any pressure greater than that of the intersection point the liquid system has a much better pressure-to-weight ratio. Generally, the gas-pressurization system will be better than the liquid-pressurization system, except where extremely great pressures are involved.

In addition to the weights of the shell structure and the pressurizing medium, the weight of the necessary protective encapsulation is a factor. Encapsulation is required to protect components from the effects of high pressure, or from the damaging liquid environment. These enclosures could also complicate placement and maintenance of the various internal components of the vehicle.

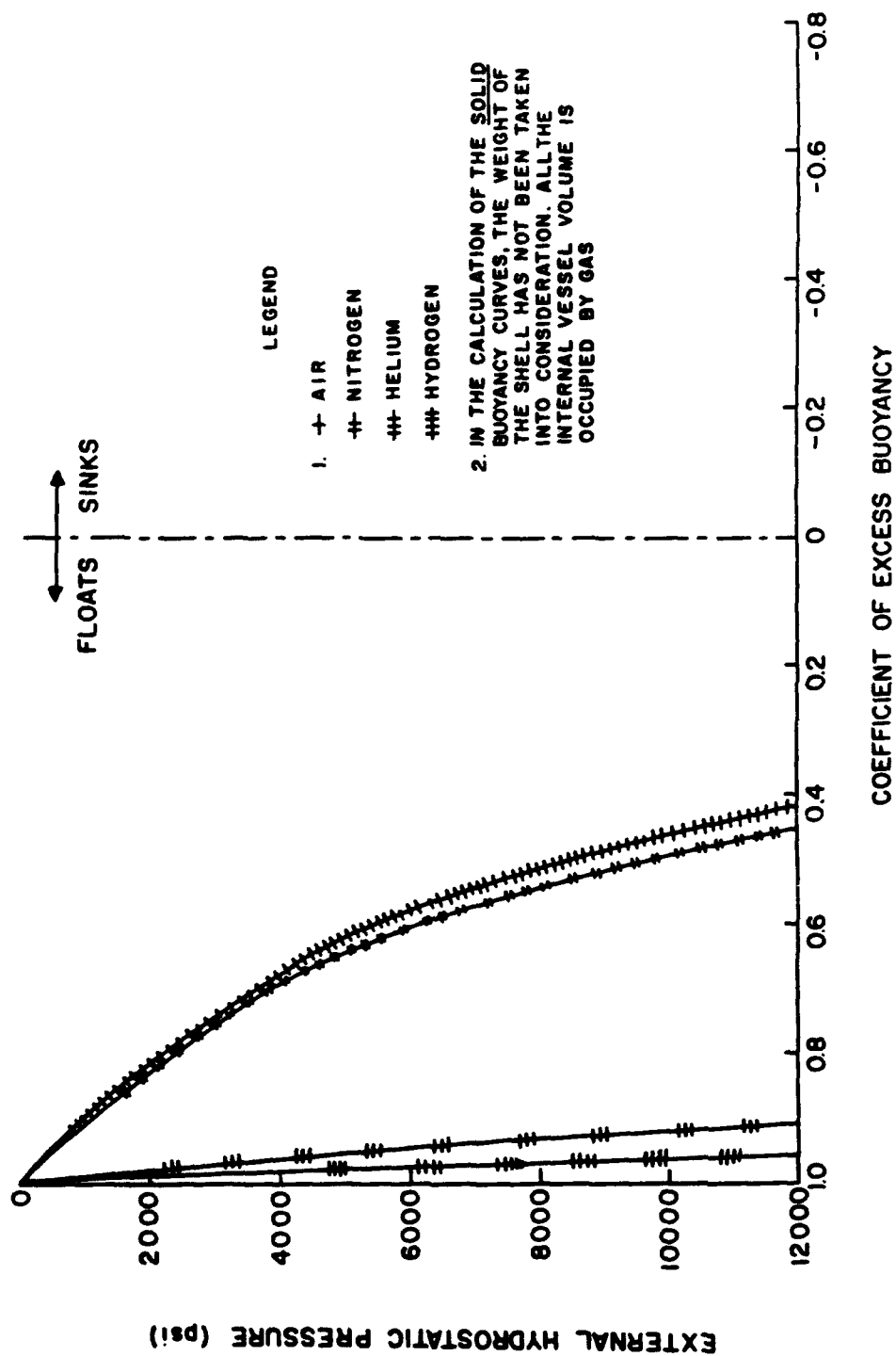


Fig. 13 - Buoyancies of Vessels Pressurized with Gas

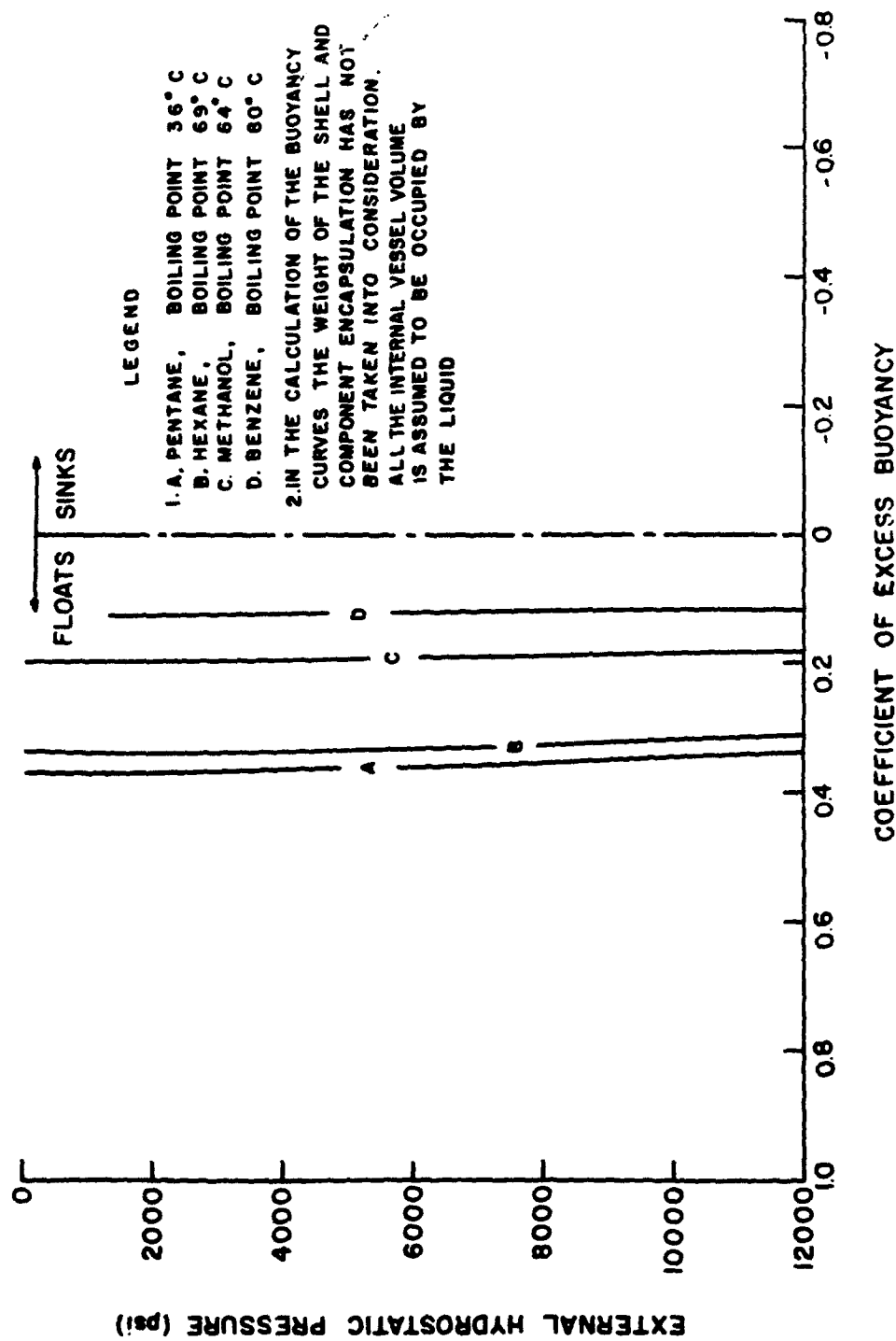


Fig. 14 - Buoyancies of Vessels Pressurized with Liquids

Summary and Evaluation of Shell Designs

Classification of Shell Designs

SHELLS for underwater vehicles can be grouped into two categories: (1) shells that utilize their structural characteristics to withstand external pressure; and (2) shells that utilize an internal pressurized fluid to withstand external pressure. Examples of the first category are ring-stiffened shells and sandwich shells. Examples of the second category are those structures, such as buoyancy or trim chambers or others, which are flooded as a necessary part of their operational functions.

Ring-stiffened shells and sandwich shells utilize the compressive strength of the material and the elastic stability of the shell structure to maintain the hydrodynamic shape of the vehicle. The ring-stiffened shell was developed in the late decades of the nineteenth century, and has been improved over the years. The sandwich-shell design was not feasible until the late nineteen forties, but it has already become accepted as the optimum shell design.

Present State of Shell Design

At the present time, the most reliable shell design is the ring-stiffened smooth cylinder. Mathematical expressions have been developed for the accurate calculation of stresses in the structure of the ring-stiffened shell. Using general equations, the designer can calculate the general instability, local instability, and local yielding of the ring-stiffened shell within ± 5 per cent of experimentally determined values.

The ring-stiffened shells derive most of their stability from ring stiffeners and bulkheads. When the weight of all the structural components, including the bulkheads, is taken into consideration, the average weight of the shell is much heavier than the weight of the material necessary to withstand simple circumferential compressive stresses in the shell. The differ-

ence in weight between the actual shell weight and the weight specified by the average circumferential stress formula $t = pD/2\sigma$ is caused by inefficient stiffening of the facing against elastic-instability collapse. This means that the ring-stiffened shells do not utilize all the compressive strength available in the material. The utilization of internal useful volume is not very good either, because of the large stiffening rings and bulkheads. For these reasons, the ring-stiffened shell is no longer considered an efficient shell design.

Sandwich shells consist of concentric cylindrical facings separated by a lightweight spacer. Depending on the type of spacer, the sandwich structure is called cellular (circumferentially stiffened), tubular (longitudinally stiffened), microballoon (material with high porosity), or solid (bimetallic). The facings carry the circumferential and axial stresses; the wide spacing between the facings provides the shell with sufficient elastic stability. Unlike the ring-stiffened shell, the sandwich shell does not require additional material, and the simple compression-strength formula predicts its weight with reasonable accuracy.

All the sandwich-shell types have been built and tested on a limited basis. Sufficient data have been accumulated to design and fabricate a sandwich shell for a given external pressure. The uniformity of shell wall thickness and the smooth uncluttered interior permit efficient utilization of internal volume. Some of the sandwich-shell walls possess annular cavities that can be used for fluid-storage or heat-exchange purposes.

Since internally pressurized shells of the ring-stiffened or sandwich type have not been utilized to any great extent, there is a lack of experimental data for design purposes. However, the derivation of mathematical expressions for the calculation of the structural dimensions of the shell does not present any difficulty.

Future Research

Each of the methods for adapting underwater vehicle shells to high external pressures has its limitations and represents a compromise among all the parameters present. The ring-stiffened shell does not provide sufficient elastic stability and does not utilize all the available compressive strength of the shell material.

The sandwich-type shells are limited by the compressive-yield strength and the density of the material. The internally pressurized shells, on the other hand, are limited by the compressibility and specific gravity of the pressurizing medium.

The limitations of these shell designs point the way to future research. The possible areas of research are:

1. development of better stiffening methods for ring-stiffened smooth shells;
2. development of light shell materials with higher compressive strengths and moduli of elasticity, including the fabrication procedures; and
3. development of pressurizing media with lower compressibility and density.

Since sandwich shells have already overcome the elastic-stability limitations of the ring-stiffened shell, improvement of ring-stiffened smooth shells does not appear to be remunerative. At best, the elastic stability of improved ring-stiffened smooth shells would only equal the elastic stability of the sandwich shell.

The most promising area of research is the development of higher-strength materials. At present, the compressive strength of materials is below 300,000 psi, but fabrication of sandwich shells from these materials presents great difficulties. The best shells that have been built utilize material with only 150,000-psi compressive strength, but these are not reliable production-type shells. Thus, research in this area must also include methods of fabricating sand-

wich shells from existing high-strength materials.

The development of improved shell-pressurizing techniques could make pressurized shells competitive with sandwich shells. At present, the pressurizing techniques are in their primitive stage of development and not widely used.

Recommended Shell Designs

The sandwich shells possess the best possible strength-to-weight ratio because of their ability to fully utilize all the material used in the structure. They satisfy more of the requirements for a successful shell design than do other designs for a given pressure range. There is no particular sandwich-shell design, or construction material, however, that is best for the whole pressure range. Certain materials and construction designs among the cellular shells will result in a better shell for a given pressure range. At the present time, there is some question about the fabrication of certain of these designs; but, disregarding this factor since it is an engineering fabrication problem, materials and designs of sandwich shells can be recommended. The honeycomb or microballoon sandwich using fiber glass laminates, or their equivalent, is best for the lower pressure ranges; the cellular sandwich is best for a large range of intermediate pressures; and either cellular or solid sandwich shells are best for the higher pressures when the commonly used construction materials are considered. There is a considerable overlap of pressure ranges; in these "gray" areas only the use of good judgment will be of any help in selecting a design and material.

Some newer and untried materials, like ceramics and glass, show promise of being useful for construction of external-pressure vessels. These materials, if successfully exploited, may revolutionize the whole external-pressure-vessel art.

Appendix

FIGURES 15 through 35 give information on volume utilization and buoyancy for cylindrical shells. To describe the limitations of these data, the equations on which they are based are also presented (Fig. 15). Some of these equations have been obtained from handbooks; the others have been developed by the author on a semiempirical basis.

Figures 16 through 35 are substantiated by tests, performed at ORL, of model and full-scale acrylic resin and aluminum shells. These data have been adjusted for the stiffening action of the bulkheads and shell joints, and the plotted pressure actually represents the collapse pressure of a long cellular sandwich shell; that is, a shell whose bulkheads are widely spaced so that they do not substantially contribute to the collapse resistance of the shell. If shorter bulkhead spacing is considered, the curves cannot be read directly, but must be adjusted for the bulkhead strengthening effect.

The volume-utilization and buoyancy curves should be used for a general comparison of different materials and shell designs. They should never be used for actual design because greater accuracy can be obtained by detailed calculations based on shell application. In such detailed calculations, it is possible to take into account the effect of facing thickness on the stress distribution in the shell wall, the stress concentrations caused by stress raisers, and other factors that cannot be taken into consideration when plotting curves on nondimensional scales.

Figures 18 through 35 show only the maxima and minima of buoyancy and internal volume coefficient for cellular sandwich shells. Figures 18 through 23 are graphs of the cellular shell's coefficient of useful internal volume for selected premium materials. Figures 24 through 29 are curves of available buoyancy and internal volume utilization for all commonly used construction materials.

Figures 18 through 35 can also be used for the approximate determination of excess buoyancy, internal volume utilization, and useful internal volume for tubular, honeycomb, and microballoon sandwich shells. The shell properties for these sandwich shells can be only approximately determined from the plotted curves because the structural components add weight to the shell but do not carry any circumferential stresses. For this reason, the excess buoyancy of honeycomb, tubular, and microballoon shells will be less than that shown for cellular shells, but the useful internal volume will be approximately the same. The excess buoyancy will be approximately 30 per cent below that of the cellular shell.

No curves have been plotted for the solid sandwich shell because of the large selection of sandwich spacer materials, but the formulas for calculation of solid sandwich shell data are available. Depending on the materials used for the sandwich facings and sandwich filler, shells with widely varying collapse resistances and buoyancies can be fabricated. Particularly, sandwich designs with a light metal spacer material and high strength facing would result in shells with high pressure-to-weight ratios.

Although Figures 16 through 35 include data for various sandwich-shell materials, there is no assurance that the sandwich shell can be built from the material for a given external pressure because of fabrication limitations. For each material, sandwich-shell design, and shell diameter, there are minimum thicknesses for shell facing and cellular stiffeners below which a shell cannot be built by existing fabrication methods. This, of course, imposes a limit on the coefficient of buoyancy for which the shells can be economically designed. Figure 17 shows the maximum coefficient of buoyancy for which cellular shells of 36-in. diameter can be designed; similar curves can be plotted for each shell design, material, and diameter.

I

COMPRESSIVE STRENGTH OF A LONG SMOOTH SHELL

$$pD = 2A\sigma_{yp}$$

WHERE p = EXTERNAL HYDROSTATIC PRESSURE (psi)

D = EXTERNAL VESSEL DIAMETER (in.)

A = WALL CROSS SECTION (in² per in.)

σ_{yp} = YIELD STRENGTH OF THE MATERIAL (psi)

II

ELASTIC INSTABILITY OF A LONG SMOOTH SHELL

$$p = \frac{2E_t}{(1-\mu^2)} \left(\frac{t}{D} \right)^3$$

WHERE E_t = TANGENT MODULUS OF ELASTICITY, VARIES WITH σ (psi)

μ = POISSON'S RATIO

t = WALL THICKNESS (in.)

III

COEFFICIENT OF EXCESS BUOYANCY = I - SHELL WEIGHT/DISPLACEMENT

IV

COEFFICIENT OF INTERNAL VOLUME = [DISPLACEMENT - SHELL MATERIAL VOLUME]/DISPLACEMENT

V

COEFFICIENT OF USEFUL INTERNAL VOLUME

$$= D_i^3/D_o^3$$

VI

ELASTIC INSTABILITY OF A LONG SANDWICH SHELL

$$p = \frac{2E_t}{(1-\mu^2)} \left[\frac{h^3 - (h-t)^3}{D_o^2 D_o} \right]$$

WHERE h = OVER-ALL DEPTH OF THE WALL (in.)

$$t = t_o + t_i$$

t_o = EXTERNAL SANDWICH FACING THICKNESS (in.)

t_i = INTERNAL SANDWICH FACING THICKNESS (in.)

D_o = DIAMETER OF THE NEUTRAL WALL PLANE;
IN CASE OF ORL SHELLS $D_o = (D_o + D_i)/2$
 E_t = WAS ASSUMED TO BE CONSTANT, AND
ITS MAGNITUDE EQUAL TO E_t AT σ_{yp}

Fig. 15 - Equations for Volume-Utilization and Buoyancy Curves

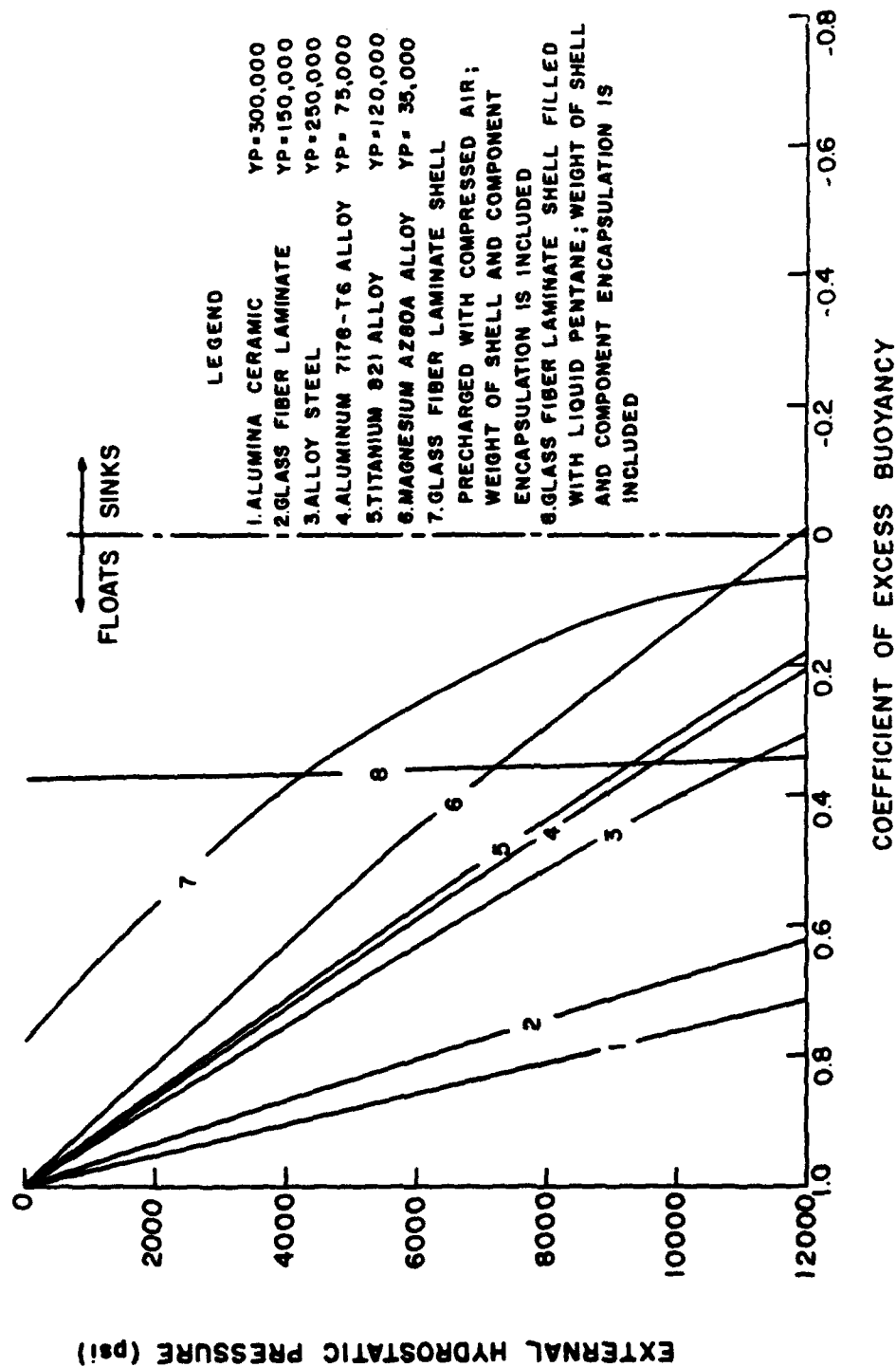


Fig. 16 - Limits of Theoretically Attainable Buoyancies for Cylindrical Shells Fabricated from Premium Materials

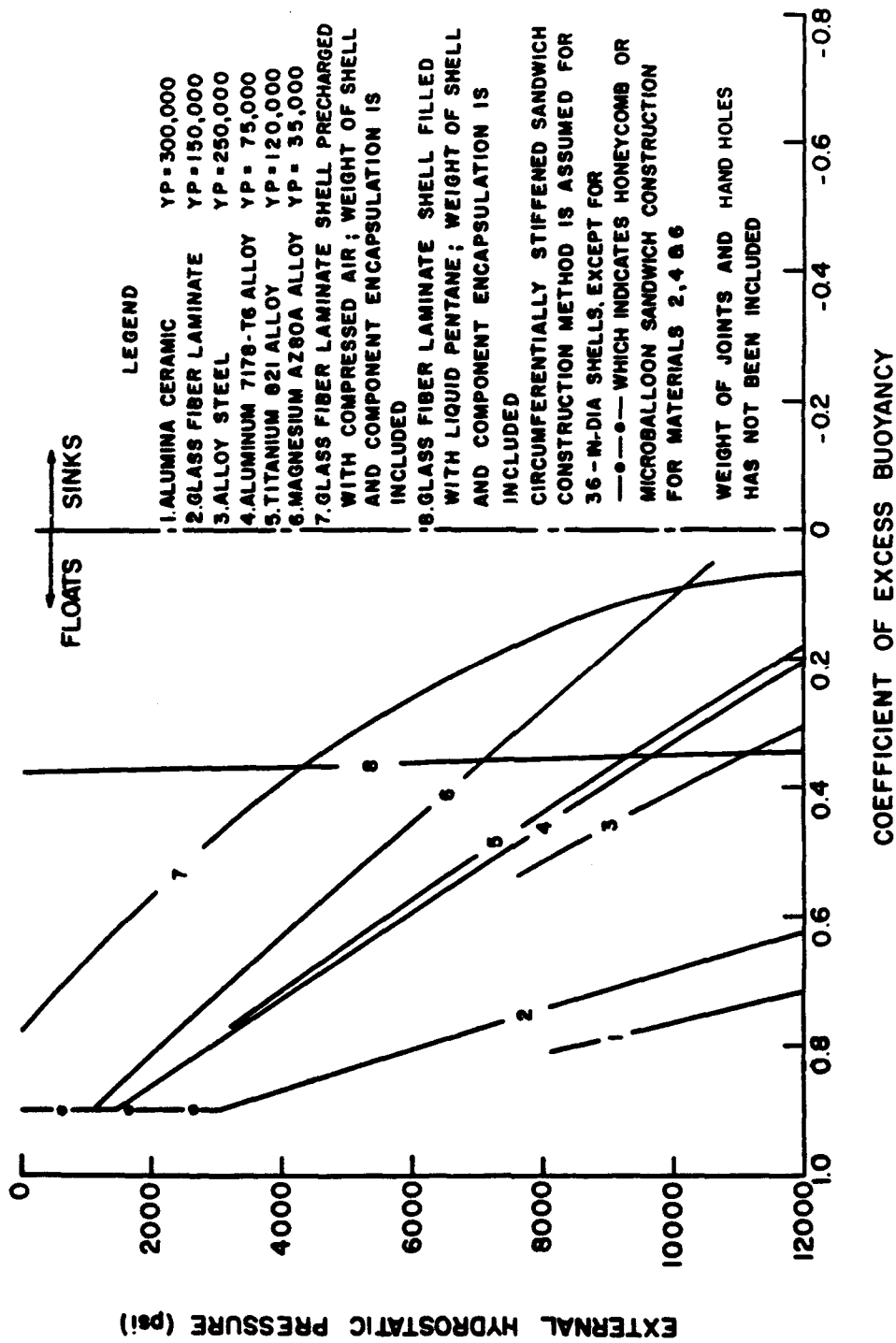
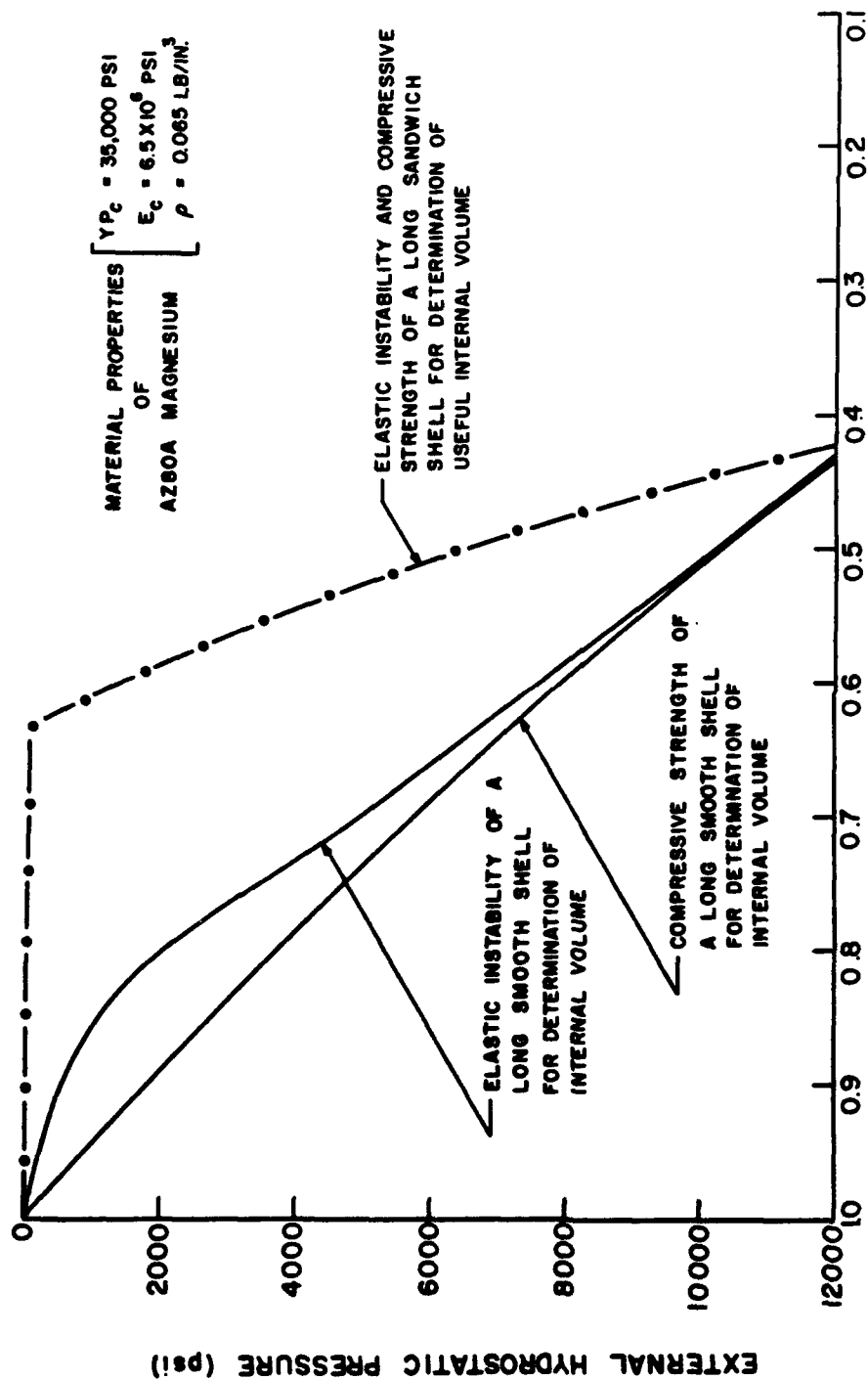


Fig. 17 - Actually Attainable Buoyancies for Cylindrical Shells Fabricated from Premium Materials



COEFFICIENTS OF INTERNAL AND USEFUL INTERNAL VOLUME

Fig. 18 - Internal and Useful Internal Volumes for Cylindrical Shells Fabricated from Premium Magnesium

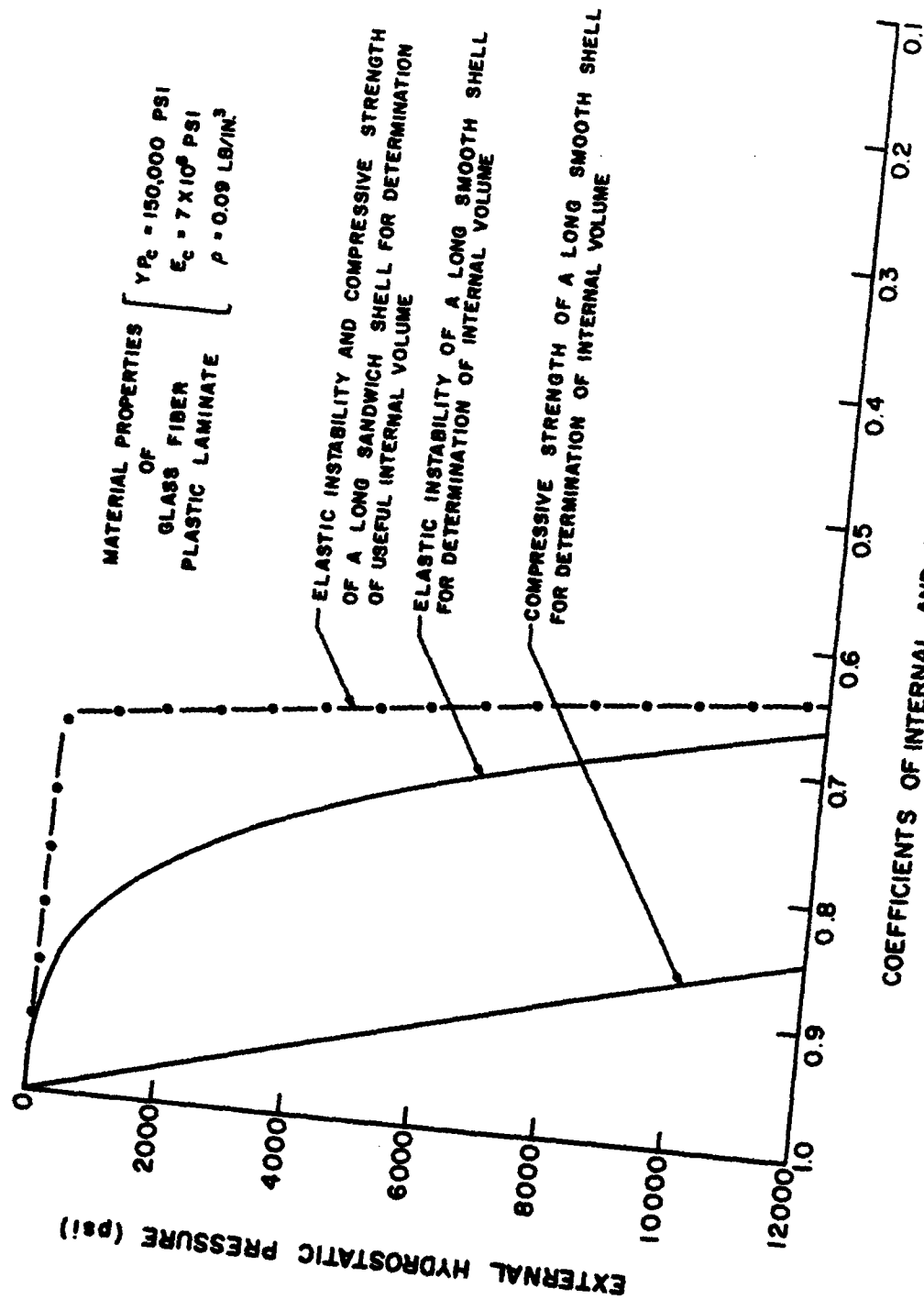


Fig. 19 - Internal and Useful Internal Volumes for Cylindrical Shells
Fabricated from Premium Glass Fiber Plastic Laminate

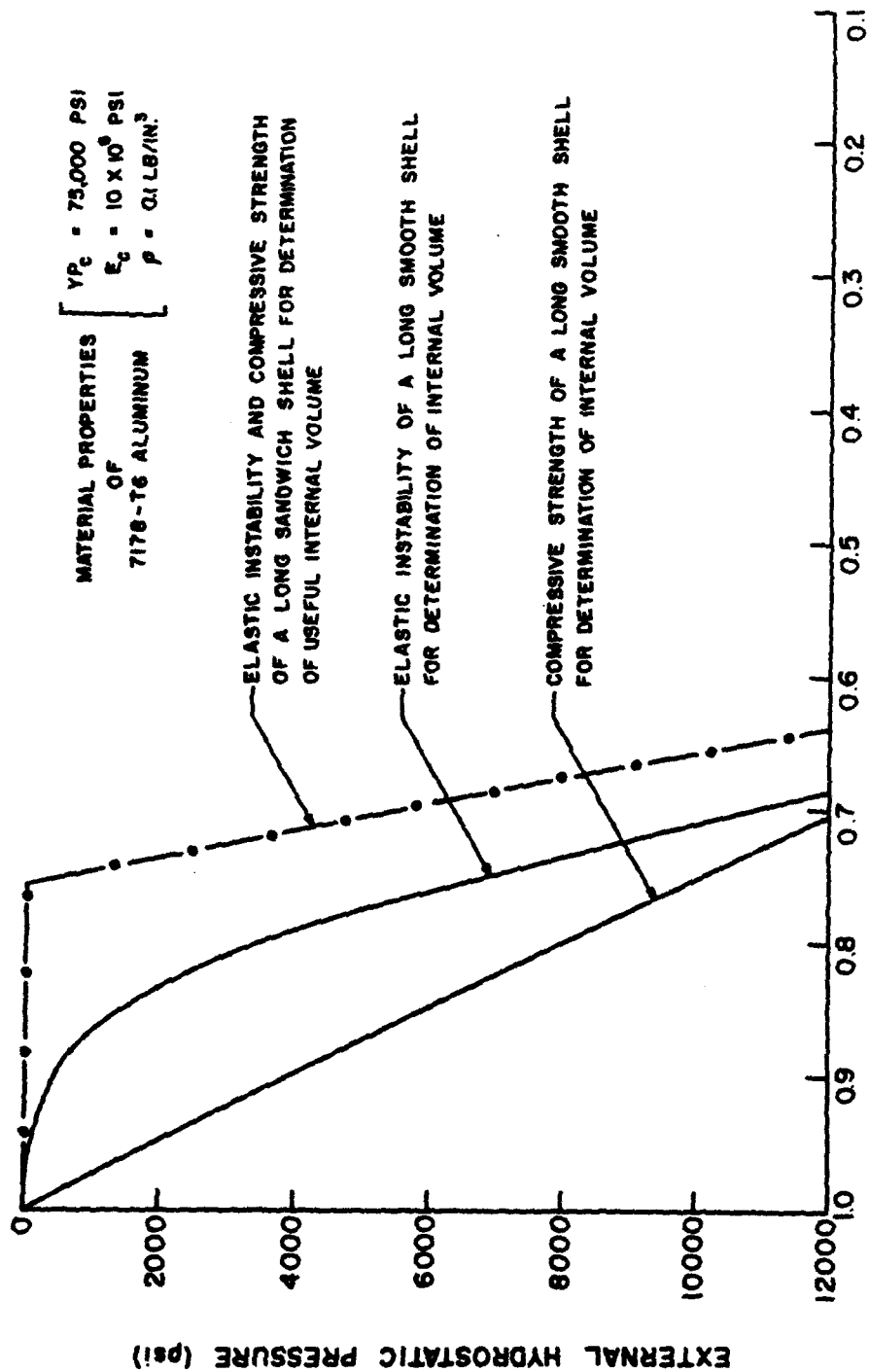


Fig. 20 - Internal and Useful Internal Volumes for Cylindrical Shells
Fabricated from Premium Aluminum

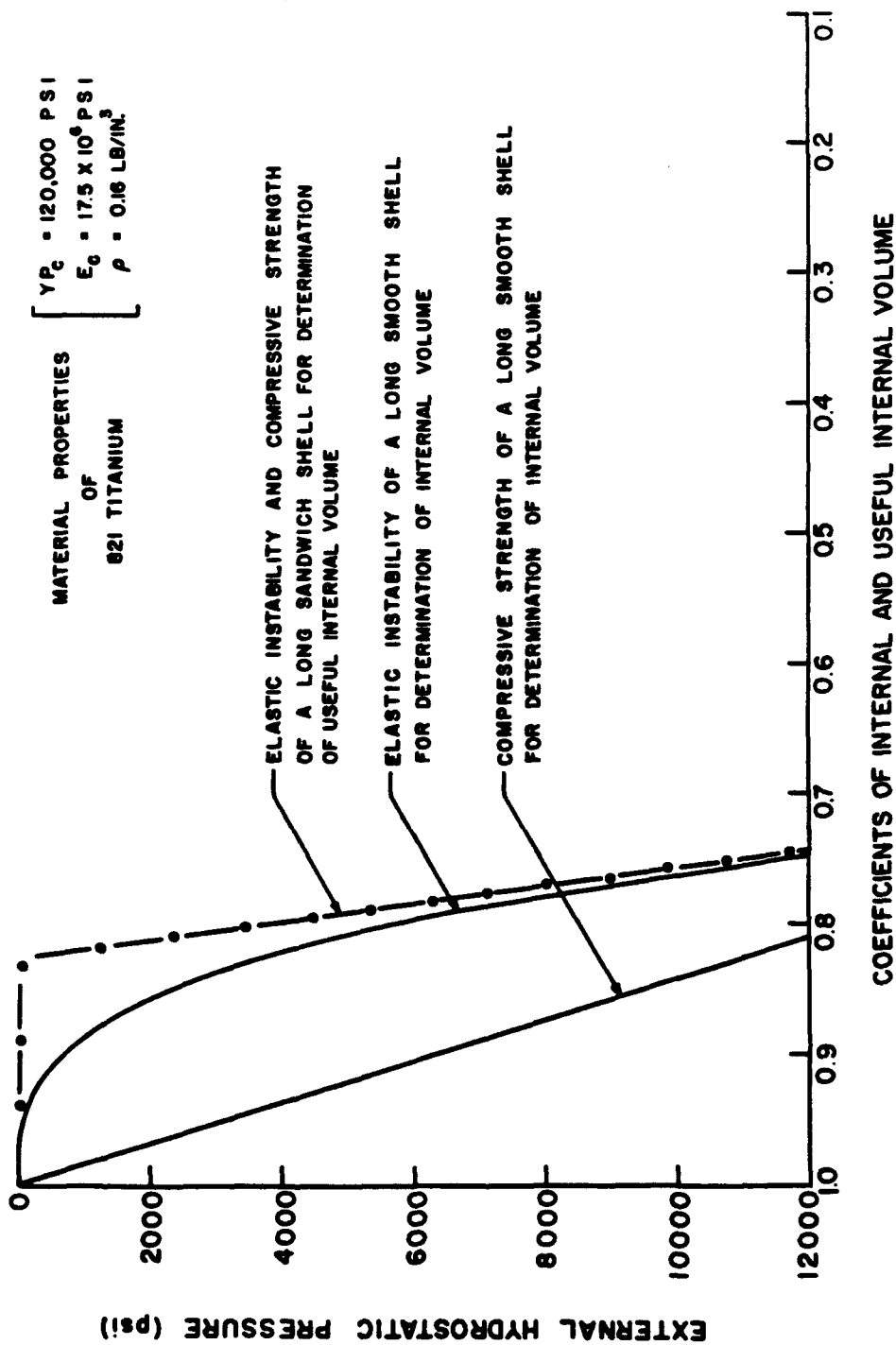


Fig. 21 - Internal and Useful Internal Volumes for Cylindrical Shells
Fabricated from Premium Titanium

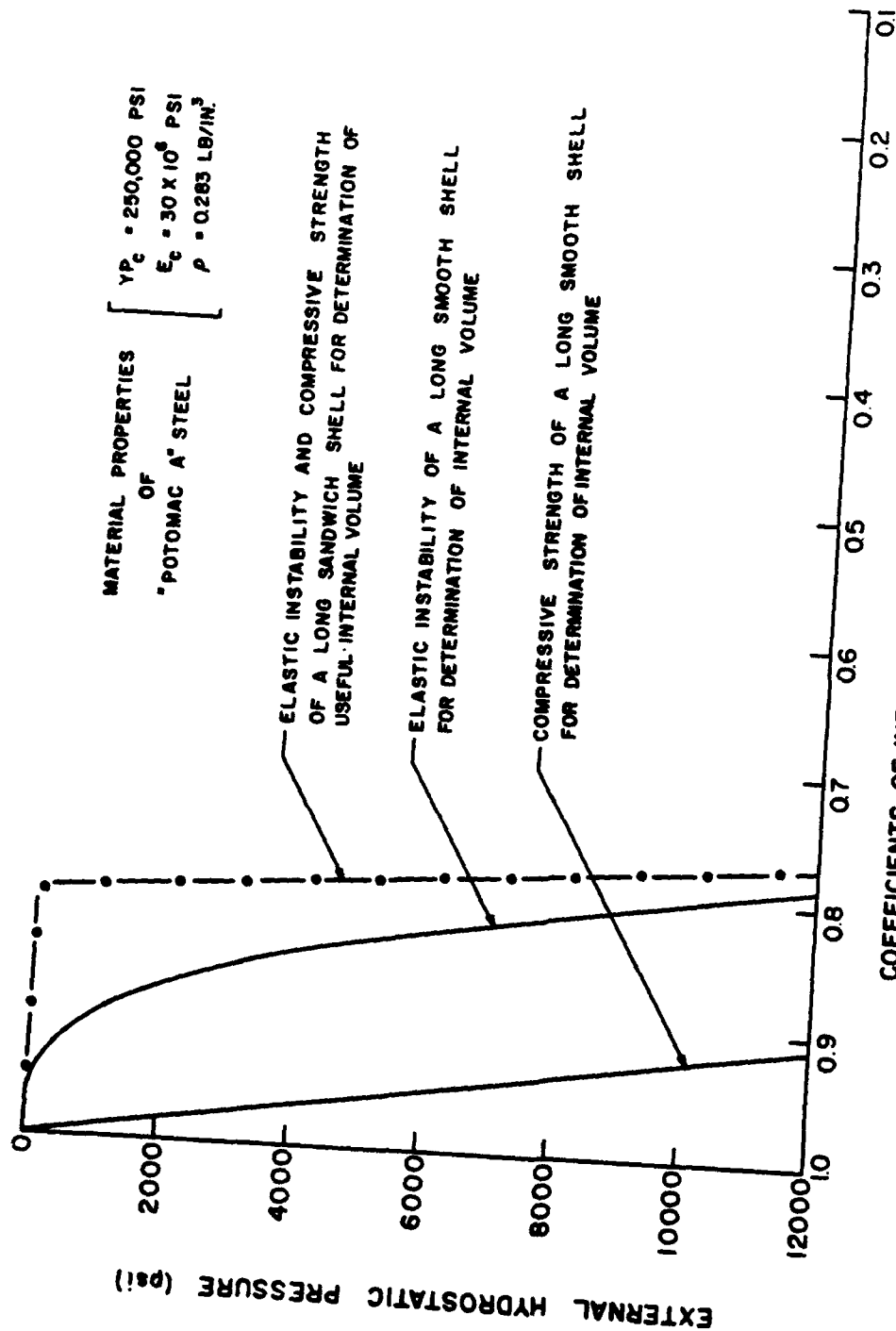
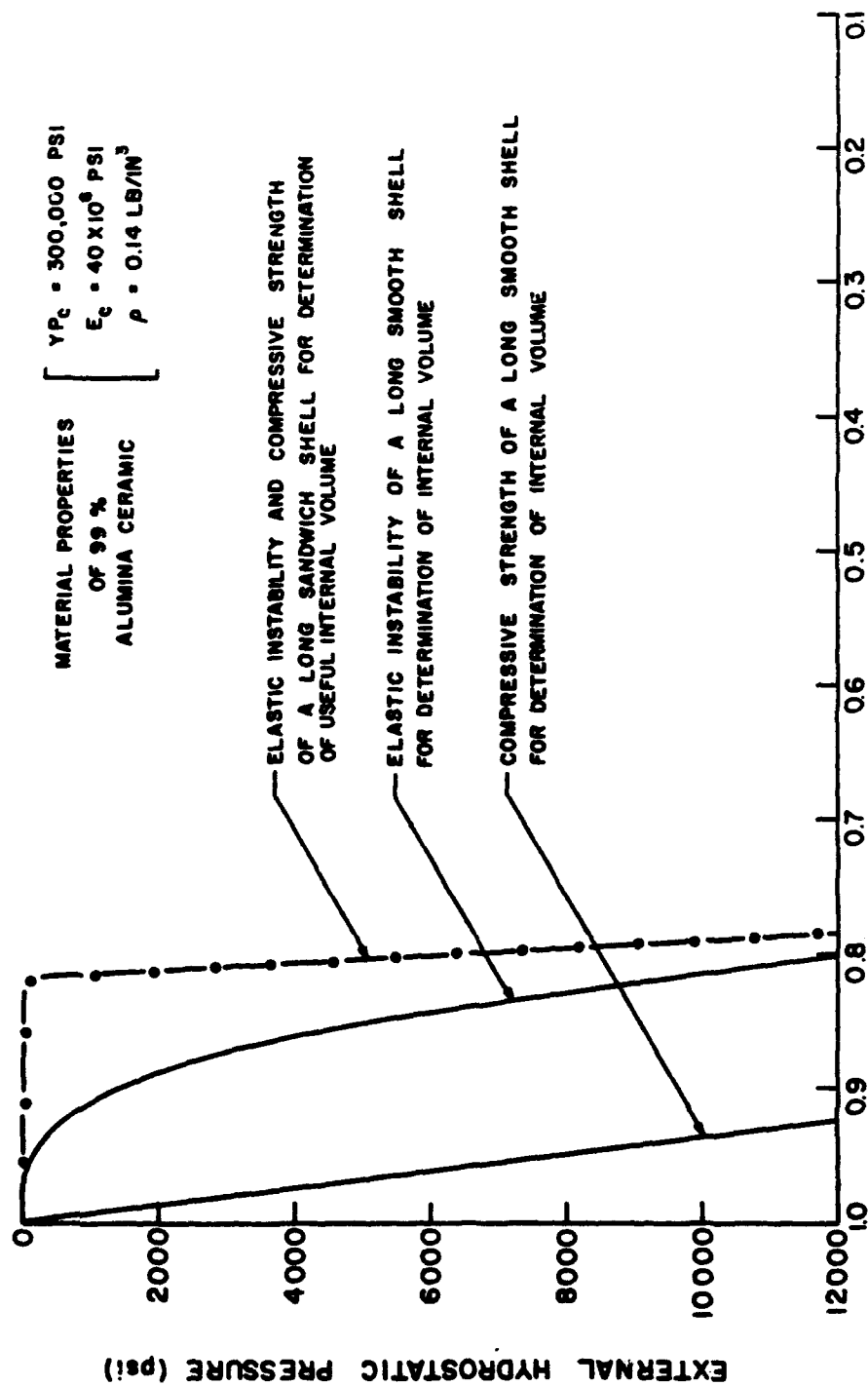


Fig. 22 - Internal and Useful Internal Volumes for Cylindrical Shells Fabricated from Premium Steel



COEFFICIENTS OF INTERNAL AND USEFUL INTERNAL VOLUME

Fig. 23 - Internal and Useful Internal Volumes for Cylindrical Shells
Fabricated from Premium Alumina Ceramic

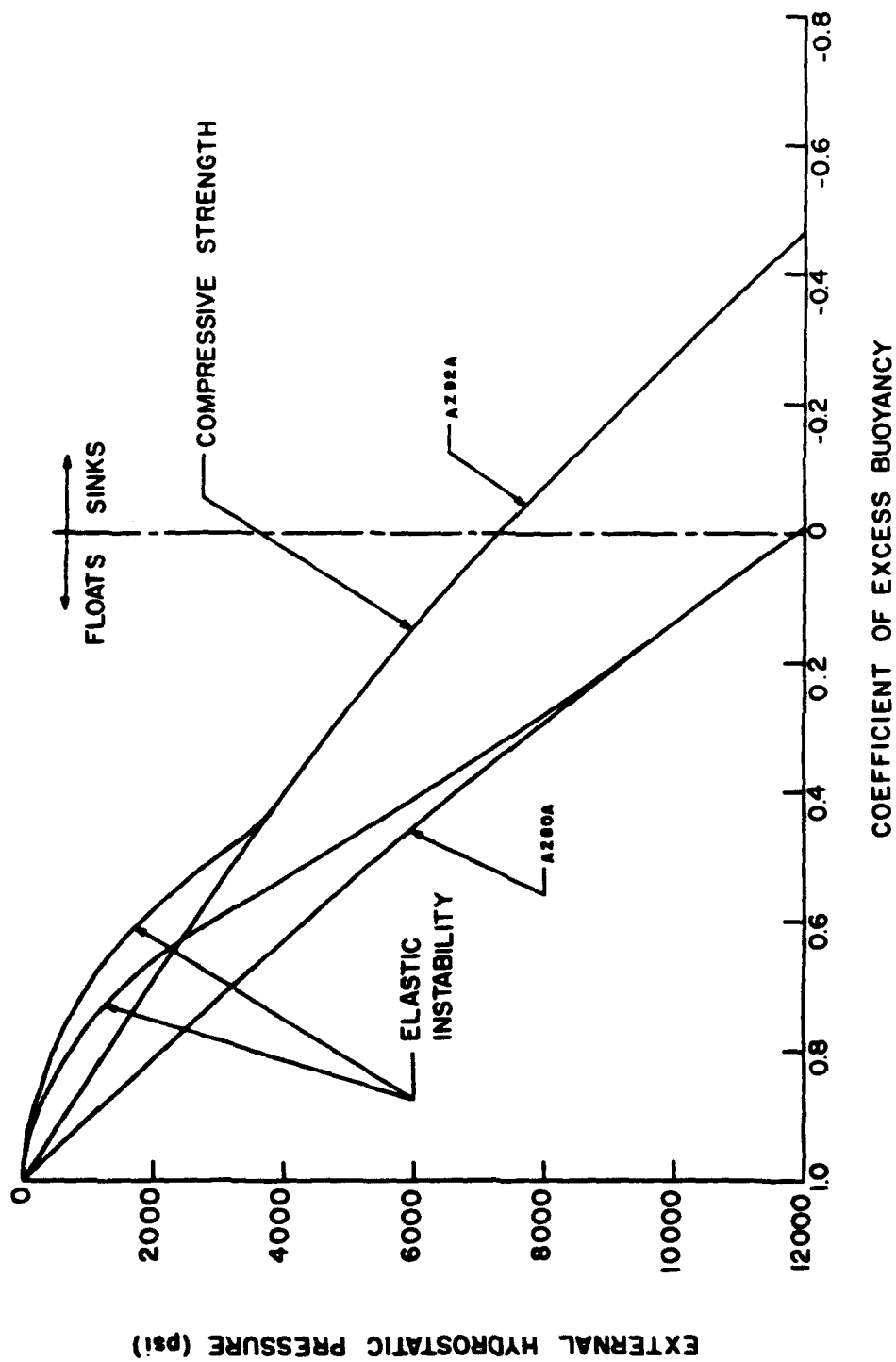


Fig. 24 - Buoyancies of Magnesium Cylindrical Shells

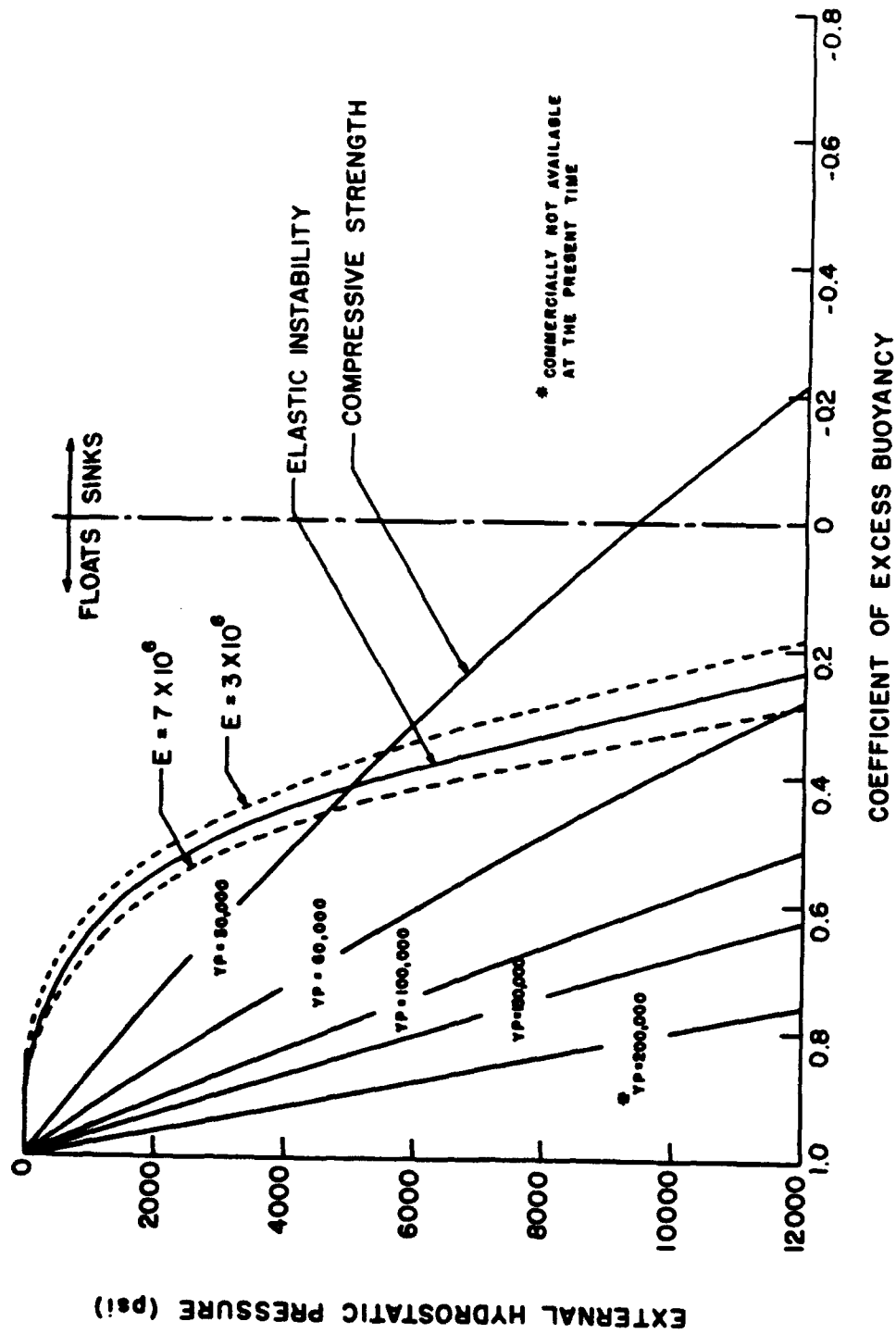


Fig. 25 - Buoyancies of Glass Fiber Plastic Laminate Cylindrical Shells

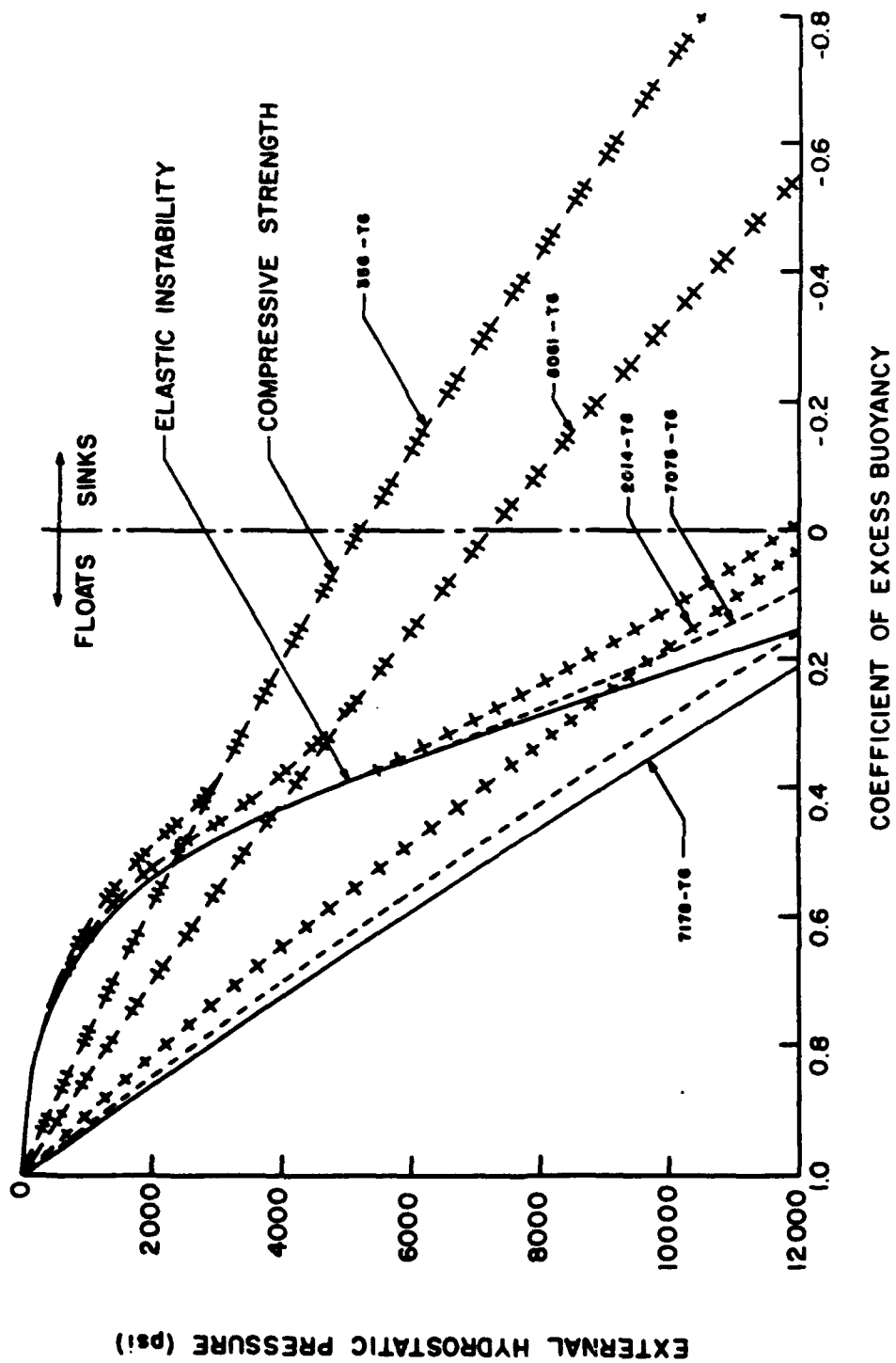


Fig. 26 - Buoyancies of Aluminum Cylindrical Shells

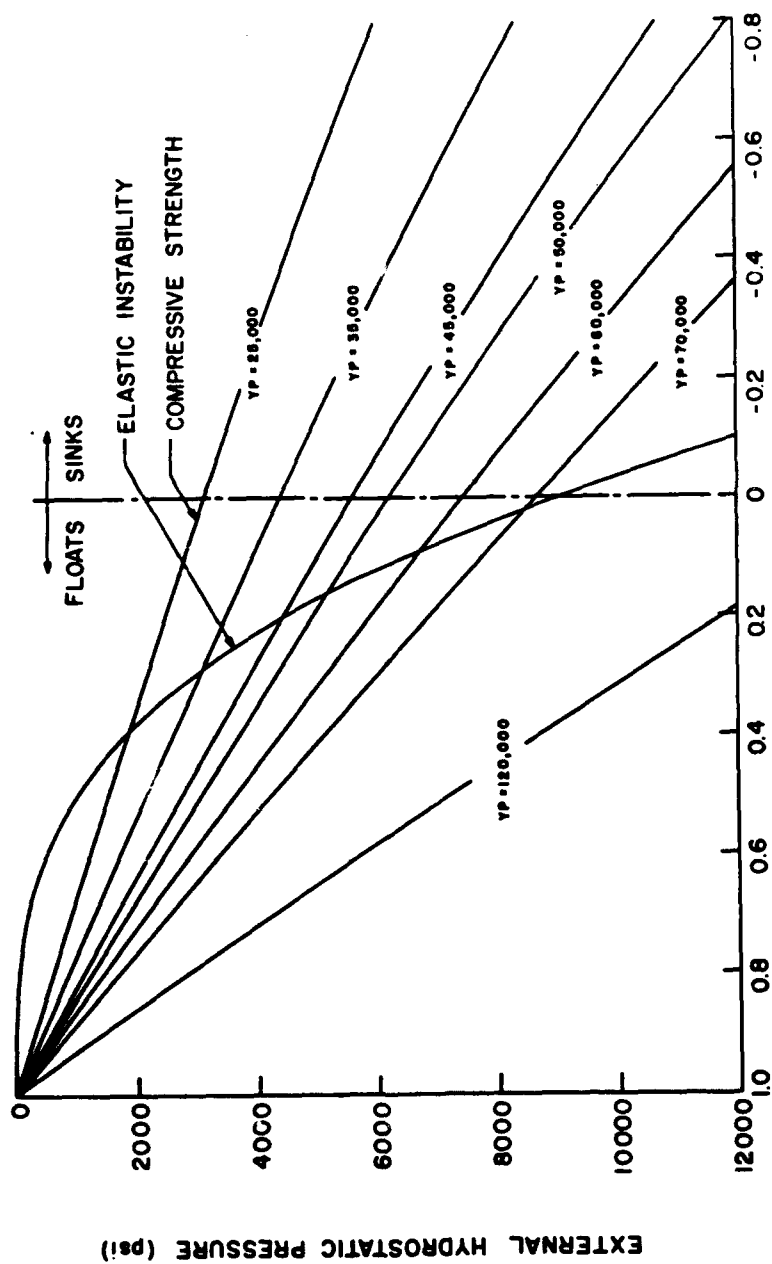
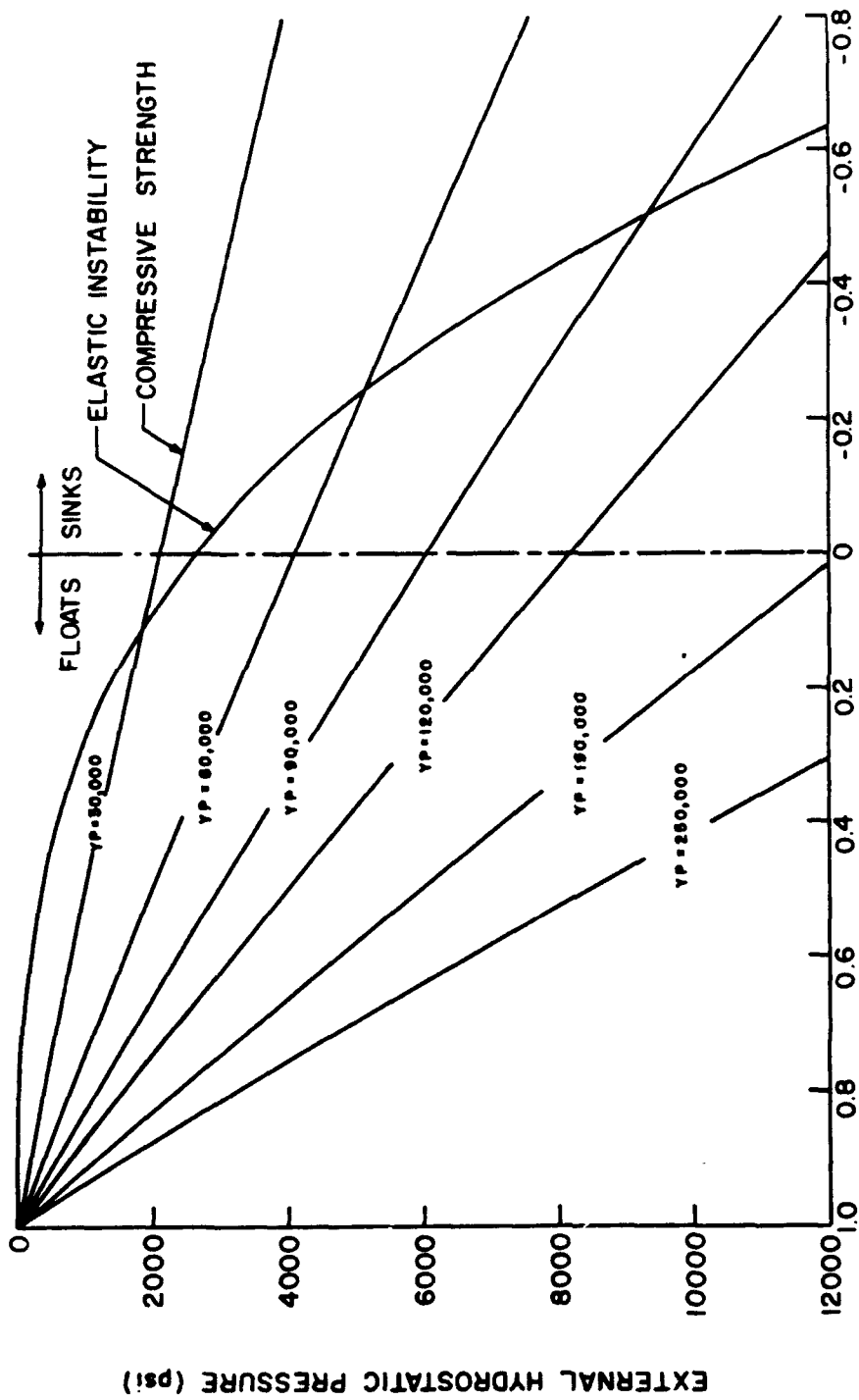


Fig. 27 - Buoyancies of Titanium Cylindrical Shells



COEFFICIENT OF EXCESS BUOYANCY

Fig. 28 - Buoyancies of Steel Cylindrical Shells

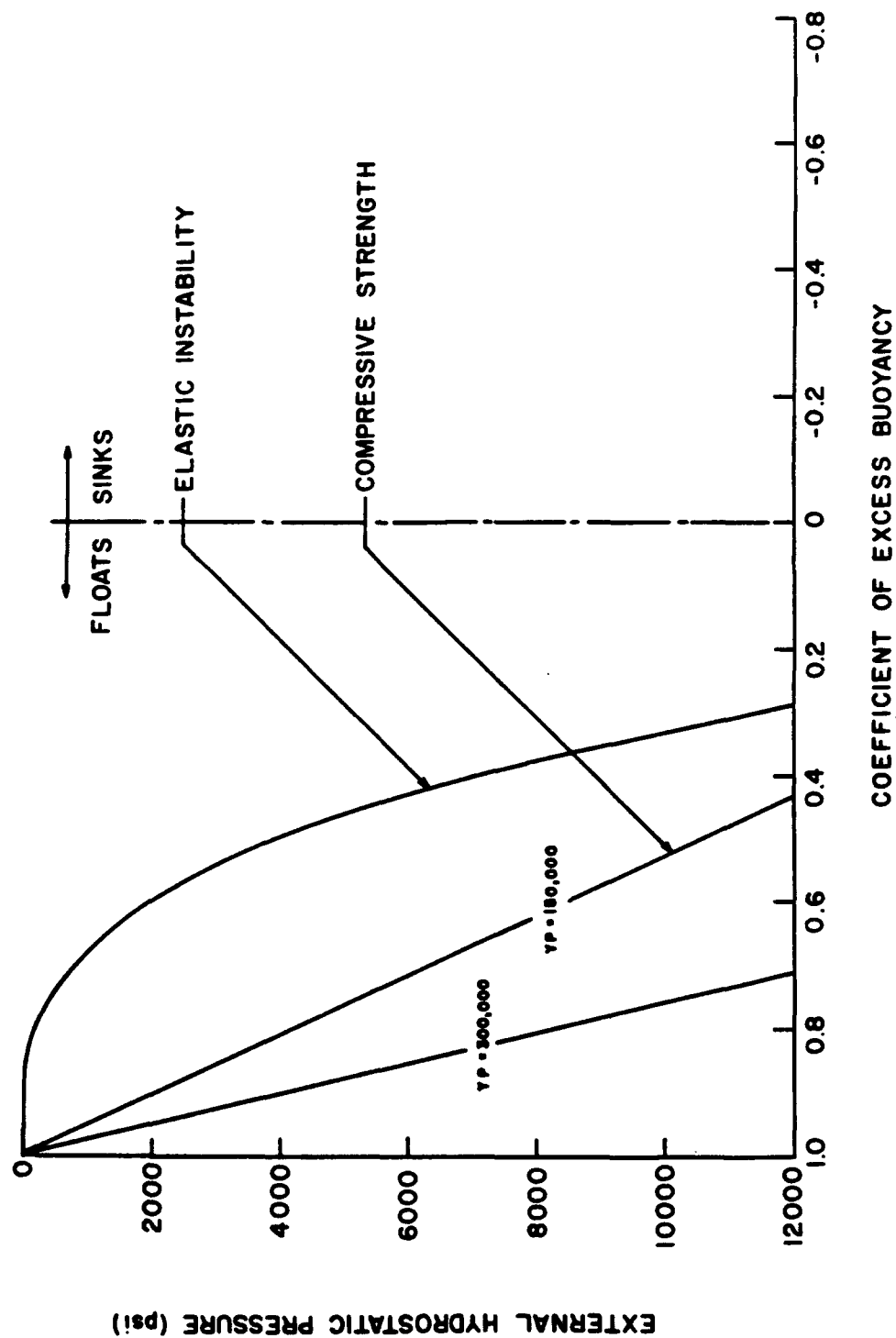


Fig. 29 - Buoyancies of Alumina Ceramic Cylindrical Shells

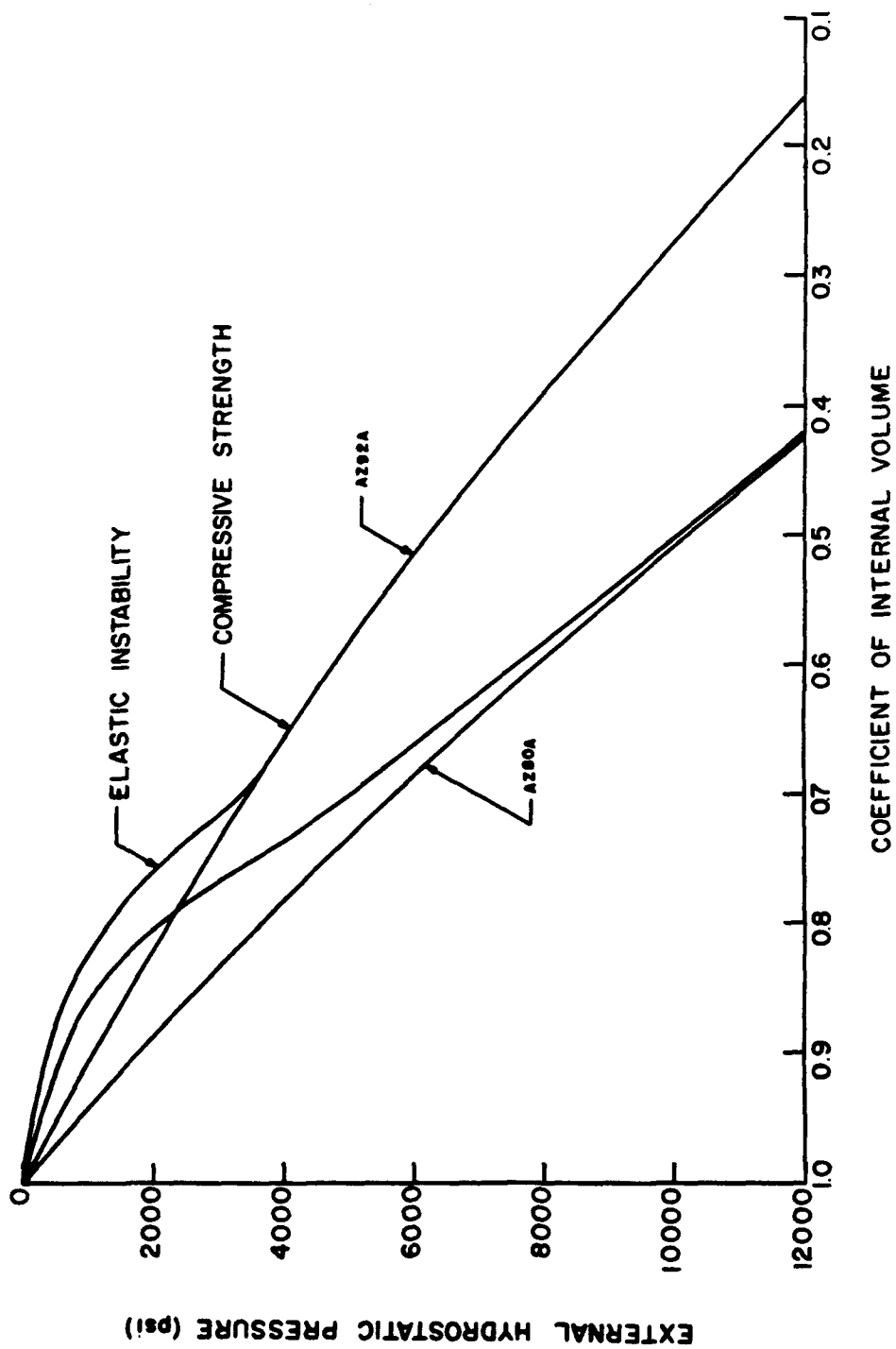


Fig. 30 - Internal Volumes of Cylindrical Shells Fabricated from Magnesium

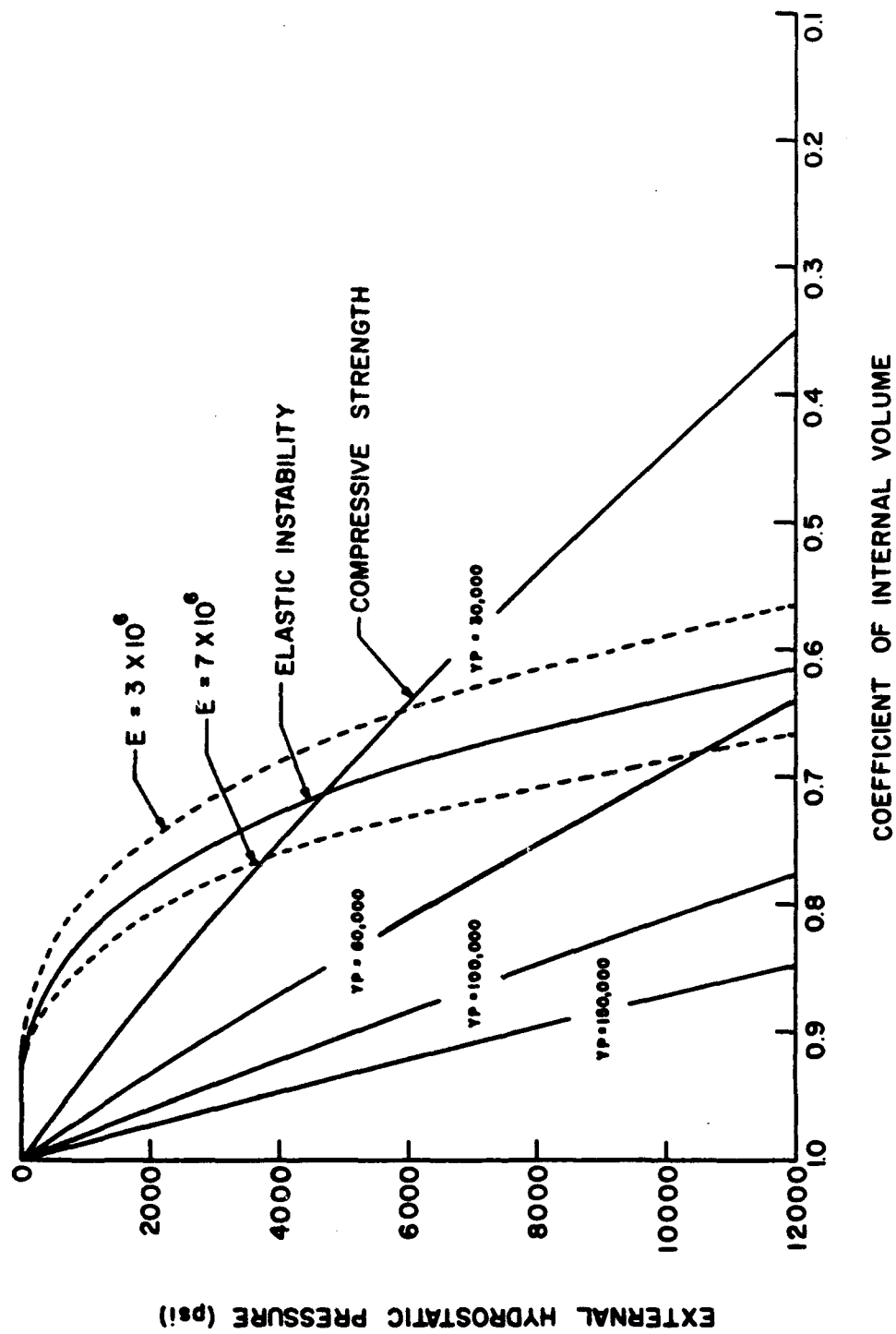


Fig. 31 - Internal Volumes of Cylindrical Shells Fabricated from Glass Fiber Plastic Laminate

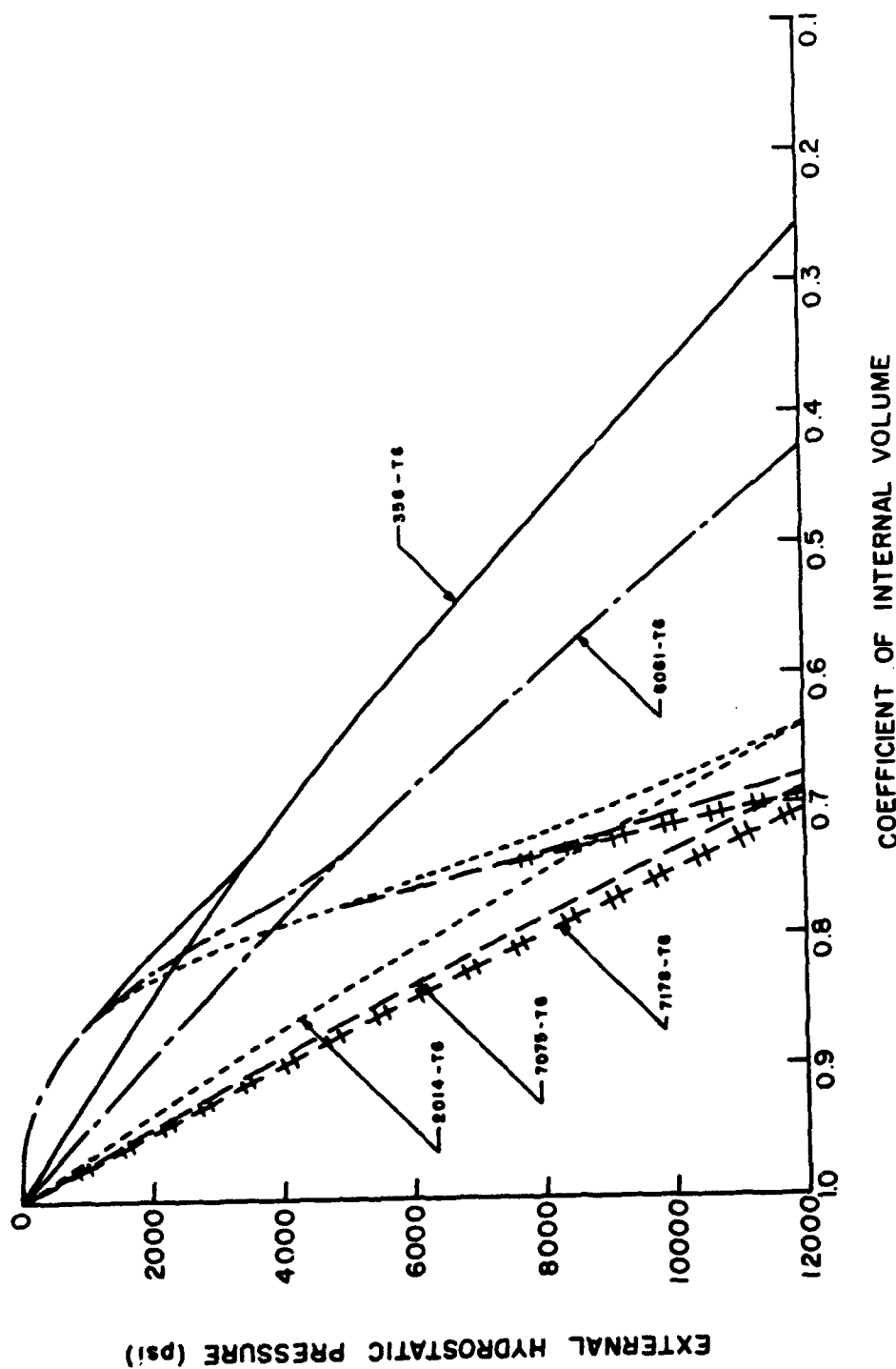
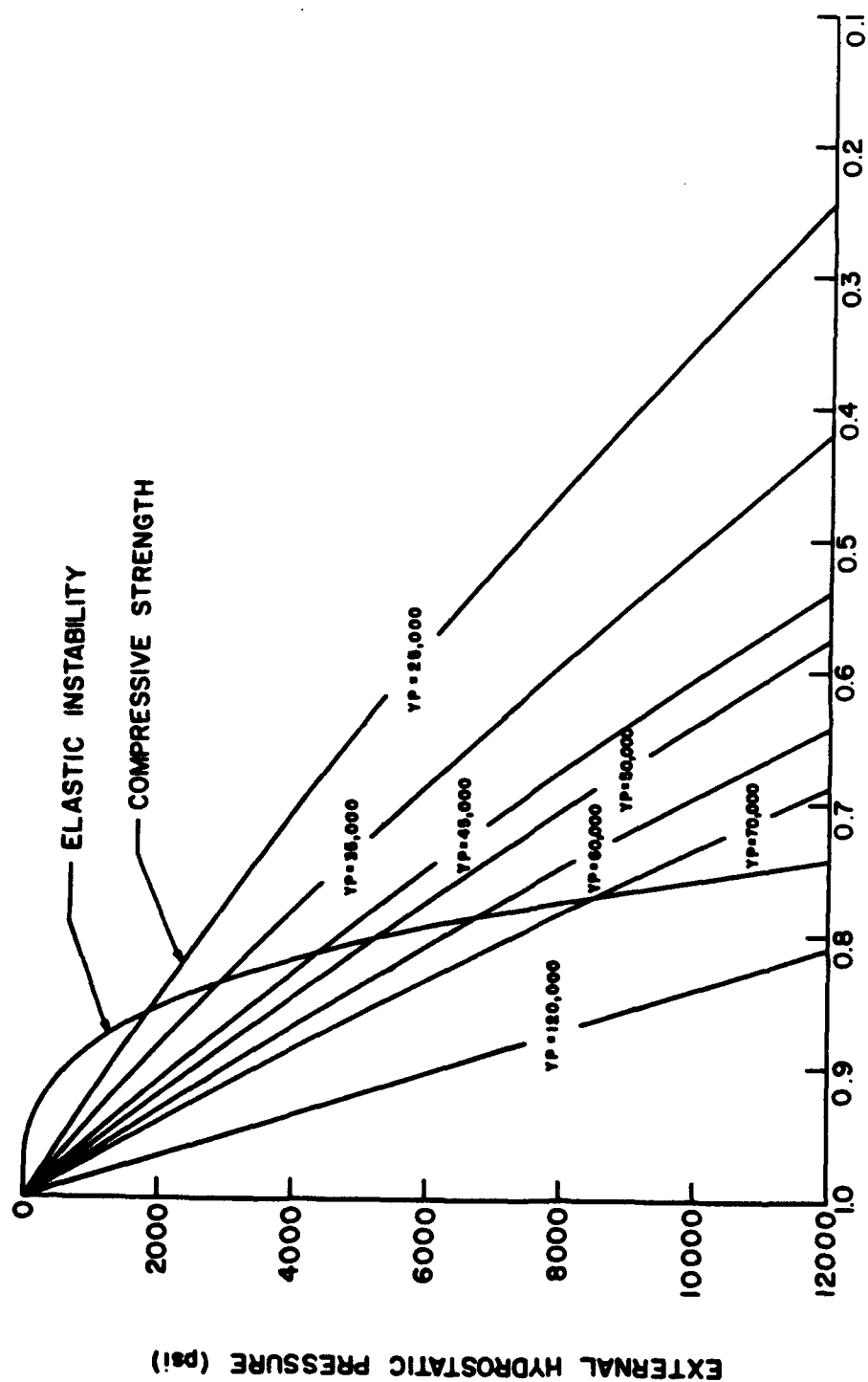


Fig. 32 - Internal Volumes of Cylindrical Shells Fabricated from Aluminum



COEFFICIENT OF INTERNAL VOLUME

Fig. 33 - Internal Volumes of Cylindrical Shells Fabricated from Titanium

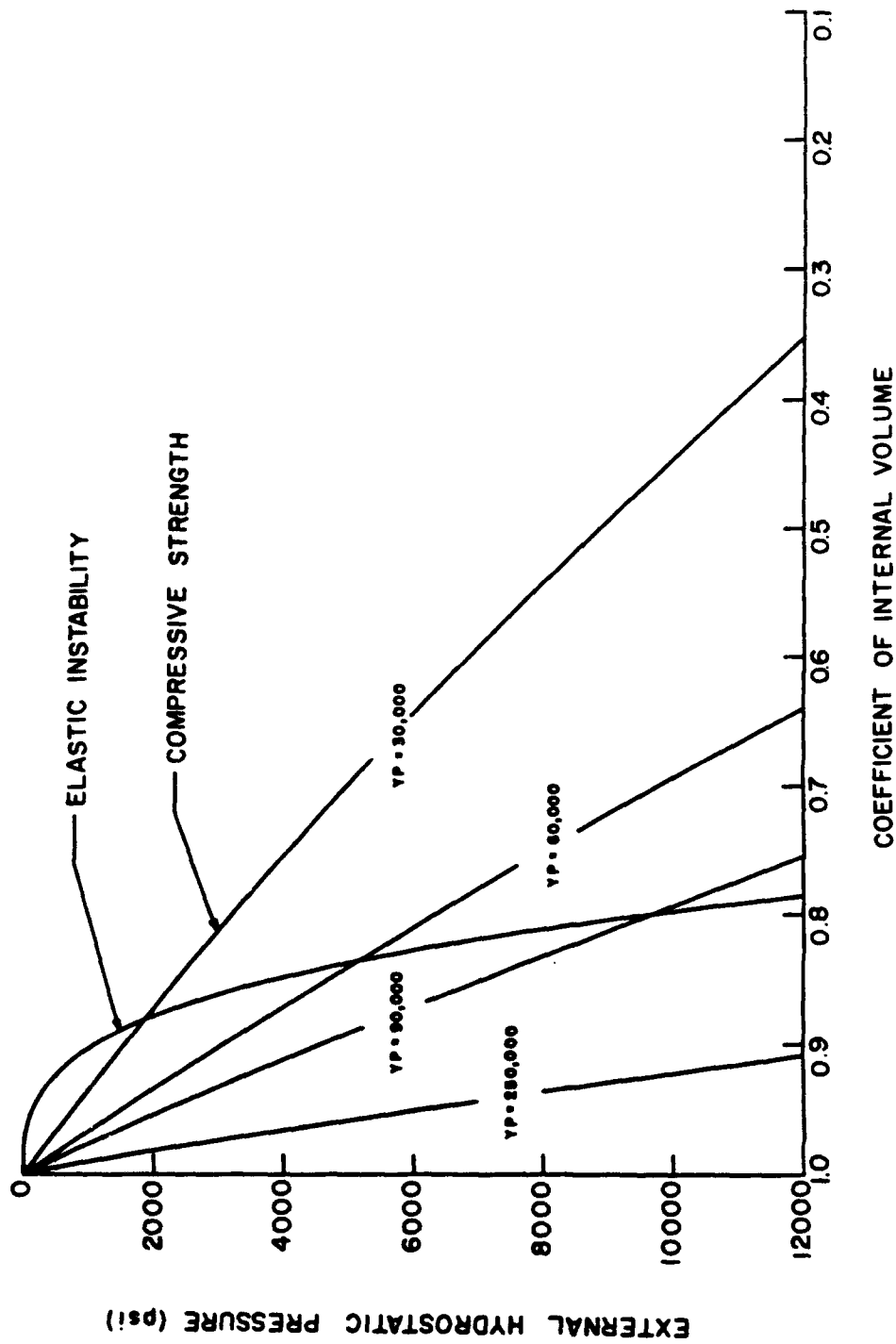


Fig. 34 - Internal Volumes of Cylindrical Shells Fabricated from Steel

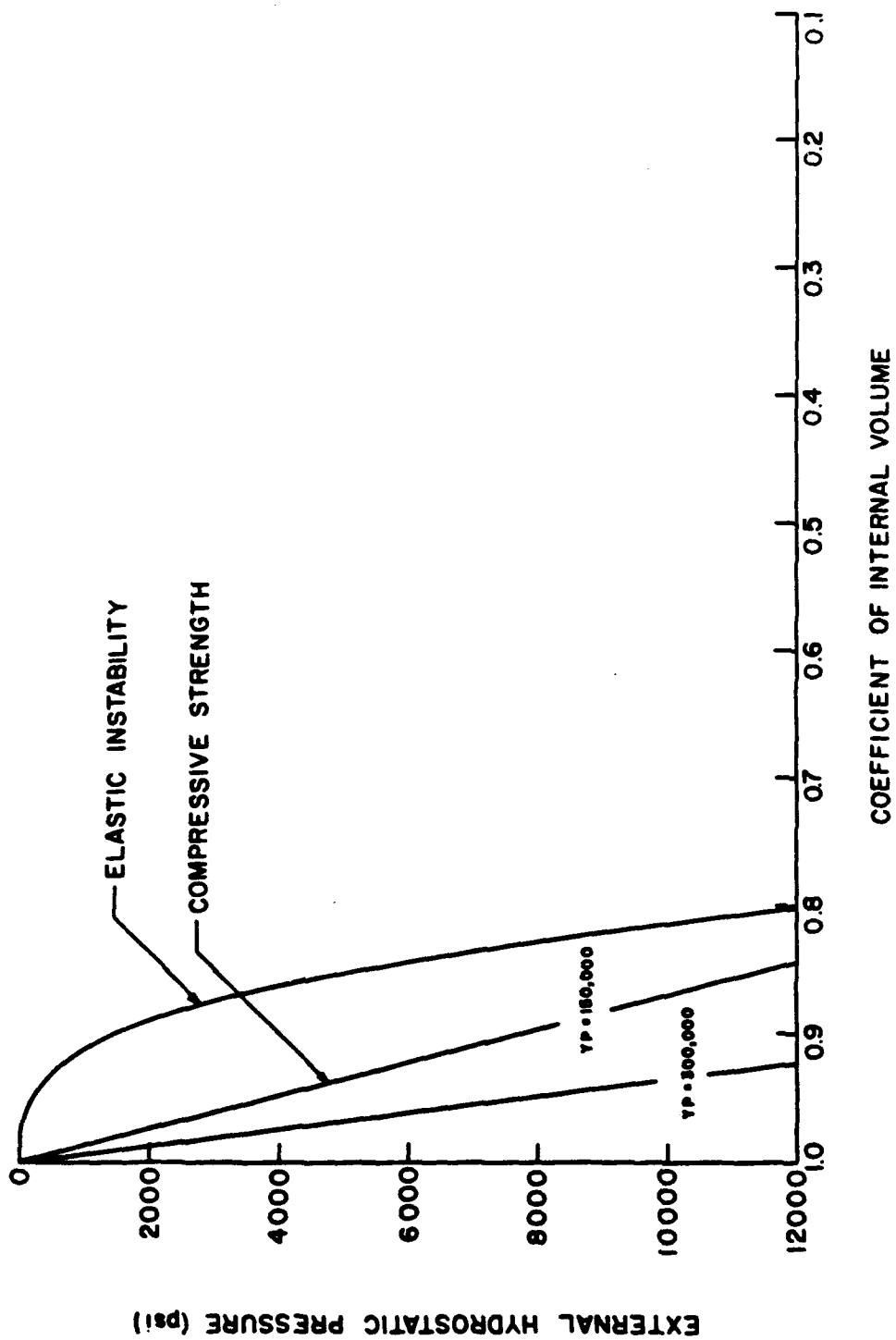


Fig. 35 - Internal Volumes of Cylindrical Shells Fabricated from Alumina Ceramic

Bibliography

Cylindrical Ring-Stiffened Shells

- Batdorf, S. B., A Simplified Method of Elastic Stability Analysis for Thin Cylindrical Shells, National Advisory Committee for Aeronautics, NACA Report 874, 1947.
- Bresse, M., Cours de Mécanique Appliquée, 3rd Ed., Paris, 1880.
- Bryan, G. H., "Application of the Engergy Test to the Collapse of Long Thin Pipe under External Pressure," Proceedings of the Cambridge Philosophical Society, London, Vol. VI, 1888, pp. 287-292.
- Donnell, L. H., "A New Theory for the Buckling of Thin Cylinders under Axial Compression and Bending," ASME Transactions, Vol. 56, No. 11, 1934, pp. 795-806.
- Engesser, F., "Knickfestigkeit gerader Stäbe," Zeitschrift für Architektur und Ingenieurwesen, 1889.
- Kendrick, S., The Buckling, under External Pressure, of Circular Cylindrical Shells with Evenly Spaced, Equal Strength Circular Ring Frames - Part I, Report 211; Part II, Report 243; Part III, Report 244; Naval Construction Research Establishment, 1953.
- Lunchick, M. E., "Yield Failure of Stiffened Cylinders under Hydrostatic Pressure," Proceedings of the Third U. S. Congress of Applied Mechanics, 1959.
- Mises, Richard von, "Der Kritische Aussendruck Zylindrischer Rohre," Stodolas Festschrift, Zurich, 1929, pp. 418-430.
- Salerno, V. L. and J. G. Pulos, Stress Distribution in a Circular Cylindrical Shell under Hydrostatic Pressure Supported by Equally Spaced Circular Ring Frames: Part I, Theory, Polytechnic Institute of Brooklyn, Report No. 171A, 1951.
- Sanden, K. von and K. Gunther, "Ueber das Festigkeitsproblem querversteifter Hohlzylinder unter allseitig gleichmässigem Aussendruck," Werft und Reederei, Vol. 1, No. 9, pp. 189-198; Vol. 1, No. 10, pp. 216-221, 1920.
- Southwell, R. V., "On the Collapse of Tubes by External Pressure," London, Edinburgh, and Dublin Philosophical Magazine and Journal of Science, Vol. 25, May 1913, pp. 687-698; Vol. 26, September 1913, pp. 502-511; Vol. 29, January 1915, pp. 67-77.
- Tokugawa, T., "Model Experiments on the Elastic Stability of Closed and Cross-Stiffened Circular Cylinders under Uniform External Pressure," Proceedings of the World Engineering Congress, Tokyo, Vol. 29, 1929, pp. 249-279.
- Trilling, C., The Influence of Stiffening Rings on the Strength of Thin Cylindrical Shells under External Pressure, U. S. Experimental Model Basin, Report 396, 1935.

- Wenk, E., Jr., R. E. Stark, and D. E. Peugh, Tests of the Yield Strength of Ring-Stiffened Cylindrical Shells Subjected to Hydrostatic Pressure, David Taylor Model Basin, C-Report 440, 1954.
- Windenburg, D. F., The Elastic Stability of Tee Stiffeners, U. S. Experimental Model Basin, Report 457, 1938.

Sandwich Plates

- Anderson, M. S., Local Instability of the Elements of a Truss-Core Sandwich Plate, National Advisory Committee for Aeronautics, NACA Technical Note 4292, July 1958.
- Anderson, M. S., Optimum Proportions of Truss-Core and Web-Core Sandwich Plates Loaded in Compression, National Aeronautics and Space Administration, NASA Technical Note D-98, 1959.
- Anderson, M. S. and R. G. Updegraff, Some Research Results on Sandwich Structures, National Advisory Committee for Aeronautics, NACA Technical Note 4009, 1957.
- Ashley, H. R., Sandwich Structure for High Temperature Vehicles, AGARD Report 216, 1958.
- Bijlaard, P. P., "Analysis of the Elastic and Plastic Stability of Sandwich Plates by the Method of Split Rigidities," Journal of the Aeronautical Sciences, Vol. 18, No. I, May 1951; Vol. 18, No. II, December 1951.
- Bijlaard, P. P., "On the Elastic Stability of Sandwich Plates," Parts I and II, Koninklijke Nederlandsche Akad. Wetenschapen, Reprinted from Proceedings, Vol. L, Nos. 1 and 2, 1947.
- Bijlaard, P. P., "Thermal Stresses and Deflections in Rectangular Sandwich Plates," Journal Aero/Space Science, Vol. 26, April 1959, pp. 210-218.
- Eriksen, W. S. and H. W. March, Effects of Shear Deformation in the Core of a Flat Rectangular Sandwich Panel, Forest Products Laboratory, Report No. 1583-B, 1950.
- Eringen, A. C., "Bending and Buckling of Rectangular Sandwich Plates," Proceedings of the First U. S. Congress of Applied Mechanics, 1951, pp. 381-391.
- Flugge, W., "The Optimum Problem of the Sandwich Plates," Journal of Applied Mechanics, Vol. 19, March 1952, pp. 104-108.
- Hoff, N. J., The Analysis of Structures, John Wiley and Sons, Inc., New York; Chapman and Hill, Ltd., London, 1956.
- Hoff, N. J., Bending and Buckling of Rectangular Sandwich Plates, National Advisory Committee for Aeronautics, NACA Technical Note 2225, 1950.
- Hunter-Tod, J. H., The Elastic Stability of Sandwich Plates, College of Aeronautics, Cranfield, England, Report No. 25, March 1949.
- Johnson, A. E. and J. W. Semonian, A Study of the Efficiency of High-Strength, Steel, Cellular-Core Sandwich Plates in Compression, National Advisory Committee for Aeronautics, NACA Technical Note 3751, 1956.
- Kimel, W. R., Elastic Buckling of a Simply Supported Rectangular Sandwich Panel Subjected to Combined Edgewise Bending and Compression, Forest Products Laboratory, Report No. 1857, September 1956; Report No. 1857-A, November 1956.

- Kuenzi, E. W., Mechanical Properties of Aluminum Honeycomb Core, Forest Products Laboratory, Report No. 1849, September 1955.
- Libove, Charles, "A Small-Deflection Theory for Flexurally Orthotropic Flat Sandwich Plates," from Theory and Practice of Sandwich Construction in Aircraft, A Symposium, Institute of Aeronautical Science, Preprint No. 165, January 1948, pp. 49-56.
- Libove, Charles and S. B. Batdorf, A General Small Deflection Theory for Flat Sandwich Plates, National Advisory Committee for Aeronautics, NACA Report 899, 1948.
- Libove, Charles and Ralph E. Hubka, Elastic Constants for Corrugated-Core Sandwich Plates, National Advisory Committee for Aeronautics, NACA Technical Note 2289, 1951.
- March, H. W., Effects of Shear Deformation in the Core of a Flat Rectangular Sandwich Panel: 1, Buckling under Compressive End Load; 2, Deflection under Uniform Transverse Load, Forest Products Laboratory, Report No. 1583, 1955.
- Mathauser, E. E. and R. A. Pride, Compressive Strength of Stainless-Steel Sandwiches at Elevated Temperatures, National Aeronautics and Space Administration, NASA Memo 6-2-59L, 1959.
- Matsunaga, S., "On the Theory of Bi-Metals," Zeitschrift für Angewandte Mathematik und Mechanik, Vol. 38, September-October 1958.
- Neuber, H. von, "Theorie der Druckstabilität der Sandwichplatte," Zeitschrift für Angewandte Mathematik und Mechanik, Vol. 32, November-December 1952; Vol. 33, January-February 1953.
- Norris, C. B., Compressible Buckling Design Curves for Sandwich Panels with Isotropic Facings and Orthotropic Cores, Forest Products Laboratory, Report No. 1854, February 1956.
- Prusakov, A. P., "Fundamental Bending and Stability Equations of Three-Layered Sandwich Plates with a Light Core" (in Russian), Prikladnaya Matematika i Mekhanika, Vol. 15, 1951, pp. 27-36.
- Rabinovich, A., Stability of Sandwich Plates in Compression (in Russian), Trudy TSAGI, No. 595, 1946.
- Raville, M. E., Deflection and Stresses in a Uniformly Loaded, Simply Supported, Rectangular Sandwich Plate, Forest Products Laboratory, Report No. 1847, December 1955.
- Reissner, Eric, "Finite Deflections of Sandwich Plates," Journal of the Aeronautical Sciences, Vol. 15, No. 7, July 1948, pp. 435-440.
- Reissner, Eric, "Errata, Finite Deflections of Sandwich Plates," Journal of the Aeronautical Sciences, Vol. 17, No. 2, February 1950, p. 125.
- Robinson, J. R., "The Buckling and Bending of Orthotropic Sandwich Panels with All Edges Simply-Supported," The Aeronautical Quarterly, Vol. VI, Part 2, May 1955, pp. 125-248.
- Seide, P. and E. Q. Stowell, Elastic and Plastic Buckling of Simply Supported Solid-Core Sandwich Plates in Compression, National Advisory Committee for Aeronautics, NACA Technical Report No. 987, 1950.
- Setterholm, V. C. and E. W. Kuenzi, Performance of Stainless Steel Sandwich Construction at High Temperatures, U. S. Air Force, WADC Technical Report 55-417, ASTIA Document No. AD 97288, September 1956.

Thurston, G. A., "Bending and Buckling of Clamped Sandwich Plates," *Journal of the Aeronautical Sciences*, Vol. 24, June 1957, pp. 407-412.

Vlasov, V. S., "The Method of Initial Function in Application to the Problems of Equilibrium of Sandwich Plates" (in Russian), *Izvestia Akademii Nauk SSSR, Otdelniye Tekhnicheskikh Nauk*, Vol. 7, 1958, pp. 40-48.

Cylindrical Sandwich Shells

Ambartsumian, S. A., "The Calculation of Laminated Anisotropic Shells" (in Russian), *Izvestia Akademii Nauk Armyanskoy SSR, Seriya Fiziko-Matematicheskikh, Yestestvennykh i Tekhnicheskikh Nauk*, Vol. 6, No. 3, 1953, pp. 15-35.

Bijlaard, P. P., *Method of Split Rigidities and Its Application to Various Buckling Problems*, National Advisory Committee for Aeronautics, NACA Technical Note 4085, July 1958.

Eringen, A. C., "Buckling of a Sandwich Cylinder under Uniform Axial Compressive Load," *Journal of Applied Mechanics*, Vol. 18, No. 2, 1951, pp. 195-202.

Eringen, A. C., "New Numerical Results of the Theory of Buckling of Sandwich Cylinders," *Journal of Applied Mechanics*, Vol. 23, No. 3, 1956, pp. 476-477.

Freiberger, W. F., "On the Minimum Weight Design Problem for Cylindrical Sandwich Shells," *Journal of the Aeronautical Sciences*, Vol. 24, November 1957, pp. 847-848.

Fulton, R. E., *Buckling Analysis and Optimum Proportions of Sandwich Cylindrical Shells under Hydrostatic Pressure*, University of Illinois, Structural Research Series No. 199, 1960.

Gerard, George, "Bending Buckling Tests of Sandwich Cylinders," *Journal of the Aeronautical Sciences*, Vol. 20, No. 9, September 1953, pp. 639-641.

Gerard, George, "Compressive and Torsional Instability of Sandwich Cylinders," *Symposium on Structural Sandwich Construction*, American Society for Testing Materials, Special Technical Publication No. 118, 1952, pp. 56-69.

Gerard, George, *Symmetrical Buckling of Sandwich Cylinders under Compressive End Load*, Report to Office of Naval Research, Guggenheim School of Aeronautics, New York University, 1959.

Gerard, George, "Torsional Instability of a Long Sandwich Cylinder," *Proceedings of the First U. S. Congress of Applied Mechanics*, 1951, pp. 391-394.

Gerard, G., F. K. Teichmann, and G. G. Gould, *Torsional Buckling Tests of Thin Sandwich Cylinders*, Report to Office of Naval Research, New York University, 1951.

Grigolyuk, E. I., "Buckling of Sandwich Construction Beyond the Elastic Limit," *Journal of Mechanics and Physics of Solids*, Vol. 6, July 1958, pp. 253-266.

Grigolyuk, E. I., "Calculation for Stability of Bimetallic Cylindrical Shells" (in Russian), *Inzhenernyi Sbornik*, No. 23, 1956, pp. 28-35.

Grigolyuk, E. I., "The Elastic Stability of Orthotropic and Layered Conical and Cylindrical Shells," *Space Systems*, Vol. III, Gosezdat in Structures and Architecture, USSR, 1953.

- Grigolyuk, E. I., "Equations of Axially Symmetric Bimetallic Elastic Shells" (in Russian), *Inzhenernyi Sbornik*, No. 18, 1954, pp. 89-98.
- Grigolyuk, E. I., "Equations of Three Layer Sandwich Shells with Light Packing" (in Russian), *Izvestia Akademii Nauk SSSR, Otdelnye Tekhnicheskikh Nauk*, No. 1, 1957, pp. 77-84.
- Grigolyuk, E. I., "Finite Deflections of Sandwich Shells with a Rigid Core" (in Russian), *Izvestia Akademii Nauk SSSR, Otdelnye Tekhnicheskikh Nauk*, No. 1, 1958, pp. 26-34.
- Grigolyuk, E. I., "Loss of Stability with Large Deflections of a Closed, Multi-Layer Conical Shell under Action of Normal Uniform Surface Pressure" (in Russian), *Inzhenernyi Sbornik*, No. 22, 1955, pp. 111-119.
- Grigolyuk, E. I., "On the Stability of a Closed Two-Layered Conical Shell Subjected to Uniform Normal Pressure," *David Taylor Model Basin, Translation 265*, March 1956.
- Grigolyuk, E. I., "Stability of Non-Homogeneous Elasto-Plastic Shells," *Soviet Physics-Doklady*, Vol. 3, No. 2, December 1958, pp. 438-441. (Translated by American Institute of Physics, Inc., New York.)
- Grigolyuk, E. I., "Strength and Stability of Cylindrical Bimetallic Shells" (in Russian), *Inzhenernyi Sbornik*, No. 16, 1953, pp. 119-148.
- Grigolyuk, E. I., "Thin Bimetallic Shells and Plates" (in Russian), *Inzhenernyi Sbornik*, No. 17, 1953, pp. 69-120.
- Haft, E. E., *Elastic Stability of Cylindrical Sandwich Shells under Axial and Lateral Load*, Forest Products Laboratory, Report No. 1852, 1955.
- Korolev, V. I., "Thin Two-Layer Plates and Shells" (in Russian), *Inzhenernyi Sbornik*, Vol. 22, 1955, pp. 98-110. (Translated for AVCO RAD.)
- Kuenzi, E. W., *Design Criteria for Long Curved Panels of Sandwich Construction in Axial Compression*, Forest Products Laboratory, Report No. 1558, December 1946.
- Kuenzi, E. W., *Effect of Length on the Buckling Stresses of Thin-Walled Plywood Cylinders in Axial Compression*, Forest Products Laboratory, Report No. 1514, March 1948.
- Kurshin, L. M., "Equations of Triple Sandwich Shells" (in Russian), *Izvestia Akademii Nauk SSSR, Otdelnye Tekhnicheskikh Nauk*, No. 3, 1958, pp. 142-144.
- Leggett, D. M. A. and H. G. Hopkins, *Sandwich Panels and Cylinders under Compressive End Loads*, British Aeronautical and Research Council, R. and M. No. 2262, 1942.
- Librescu, L., "Some Problems in Theory of a Class of Non-Homogeneous Elastic Thin Shells" (in Romanian), *Studii si Cercetari Mecan*, Vol. 10, No. 1, 1959, pp. 187-202.
- March, H. W. and E. W. Kuenzi, *Buckling of Cylinders of Sandwich Construction in Axial Compression*, Forest Products Laboratory, Bulletin 1830, 1952. (Revised 1957.)
- March, H. W. and E. W. Kuenzi, *Buckling of Sandwich Cylinders in Torsion*, Forest Products Laboratory, Report No. 1840, June 1953. (Revised 1958.)
- March, H. W., C. B. Norris, and E. W. Kuenzi, *Buckling of Long, Thin, Plywood Cylinders in Axial Compression*, Forest Products Laboratory, Report No. 1322, 1943.

- March, H. W., Supplement to Buckling of Long, Thin, Plywood Cylinders in Axial Compression-Mathematical Treatment, Forest Products Laboratory, Report No. 1322-A, 1943. (Reviewed and reaffirmed March 1956.)
- March, H. W., C. B. Norris, C. B. Smith, and E. W. Kuenzi, Buckling of Thin-Walled Plywood Cylinders in Torsion, Forest Products Laboratory, Report No. 1529, 1945.
- Nash, W. A., "Recent Advances in the Buckling of Thin Shells," Applied Mechanics Reviews, Vol. 13, No. 3, March 1960, pp. 161-164.
- Norris, C. B. and E. W. Kuenzi, Buckling of Long, Thin, Plywood Cylinders in Axial Compression-Experimental Treatment, Forest Products Laboratory, Report No. 1322-B, 1943.
- Panov, D. Iu., "On the Stability of Bimetallic Shells Subjected to Heat" (in Russian), Prikladnaya Matematika i Mekhanika, Vol. 11, No. 6, 1947.
- Radkowski, P. P., "Buckling of Single and Multi-Layer Conical and Cylindrical Shells with Rotationally Symmetric Stresses," Proceedings of the Third U. S. Congress of Applied Mechanics, 1959, pp. 443-449.
- Radkowski, P. P., Elastic Stability of Thin Single- and Multi-Layer Conical and Cylindrical Shells Subjected to External Pressure, AVCO Report RAD-TR-2-57-34, 1957.
- Raville, M. E., Analysis of Long Cylinders of Sandwich Construction under Uniform External Lateral Pressure, Forest Products Laboratory, Report No. 1844, 1954.
- Raville, M. E., Supplement to Analysis of Long Cylinders of Sandwich Construction under Uniform External Lateral Pressure: Facings of Moderate and Unequal Thicknesses, Forest Products Laboratory, Report No. 1844-A, February 1955.
- Raville, M. E., Buckling of Sandwich Cylinders of Finite Length under Uniform External Lateral Pressure, Forest Products Laboratory, Report No. 1844-B, May 1955.
- Reissner, Eric, Small Bending and Stretching of Sandwich-Type Shells, National Advisory Committee for Aeronautics, NACA Report 975, 1950.
- Stachiw, Jaroslaw D., General Instability of Circumferentially Stiffened Sandwich Shells Subjected to Uniform External Pressure, Master's Thesis, The Pennsylvania State University, 1961.
- Stein, Manuel and J. Mayers, A Small Deflection Theory for Curved Sandwich Plates, National Advisory Committee for Aeronautics, NACA Report 1008, 1951.
- Stein, Manuel and J. Mayers, Compressive Buckling of Simply Supported Curved Plates and Cylinders of Sandwich Construction, National Advisory Committee for Aeronautics, NACA Technical Note 2601, 1952.
- Teichmann, F. K. and G. Gerard, Tests of Thin Sandwich Cylinders under Compressive End Loads, Report to Office of Naval Research, Guggenheim School of Aeronautics, New York University, 1949.
- Teichmann, F. K., C.-T. Wang, and George Gerard, "Buckling of Sandwich Cylinders under Axial Compression," Journal of the Aeronautical Sciences, Vol. 18, No. 6, June 1951, pp. 398-406.
- Teichmann, F. K. and C.-T. Wang, Finite Deflections of Curved Sandwich Plates and Sandwich Cylinders, Institute of Aeronautical Science, FF4, 1951.

- Wang, C.-T., General Theory on the Buckling of Sandwich Cylinders, Report to the Office of Naval Research, Guggenheim School of Aeronautics, New York University, 1949.
- Wang, C.-T., Principle and Application of Complementary Energy Method for Thin Homogeneous and Sandwich Plates and Shells with Finite Deflections, National Advisory Committee for Aeronautics, NACA Technical Note 2260, 1952.
- Wang, C.-T. and D. F. DeSanto, "Buckling of Sandwich Cylinders under Axial Compression, Torsion, Bending, and Combined Loads," Journal of Applied Mechanics, Vol. 22, No. 3, September 1955.
- Wang, C.-T. and G. V. R. Rao, "A Study of an Analogous Model Giving the Non-Linear Characteristics in the Buckling Theory of Sandwich Cylinders," Journal of the Aeronautical Sciences, Vol. 19, No. 2, July 1952, pp. 93-100.
- Wang, C.-T. and D. P. Sullivan, "Buckling of Sandwich Cylinders under Bending and Combined Bending and Axial Compression," Journal of the Aeronautical Sciences, Vol. 19, No. 2, July 1952, pp. 468-470, 485.
- Wang, C.-T., R. J. Vaccaro, and D. F. DeSanto, "Buckling of Sandwich Cylinders under Combined Compression, Torsion, and Bending Loads," Journal of Applied Mechanics, Vol. 22, No. 3, September 1955, pp. 324-328.

General

- Bleich, F., Buckling Strength of Metal Structures, McGraw-Hill Book Company, Inc., New York, 1952.
- Geckeler, N., Statika Uprugovo Tyela, Gosezdat, Moskva, 1934.
- Gerard, G. and S. Wildhorn, A Study of Poisson's Ratio in the Yield Region, National Advisory Committee for Aeronautics, NACA Technical Note 2561, 1952.
- Ilyushin, A. A., Stability of Plates and Shells Beyond the Proportional Limit, National Advisory Committee for Aeronautics, NACA Technical Note 1116, 1947.
- Karman, Th. von, "Untersuchungen über Knickfestigkeit," Mitteilungen über Forschungsarbeiten auf dem Gebiete des Ingenieurwesens, 1910, p. 81.
- Marks, Lionel S., Mechanical Engineers Handbook, McGraw-Hill Book Company, Inc., New York, 1958.
- Mises, Richard von, "Der Kritische Aussendruck Zylindrischer Rohre," Verein Deutscher Ingenieure, Vol. 59, No. 19, 1914, pp. 750-755.
- Nash, A. W., Bibliography on Shells and Shell-Like Structures (1800-1954 Period), David Taylor Model Basin, Report 863, 1954.
- Nash, A. W., Bibliography on Shells and Shell-Like Structures (1954-1956 Period), Engineering and Industrial Experiment Station, University of Florida, 1957.
- Timoshenko, S., Strength of Materials - Part I, D. Van Nostrand Company, Inc., New York, 1956.
- Timoshenko, S., Strength of Materials - Part II, D. Van Nostrand Company, Inc., New York, 1956.

Timoshenko, S., Theory of Elastic Stability, McGraw-Hill Book Company, Inc., New York, 1936.

Timoshenko, S. and J. N. Goodier, Theory of Elasticity, McGraw-Hill Book Company, Inc., New York, 1951.

Timoshenko, S., Theory of Plates and Shells, McGraw-Hill Book Company, Inc., New York, 1940.

<p style="text-align: center;">UNCLASSIFIED</p> <p>Ordnance Research Laboratory Report No. NOrd 16597-89 The Pennsylvania State University, University Park, Pa.</p> <p style="text-align: center;">SHELLS FOR UNDERWATER VEHICLES</p> <p style="text-align: center;">J. D. Stachiw</p> <p>September 28, 1962; 56 pp. & figs.</p> <p>The design criteria for underwater shells are discussed, and the basic shell designs are evaluated on the basis of these criteria. Internally pressurized shells and shell-pressurization methods are also discussed.</p> <p>At present, the sandwich-shell design offers the highest pressure-to-weight ratio consistent with the shell-design criteria. The honeycomb or microballoon fiber glass sandwich shells could be best used in the lower pressure ranges and cellular sandwich shells, for a large band of intermediate pressure ranges; the cellular or solid sandwich shells would be better used at the high pressure ranges.</p> <p style="text-align: right;">(over)</p> <p style="text-align: center;">UNCLASSIFIED</p>	<p style="text-align: center;">UNCLASSIFIED</p> <p>Ordnance Research Laboratory Report No. NOrd 16597-89 The Pennsylvania State University, University Park, Pa.</p> <p style="text-align: center;">SHELLS FOR UNDERWATER VEHICLES</p> <p style="text-align: center;">J. D. Stachiw</p> <p>September 28, 1962; 56 pp. & figs.</p> <p>The design criteria for underwater shells are discussed, and the basic shell designs are evaluated on the basis of these criteria. Internally pressurized shells and shell-pressurization methods are also discussed.</p> <p>At present, the sandwich-shell design offers the highest pressure-to-weight ratio consistent with the shell-design criteria. The honeycomb or microballoon fiber glass sandwich shells could be best used in the lower pressure ranges and cellular sandwich shells, for a large band of intermediate pressure ranges; the cellular or solid sandwich shells would be better used at the high pressure ranges.</p> <p style="text-align: right;">(over)</p> <p style="text-align: center;">UNCLASSIFIED</p>
<p style="text-align: center;">UNCLASSIFIED</p> <p>Ordnance Research Laboratory Report No. NOrd 16597-89 The Pennsylvania State University, University Park, Pa.</p> <p style="text-align: center;">SHELLS FOR UNDERWATER VEHICLES</p> <p style="text-align: center;">J. D. Stachiw</p> <p>September 28, 1962; 56 pp. & figs.</p> <p>The design criteria for underwater shells are discussed, and the basic shell designs are evaluated on the basis of these criteria. Internally pressurized shells and shell-pressurization methods are also discussed.</p> <p>At present, the sandwich-shell design offers the highest pressure-to-weight ratio consistent with the shell-design criteria. The honeycomb or microballoon fiber glass sandwich shells could be best used in the lower pressure ranges and cellular sandwich shells, for a large band of intermediate pressure ranges; the cellular or solid sandwich shells would be better used at the high pressure ranges.</p> <p style="text-align: right;">(over)</p> <p style="text-align: center;">UNCLASSIFIED</p>	<p style="text-align: center;">UNCLASSIFIED</p> <p>Ordnance Research Laboratory Report No. NOrd 16597-89 The Pennsylvania State University, University Park, Pa.</p> <p style="text-align: center;">SHELLS FOR UNDERWATER VEHICLES</p> <p style="text-align: center;">J. D. Stachiw</p> <p>September 28, 1962; 56 pp. & figs.</p> <p>The design criteria for underwater shells are discussed, and the basic shell designs are evaluated on the basis of these criteria. Internally pressurized shells and shell-pressurization methods are also discussed.</p> <p>At present, the sandwich-shell design offers the highest pressure-to-weight ratio consistent with the shell-design criteria. The honeycomb or microballoon fiber glass sandwich shells could be best used in the lower pressure ranges and cellular sandwich shells, for a large band of intermediate pressure ranges; the cellular or solid sandwich shells would be better used at the high pressure ranges.</p> <p style="text-align: right;">(over)</p> <p style="text-align: center;">UNCLASSIFIED</p>

UNCLASSIFIED

It is recommended that research be directed toward development of higher-strength materials and improved fabrication methods. It is also recommended that fluids of lower compressibility and density be developed for shell pressurization.

UNCLASSIFIED

UNCLASSIFIED

It is recommended that research be directed toward development of higher-strength materials and improved fabrication methods. It is also recommended that fluids of lower compressibility and density be developed for shell pressurization.

UNCLASSIFIED

UNCLASSIFIED

It is recommended that research be directed toward development of higher-strength materials and improved fabrication methods. It is also recommended that fluids of lower compressibility and density be developed for shell pressurization.

UNCLASSIFIED

UNCLASSIFIED

It is recommended that research be directed toward development of higher-strength materials and improved fabrication methods. It is also recommended that fluids of lower compressibility and density be developed for shell pressurization.

UNCLASSIFIED



THE PENNSYLVANIA STATE UNIVERSITY
UNIVERSITY PARK, PENNSYLVANIA

General Instability of Circumferentially Stiffened Sandwich Shells Subjected to Uniform External Pressure

SERIAL NO. NOrd 16597-91

December 10, 1962

Copy No.

General Instability of Circumferentially Stiffened Sandwich Shells Subjected to Uniform External Pressure

By J. D. Stachiw

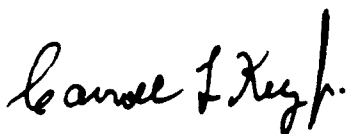
ORDNANCE RESEARCH LABORATORY

The Pennsylvania State University

University Park, Pennsylvania

December 10, 1962

APPROVED FOR DISTRIBUTION



ASSISTANT DIRECTOR

APPROVED FOR DISTRIBUTION



DIRECTOR

Distribution List

Chief, Bureau of Naval Weapons (RU-2) Department of the Navy Washington 25, D. C.	1 copy	Commander U. S. Naval Ordnance Laboratory White Oak Silver Spring 19, Maryland	2 copies
Chief, Bureau of Naval Weapons (RUTO-33) Department of the Navy Washington 25, D. C.	2 copies	Commander U. S. Naval Ordnance Laboratory White Oak Silver Spring 19, Maryland Attn: Dr. S. J. Raff	1 copy
Chief, Bureau of Naval Weapons (RUDC) Department of the Navy Washington 25, D. C.	1 copy	Commander U. S. Naval Ordnance Test Station 3202 East Foothill Boulevard Pasadena Annex Pasadena 8, California	2 copies
Chief, Bureau of Naval Weapons (RUSD) Department of the Navy Washington 25, D. C.	1 copy	Commanding Officer U. S. Naval Torpedo Station Keyport, Washington	1 copy
Chief, Bureau of Naval Weapons (DLI-3) Department of the Navy Washington 25, D. C.	2 copies	Commanding Officer U. S. Naval Torpedo Station Quality Evaluation Technical Library Keyport, Washington	1 copy
Chief, Naval Operations (OP 721) Department of the Navy Washington 25, D. C. For: IEP AEC 28	5 copies	Officer in Charge U. S. Navy Central Torpedo Office Newport, Rhode Island	1 copy
Chief, Naval Operations (OP 31) Department of the Navy Washington 25, D. C.	1 copy	Director (Code 2021) U. S. Naval Research Laboratory Washington 25, D. C.	3 copies
Chief, Naval Operations (OP 312) Department of the Navy Washington 25, D. C.	1 copy	Director (Code 2027) U. S. Naval Research Laboratory Washington 25, D. C.	1 copy
Chief, Naval Operations (OP 71) Department of the Navy Washington 25, D. C.	1 copy	Commanding Officer and Director U. S. Navy Electronics Laboratory San Diego 52, California	1 copy
Chief, Naval Operations (OSEG) Department of the Navy Washington 25, D. C.	1 copy	Commanding Officer and Director David Taylor Model Basin Washington 7, D. C.	1 copy
Chief, Naval Operations (OPO7TC) Technical Analysis and Advisory Group Rm5E613, Pentagon Washington 25, D. C.	1 copy	Commanding Officer U. S. Navy Mine Defense Laboratory Panama City, Florida	1 copy
Chief, Bureau of Ships Department of the Navy Washington 25, D. C.	3 copies	Commanding Officer and Director U. S. Navy Underwater Sound Laboratory Fort Trumbull New London, Connecticut	1 copy
Commander Armed Services Technical Information Agency Attention TIPDR Arlington Hall Station Arlington 12, Virginia	10 copies	Commander U. S. Naval Missile Center Point Mugu Port Hueneme, California	1 copy
Commanding Officer U. S. Naval Underwater Ordnance Station Newport, Rhode Island	3 copies		

Commander U. S. Naval Air Development Center Johnsville, Pennsylvania	1 copy	Commander, Test and Evaluation Force U. S. Atlantic Fleet U. S. Naval Base Norfolk 11, Virginia	1 copy
Officer in Charge Naval Aircraft Torpedo Unit Naval Air Station Quonset Point, Rhode Island	1 copy	Clevite Ordnance 540 East 105th Street Cleveland, Ohio	1 copy
Scientific and Technical Information Facility P. O. Box 5700 Bethesda, Maryland Attn: NASA Representative (S-AK/DL)	1 copy	Vitro Corporation of America 14,000 Georgia Avenue Silver Spring, Maryland	1 copy
Director, Applied Physics Laboratory University of Washington Seattle, Washington	2 copies	Westinghouse Electric Corporation Lansdowne Plant Baltimore, Maryland	1 copy
Director, Marine Physical Laboratory Scripps Institution of Oceanography San Diego 52, California	1 copy	Woods Hole Oceanographic Institution Woods Hole, Massachusetts	1 copy
Hudson Laboratories Dobbs Ferry, New York	1 copy	Aerojet General Corporation Azusa, California Attn: G. M. McRoberts	1 copy

Acknowledgment

*T*HIS REPORT is based on research required for the degree of Master of Science at the College of Engineering and Architecture, The Pennsylvania State University. This research, which is described in the thesis "General Instability of Circumferentially Stiffened Sandwich Shells Subjected to Uniform External Pressure," was performed at the Ordnance Research Laboratory from 1959 to 1961. The author wishes to acknowledge the financial and administrative assistance extended by the Ordnance Research Laboratory and the guidance in the writing of the thesis provided by the Mechanics Department of the College of Engineering and Architecture.

Table of Contents

General Instability of Circumferentially Stiffened Sandwich Shells Subjected to Uniform External Pressure	1
Introduction	1
Theoretical Consideration and Discussion	2
Experimental and Testing Procedures	6
Experimental Results	10
Comparison of Experimental and Theoretical Results	11
Summary and Conclusions	12
References	13

List of Illustrations*

- Fig. 1. Aluminum Cellular Sandwich Shell
- Fig. 2. Structure of Cellular Sandwich Shell
- Fig. 3. Acrylic Resin Cellular Sandwich Shell
- Fig. 4. Structural Components of Acrylic Resin Cellular Sandwich Shell
- Fig. 5. Acrylic Resin Tubular Sandwich Shell
- Fig. 6. Acrylic Resin Smooth Shell
- Fig. 7. Acrylic Resin Smooth Shell Stiffened by Equally Spaced Circumferential Plain Ribs
- Fig. 8. Acrylic Resin Smooth Shell Stiffened by Equally Spaced Circumferential T Ribs
- Fig. 9. Buckling of Slender Aluminum Rods
- Fig. 10. Assembly Drawing of Acrylic Resin Shells
- Fig. 11. Equipment Required for Implosion Testing of Acrylic Resin Shells
- Fig. 12. Assembly Drawing of Aluminum Cellular Sandwich Shell
- Fig. 13. End Supports for Shells Subjected to External Pressure
- Fig. 14. Method of Implosion Testing of Aluminum Cellular Sandwich Shells
- Fig. 15. Location of Instruments during Pressure-Cycling Test
- Fig. 16. Location of Instruments during Implosion Test
- Fig. 17. Cellular Sandwich Shell after Implosion
- Fig. 18. Deformation of Cellular Sandwich Shells after Implosion
- Fig. 19. Dissected Collapsed Shell (Model A)
- Fig. 20. Shell Wall Section
- Fig. 21. Stresses in Shell Models A and A' during Pressure Cycling -
Locations 1 through 6

*Illustrations will be found at the end of the report, following the colored divider.

- Fig. 22. Stresses in Shell Models A and A' during Pressure Cycling -
Locations 7 through 12
- Fig. 23. Stresses in Shell Models A and A' during Pressure Cycling -
Locations 16 through 18 and 22 through 24
- Fig. 24. Stresses in Shell Models A and A' during Pressure Cycling -
Locations 13 through 15 and 19 through 21
- Fig. 25. Strains in Shell Models A and A' during Implosion Testing -
Locations 1 through 6
- Fig. 26. Strains in Shell Models A and A' during Implosion Testing -
Locations 7 through 12
- Fig. 27. Strains in Shell Models A and A' during Implosion Testing -
Locations 19 through 24
- Fig. 28. Collapse Pressure of an Infinitely Long Aluminum Cellular Sandwich Shell
- Fig. 29. Collapse Pressure of an Infinitely Long Acrylic Resin Cellular Sandwich Shell
- Fig. 30. Tangent Modulus of Elasticity vs Compressive Stress for 6061-T6 Aluminum Alloy
- Fig. 31. Stress-Strain Curve for Acrylic Resin Shell Material

Abstract

THE Bresse equation for the buckling of rings under radial pressure is modified to predict the general-instability collapse pressure of cellular sandwich shells under hydrostatic pressure. The validity of the equation is demonstrated by implosion experiments with carefully designed cellular sandwich shells, the general-instability collapse pressures of which are compared with the results obtained by the modified Bresse equation. The results indicate that the modified equation predicts the general-instability collapse pressure of cellular sandwich shells within 5 per cent. This equation is recommended for use only when the ratio of shell ring depth to shell mean diameter is less than 0.1.

General Instability of Circumferentially Stiffened Sandwich Shells Subjected to Uniform External Pressure

Introduction

CELLULAR sandwich shells are preferred for many underwater applications because of their ability to withstand great hydrostatic pressures. The cellular sandwich shell, sometimes referred to as a circumferentially stiffened sandwich shell, consists of two concentric cylinders joined by a series of equally spaced circumferential annular stiffeners (Figs. 1 through 4). On the basis of theories postulated by some authorities (1,2),* it appears that cellular sandwich shells possess the highest pressure-to-weight ratio and thus represent the optimum design for pressure vessels subjected to external hydrostatic pressure. However, the advantages of this design are offset by the lack of design data for accurately predicting the hydrostatic-pressure capability of the shell. There is a need for a simple equation that will accurately predict the hydrostatic collapse pressure of the cellular sandwich shell.

PURPOSE OF THE INVESTIGATION

Cellular sandwich shells, like other types of shells, are subject to two broad categories of shell failure: elastic instability, and failure of the material. Of the two types of failure, elastic instability is less predictable and thus of greater interest. There are many types of elastic instability, but this investigation was concerned with general instability - a type of elastic failure in which all the shell components buckle simultaneously. It was the purpose of this investigation to theoretically and experimentally develop a simple equation for predicting the general-instability collapse pressure of a cellular sandwich shell subjected to hydrostatic pressure.

HYPOTHESIS AND METHOD OF INVESTIGATION

The theoretical basis of this investigation was Bresse's theory for the buckling of rings under radially applied external pressure(3). It is postulated that a modified Bresse equation accurately predicts the uniform external pressure at which general-instability failure of a cellular sandwich shell occurs. The advantages of cellular sandwich shell construction were determined by tests in which five types of acrylic resin shells were imploded (Figs. 3 and 5 through 8). To verify the validity of the modified Bresse equation, two identical aluminum cellular shells and one acrylic resin cellular shell were imploded in a carefully controlled pressurization system. Both types of shells were designed to collapse by general instability, and their collapse pressures were then compared with those predicted by the modified Bresse equation. The criterion by which the validity of the modified Bresse equation was judged is its ability to predict collapse pressure within 10 per cent of the experimental results.

This investigation was limited to the collapse of cellular sandwich shells by general instability, and only those shell parameters and experimental data that have direct bearing on this method of

*Numbers in parentheses refer to References on p. 13.

collapse were investigated. However, local buckling of sandwich-shell facings and circumferential stiffeners is discussed in a general way.

BRIEF SUMMARY OF RESULTS AND CONCLUSIONS

The two aluminum shells were tested together, and collapsed at 2300 psi; the acrylic resin shell collapsed at 1650 psi. When both collapse pressures were corrected for end conditions and compared with those obtained by the modified Bresse equation, the difference was less than 5 per cent. On the basis of this and other investigations, it is concluded that the modified Bresse equation accurately predicts the general-instability collapse pressure of cellular sandwich shells, provided the proper corrections for end conditions are made.

Theoretical Consideration and Discussion

STRUCTURAL ANALYSIS OF THE CELLULAR SANDWICH SHELL

The derivation of an equation describing the safe load of a novel structure can generally be approached from two diametrically opposite viewpoints. One viewpoint is based on the supposition that an equation describing the safe load for any new structure can be derived from the basic tenets of statics and from the theory of elasticity, providing that a thorough analysis of the distribution of loads and boundary conditions has been made previously. The other viewpoint is based on the supposition that any new structure can be considered as a combination of several structural elements for which load-carrying capabilities already have been obtained.

If an approach to the solution of a problem could be characterized by one word, the first viewpoint might be called scientific and the second, engineering. Both viewpoints have their value, depending on the aims of the investigation. The scientific formula derivation has its value when the aim of the investigation is the discovery of a basic set of equations. However, when the aim of the investigation is applicable to a specific engineering structure only, the engineering approach is much more desirable since the emphasis is on the utilitarian value of the formula and not on its value as a contribution to the theoretical body of knowledge.

As this investigation was initiated to acquire an engineering design formula for the prediction of a particular mode of failure of a special type of structure, it was decided at the very outset that only the engineering approach was desirable. This decision was further substantiated by other reasons, such as limited funds and a short period of time in which to conduct the investigation.

DEFINITION OF TERMS

The terms used in this report are defined below. Some of the structural members (such as I rings and I-ring flanges) do not exist as such, but are referred to for purposes of analysis. The cellular sandwich shell, for instance, can be thought of as concentric cylinders joined by annular stiffeners; or as a series of wide-flange I beams formed into rings, the flanges of which form the inner and outer cylinders (Fig. 2).

Annular Stiffeners - Rings joining the outside and inside shell facings to form an integral structure (Fig. 2).

Shell Facings - Thin shell-like cylinders joined by annular stiffeners (Fig. 2).

I Ring - A wide-flange I beam rolled into a circular shape (Fig. 2).

I-Ring Flange - That portion of the I beam forming the inside and outside facing of the shell (Fig. 2).

I-Ring Web - That portion of the I beam supporting the flanges.

Pressure-to-Weight Ratio - An arbitrary ratio for the comparison of various shells subjected to internal or external pressure. This comparison index takes into account both the strength-to-

weight ratio of the structural material and the buckling resistance of the shell design. The ratio is defined as:

$$\eta = P_{ce} \left(\frac{V_i}{W_i} \right),$$

where

P_{ce} = the experimentally determined hydrostatic collapse pressure of the shell,

V_i = displacement volume of the vessel per unit shell length (in.³ per in.),

and

W_i = weight of the shell per unit length (lb per in.).

Hydrostatic Pressure - External pressure of uniform magnitude applied both axially and radially to the enclosed pressure vessel.

Collapse Pressure - External hydrostatic pressure that causes the pressure vessel to lose its structural integrity.

Infinitely Long Pressure Vessel - Pressure vessel possessing bulkhead spacing such that any further increase in the spacing will not decrease the collapse pressure of the vessel.

Short Pressure Vessel - Pressure vessel whose collapse pressure depends to some extent on the reinforcing action of the bulkheads.

Failure by General Instability - Type of failure in which all the structural components of the shell fail simultaneously by buckling.

General Instability Equation - Bresse's theory for the buckling of rings adapted for the calculation of the external hydrostatic pressure at which an infinitely long cellular sandwich shell will collapse because of general instability.

APPLICATION OF BRESSE RING-BUCKLING EQUATION

The sandwich shell, when analyzed structurally, can be thought of as either an assembly of typical wide-flange I rings, or as outer and inner cylinders joined by circumferential annular stiffeners at regular intervals. Although equations describing the general-instability collapse of smooth shells and circumferential rings exist, the structural interaction between these shell components is such that the general-instability collapse pressure of the assembly is not necessarily equal to the sum of the individual collapse resistances of the components. Thus, for the engineering type of investigation, it is fruitless to pursue the structural analysis approach, which treats the shell as a combination of inner and outer smooth cylinders joined by annular stiffeners. The method that logically promises a solution to the problem is the one in which the shell is considered to be made up of infinitely repeatable wide-flange I rings (Fig. 2).

When the hypothesis is made that the shell is only a series of wide-flange I rings, then it follows that the over-all collapse resistance of the shell to external pressure is equal to the buckling resistance of the structural module, the wide-flange I ring. Therefore, the over-all collapse resistance of the shell can be determined if the buckling strength of a single wide-flange I ring is known. Fortunately, the problem of ring stability under uniform, radially applied, external loading was solved long ago by Bresse(3); the solution was then extended into the plastic strain regions by Engesser(4). The difference between the loading of Bresse's ring and that of the typical shell I ring being investigated is in the superimposition of axial load upon the ring along its outer and inner flanges.

The expression for the uniformly applied radial loading that produces radial buckling of the ring has been very lucidly presented by Timoshenko(5), and his notation is used in deriving the general-instability equation for the cellular sandwich shell. This equation actually represents a semiempirical adaptation of the Bresse ring-buckling theory(3) to the buckling of sandwich shells

by general instability. The adaptation is performed on the basis of structural similarity, and the validity of the adaptation is supported by experimental data.

BUCKLING OF A CELLULAR SANDWICH SHELL UNDER HYDROSTATIC PRESSURE

In the original Bresse ring-buckling equation,

$$q_{ct} = \frac{3EI}{R^3} \quad 1$$

where

q_{ct} = the radial external collapse pressure of the ring (lb per in. of circumference measured along the neutral axis of the ring),

E = modulus of elasticity in compression (psi),

I = moment of inertia of the ring (in.⁴),

and

R = radius of the neutral axis of the ring (in.).

The Bresse equation is correct for only a single ring under radially applied external pressure. This means that there is no loading perpendicular to the plane of the ring and no external restraint on the buckling ring. When shells of typical wide-flange I rings are considered, it becomes apparent that the flanges of an individual I ring are restrained from distortion by the adjacent I rings, and that they are subjected not only to radial loading but also to axial loading. The restraint on I-ring flanges and the superimposed axial loading must be accounted for in some manner; otherwise, erroneous answers will be obtained from Eq. 1.

The simplest approach to the problem of restraint on the flanges of an I ring by neighboring I rings is to assume that the cross sections of the I rings will not become distorted during compression because the adjoining flanges will prevent them from distorting. This assumption is basically the same as that made for the derivation of the buckling formula of an infinitely long smooth shell subjected to uniform external radial pressure(6). Since the cross section of the flanges will not be distorted during the compression of the rings under load, a new expression(5) must be substituted for the modulus of elasticity in Eq. 1. Thus, $E/(1-\mu^2)$ is substituted for E in Eq. 1, giving a new expression:

$$P_{ct} = \frac{3EI}{R^3} \times \frac{1}{1-\mu^2} \times \frac{R}{R_o} \quad 2$$

where

P_{ct} = the external hydrostatic collapse pressure of the shell assembly,

R_o = external shell radius,

and

μ = Poisson's ratio in the elastic range of the material under uniaxial compression.

The factor R/R_o is used to correct for the large difference between the outside shell radius and the radius of the neutral axis of the ring. For thin-walled smooth shells, such a correction is not necessary; but, for thick-walled shells, or for sandwich shells whose ratio of ring depth to ring

external surface radius is greater than 0.1 ($h/R_0 > 0.1$), such a correction is mandatory because it generally amounts to approximately 10 per cent of the uncorrected value of P_{ct} . Even with the correction, Eq. 2 is not exactly correct since the flanges of the I rings do not constitute the whole I ring but only a part of it. However, a detailed correction of Eq. 2 is not necessary: a comparison of the inertias of the web and the flanges shows that the contribution of the web to the moment of inertia of the I ring is very small.

In the derivation of Eq. 2, it was assumed that the ring material followed Hooke's law faithfully from zero stress to the moment of buckling. There are very few materials that behave in such a manner; therefore, the equation must be modified to account for materials that do not follow Hooke's law. Engesser(4) and Southwell(7) have developed expressions that allow for the deviation of materials from Hooke's law and yet predict the buckling of structural members.

The Engesser solution must be used to calculate the general-instability collapse pressure of a ring or cylinder fabricated from aluminum. For the buckling of structures fabricated from materials not having linear stress-strain properties, the Engesser solution substitutes the tangent modulus of elasticity for the modulus of elasticity in Eq. 2. Little experimental data have been found on the correctness of the Engesser solution as applied to the collapse of shells or rings, but some data have been accumulated on its application to the buckling of slender rods, as shown in Fig. 9. This figure shows that the experimental points follow the theoretical curve predicting the buckling of slender rods. Since the buckling of both rods and shells is based on similar structural parameters, it is felt that the Engesser solution will hold equally well for shells and composite shells.

Equation 2 can be further refined by substitution of μ_s for μ since μ_s is Poisson's ratio of the shell material at a given stress level. In the elastic strain region, Poisson's ratio changes very little with the increasing stress level; but, in the plastic strain region, Poisson's ratio increases considerably as compared to its value in the elastic strain region. When μ_s is used instead of μ in Eq. 2, the magnitude of the calculated collapse values for the plastic strain region may increase by as much as 18 per cent(8). The difficulty in applying this correction is the scarcity of published data on the change of μ_s with the change in the stress level; thus, μ is usually used instead of μ_s . By not using μ_s , some of the calculated collapse-pressure values are placed in error; but, since it makes the calculated values smaller, it is accepted as a safe and conservative practice.

Although specifically derived for radial loading of rings, Eq. 2 can also be used to predict the general instability of cellular sandwich shells under the joint action of axial and radial external pressures. The applicability of Eq. 2 to cellular sandwich shells subjected to radial pressure, or to combined axial and radial pressures, is based on the fact that buckling in a smooth cylinder requires a much greater axial pressure than a radial pressure or combined axial and radial pressures(9). Since the axial and radial external pressures are of equal magnitude in the hydrostatic loading of a shell, the cylinder will become unstable because of radial pressure long before buckling because of axial pressure will occur. Although this has been proved experimentally and theoretically for smooth cylinders only, it is assumed that it will also apply to sandwich shells because of the similarity of the relevant shell parameters.

The final version of the Bresse ring-buckling equation, modified to include the tangent modulus of elasticity in compression E_t , Poisson's ratio at a given strain level μ_s , and the correction factor R/R_0 , can be now written as

$$P_{ct} = \left(\frac{3I_{ns}}{R^3} \right) \left(\frac{1}{1-\mu_s} \right) \left(\frac{R}{R_0} \right) E_t, \quad 3$$

where

$$I_{ns} = \frac{\left[\frac{h^3 - (h-t_o-t_i)^3}{12} \right] L_r + \frac{(h-t_o-t_i)^3 t_w}{12}}{L_r},$$

h = over-all wall thickness, t_o = outside flange thickness, t_i = inside flange thickness, L_r = annular stiffener spacing, and t_w = annular stiffener width. Equation 3 will be used to calculate the general-instability collapse of sandwich shells.

When the shell material has a definite yieldpoint and becomes plastic without strain hardening, Engesser's solution does not apply; Southwell's modification(7), or some other modification, must be applied. Since this investigation does not concern itself with shells fabricated from such materials, these modifications to the Bresse equation will not be discussed.

Experimental and Testing Procedures

ACRYLIC RESIN SHELLS

Five inexpensive acrylic resin shells were constructed to determine the relative merits of the different types of shell construction. These shells, shown in Fig. 3 and Figs. 5 through 8, were of identical weight, length, outside diameter, and usable inside diameter. They were fabricated from commercially available tubes, and their rings were cut from commercial acrylic resin sheet stock. All the structural components were joined into a single homogeneous structure with acrylic resin solvent. To eliminate residual stresses introduced by machining and bonding of the material, the finished shell assemblies were annealed in temperature-controlled ovens. Figure 10 is an assembly drawing of the acrylic resin shells.

For implosion testing, the shell ends were sealed with identical friction-type closures and immersed in a 2000-psi-capacity pressure chamber (Fig. 11). The collapse pressures for all the shells were carefully recorded, and are presented in Table I. The results indicate that, among those tested, cellular sandwich construction is the best method of stiffening shells against external pressure.

TABLE I
COLLAPSE PRESSURES OF ACRYLIC RESIN SHELLS

Description*	Collapse Pressure** (psi)	Pressure-to-Weight Ratio $\eta = P_{cs} \left(\frac{V_i}{W_i} \right)$
Smooth shell	590	0.585×10^5
Smooth shell stiffened by equally spaced circum- ferential plain rings	1200	1.185×10^5
Smooth shell stiffened by equally spaced circum- ferential T rings	1450	1.44×10^5
Longitudinally stiffened sandwich shell	1100	1.09×10^5
Cellular sandwich shell	1650	1.63×10^5

*Material properties are shown in Fig. 31.

**Pressurization rate: 20 psi per sec.

ALUMINUM CELLULAR SANDWICH SHELLS

Equation 3 was used to design two larger aluminum cellular sandwich shells (models A and A') to test the general-instability collapse theory postulated. The shells were constructed of wrought aluminum, a typical construction material, which was selected solely on the basis of cost and ease of fabrication. Since engineering design formulas for this type of shell were not available at that time, both the shell facings and the rib spacing were selected on the basis of general engineering stability principles(10, 5). The thickness of the shell facings and the spacing of the ribs were critical and were selected so that local buckling(11) or yielding would not occur before the shell collapsed as a whole under the action of external pressure. Figure 12 is the assembly drawing for the aluminum cellular sandwich shells.

Since so many variables enter into the design of a sandwich shell, it is not prudent to accept the experimental collapse pressure of a single shell as the typical collapse pressure of that sandwich shell design. The best approach would be to test as many shells of the same design as possible and to evaluate the collapse pressures by statistical methods, but such an approach would be too expensive for this investigation. To overcome this limitation and to obtain at least a semblance of a typical collapse pressure, it was decided to make both aluminum shells of identical dimensions and to average their collapse pressures. The dimensional tolerances for the fabrication of both shells were very "tight," as indicated in Fig. 12. These tolerances ensured that the shells would be as nearly identical as possible and that they would collapse simultaneously during testing.

During the fabrication of the shells, all conceivable quality controls were instituted and adhered to in order to make certain that the final product tested was the same as that described in Fig. 12. The shell design demanded an unusually high degree of attention to manufacturing details on the part of the contractor - details that are generally ignored in everyday shop practice. The welding fabrication method, in particular, presented more than the usual problems.

Because of the extreme length of welds, and the required postweld heat treatment, the wrought aluminum shells required special care to avoid residual-stress distortions. Only by the use of elaborate welding jigs and uniform welding rates was it possible to keep the distortion of the shells within the design specifications. The most important single item in the structural strength of the wrought aluminum shells was the quality of the welds, which was so high that it surpassed the fabrication specifications by 21 per cent, as shown in Table II.

Another important item in the design and fabrication of these shells was the location of the welds. Actually, there are several ways in which shell components can be joined to form a welded shell structure; the selection of the weld type and its location depends primarily upon the stresses created by external pressure application. Since external pressure loading generates the greatest stresses in the circumferential direction, the welds had to be located along the circumference of the shell; but, even at this location, there were several alternatives for the selection of weld type and placement.

After a careful evaluation of all the possible weld types and locations, a weld was selected that would be almost as strong as the parent material, provided it was properly applied and located. This weld, which is shown in Fig. 12, was placed in the circumferential direction and joined the flanges of individual wide-flange I rings.

Each of the shells was provided with a wedge-band joint at each end for coupling with another shell of identical construction. The joints were equipped with standard neoprene O rings in a radial-type sealing arrangement that effectively sealed the shell assembly against high external testing pressures.

TEST APPARATUS AND SHELL END SUPPORTS

The basic apparatus required for implosion testing consisted of two shell end closures, an internal pressure vessel, a hydraulic pump, and several accurate pressure indicators. At the time this investigation was conducted, the Ordnance Research Laboratory did not have pressurizing equipment of sufficient capacity to test the two aluminum experimental shells. All experimental testing of the aluminum shells was performed at the Southwest Research Institute, San Antonio, Texas.

TABLE II
MATERIAL PROPERTIES OF COLLAPSED ALUMINUM SHELLS

Test Sample	No.	Cross Section (in. ²)	Elongation in 1 in. (per cent)	Load (lb)	Ultimate Strength (psi)
Parent material	1	0.0986	17.47	4765	48,327
	2	0.095	19.50	4650	48,947
Weld coupon	1	0.1005	4.42	4010	39,900
	2	0.1003	3.90	4005	39,930
	3	0.0995	5.18	4200	42,211
	4	0.102	4.06	4110	40,294
	5	0.0997	3.68	3910	39,218
	6	0.1003	4.60	4045	40,329
	7	0.101	4.08	3855	38,168
	8	0.1005	4.46	4260	42,388
	9	0.1005	4.89	4180	41,592
	10	0.1005	4.89	4165	41,443

Material and Construction

Parent material - 6061-T6 aluminum alloy

Welds -

Root pass: 5356 filler, heliarc-welded

Filler passes: 4043 filler, Sigma-welded

Weld type - 90-deg single-vee butt weld

Material Strengths

Specified weld strength - 33,500 psi (see Fig. 12)

Average weld strength - 40,547 psi; 83.5 per cent of average parent material strength

Specified parent material strength - 42,000 psi (see Fig. 12)

Average parent material strength - 48,637 psi

Test Description

Method of testing - tensile

Strain rates - 0.001 in. per sec

The method of mounting the shells inside the tank requires careful consideration. Depending on the type of shell support inside the tank, the experimental collapse of a given shell will vary anywhere from 5 to 500 per cent of an infinitely long shell collapse pressure. These percentages depend on the shell's ratio of ring depth to mean diameter (h/D) and its ratio of length to mean diameter (L/D).

There are four types of shell end supports: rigid, simple, friction, and elastic (Fig. 13). Each type of end support imposes a different shell end condition, which, in turn, usually changes the experimental collapse strength of the shell. There is, generally speaking, no one preferred type

of shell support; they all have their value, depending on what the testing arrangement is supposed to simulate. For this investigation, the friction type of end support was selected.

Shells are classified as infinitely long when their dimensions are such that a further increase in length will not change their collapse pressure. Shells of interest to the Laboratory - that is, shells whose L/D ratio is greater than 5 and whose h/D ratio is between 0.1 and 0.05 - are considered to be infinitely long shells.

Two approaches to shell testing are possible: the most straightforward, but more expensive, approach requires experimental shells whose bulkhead lengths are more than five times their diameters ($L > 5D$) and whose ends are rigidly or simply supported; and a less accurate, but also less expensive, approach that uses shorter shells equipped with friction end supports to simulate the collapse strength of longer shells ($L > 5D$).

The reasoning behind the second approach is based on the assumption that the collapse resistance (psi of external pressure) of a short shell is actually the collapse resistance of an infinitely long shell stiffened by the presence of friction end supports at each end of the shell. The stiffness of the end rings, and the friction between the end rings and the closure plates, are calculable; their effect on the shell collapse strength can be subtracted from the over-all short sandwich shell collapse pressure - the end result being the collapse pressure of a long sandwich shell. This type of end support was used for the testing of both the small-scale acrylic resin shells and the large aluminum shells. The stiffness of the end rings, and the friction between the end adapter rings and closure plates, were different for the two types of shells; but, in each case, the variable parameters were the same and could be calculated by the same equations.

TEST FACILITIES AT THE SOUTHWEST RESEARCH INSTITUTE

Pressurization System. The pressure tank in which the implosion testing of the shells was conducted (Fig. 14) is located at the Mechanics Laboratory of SRL. The dimensions of the tank are 30 in. in diameter by 150 in. long, and it is able to safely contain pressures up to 10,000 psi. The tank is actually composed of a section of straight thick tube threaded internally at both ends and capped with solid steel discs. The sealing between the discs and the tube is accomplished by standard O rings backed with steel expansion rings. The cap on the loading end of the tube has an 8-in.-diameter opening that permits observation of the inside of the shell during implosion testing. The whole tank assembly is positioned inside a concrete-lined silo in the floor of the building, with the loading end of the tank being almost flush with the floor.

Instrumentation. To record the strains and deflections of the shell inside the pressure chamber, several types of instruments are available at SRL. However, electrical resistance strain gages and strain-recording equipment were used exclusively for this investigation.

For the recording of strains indicated by the strain gages, an automatic scanner-recorder was used, permitting the balancing and recording of 48 gage circuits in 1 min. The rapidity with which all the strains could be read and recorded eliminated any discrepancies resulting from creep of shell material or from creep of the adhesive with which the gages were attached to the shell.

The electrical-resistance strain gages were mounted on critical areas of the shell assembly. The location and the identification of gages are shown in Figs. 15 and 16. Since all the strain gages were mounted on the inside of the shell, only a temperature-compensating gage was required, and the pressure-compensating gage was eliminated.

TESTING PROCEDURE FOR SHELL MODELS A AND A'

Both the instrumentation and testing procedures were planned to provide the greatest amount of information possible. In addition to obtaining the collapse pressures of Models A and A', it was desirable to obtain information about the influence of end conditions on collapse pressure.

The twin shells were assembled into one pressure vessel assembly capped at both ends with friction-type end closure plates (Fig. 14). The assembly was placed inside the pressure chamber, the chamber cover was screwed down tight, and the entrapped air in the chamber was bled off to

the atmosphere. After the chamber was checked for leakage, the oil inside the chamber was pressurized to 100 psi, and all the strain gages were balanced at that pressure. The pressurizing of the oil in the tank and the recording of strains were performed simultaneously by two operators, the pump operator following orders from the strain-recorder operator. Upon command, the pump operator increased the pressure to 200 psi for the duration of the automatic scanner-recorder's strain-recording cycle. When the recording cycle was completed, the pressure was raised to 300 psi and the recording cycle was repeated. This procedure was repeated until a pressure of 1100 psi was reached.

At 1100 psi the strain recorder was disconnected and the pressure was cycled from 0 to 1100 psi 25 times. The cycling of pressure at 1100 psi eliminated any residual stresses caused by the prior welding and heat treating of the shell assembly. After the cycling was completed, the strains were recorded again in an identical manner to check for any creep or redistribution of strains that might have occurred during the repeated pressure cycling. Upon completion of the pressure-cycling, stress-relieving program, the shells were coupled in reverse order and again positioned inside the pressure chamber to obtain some strain readings at the shell assembly ends resting against the end closure plates. The comparison of circumferential strain readings at the center and ends of the shell assembly showed the influence of the end adapter rings sliding upon the end closure plates.

For the actual implosion test, the pressure was raised in 200-psi increments, and the strains were recorded at each level. The pressure increases were continued until implosion of the shell assembly occurred at 2300 psi. Both shells collapsed simultaneously, so further testing was not necessary. Figure 17 shows a collapsed shell; Fig. 18 shows the deformation of the shells after implosion.

The collapsed shells were dissected (Figs. 19 and 20), and the thicknesses of the I-ring flanges and webs were compared to the specifications (Fig. 12) to determine any possible deviations. Since the welds comprise a large amount of filler material on the shell, coupons were cut from the imploded shells and tested to destruction to determine their strength.

Experimental Results

SHELL STRAINS UNDER EXTERNAL PRESSURE

The strains recorded by the strain gages (Figs. 21 through 27) give considerable information about the behavior of the shells under load. There was no difference between the readings of the mid-bay strain gages at the beginning and end of the cycling test, so only one set of curves was plotted (Figs. 21 through 24). These curves indicate that only a negligible amount of residual stress was present; otherwise, the difference between the strains recorded at the beginning and at the end of the test would have been noticeable, indicating that some realigning of stresses had taken place. This realigning was expected because of the repeated elastic loading and unloading of the shell structure, but the results do not bear this out. There is a considerable difference between the strains at the shell mid-bays and at the shell ends, proving that individual shell ends are stiffer than the I rings.

Both shells imploded simultaneously, but the rate of deformation and the extent of damage were not the same. The strain gages at mid-bay locations did not indicate any noticeable difference in circumferential strains, but the gages located at the ends of the shells showed a difference. When the circumferential strains at the ends of the two shells were compared, it became apparent that the ends deformed at different rates and thus supplied different amounts of restraint to the shells, causing one to fail sooner than the other. The difference in the final amount of deformation can be deduced from the measurements of the outside shell diameters at different points along the length of the shell (Fig. 18). From the difference in the plastic deformation of the two shells, it is estimated that the collapse strengths of the two shells differed by 50 to 100 psi, which is less than 5 per cent of the actual experimental collapse pressure of 2300 psi.

DISSECTION OF IMPOLODED SHELLS

An examination of the collapsed shell (Fig. 17) and of the dissected collapsed shell (Fig. 19) did not indicate that any local buckling occurred before total collapse by general instability. Detailed observation of the I-ring flanges and webs indicated that these members were in excellent condition. These results are of great importance, for they eliminate the need to consider the influence of local instability on the buckling by general instability. The fact that local buckling did not occur is the single most important result of this investigation. If local buckling were present, the comparison between theoretically predicted and experimentally determined collapse pressures would be difficult. As mentioned previously, the theory developed in this report presupposes only the existence of general instability unimpaired by the influence of failures caused by local buckling of material.

To determine whether the shells actually represent the shell specified in Fig. 12, accurate measurements of the I-ring flanges, webs, and web spacings were made at various locations. The measurements failed to disclose any deviation from the specifications. Coupons were cut at various locations and subjected to tensile tests in a hydraulic press (refer to Table II). Both the material and the welds were found to surpass the specification tolerances by approximately 20 per cent.

Comparison of Experimental and Theoretical Results

Figure 28 compares the collapse pressure calculated by means of Eq. 3 with the collapse pressure obtained experimentally. The corrected theoretical collapse pressure for the two shells almost coincides with the experimental collapse pressure. Figure 28 actually shows the relationship between the over-all depth of a sandwich wall and the collapse pressure, providing the cross-sectional area of the sandwich wall remains constant as the depth of the wall varies. Such a graph is especially useful in the design of sandwich shells, and was used in designing Models A and A'. Once Eq. 3 has been plotted, it is easy to select the optimum wall depth for a shell of given outside diameter, material, and weight. The optimum wall depth (denoted in calculations by h , Fig. 2) is represented by the sandwich wall that provides the most rigidity for the shell and occupies the least internal shell volume. The optimum wall depth for the aluminum shells is shown in Fig. 28 and that for the acrylic resin shell, in Fig. 29.

For the aluminum shells, a point on the graph (Fig. 28) has been selected where the rate of gain in resistance to collapse is the least and the rate of increase in the wall depth, h , is the greatest. This point is located immediately after the change-over from the linear slope to the almost horizontal slope in Fig. 28. This point also represents the shell wall depth that gives the maximum internal shell diameter. Selection of any other point on the graph will result in a shell that has considerably lower collapse pressure and slightly larger internal diameter, or in a shell that has slightly higher collapse pressure but considerably smaller inside diameter.

For the plotting of Eq. 3, it was necessary to obtain data on the behavior of both 6061-T6 aluminum alloy and acrylic resin. These data consisted of three curves: a stress-strain curve, a tangent-modulus-of-elasticity-vs-stress curve, and a Poisson's-ratio-vs-stress curve. The first two curves for 6061-T6 aluminum alloy were obtained from Alcoa Research Laboratories, and the most important one is reproduced in Fig. 30. Since a literature search failed to unearth any data on the third curve and since funds were not available to determine it experimentally, the curve of Fig. 30 was plotted by means of Poisson's ratio for zero stress level, obtained from Alcoa. It was assumed that the error introduced by this simplification is of only minor magnitude. The assumption that the error introduced by the use of μ instead of μ_t is small is based on the known change of Poisson's ratio for 2014-T6 aluminum alloy. Poisson's ratio at a given strain level of this alloy increases to 0.4 in the intermediate plastic strain region. If this ratio also becomes 0.4 for 6061-T6 aluminum alloy in the intermediate plastic strain region, failure to take this into account would introduce only a 6 per cent error in the calculated collapse pressure of the shell. The data for the determination of the tangent modulus of elasticity for acrylic resin were obtained experimentally, and are presented in Fig. 31.

When comparison is made between the theoretical and experimental collapse pressures, a distinction must be made between experimental values and corrected experimental values. The

recorded experimental collapse pressures must be corrected to take into account the reinforcement of the shell by individual shell joints, end adapter rings, and friction end closure plates. If corrections were not made for this strengthening effect, the experimentally obtained collapse values would not represent the collapse pressure of a long shell, but would represent the collapse pressure of a short section stiffened at the ends, for which Eq. 3 is not applicable. When all the end conditions were taken into account, the collapse strength of the aluminum shell assembly tested was calculated to be 380 psi greater than that of an infinitely long shell of the same design. The difference between the corrected, experimentally obtained, collapse pressure and the collapse pressure predicted on the basis of Eq. 3 is 80 psi, which is less than 5 per cent, and thus satisfactory for engineering design purposes.

The corrected collapse pressure of Fig. 28 shows very close agreement with the collapse value theoretically calculated on the basis of the modified Bresse equation (Eq. 3). However, because some of the assumptions on which the corrections are based may contain inaccuracies, the coincidence of the two values alone is not construed as absolute proof that Eq. 3 predicts the general-instability collapse pressure of a cellular sandwich shell.

Further evidence that Eq. 3 predicts the general-instability collapse of sandwich shells was obtained from calculation of the collapse pressure of the acrylic resin sandwich shell (Fig. 29) and from calculation of the collapse pressure of steel cellular shells tested by the David Taylor Model Basin(12). The experiments performed at DTMB utilized steel shells of similar sandwich construction but of different h/D ratios; and their collapse pressures, when recalculated by means of Eq. 3, also agree with the experimental collapse pressures.

When all this experimental evidence is taken into consideration, it can be stated that sufficient support exists to substantiate the hypothesis that Eq. 3 accurately predicts the general-instability collapse of cellular sandwich shells.

Summary and Conclusions

Both aluminum cellular sandwich shells collapsed at 2300 psi because of general instability. When this pressure was corrected for the reinforcing effect of joint rings and friction-type end supports, a corrected collapse pressure of 1920 psi was obtained. The corrected experimental collapse pressure of 1920 psi, when compared with the collapse pressure of 2000 psi calculated by the modified Bresse equation, shows little difference. Similar results were obtained when the corrected experimental collapse pressure of the acrylic resin cellular sandwich shell was compared with the collapse pressure calculated by the modified Bresse equation. In both cases, the accuracy of the modified Bresse equation is less than 5 per cent.

It is concluded that the modified Bresse equation accurately predicts the general-instability collapse pressure of infinitely long cellular sandwich shells. This conclusion is based on the comparison of theoretically and experimentally determined collapse pressures. Although the modified Bresse equation is intended for infinitely long cellular sandwich shells, it can also be used for short shells provided the proper corrections for end conditions are made.

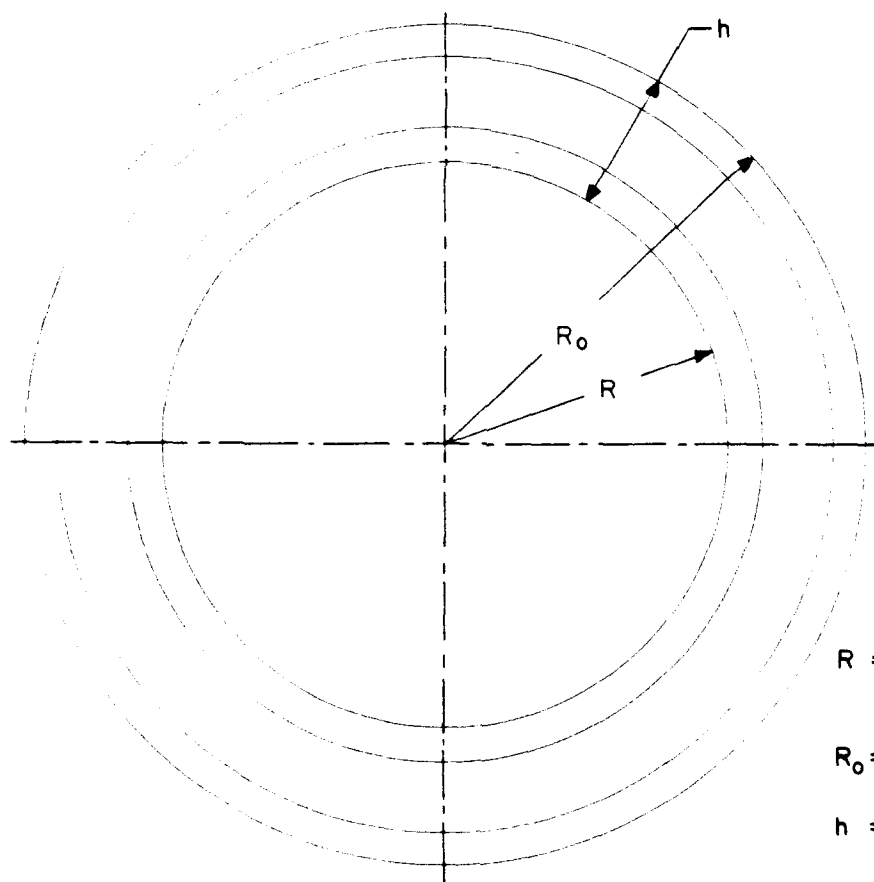
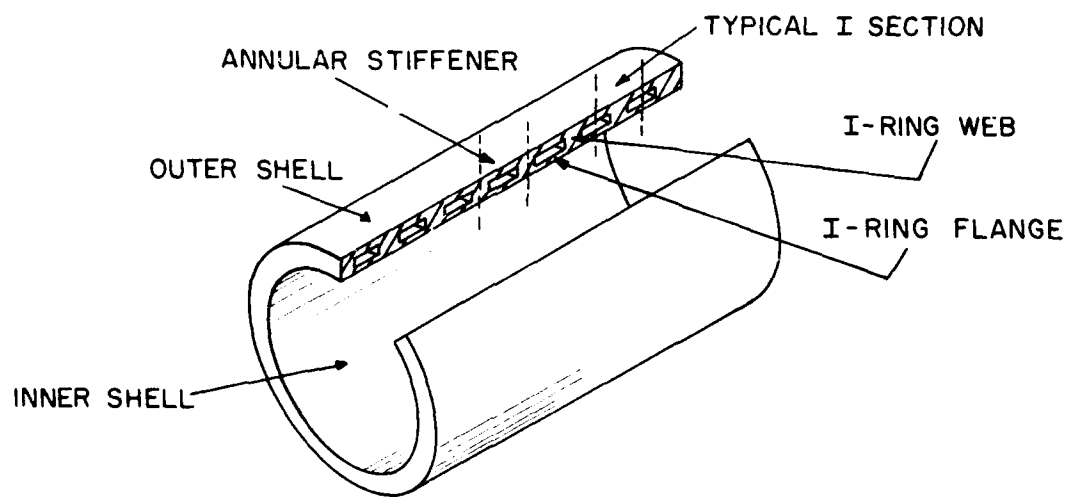
The modified Bresse equation is limited to the collapse of cellular sandwich shells by general instability. However, there are many other types of shell failure that should be investigated: local buckling of ring flanges, local buckling of ring webs, or local yielding of the shell material. The greatest impediment to these investigations is the lack of well documented implosion-test data for cellular sandwich shells of different lengths and diameters. Both experimental and theoretical approaches are necessary to obtain workable design equations for cellular sandwich shells.

References

1. E. I. Grigolyuk, "Buckling of Sandwich Construction Beyond the Elastic Limit," *Journal of Mechanics and Physics of Solids*, Vol. 6, July 1958, pp. 253-266.
2. R. E. Fulton, "Buckling Analysis and Optimum Proportions of Sandwich Cylindrical Shells under Hydrostatic Pressure," *University of Illinois, Structural Research Series No. 199*, June 1960.
3. M. Bresse, *Cours de Mécanique Appliquée*, 3rd Ed., Paris, 1880.
4. F. Engesser, "Knickfestigkeit gerader Stäbe," *Zeitschrift für Architektur und Ingenieurwesen*, 1889, p. 455.
5. S. Timoshenko, *Strength of Materials - Part II*, D. Van Nostrand Company, Inc., New York, 1956, pp. 178-190.
6. G. H. Bryan, "Application of the Energy Test to the Collapse of Long Thin Pipe under External Pressure," *Proceedings of the Cambridge Philosophical Society*, London, Vol. VI, 1888, pp. 287-292.
7. R. V. Southwell, "On the Collapse of Tubes by External Pressure," *London, Edinburgh, and Dublin Philosophical Magazine and Journal of Science*, Vol. 25, May 1913, pp. 687-698; Vol. 26, September 1913, pp. 502-511; Vol. 29, January 1915, pp. 67-77.
8. E. Gratzel and H. Schlechtweg, "Stress Distribution in a Cylindrical Brittle Tube under Uniform Internal and External Pressure," *Zeitschrift für Angewandte Mathematik und Mechanik*, Vol. 34, No. 3, March 1954, pp. 81-104.
9. S. B. Batdorf, *A Simplified Method of Elastic Stability Analysis for Thin Cylindrical Shells*, National Advisory Committee for Aeronautics, NACA Report 874, 1947.
10. S. Timoshenko, *Strength of Materials - Part I*, D. Van Nostrand Company, Inc., New York, 1956.
11. R. von Mises, "Der Kritische Aussendruck Zylindrischer Rohre," *Verein Deutscher Ingenieure*, Vol. 59, No. 19, 1914, pp. 750-755.
12. E. E. Johnson, *Structural Research on Hulls for Extreme Depth*, David Taylor Model Basin, Report C-1214, September 1960.



Fig. 1 - Aluminum Cellular Sandwich Shell



R = RADIUS OF THE
NEUTRAL AXIS OF
THE RING
 R_0 = RADIUS OF THE
EXTERNAL SHELL
 h = WALL DEPTH

Fig. 2 - Structure of Cellular Sandwich Shell

Table of Contents

The Effects of Shell Joints and Bonding on the Stability of Acrylic Resin Cellular Shells	1
Introduction	1
Effects of Joints and Bonding on Shell Stability	1
Calculation of Stresses in Cellular Shells	3
Comparison of Calculated and Experimental Results	3
Photoelastic Analysis of Stress Concentrations in Cellular Shells	4
Conclusions	5
References	6

Abstract

SIX ACRYLIC resin cellular shells were tested under external hydrostatic pressure to determine the effects of joints between individual shell structure components and the effects of bonding on cellular shell stability. When the shell stiffeners were restrained from moving laterally, the location of joints and the degree of bonding did not affect the general elastic stability enough to cause failure by elastic buckling. All shells failed by material yielding except the one in which the stiffeners were not restrained from moving laterally. However, the distribution of stresses and strains on the other shell surfaces was considerably influenced by the location of joints and the degree of bonding. The shell stresses were calculated by Pulos' and Mehta's formulas and compared with the experimentally determined stresses. The calculated and experimental values agreed within ± 15 per cent except for the principal axial stresses on the shell facings at the stiffeners. Four epoxy resin models of the cellular shells were pressure-tested and analyzed photoelastically to determine the effects of stress concentrations at the junctures of the stiffeners and the inner and outer shell facings.

Distribution List

Chief, Bureau of Naval Weapons (RU-2) Department of the Navy Washington 25, D. C.	1 copy	Commander U. S. Naval Ordnance Laboratory White Oak Silver Spring 19, Maryland	2 copies
Chief, Bureau of Naval Weapons (RUTO-33) Department of the Navy Washington 25, D. C.	2 copies	Commander U. S. Naval Ordnance Laboratory White Oak Silver Spring 19, Maryland Attn: Dr. S. J. Raff	1 copy
Chief, Bureau of Naval Weapons (RUDC) Department of the Navy Washington 25, D. C.	1 copy	Commander U. S. Naval Ordnance Test Station 3202 East Foothill Boulevard Pasadena Annex Pasadena 8, California	2 copies
Chief, Bureau of Naval Weapons (DLI-3) Department of the Navy Washington 25, D. C.	2 copies	Commanding Officer U. S. Naval Torpedo Station Keyport, Washington	1 copy
Chief, Naval Operations (OP 721) Department of the Navy Washington 25, D. C. For: IEP ABC 28	5 copies	Commanding Officer U. S. Naval Torpedo Station Quality Evaluation Technical Library Keyport, Washington	1 copy
Chief, Naval Operations (OP 31) Department of the Navy Washington 25, D. C.	1 copy	Commanding Officer U. S. Naval Underwater Ordnance Station Newport, Rhode Island	2 copies
Chief, Naval Operations (OP 312) Department of the Navy Washington 25, D. C.	1 copy	Director (Code 2021) U. S. Naval Research Laboratory Washington 25, D. C.	3 copies
Chief, Naval Operations (OP 71) Department of the Navy Washington 25, D. C.	1 copy	Director (Code 2027) U. S. Naval Research Laboratory Washington 25, D. C.	1 copy
Chief, Naval Operations (O3EG) Department of the Navy Washington 25, D. C.	1 copy	Commanding Officer and Director U. S. Navy Electronics Laboratory San Diego 52, California	1 copy
Chief, Naval Operations (OPO7TC) Technical Analysis and Advisory Group Rm5E613, Pentagon Washington 25, D. C.	1 copy	Commanding Officer and Director David Taylor Model Basin Washington 7, D. C.	1 copy
Chief, Bureau of Ships Department of the Navy Washington 25, D. C.	3 copies	Commanding Officer U. S. Navy Mine Defense Laboratory Panama City, Florida	1 copy
Commander Armed Services Technical Information Agency Attention TIPDR Arlington Hall Station Arlington 12, Virginia	10 copies	Commanding Officer and Director U. S. Navy Underwater Sound Laboratory Fort Trumbull New London, Connecticut	1 copy
Officer in Charge U. S. Naval Underwater Weapons Systems Engineering Center Newport, Rhode Island	1 copy	Commander U. S. Naval Missile Center Point Mugu Port Hueneme, California	1 copy

Commander U. S. Naval Air Development Center Johnsville, Pennsylvania	1 copy	Commander, Test and Evaluation Force U. S. Atlantic Fleet U. S. Naval Base Norfolk 11, Virginia	1 copy
Officer in Charge Naval Aircraft Torpedo Unit Naval Air Station Quonset Point, Rhode Island	1 copy	Clevite Ordnance 540 East 105th Street Cleveland, Ohio	1 copy
Scientific and Technical Information Facility P. O. Box 5700 Bethesda, Maryland Attn: NASA Representative (S-AK/DL)	1 copy	Vitro Corporation of America 14,000 Georgia Avenue Silver Spring, Maryland	1 copy
Director, Applied Physics Laboratory University of Washington Seattle, Washington	2 copies	Westinghouse Electric Corporation Lansdowne Plant Baltimore, Maryland	1 copy
Director, Marine Physical Laboratory Scripps Institution of Oceanography San Diego 52, California	1 copy	Woods Hole Oceanographic Institution Woods Hole, Massachusetts	1 copy
Hudson Laboratories Dobbs Ferry, New York	1 copy	Aerojet General Corporation Azusa, California Attn: G. M. McRoberts	1 copy

The Effects of Shell Joints and Bonding on the Stability of Acrylic Resin Cellular Shells

By J. D. Stachiw

The Pennsylvania State University
Institute for Science & Engineering
ORDNANCE RESEARCH LABORATORY
University Park, Pennsylvania

September 25, 1963

APPROVED FOR DISTRIBUTION

ASSISTANT DIRECTOR

APPROVED FOR DISTRIBUTION

DIRECTOR



THE PENNSYLVANIA STATE UNIVERSITY
INSTITUTE FOR SCIENCE & ENGINEERING
UNIVERSITY PARK, PENNSYLVANIA

The Effects of Shell Joints and Bonding on the Stability of Acrylic Resin Cellular Shells

September 25, 1963

SERIAL NO. NOrd 16597-97

Copy No. 63

UNCLASSIFIED

Ordnance Research Laboratory Report No. NORD 16597-91
The Pennsylvania State University, University Park, Pa.

GENERAL INSTABILITY OF CIRCUMFERENTIALLY STIFFENED SANDWICH SHELLS
SUBJECTED TO UNIFORM EXTERNAL PRESSURE

J. D. Stachiw

December 10, 1962; 13 pp. & figs.

The Bresse equation for the buckling of rings under radial pressure is modified to predict the general-instability collapse pressure of cellular sandwich shells under hydrostatic pressure. The validity of the equation is demonstrated by implosion experiments with carefully designed cellular sandwich shells, the general-instability collapse pressures of which are compared with the results obtained by the modified Bresse equation. The results indicate that the modified equation predicts the general-instability collapse pressure of cellular sandwich shells within 5 per cent. This equation is recommended for use only when the ratio of shell ring depth to shell mean diameter is less than 0.1.

UNCLASSIFIED

Ordnance Research Laboratory Report No. NORD 16597-91
The Pennsylvania State University, University Park, Pa.

GENERAL INSTABILITY OF CIRCUMFERENTIALLY STIFFENED SANDWICH SHELLS
SUBJECTED TO UNIFORM EXTERNAL PRESSURE

J. D. Stachiw

December 10, 1962; 13 pp. & figs.

The Bresse equation for the buckling of rings under radial pressure is modified to predict the general-instability collapse pressure of cellular sandwich shells under hydrostatic pressure. The validity of the equation is demonstrated by implosion experiments with carefully designed cellular sandwich shells, the general-instability collapse pressures of which are compared with the results obtained by the modified Bresse equation. The results indicate that the modified equation predicts the general-instability collapse pressure of cellular sandwich shells within 5 per cent. This equation is recommended for use only when the ratio of shell ring depth to shell mean diameter is less than 0.1.

UNCLASSIFIED

UNCLASSIFIED

Ordnance Research Laboratory Report No. NORD 16597-91
The Pennsylvania State University, University Park, Pa.
GENERAL INSTABILITY OF CIRCUMFERENTIALLY STIFFENED SANDWICH SHELLS
SUBJECTED TO UNIFORM EXTERNAL PRESSURE

J. D. Stachiw

December 10, 1962; 13 pp. & figs.

The Bresse equation for the buckling of rings under radial pressure is modified to predict the general-instability collapse pressure of cellular sandwich shells under hydrostatic pressure. The validity of the equation is demonstrated by implosion experiments with carefully designed cellular sandwich shells, the general-instability collapse pressures of which are compared with the results obtained by the modified Bresse equation. The results indicate that the modified equation predicts the general-instability collapse pressure of cellular sandwich shells within 5 per cent. This equation is recommended for use only when the ratio of shell ring depth to shell mean diameter is less than 0.1.

UNCLASSIFIED

UNCLASSIFIED

Ordnance Research Laboratory Report No. NORD 16597-91
The Pennsylvania State University, University Park, Pa.
GENERAL INSTABILITY OF CIRCUMFERENTIALLY STIFFENED SANDWICH SHELLS
SUBJECTED TO UNIFORM EXTERNAL PRESSURE

J. D. Stachiw

December 10, 1962; 13 pp. & figs.

The Bresse equation for the buckling of rings under radial pressure is modified to predict the general-instability collapse pressure of cellular sandwich shells under hydrostatic pressure. The validity of the equation is demonstrated by implosion experiments with carefully designed cellular sandwich shells, the general-instability collapse pressures of which are compared with the results obtained by the modified Bresse equation. The results indicate that the modified equation predicts the general-instability collapse pressure of cellular sandwich shells within 5 per cent. This equation is recommended for use only when the ratio of shell ring depth to shell mean diameter is less than 0.1.

UNCLASSIFIED

siderably influenced by these structural factors. The difference between strains and stresses (Figs. 14 through 19) in the various models indicates the presence of different edge conditions. Since the stress-strain relationship of acrylic resin (Fig. 20) ceases to be linear at stresses above 10,000 psi, which corresponds to approximately 1000 psi of external hydrostatic pressure, the curves have not been plotted beyond these values.

The least variation in principal circumferential stresses occurred on the external shell facing above the stiffeners. The greatest variation in principal circumferential stresses took place on the internal facing of the shell at midway between stiffeners. The principal stresses in the axial direction differed at all locations among the shell models.

Calculation of Stresses in Cellular Shells

The distribution of stresses in cellular shells can be calculated by either Pulos' or Mehta's method of stress analysis(2, 3). Pulos' analysis is based on the application of edge coefficients of the cellular wall module; the shell is divided into annular stiffeners and short inner and outer cylindrical facing elements between the stiffeners. Mehta's solution is simpler and does not apply edge coefficients; the cellular shell is broken down into continuous inner and outer cylindrical shell facings and individual annular stiffeners. In both methods of analysis, the equilibrium and compatibility conditions are used to determine the forces and moments at the junctures of the shell elements. The shell stresses calculated by both methods agree within ± 15 per cent (Figs. 21 and 22).

Comparison of Calculated and Experimental Results

The calculated and experimentally determined stresses for the acrylic resin shells agree within ± 15 per cent except for the principal axial stresses on the outer surface of the outer facing, and on the inner surface of the inner facing, at the stiffeners. The discrepancies at these locations are large - from 200 to 300 per cent - but this can be explained by the use of 1/4-in. SR-4 strain-gage rosettes for the measurement of strains. Since the maximum calculated stresses at these points apply only to stress peaks on the shell facings along the centerline of the stiffeners, they cannot be accurately measured by 1/4-in. SR-4 strain gages. If 1/64-in. SR-4 gages were used, probably there would be better agreement between calculated and experimentally determined results at these points.

Evidence that the SR-4 gages were responsible for the large discrepancies can be found in test data obtained from larger diameter shells in which 1/4-in. SR-4 gages were used. In tests(4) of a large diameter aluminum shell (Model F), 1/4-in. SR-4 rosettes were used to measure the stress peaks on the shell facings at the stiffeners. The stiffeners were thicker than those of the acrylic resin shells, and thus the 1/4-in. SR-4 rosettes were able to measure the peak stresses on the shell facings at the stiffeners more accurately. When the calculated and experimentally determined stresses were plotted on the same pressure-stress coordinates, the agreement was better (Fig. 23).

The agreement between calculated and experimental stresses may also depend on the h/R_c ratio of the shell. The h/R_c ratio of the aluminum cellular shell is 1/10, whereas that of the acrylic resin shells is 1/4. This means that the Model F shell is a thin-wall shell and that the acrylic resin shells are thick-wall shells with different stress distributions.

Another factor in the agreement between calculated and experimentally determined stresses is the machining tolerances specified in the design of a shell. In the machining of the aluminum and acrylic resin shells, these tolerances amounted to as much as ± 15 per cent of the outside or inside facing thicknesses. Since all the stresses were calculated for nominal facing and stiffener thicknesses, the machining tolerances alone could cause a difference of ± 15 per cent between calculated and experimentally determined stresses.

When all the sources of error are taken into account, it can be concluded that the difference between the calculated and experimentally determined stresses for the acrylic resin shells is not significant. It can be further concluded that both Pulos' and Mehta's stress analyses can be used in the design of cellular shells, provided a minimum safety margin of 1.5 is used. This safety margin is based on the assumption that the material properties may vary from the average value by 15 per cent, that the machined surfaces may vary from the nominal size by 20 per cent, and that the calculated stresses may vary from the actual stresses by 15 per cent. In the absence of further experimental evidence, neither Pulos' nor Mehta's analysis can be considered superior.

Photoelastic Analysis of Stress Concentrations in Cellular Shells

Photoelastic analysis(5) of stress concentrations is superior to the electric strain gage method of analysis. The latter method, which was used to record the stresses in the acrylic resin shells, has the disadvantage that the section in which a stress concentration occurs must be known beforehand so that the strain gage can be positioned properly. Since the strain gages are large, they measure only the average strains of the area covered, not the peak strains. The photoelastic method, however, permits analysis of both average and peak strains in a given shell section. The stresses, when permanently frozen into the material during the load application, become visible when the section is exposed to polarized light (Figs. 24 and 25).

Although acrylic resin is a photoelastically active material, it does not lend itself to freezing of stresses. Epoxy resin is a more photoelastically sensitive material, and permits the freezing in of stresses; therefore, it was selected as the construction material for four cellular shell models. These shells (Fig. 26), which are approximately 1/5-scale models of the ORL cellular shells, were subjected to an intricate wax investment casting process and machined to size.

The shells were pressurized at temperatures sufficient to soften the shell material. While still under hydrostatic pressure, the shells were gradually cooled so that the stresses could be frozen in. Sections of the shell material were then removed from the shell, polished, exposed to polarized light, and photographed. All these operations, including casting and machining of the shells, were performed by the Department of Engineering Mechanics at The Pennsylvania State University (6).

Figures 24, 25, and 27 show the stress concentrations introduced into the shell structure by the presence of small radii fillets and rigid end closures. It should be noted that these photographs show only the maximum shear stresses in the axial plane of the shell; the influence of circumferential stresses on the magnitude and location of the fringes has been eliminated from the photograph. Photoelastic analysis of the shear stresses in the circumferential plane of the shell would require shell slices in the circumferential plane of the shell. Since the stress concentration at the junctures of the annular stiffeners and the shell facings and of the rigid end closures in the shell facings are primarily due to the flexure of the facings between the stiffeners, slices in the axial plane only were taken. The rigid end closures generate stress concentrations (Figs. 27 and 28) that are much more severe than those at the junctures of the shell facings and annular stiffeners. Therefore, all the other shells tested at ORL employed nonrigid end closures on which the shell ends could slide during the test.

In addition to the stress concentrations at the junctures of the stiffeners and facings, it is important to know the relationship between the radius of the fillet and the magnitude of the stress concentration in both the elastic and plastic strain regions of the construction material. Several T-sections of various fillet radii were machined from epoxy resin to determine this relationship. These sections were subjected to bending and compressive loading and then analyzed photoelastically (Figs. 29 and 30); Figs. 31 through 35 are plots of the experimental data.

Figures 31 through 35 show that the fillet radius at the juncture of the stiffener and the facing (Fig. 32) influences the radial compressive stresses in the annular stiffeners and the flexure stresses at the stiffeners more than it affects the axial stresses. The axial compressive stresses in the facings are influenced to a much less degree by the radius of the fillet (Figs. 31 through 33). However, it can be concluded that if $r/t_f > 1/8$ the stress concentrations caused by the bending of facings, axial compression of facings, and radial compression of the stiffeners will be less than

1.25. Stress concentration factors of such magnitude can certainly be tolerated. If r/t_r decreases to 1/16, however, the situation changes drastically; the stress concentration factor then approaches 2, and cannot be tolerated in brittle shell materials.

The magnitude of stresses at the stress concentration point changes when the stresses load the construction material so that it behaves plastically instead of elastically. Generally, the high stresses at the stress concentration points will cause the material to yield locally, redistributing the stresses in the material. This causes the stresses to increase in the elastic sections and to decrease in the plastic sections. The more ductile the material, the more pronounced this effect will be. Therefore, in ductile materials, the stress concentrations caused by sharp-radii fillets are not as serious as they are in more brittle materials.

Although the behavior of materials in the plastic strain range can be investigated photoelastically, it is difficult to apply the results to nonphotoelastic materials, such as those generally used for underwater-vehicle shells. The results cannot be transferred directly because the stress-strain curves of the two materials differ nonlinearly in the plastic strain regions. On the other hand, the photoelastically determined stresses in the elastic strain region can be used to predict the magnitude of stresses in nonphotoelastic materials, provided the shells are in some scaled relationship. Thus, when the material in which the strains occur shifts from elastic to plastic behavior (Fig. 35), photoelastic analysis is of only qualitative value for the calculation of stresses in an aluminum cellular shell.

Conclusions

The following conclusions were reached on the basis of pressure tests, stress analyses, and photoelastic analysis:

1. The stability of the cellular shells tested is not affected by unbonded joints at the juncture of the annular stiffeners and the inner and outer shell facings provided the stiffeners are restrained from moving laterally.

2. The correlation between calculated and experimentally determined stresses is fairly good, being better for the larger diameter aluminum shell than for the plastic shells.

3. The greatest disagreement between calculated and experimentally determined stresses occurred along the axis of the shell on the outer surface of the outside facing, and on the inner surface of the inside facing, at the stiffeners. This disagreement was caused by failure of the large SR-4 gages to measure the peak stresses accurately and by the presence of shell joints not accounted for in the stress analysis theory. The correlation is better for the larger diameter aluminum shell than for the acrylic resin shells.

4. The least disagreement between calculated and experimentally determined stresses occurred along the circumference of the shell on the outer surface of the outer facing, and on the inner surface of the inner facing, at the stiffeners. Pulos' and Mehta's analyses predict similar stresses at these points.

5. When the fillet radius at the juncture of the stiffeners and facings is small, serious stress concentrations are present at these points along the axis of the cellular shell. A fillet radius of $r/t_r > 1/8$ is required to keep the stress concentration factors below 1.5.

6. The stress concentrations at very rigid shell closures are considerably greater than those at other points along the shell length. The use of rigid shell closures and shell joints in cellular shells should be avoided.

References

1. J. D. Stachiw, Experimental Evaluation of Shell Designs Using Miniature Acrylic Resin Shell as Test Specimens, Ordnance Research Laboratory Technical Memorandum, TM 26.3420-41, July 7, 1960.
2. J. G. Pulos, Axisymmetric Elastic Deformations and Stresses in a Web-Stiffened Sandwich Cylinder under External Hydrostatic Pressure, David Taylor Model Basin, Report 1541, November 1961.
3. P. K. Mehta, Axisymmetric Elastic Stresses in Ring-Stiffened Sandwich Shells Subjected to Uniform External Pressure, Master's Thesis, The Pennsylvania State University, June 1961.
4. J. D. Stachiw, Implosion Testing of ORL Cellular Shell Model F, Ordnance Research Laboratory Technical Memorandum, TM 26.3420-143, June 12, 1962.
5. G. U. Oppel, The Frozen Stress Method for Three-Dimensional Photoelastic Stress Analysis, NACA TM 824, 1937.
6. G. U. Oppel and H. A. Peterson, "Experimental Techniques Employed for Photoelastic Analysis of Cellular Shells," Experimental Mechanics, August 1963, pp. 184-191.

The Effects of Shell Joints and Bonding on the Stability of Acrylic Resin Cellular Shells

Introduction

UNDERWATER vehicles require shells that are elastically stable and capable of withstanding large axial and circumferential compressive stresses. Elastic stability can be provided by an optimally stable shell design, but compressive strength requires materials of high compressive yield strengths. Since most underwater vehicles must carry large payloads, the requirements of low shell weight and large internal useful volume must be added to these structural requirements.

Although structural materials with high compressive yield strengths are available, they cannot be used efficiently in ring-stiffened cylindrical shells. This construction requires more material than is necessary to reduce the compressive stresses just below the yield strength of these materials. Obviously, a shell design that utilizes the compressive strength of premium material more fully than the ring-stiffened design is desirable.

The cellular shell, or circumferentially stiffened sandwich shell (Fig. 1), permits stressing of the construction material to its yield point without premature failure because of general instability. In tests performed at the Ordnance Research Laboratory, cellular shell construction was proved to provide more elastic stability and compressive strength than ring-stiffened shells or axially stiffened sandwich shells of the same weight, outside diameter, inside diameter, and construction material(1)*. This report describes the continuation of these tests, and is concerned with the effects of joints between individual shell structure components and with the effects of bonding on cellular shell stability, particularly the theoretical and experimental determination of stress concentrations.

Effects of Joints and Bonding on Shell Stability

Six acrylic resin cellular shells were constructed to determine the relative merits of the different types of joints and methods of bonding (Figs. 2 and 3). These shells were of the same size and weight as the acrylic resin cellular shell of the previous test series(1) and were imploded under the same conditions. Although the cellular shell is of comparatively simple construction (concentric cylinders separated by stiffeners), the location and strength of joints between structural components may vary considerably. The following methods were used to fabricate the acrylic resin cellular shells:

- Model 6 - smooth tube slip-fitted over an externally ribbed tube (Fig. 4);
- Model 7 - internally ribbed tube slip-fitted over a smooth tube (Fig. 5);
- Model 8 - stacked H-ring modules (Fig. 6);
- Model 9 - stacked U-ring modules (Fig. 7);

*Numbers in parentheses refer to References at the end of this report.

- Model 10 - annular stiffeners, inserted between concentric tubes - these annular stiffeners fitted loosely and were separated by three spacers located 120 deg apart (Fig. 8); and
 Model 11 - stacked concentric rings and spacers (Figs. 9 and 10).

Strain gages were mounted on the shells (Fig. 11), and the shells were subjected to external hydrostatic pressure in a small pressure tank (Fig. 12). Both ends of the shells were closed with end closure plates that permitted the ends of the shell to contract while under external pressure (Fig. 13), and both stresses and strains were recorded during the tests. Unbonded joints were taped with 3M electrical insulation tape to prevent leaking. Table I lists the implosion pressure structural efficiency (η),* and material strength utilization (ψ)** of the shells.

TABLE I
 IMPLOSION-TEST RESULTS

Model	Implosion Pressure (psi)	Structural Efficiency	Material Strength Utilization (per cent)
6	1600	1.59×10^5	100
7	1600	1.59×10^5	100
8	1600	1.59×10^5	100
9	1600	1.59×10^5	100
10	1200	1.19×10^5	76
11	1610	1.59×10^5	100

GENERAL ELASTIC STABILITY

All models failed by material yielding except Model 10, the cellular shell in which the stiffeners were not restrained from moving laterally. Table I shows that the other shells imploded at approximately the same pressure. However, these pressures were approximately 50 psi lower than that of Model 5, the all-bonded cellular shell tested in the previous acrylic resin test series (1). The 50-psi difference in implosion pressures can be explained by a 5-deg difference in temperature between the pressurizing media used in the two tests. When the decrease in material strength caused by this temperature difference is taken into consideration, it can be stated that Models 6 through 9 and Model 11 were equal in elastic stability to Model 5, which had an η of 1.64×10^5 and a ψ of 100 per cent. The location of joints and the lack of bonding do not seem to influence the general elastic stability of cellular shells as long as the stiffeners are restrained from moving laterally. Model 10, on the other hand, failed at a much lower pressure because the annular stiffeners were not restrained along their whole circumference but were kept in place by only three spacers located 120 deg apart.

DISTRIBUTION OF STRESSES AND STRAINS

Although the general elastic stability of the shell was not affected by the location of the joints and the lack of bonding, the distribution of stresses and strains on the shell surface was con-

* η = collapse pressure \times (hull displacement/weight of shell).

** ψ = (experimental collapse pressure) (outside diameter)/2 (average thickness of solid portion of shell wall) (yield strength). The yield strength was measured at the temperature of the water used in the test.

List of Illustrations*

- Fig. 1. Cellular Shell
- Fig. 2. Acrylic Resin Cellular Shells (Models 6 through 10)
- Fig. 3. Acrylic Resin Cellular Shell (Model 11)
- Fig. 4. Assembly of Model 6
- Fig. 5. Assembly of Model 7
- Fig. 6. Assembly of Model 8
- Fig. 7. U-Ring Module Used in Assembly of Model 9
- Fig. 8. Detail of Model 10 Assembly
- Fig. 9. Structural Modules of Model 11
- Fig. 10. Assembly of Model 11
- Fig. 11. Location of Strain Gages on Acrylic Resin Cellular Shells
- Fig. 12. Equipment for Pressure Testing Acrylic Resin Shells
- Fig. 13. End Closure for Acrylic Resin Shells
- Fig. 14. Principal Stresses and Strains in Model 6
- Fig. 15. Principal Stresses and Strains in Model 7
- Fig. 16. Principal Stresses and Strains in Model 8
- Fig. 17. Principal Stresses and Strains in Model 9
- Fig. 18. Principal Stresses and Strains in Model 10
- Fig. 19. Principal Stresses and Strains in Model 11
- Fig. 20. Compressive Stress-Strain Curve for Acrylic Resin Used in Cellular Shells
- Fig. 21. Principal Stresses at Locations A and B as Calculated by Pulos' Analysis
- Fig. 22. Principal Stresses at Locations A and B as Calculated by Mehta's Analysis

* Illustrations will be found at the end of the report, following the colored divider.

- Fig. 23. Calculated and Experimentally Determined Stresses in Model F Cellular Shell
- Fig. 24. Photoelastic Fringes Obtained with Rectangular-Cell Epoxy Resin Shell
- Fig. 25. Photoelastic Fringes Obtained with Square-Cell Epoxy Resin Shell
- Fig. 26. Epoxy Resin Cellular Shells
- Fig. 27. Detail of Square -Cell Epoxy Resin Shell
- Fig. 28. Detail of Rectangular-Cell Epoxy Resin Shell
- Fig. 29. Photoelastic Fringes in Two-Dimensional T-Section Models, in the Linear Elastic Range, during Pure Flexure of the Wall
- Fig. 30. Generation of Stresses in T-Section Models
- Fig. 31. Flexural Stress Concentration Factor vs r/t_f in the Axial Plane of the Shell at the Juncture of the Stiffener and the Facing
- Fig. 32. Radial Stress Concentration Factor vs r/t_f at the Point of Maximum Flexural Stress in the Facing at the Juncture of the Stiffener
- Fig. 33. Axial Stress Concentration Factor vs r/t_f at the Point of Maximum Flexural Stress in the Facing at the Juncture of the Stiffener
- Fig. 34. Location (d/t) of Maximum Flexural Stresses vs r/t_f for a Shell Facing Subjected to Flexure in the Axial Plane of the Shell
- Fig. 35. Distribution of Maximum Shear Stresses in T-Sections Subjected to Identical Flexure

Distribution List

Chief, Bureau of Naval Weapons (RU-2) Department of the Navy Washington 25, D. C.	1 copy	Commander U. S. Naval Ordnance Laboratory White Oak Silver Spring 19, Maryland	2 copies
Chief, Bureau of Naval Weapons (RUTO-33) Department of the Navy Washington 25, D. C.	2 copies	Commander U. S. Naval Ordnance Laboratory White Oak Silver Spring 19, Maryland Attn: Dr. S. J. Raff	1 copy
Chief, Bureau of Naval Weapons (RUDC) Department of the Navy Washington 25, D. C.	1 copy	Commander U. S. Naval Ordnance Test Station 3202 East Foothill Boulevard Pasadena Annex Pasadena 8, California	2 copies
Chief, Bureau of Naval Weapons (RUSD) Department of the Navy Washington 25, D. C.	1 copy	Commanding Officer U. S. Naval Torpedo Station Keyport, Washington	1 copy
Chief, Bureau of Naval Weapons (DLI-3) Department of the Navy Washington 25, D. C.	2 copies	Commanding Officer U. S. Naval Torpedo Station Quality Evaluation Technical Library Keyport, Washington	1 copy
Chief, Naval Operations (OP 721) Department of the Navy Washington 25, D. C. For: IEP ABC 28	5 copies	Director (Code 2021) U. S. Naval Research Laboratory Washington 25, D. C.	3 copies
Chief, Naval Operations (OP 31) Department of the Navy Washington 25, D. C.	1 copy	Director (Code 2027) U. S. Naval Research Laboratory Washington 25, D. C.	1 copy
Chief, Naval Operations (OP 312) Department of the Navy Washington 25, D. C.	1 copy	Commanding Officer and Director U. S. Navy Electronics Laboratory San Diego 52, California	1 copy
Chief, Naval Operations (OP 71) Department of the Navy Washington 25, D. C.	1 copy	Commanding Officer and Director David Taylor Model Basin Washington 7, D. C.	1 copy
Chief, Naval Operations (O3EG) Department of the Navy Washington 25, D. C.	1 copy	Commanding Officer U. S. Navy Mine Defense Laboratory Panama City, Florida	1 copy
Chief, Naval Operations (OPO7TC) Technical Analysis and Advisory Group Rm5E613, Pentagon Washington 25, D. C.	1 copy	Commanding Officer and Director U. S. Navy Underwater Sound Laboratory Fort Trumbull New London, Connecticut	1 copy
Chief, Bureau of Ships Department of the Navy Washington 25, D. C.	3 copies	Commander U. S. Naval Missile Center Point Mugu Port Hueneme, California	1 copy
Commander Armed Services Technical Information Agency Attention TIPDR Arlington Hall Station Arlington 12, Virginia	10 copies		
Officer in Charge U. S. Naval Underwater Weapons Systems Engineering Center Newport, Rhode Island	1 copy		

Commander U. S. Naval Air Development Center Johnsville, Pennsylvania	1 copy	Commander, Test and Evaluation Force U. S. Atlantic Fleet U. S. Naval Base Norfolk 11, Virginia	1 copy
Officer in Charge Naval Aircraft Torpedo Unit Naval Air Station Quonset Point, Rhode Island	1 copy	Clevite Ordnance 540 East 105th Street Cleveland, Ohio	1 copy
Scientific and Technical Information Facility P. O. Box 5700 Bethesda, Maryland Attn: NASA Representative (S-AK/DL)	1 copy	Vitro Corporation of America 14,000 Georgia Avenue Silver Spring, Maryland	1 copy
Director, Applied Physics Laboratory University of Washington Seattle, Washington	2 copies	Westinghouse Electric Corporation Lansdowne Plant Baltimore, Maryland	1 copy
Director, Marine Physical Laboratory Scripps Institution of Oceanography San Diego 52, California	1 copy	Woods Hole Oceanographic Institution Woods Hole, Massachusetts	1 copy
Hudson Laboratories Dobbs Ferry, New York	1 copy	Aerojet General Corporation Azusa, California Attn: G. M. McRoberts	1 copy



Fig. 3 - Acrylic Resin Cellular Sandwich Shell

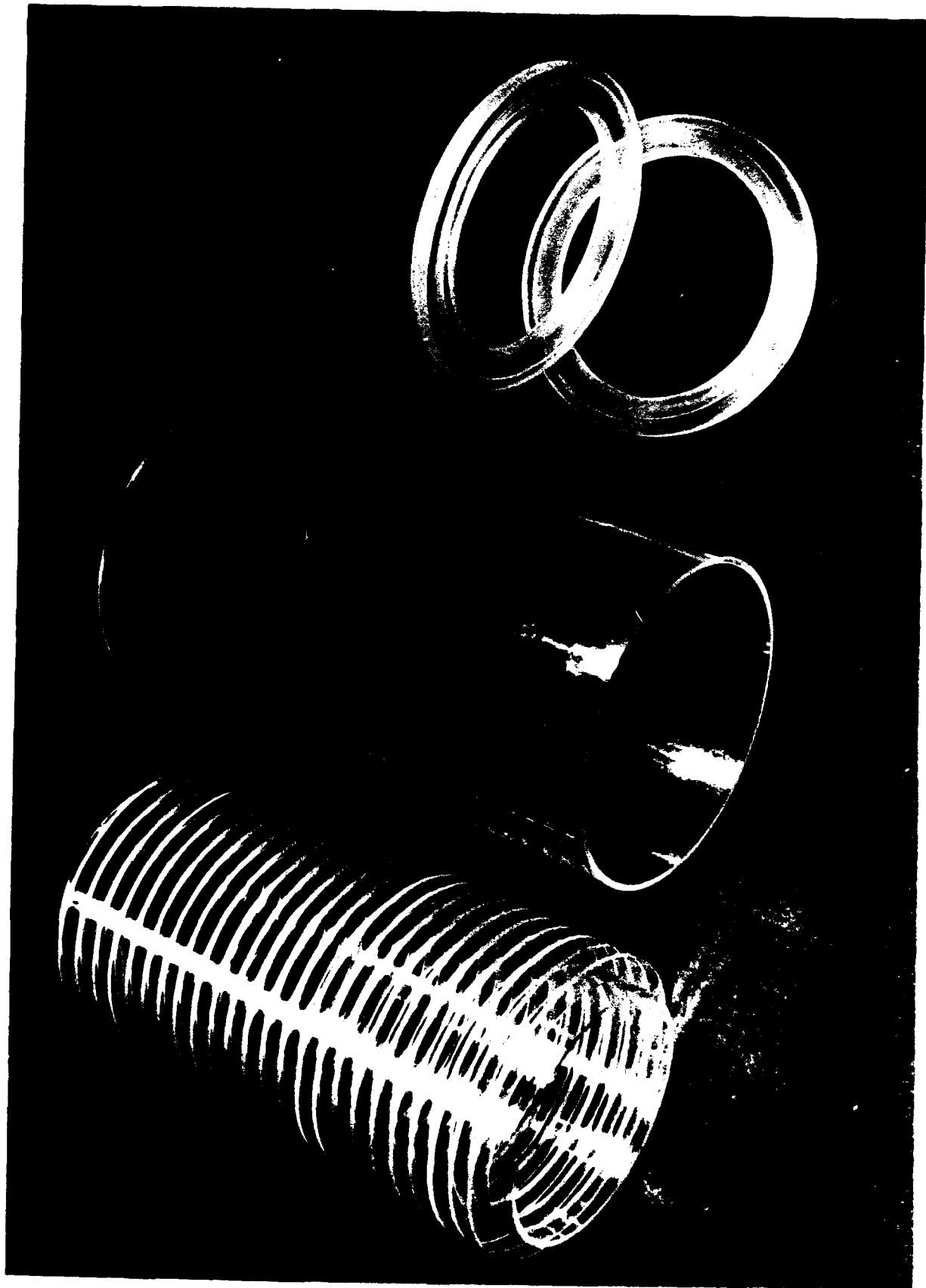


Fig. 4 - Structural Components of Acrylic Resin Cellular Sandwich Shell

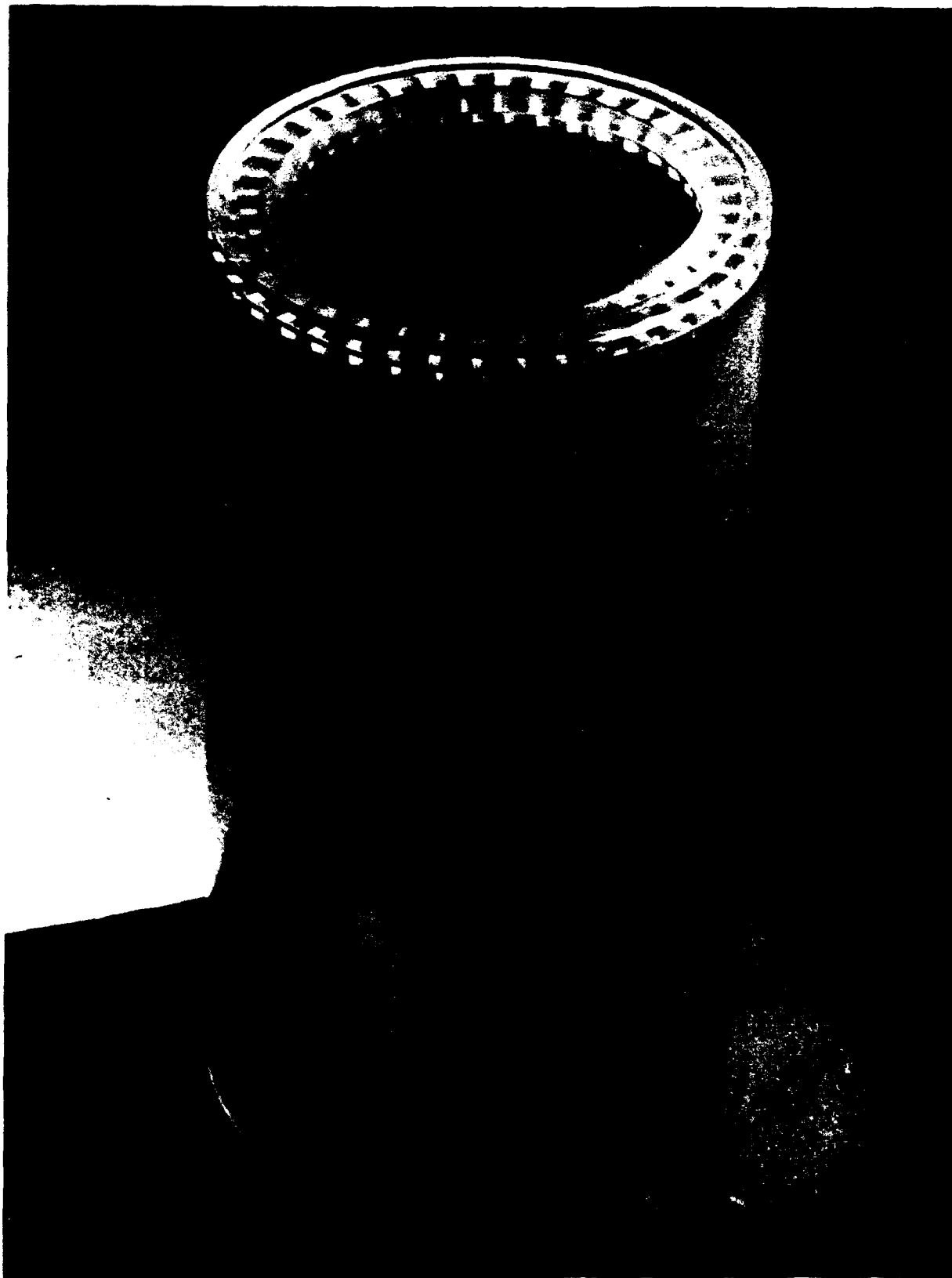


Fig. 5 - Acrylic Resin Tubular Sandwich Shell



Fig. 6 - Acrylic Resin Smooth Shell

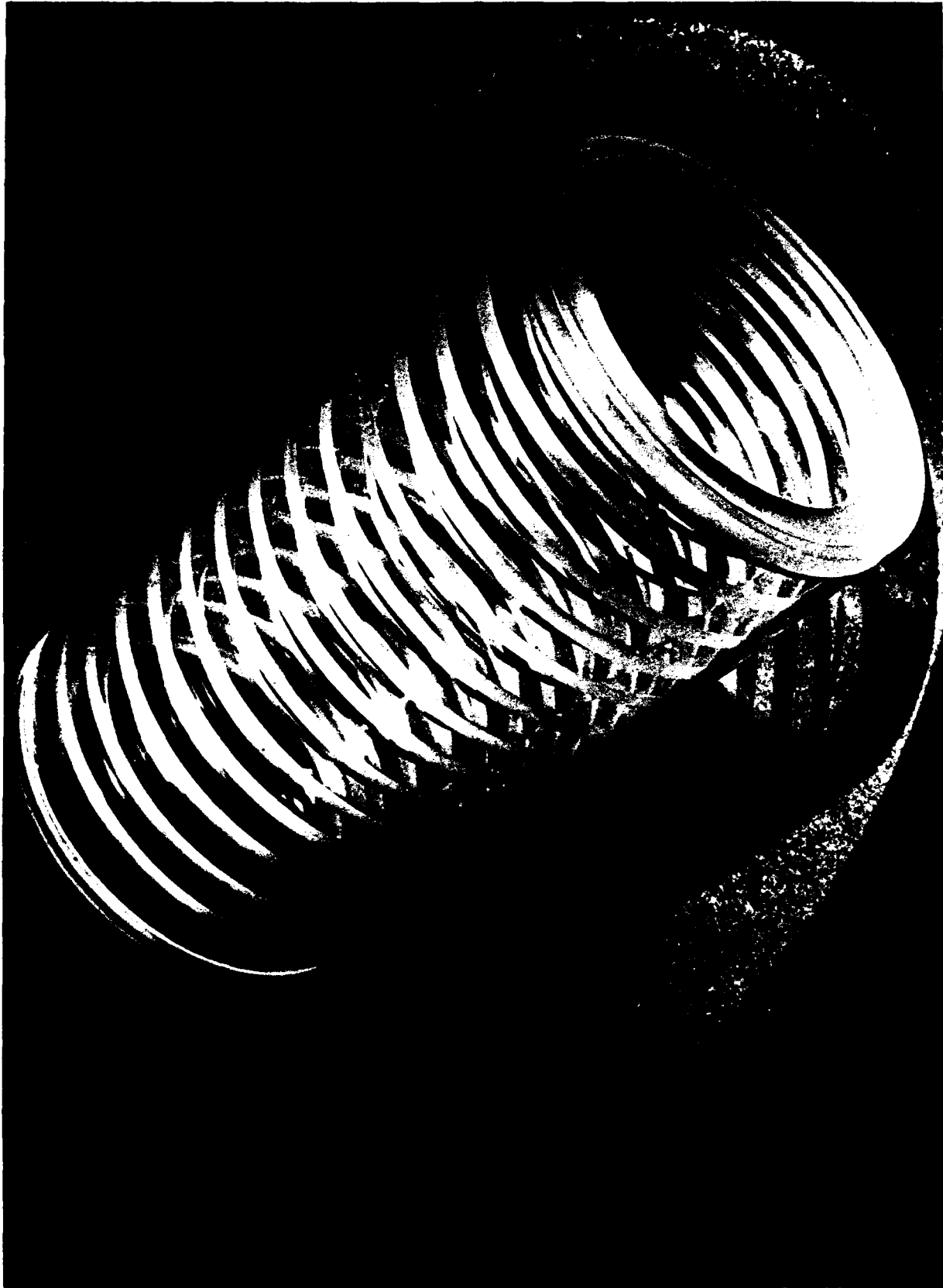


Fig. 7 - Acrylic Resin Smooth Shell Stiffened by Equally Spaced Circumferential Plain Ribs

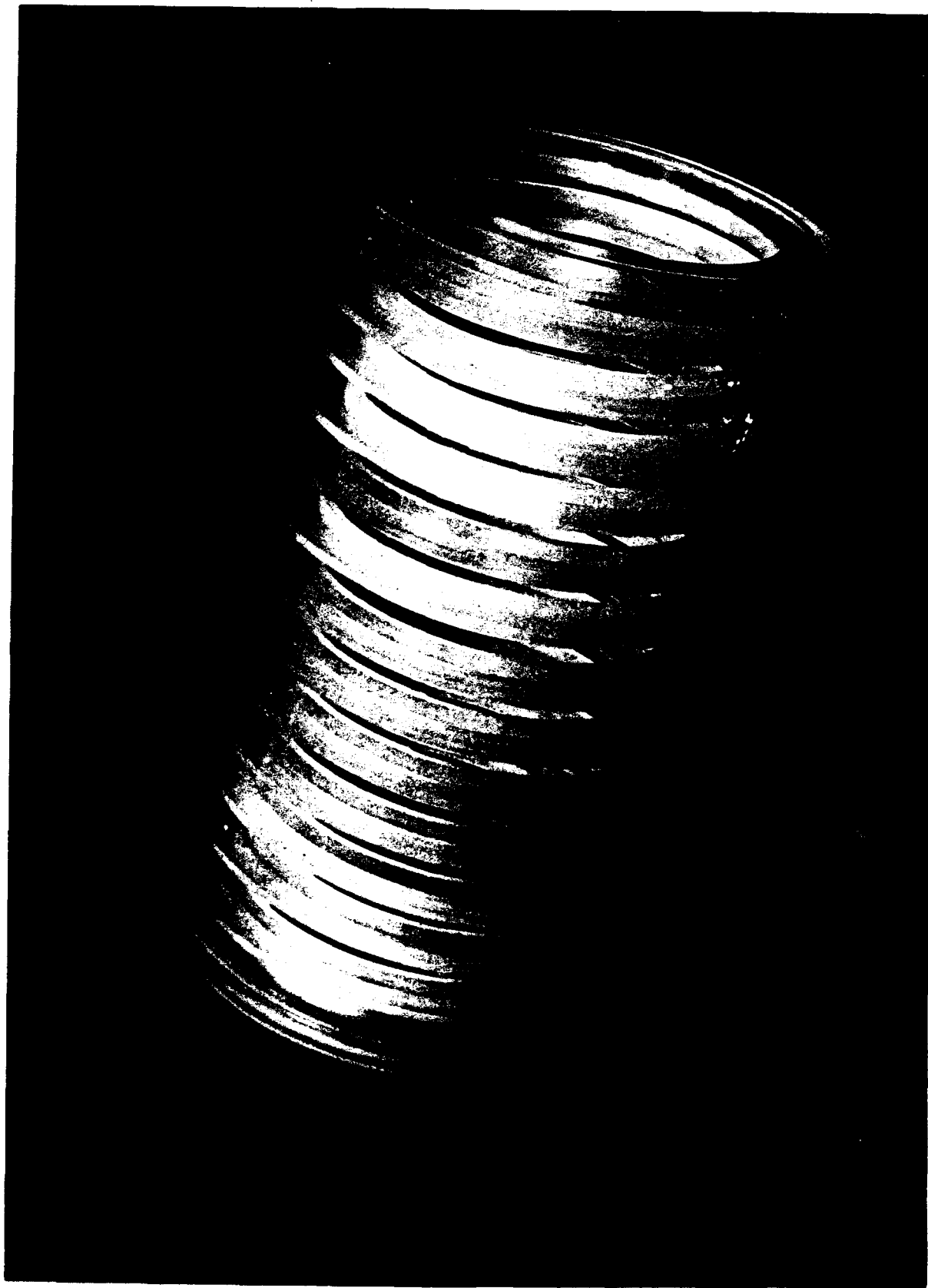


Fig. 8 - Acrylic Resin Smooth Shell Stiffened by Equally Spaced Circumferential T Ribs

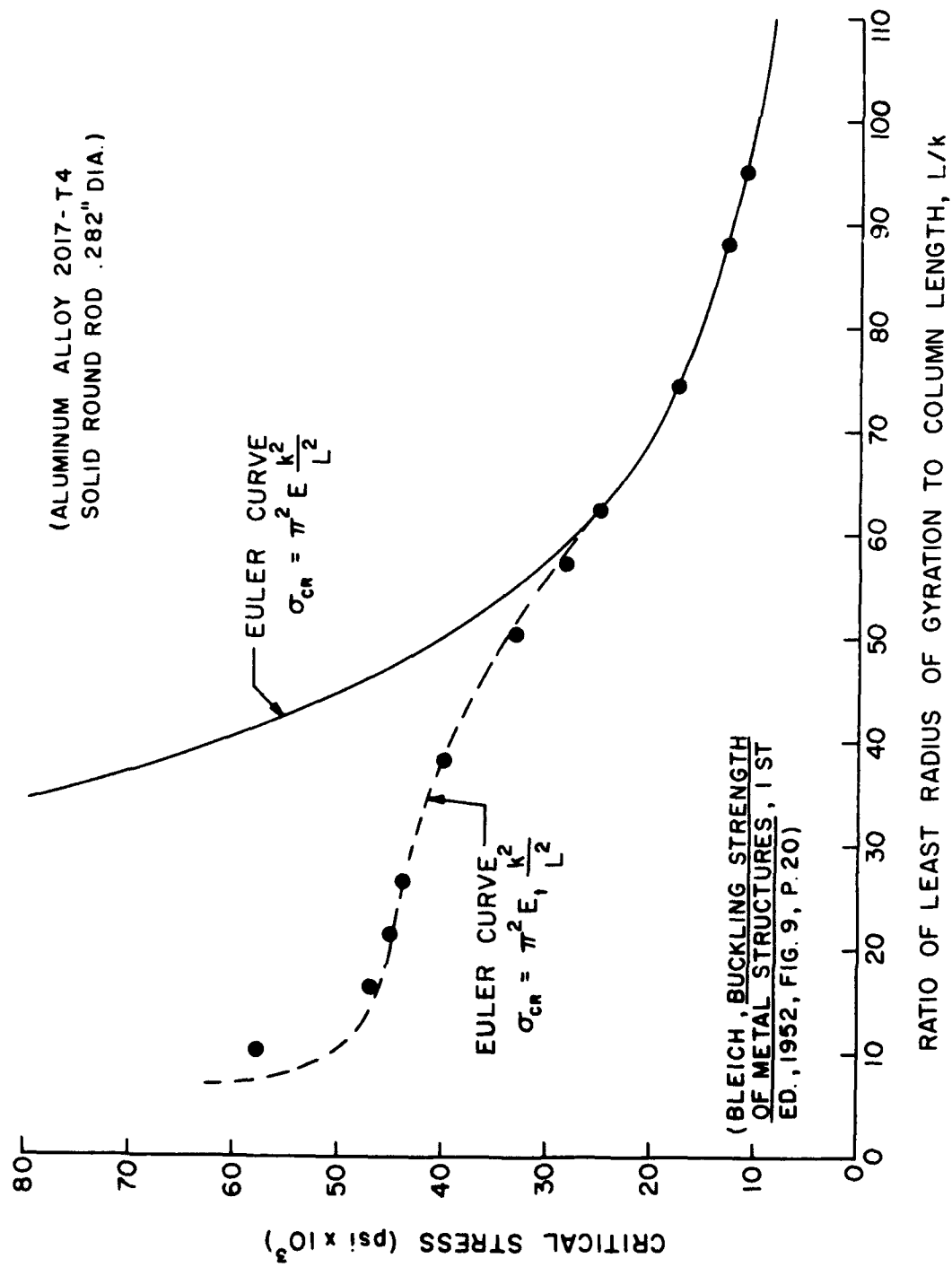


Fig. 9 - Buckling of Slender Aluminum Rods

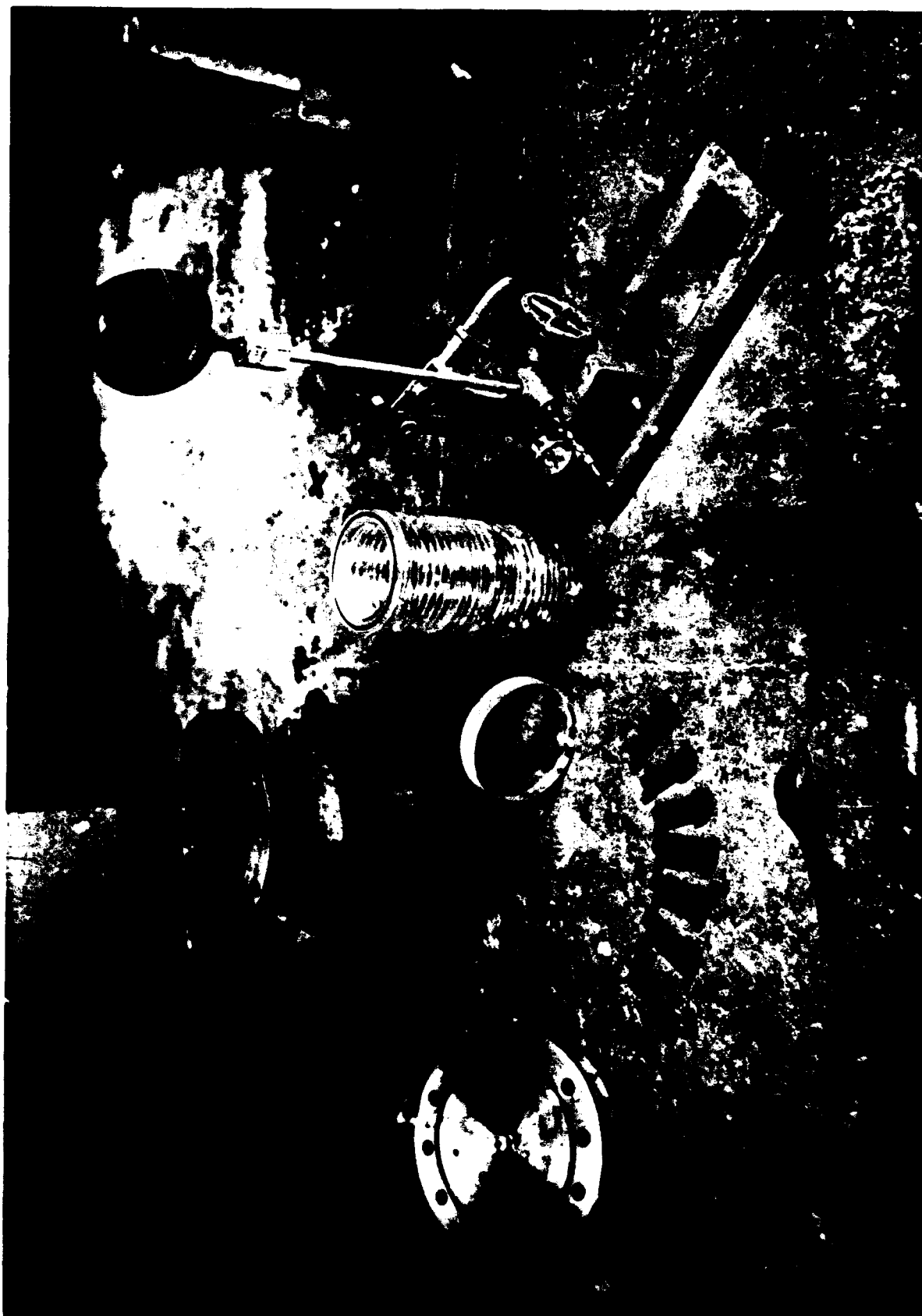
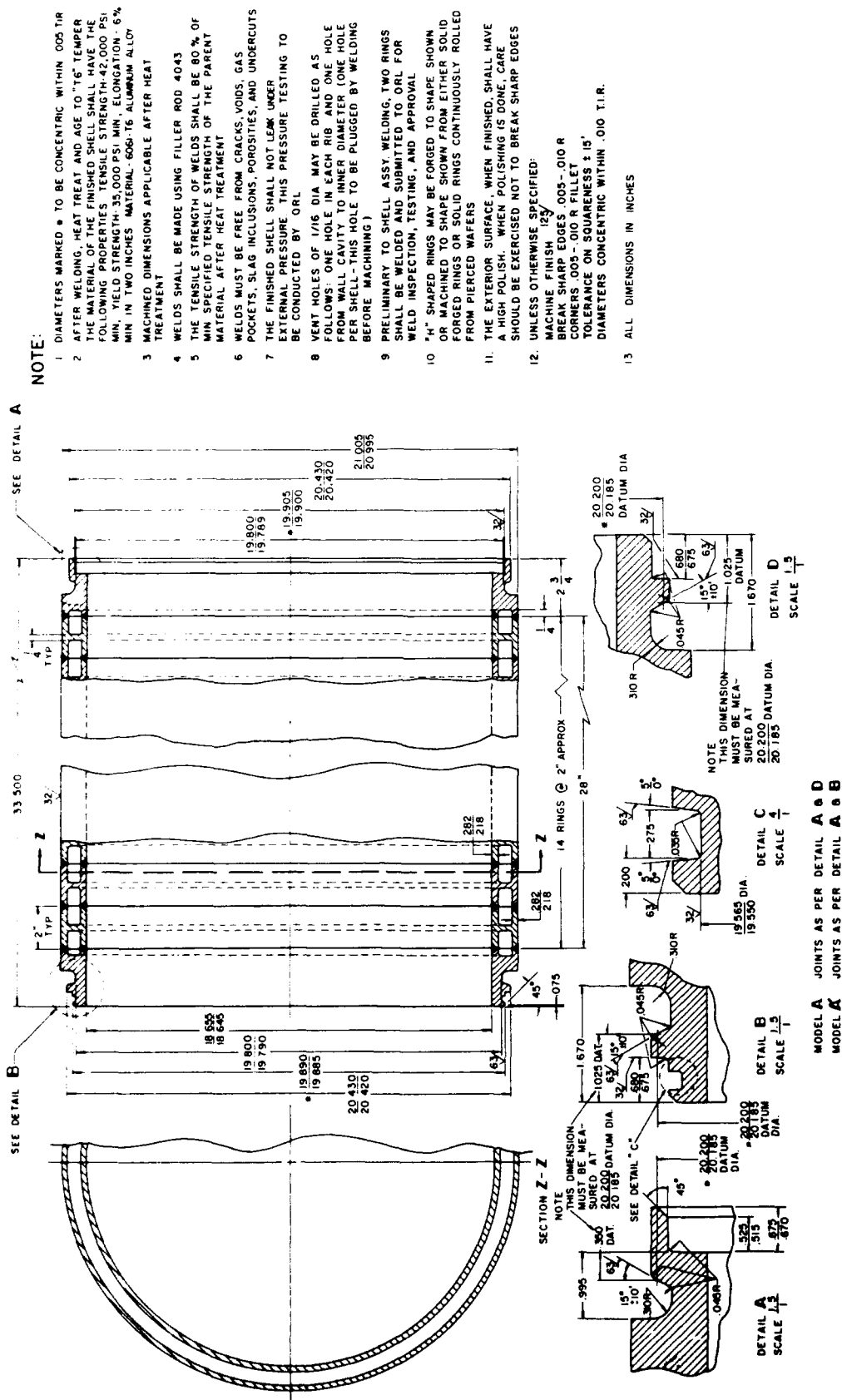
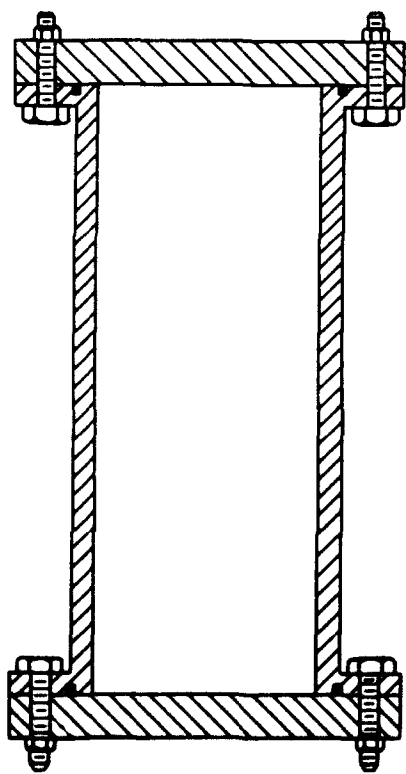
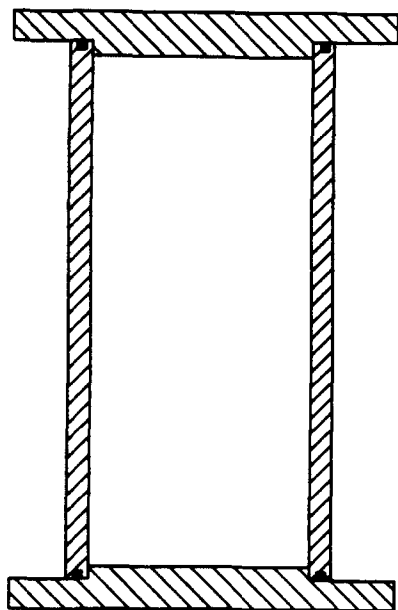


Fig. 11 - Equipment Required for Implosion Testing of Acrylic Resin Shells

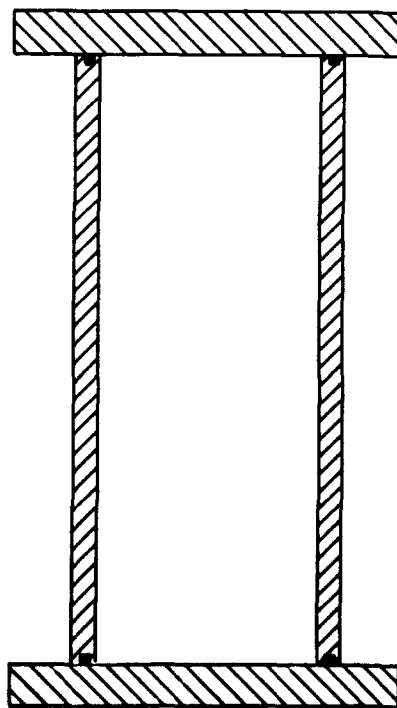




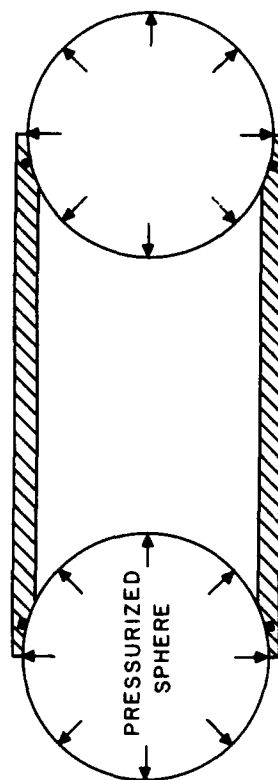
RIGID END SUPPORT



SIMPLE END SUPPORT



FRICTION END SUPPORT



ELASTIC END SUPPORT

Fig. 13 - End Supports for Shells Subjected to External Pressure

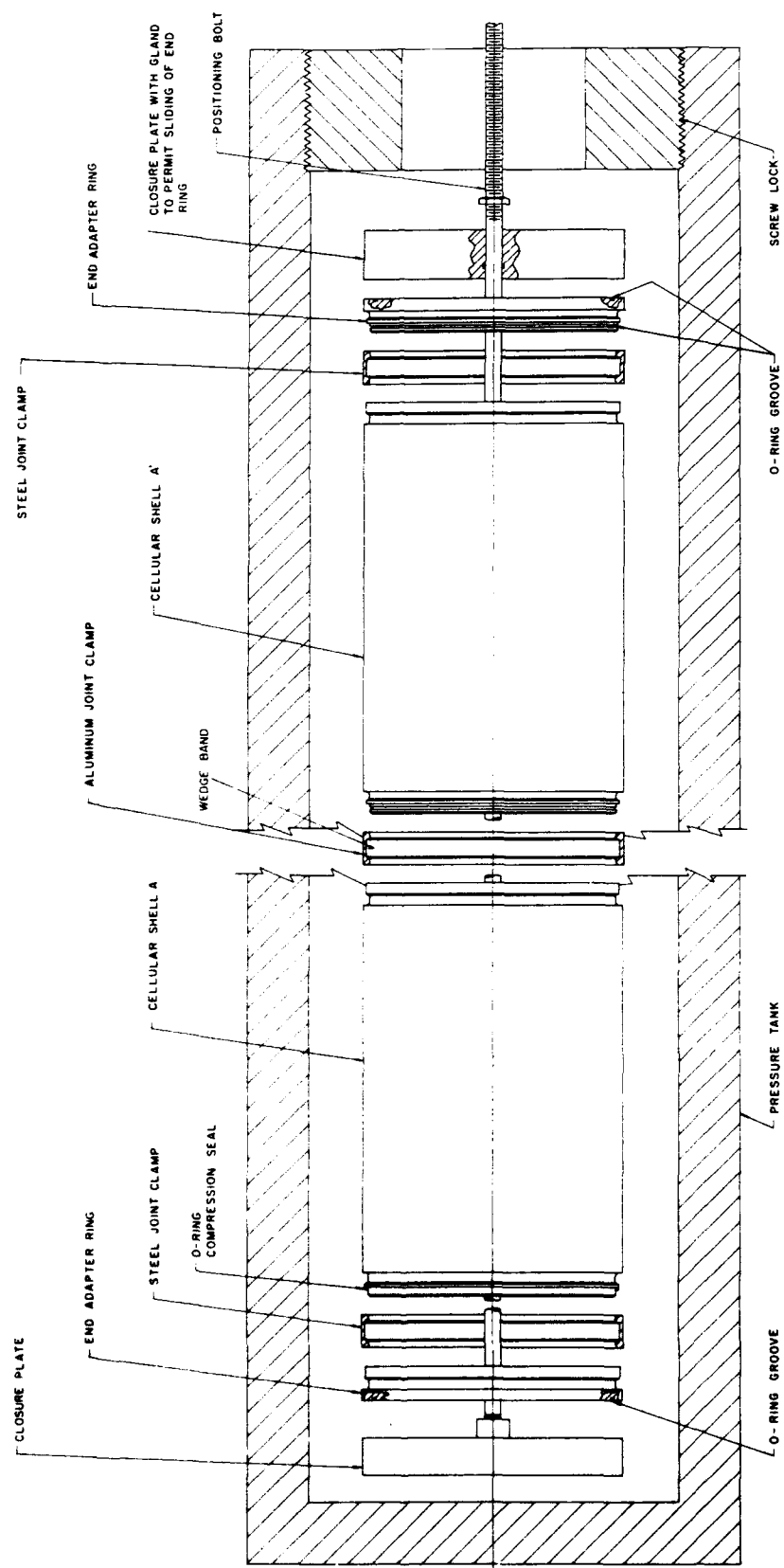


Fig. 14 - Method of Implosion Testing of Aluminum Cellular Sandwich Shells

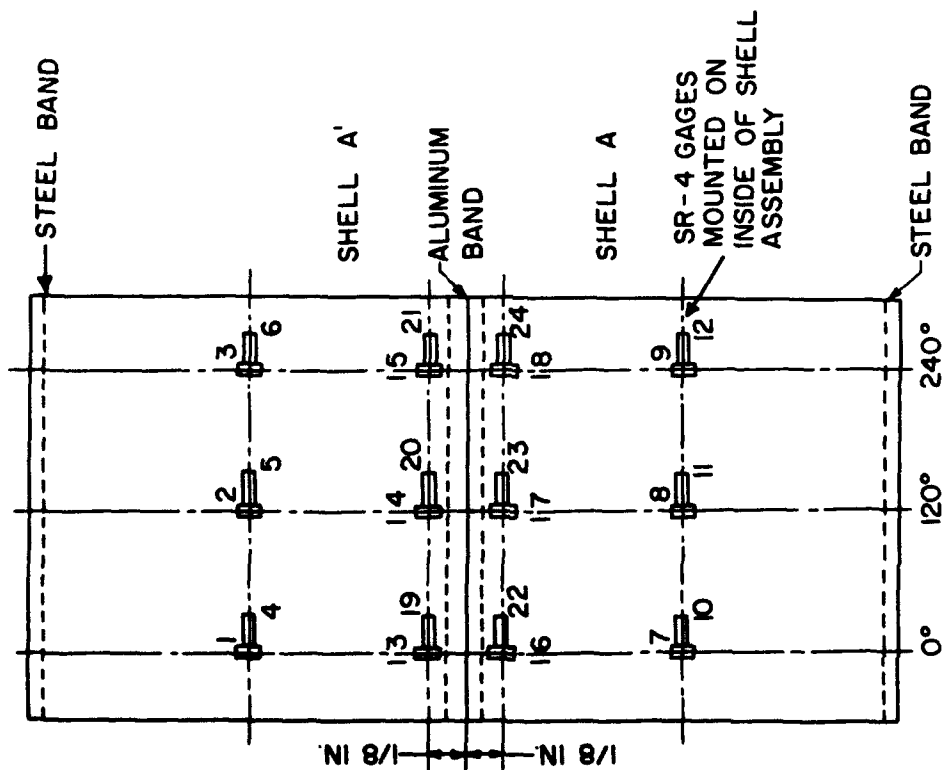


Fig. 15 - Location of Instruments during Pressure-Cycling Test

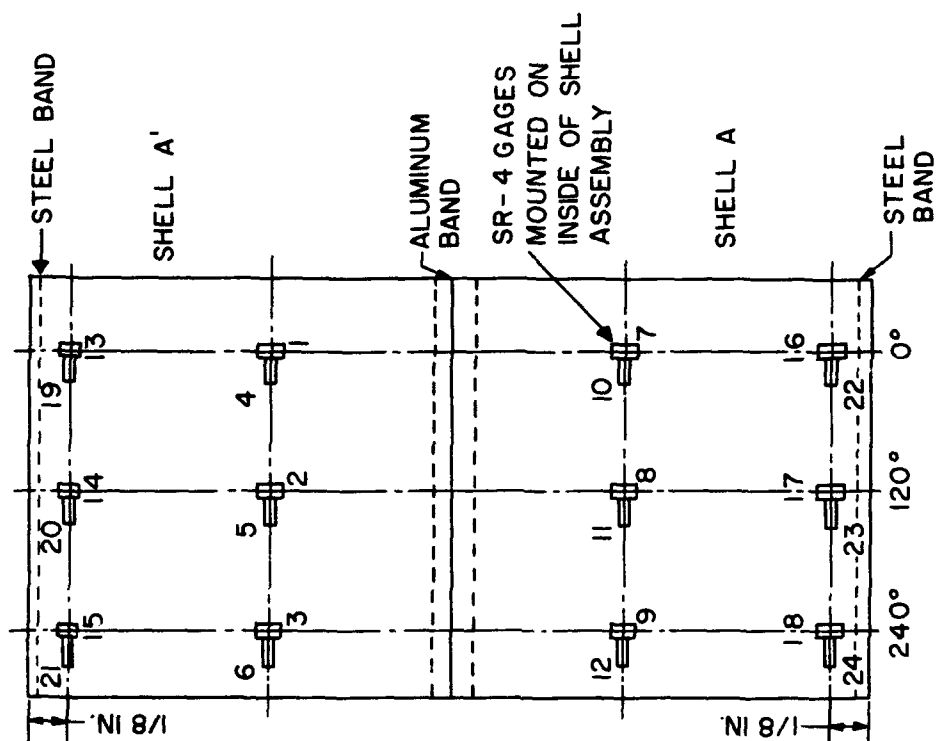


Fig. 16 - Location of Instruments during Implosion Test

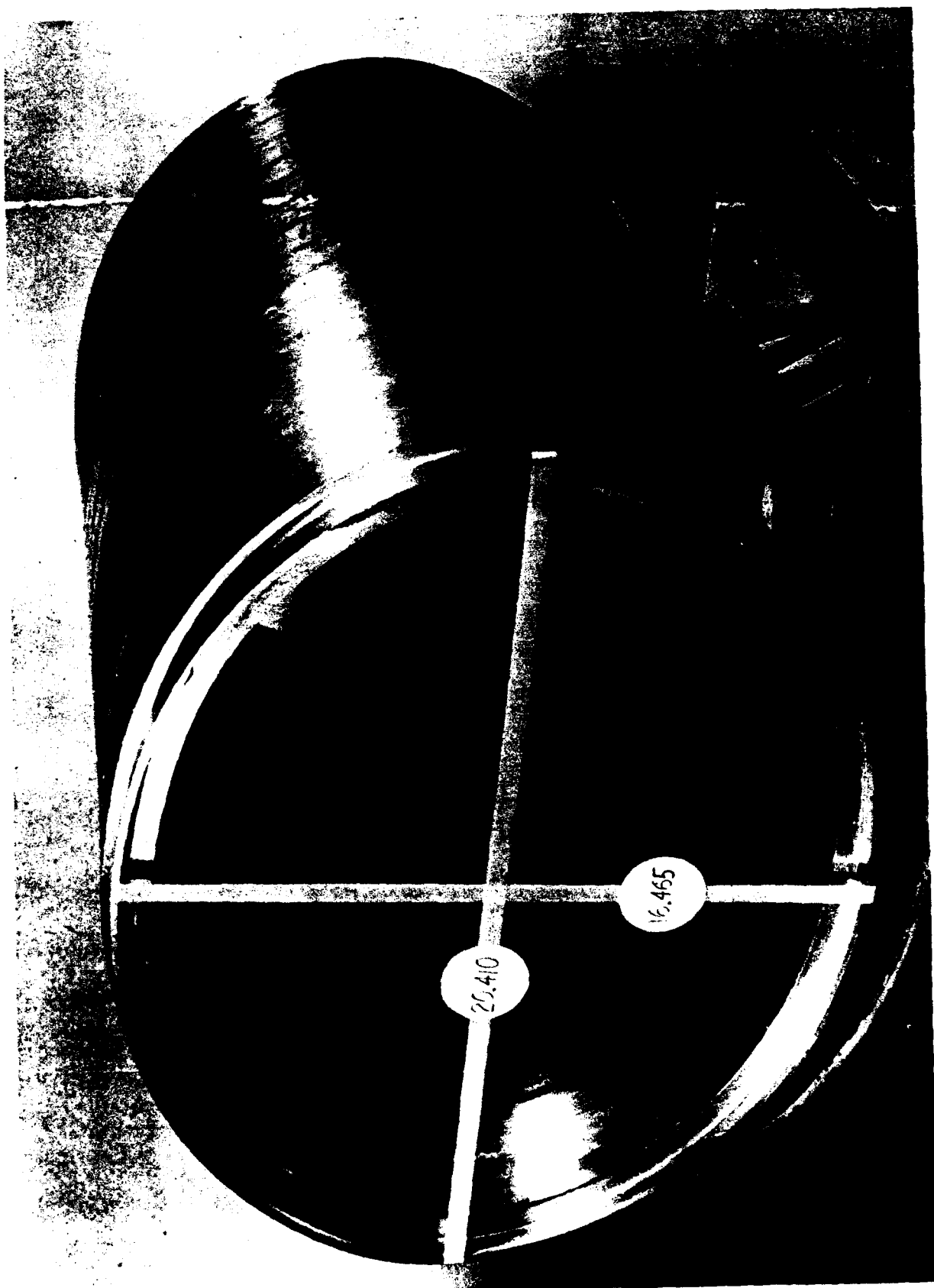


Fig. 17 - Cellular Sandwich Shell after Implosion

X(in.)	O.D. MIN. (in.)	O.D. MAX. (in.)
0	18.44	22.90
5	18.21	22.79
10	18.23	22.80
15	18.23	22.78
20	18.40	22.51
25	18.50	22.47
29.25	19.01	22.32
0	19.41	22.34
5	19.41	21.85
10	19.82	21.60
15	19.92	21.35
20	20.22	21.10
25	20.40	21.00
29.25	20.51	20.90

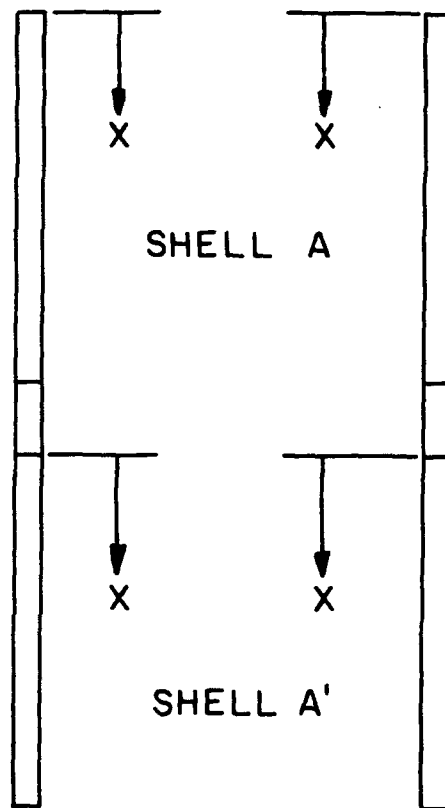


Fig. 18 - Deformation of Cellular Sandwich Shells after Implosion



Fig. 19 - Dissected Collapsed Shell (Model A)

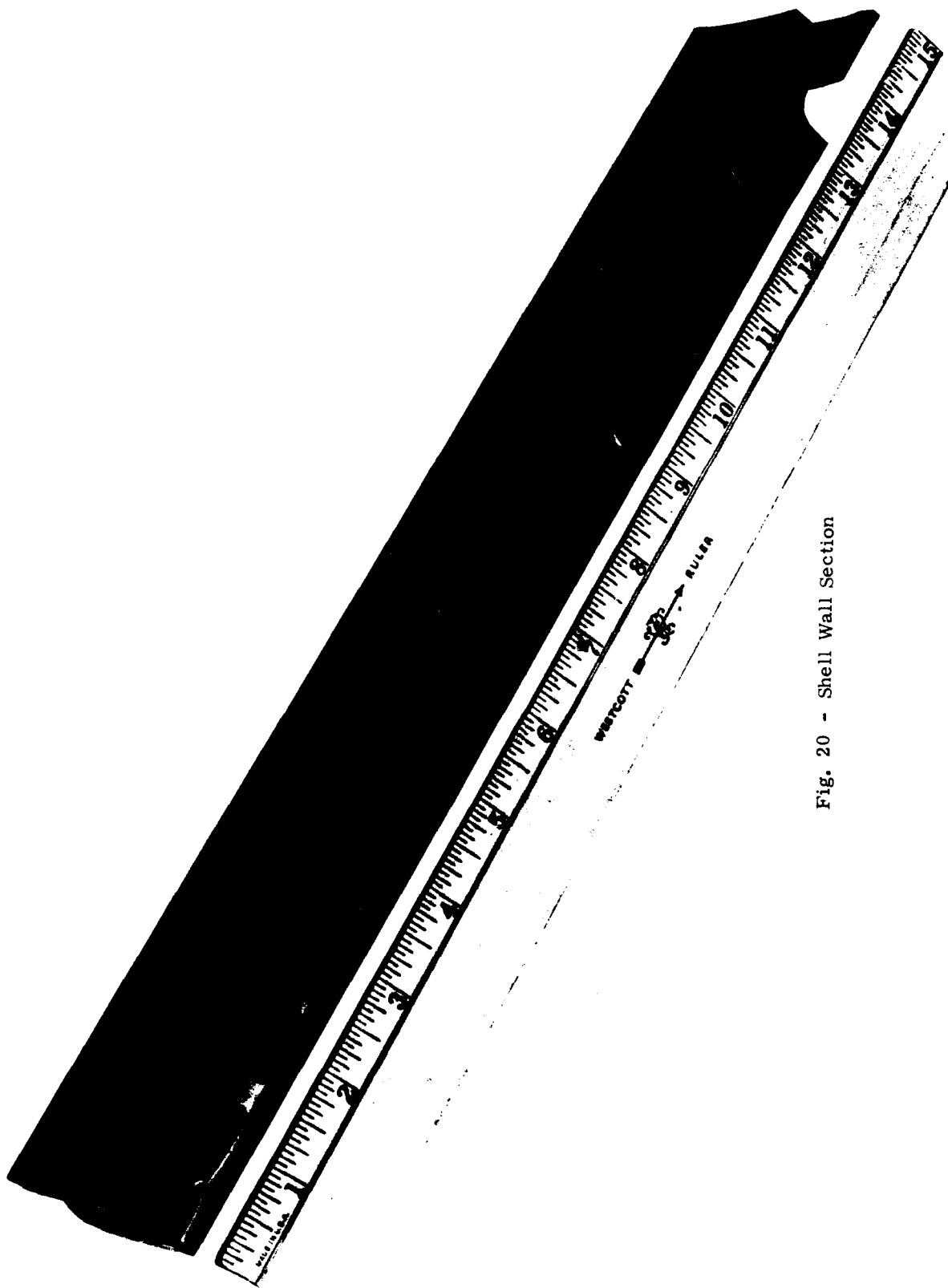


Fig. 20 - Shell Wall Section

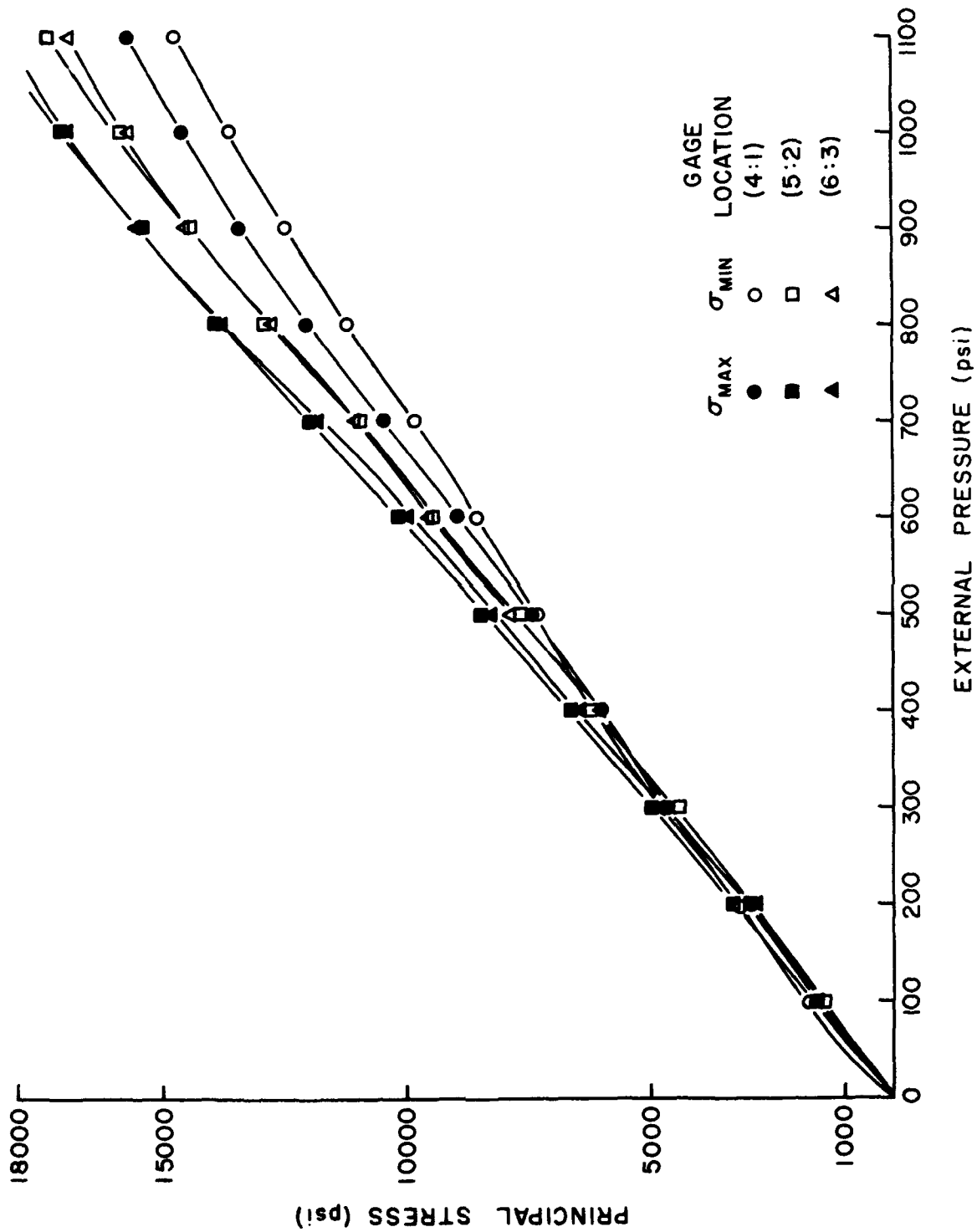


Fig. 21 - Stresses in Shell Models A and A' during Pressure Cycling -
Locations 1 through 6 (See Fig. 15)

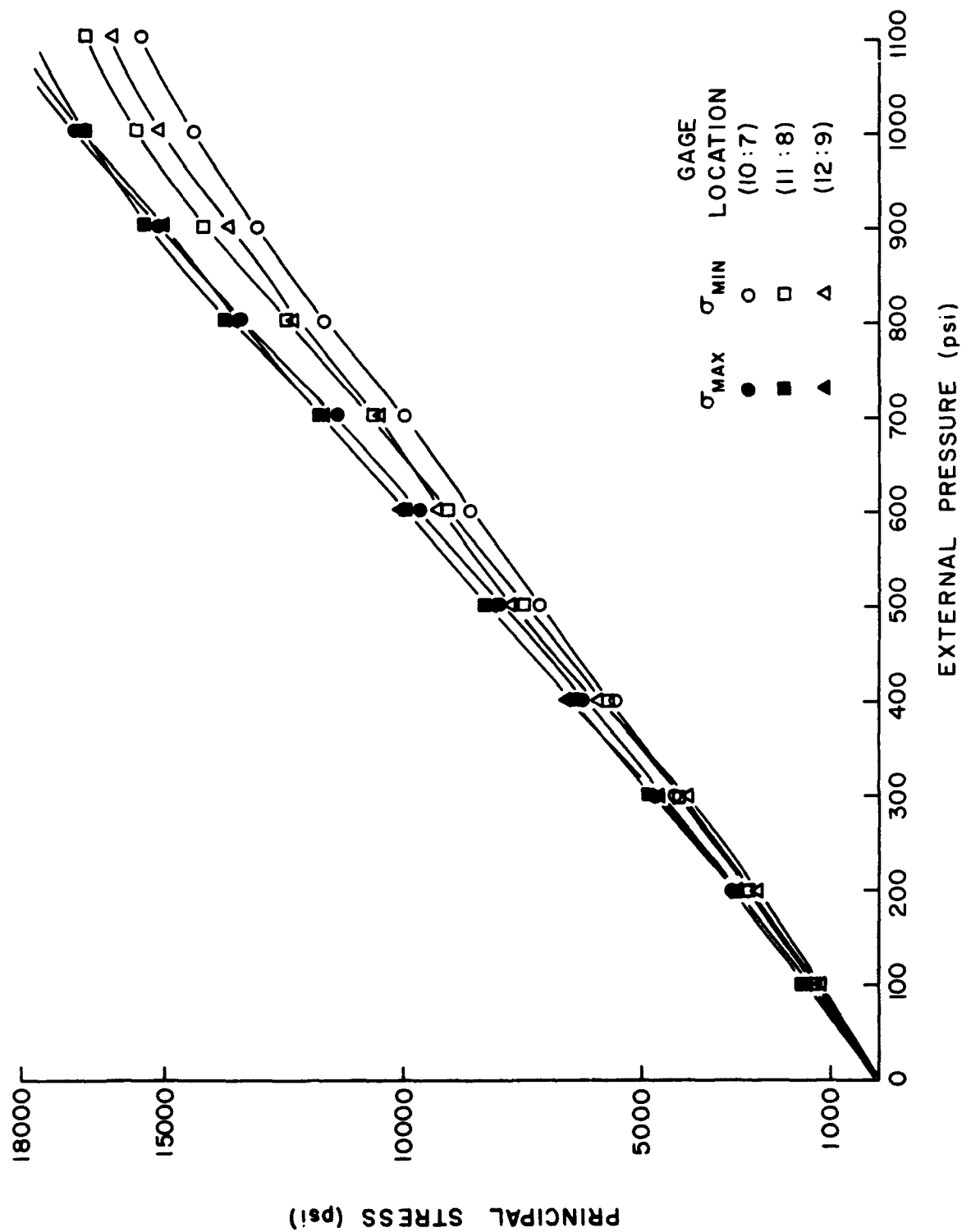


Fig. 22 - Stresses in Shell Models A and A' during Pressure Cycling -
Locations 7 through 12 (See Fig. 15)

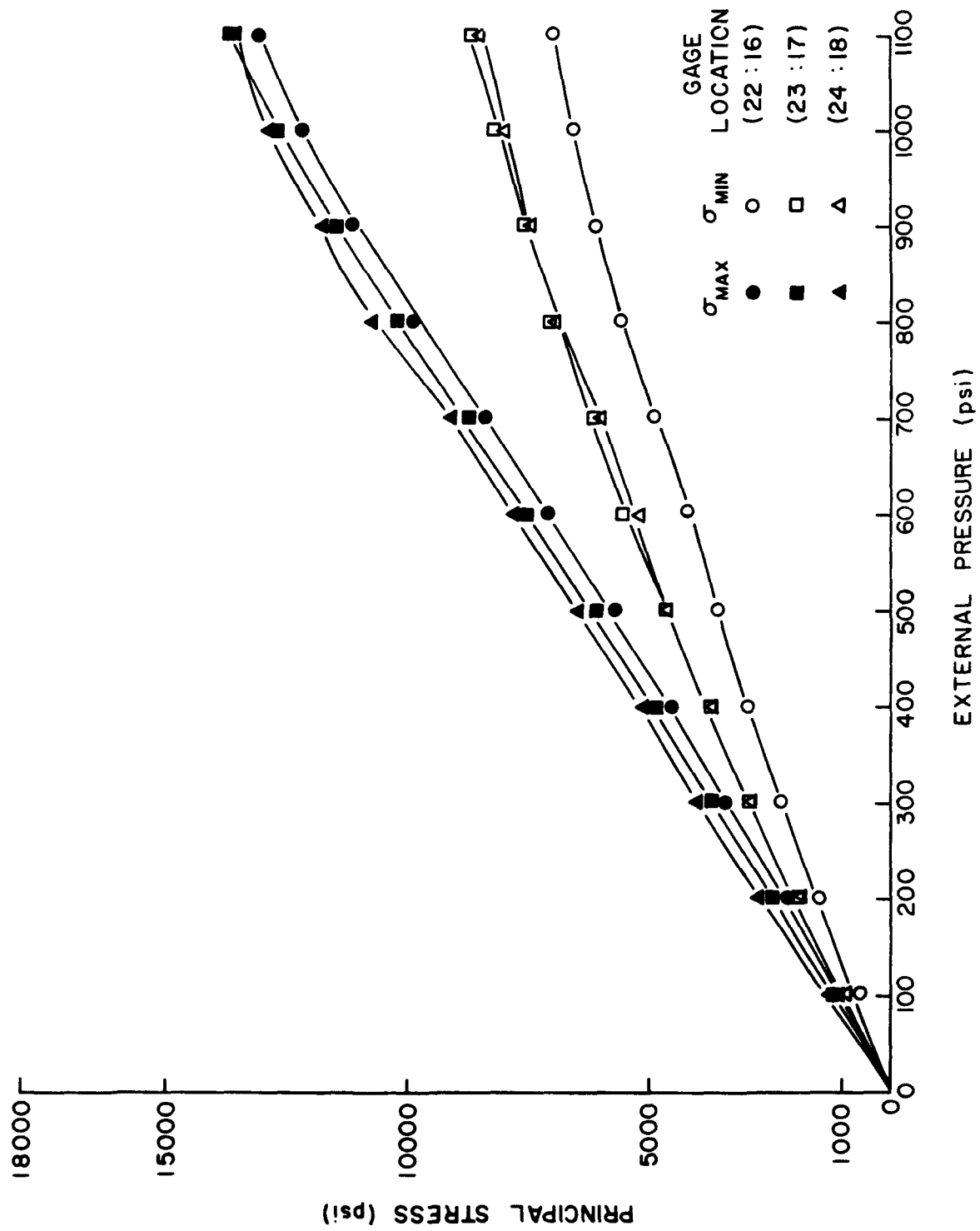


Fig. 23 - Stresses in Shell Models A and A' during Pressure Cycling -
Locations 16 through 18 and 22 through 24 (See Fig. 15)

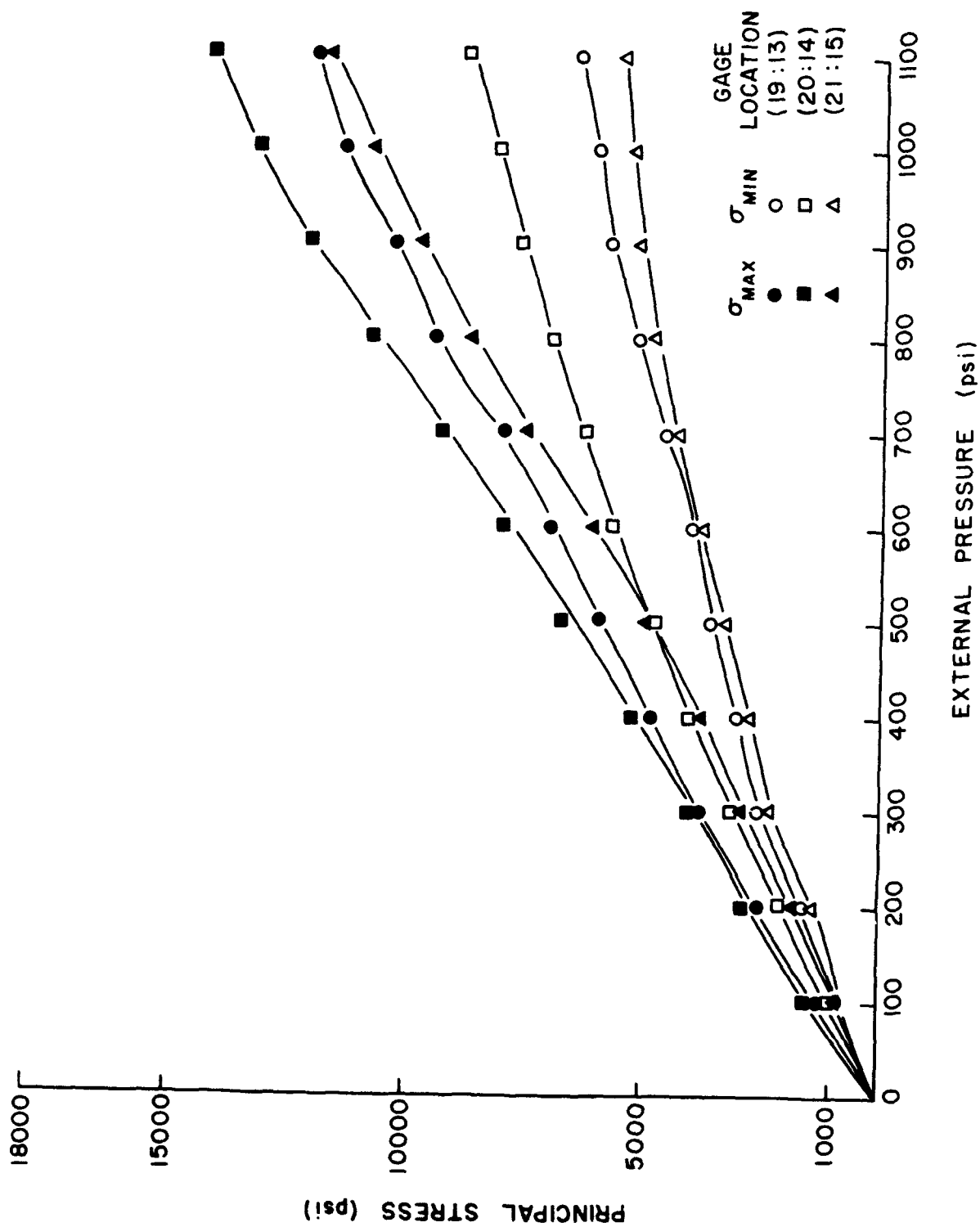


Fig. 24 - Stresses in Shell Models A and A' during Pressure Cycling - Locations 13 through 15 and 19 through 21 (See Fig. 15)

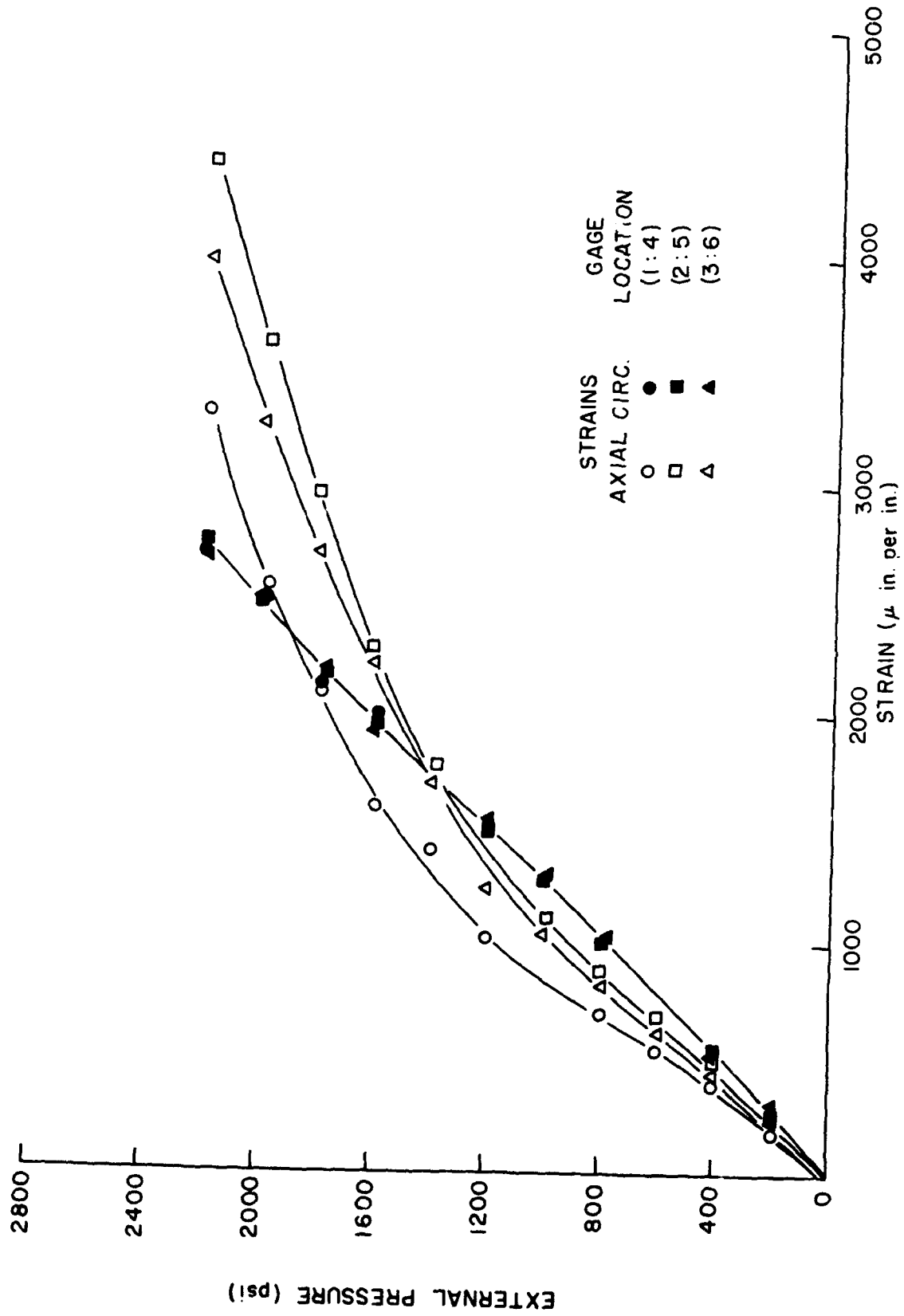


Fig. 25 - Strains in Shell Models A and A' during Implosion Testing -
Locations 1 through 6 (See Fig. 16)

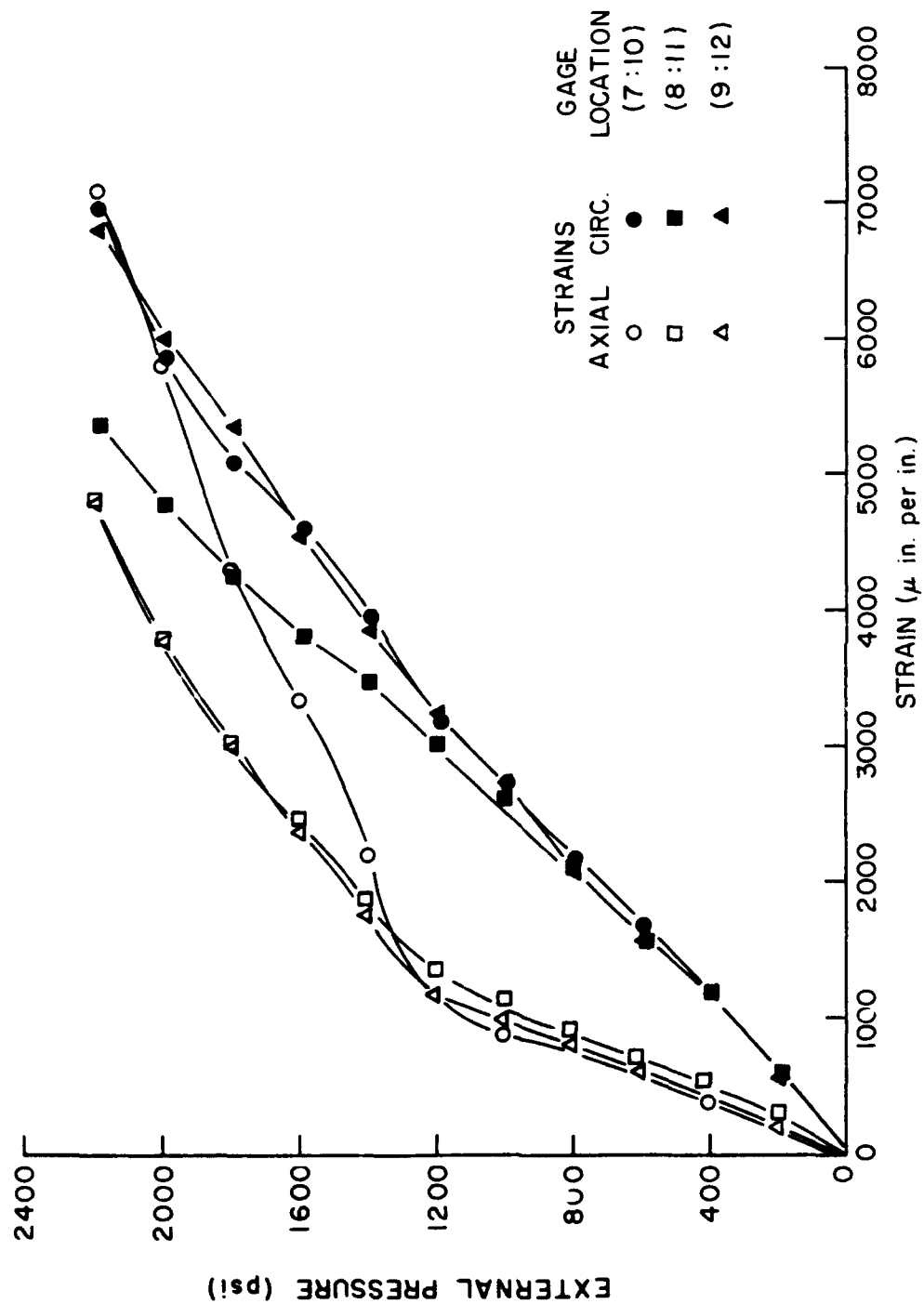


Fig. 26 - Strains in Shell Models A and A' during Implosion Testing -
Locations 7 through 12 (See Fig. 16)

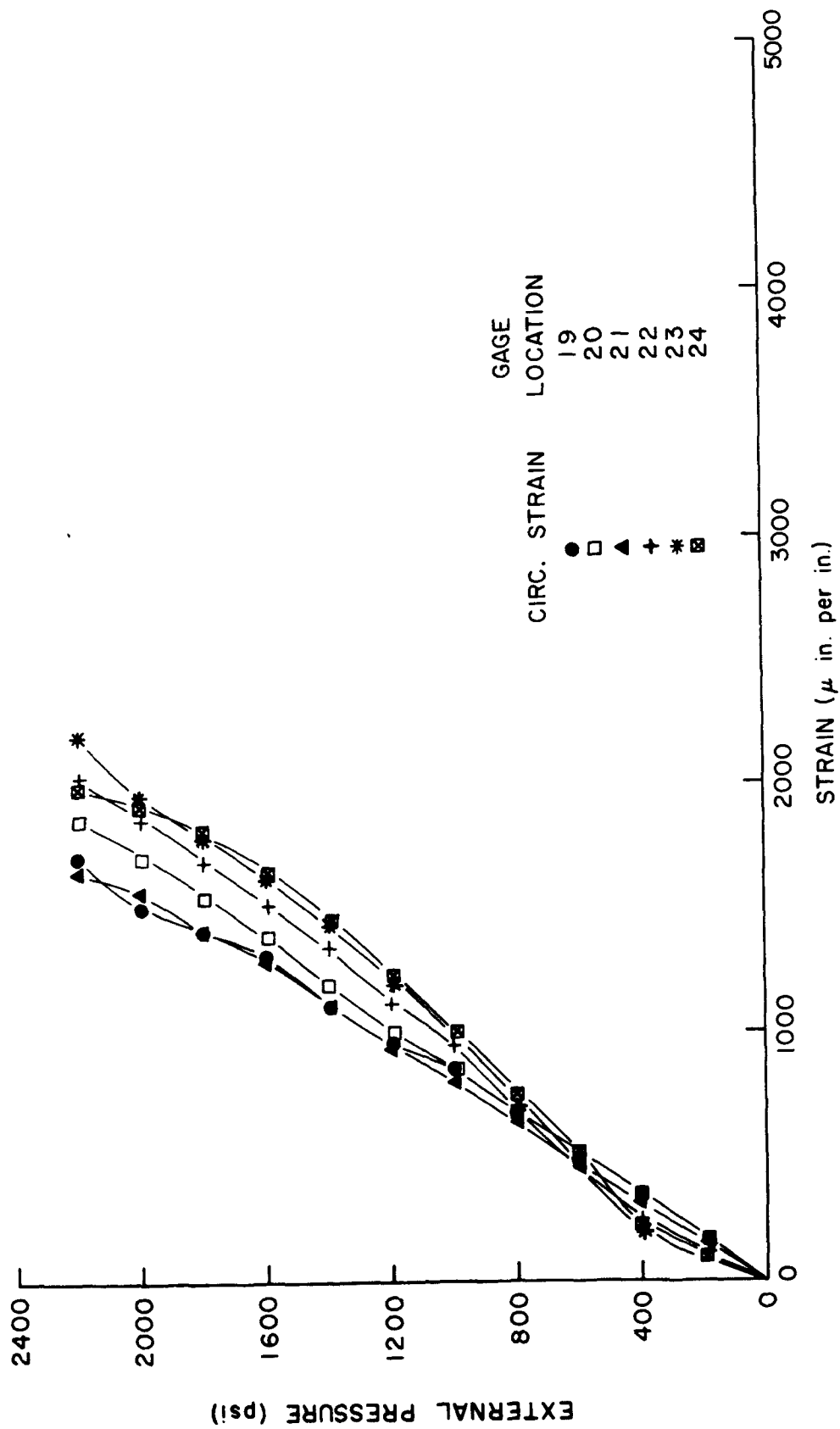


Fig. 27 - Strains in Shell Models A and A' during Implosion Testing -
Locations 19 through 24 (See Fig. 16)

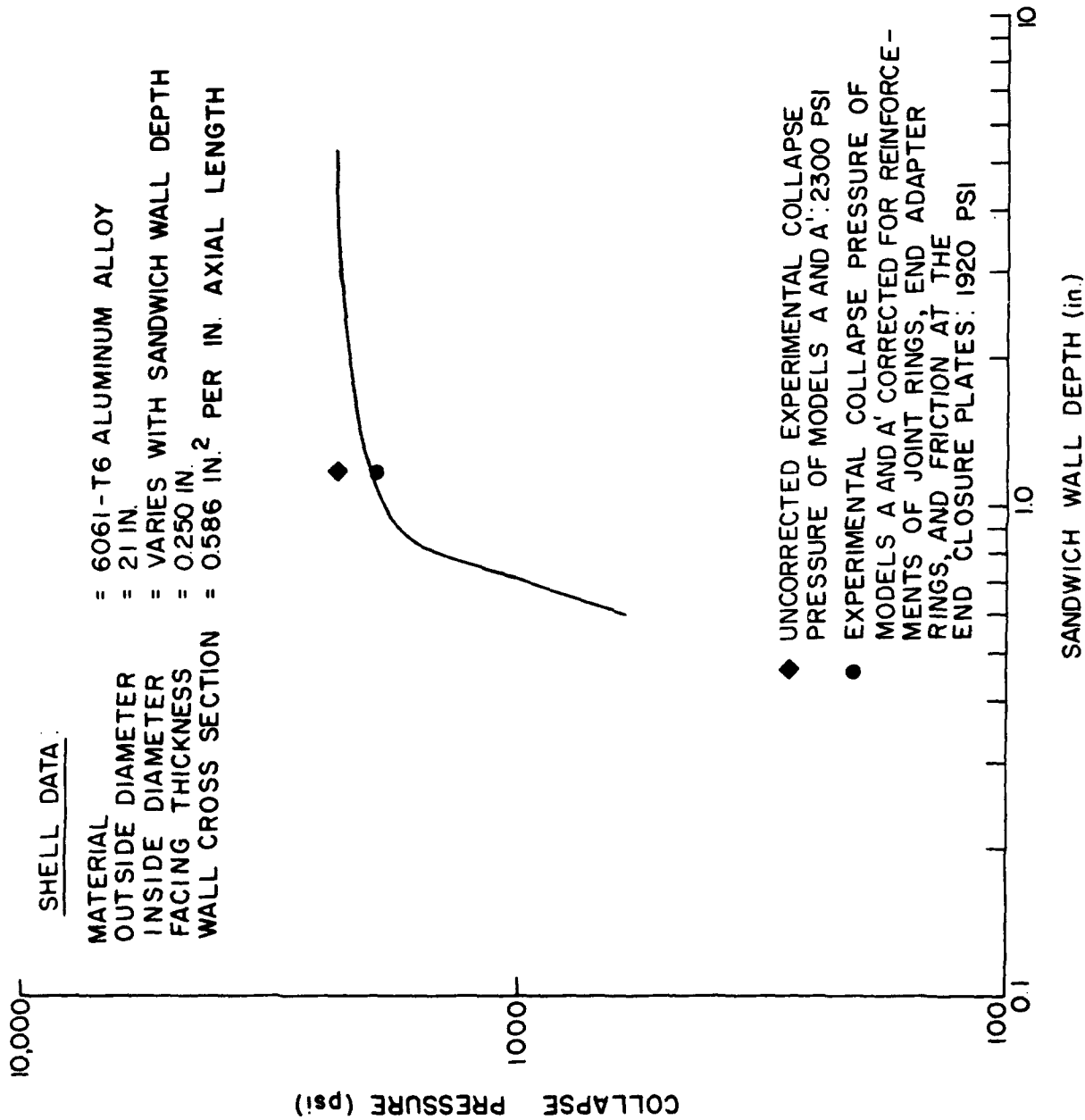


Fig. 28 - Collapse Pressure of an Infinitely Long Aluminum Cellular Sandwich Shell

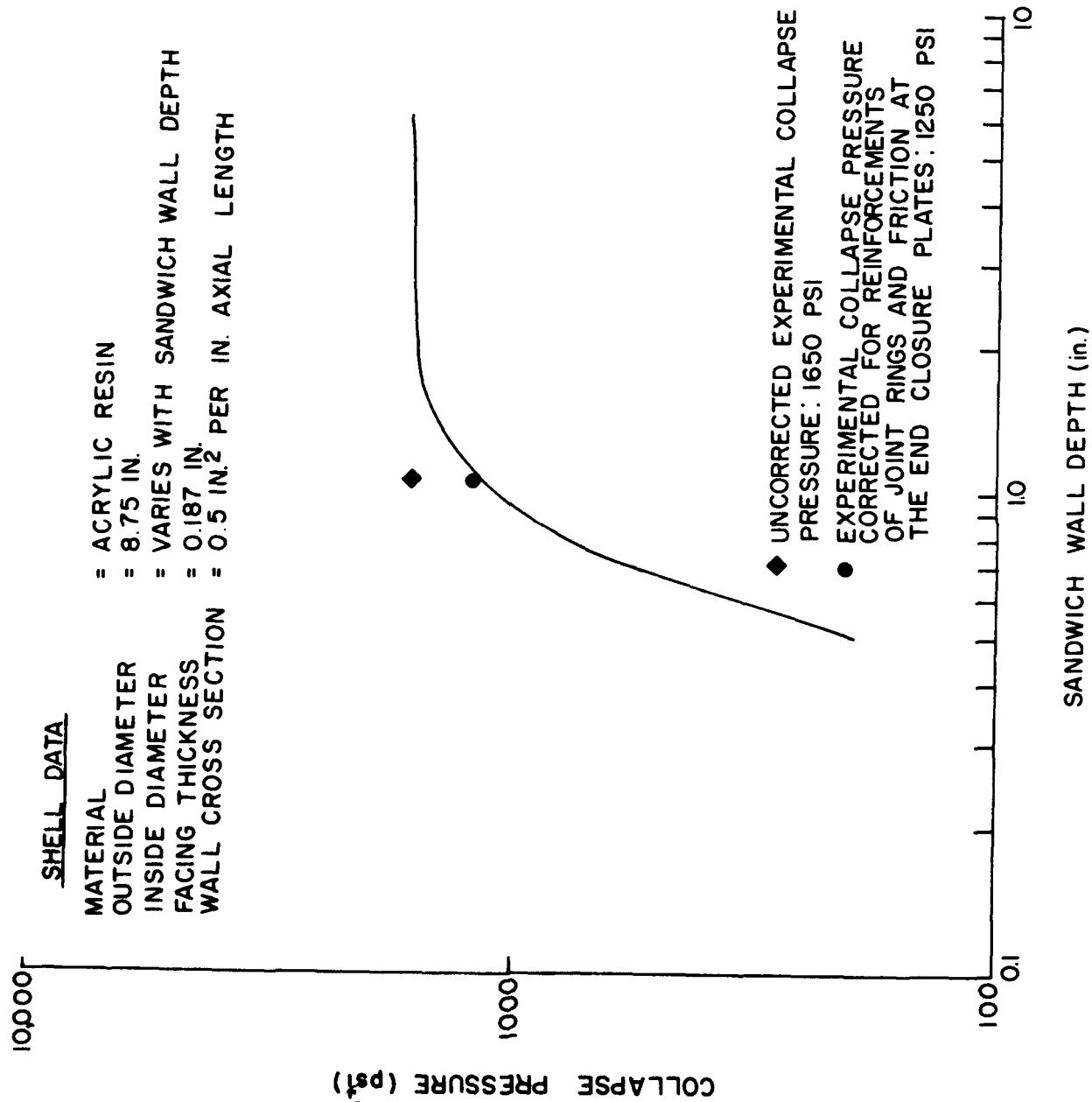


Fig. 29 - Collapse Pressure of an Infinitely Long Acrylic Resin Cellular Sandwich Shell

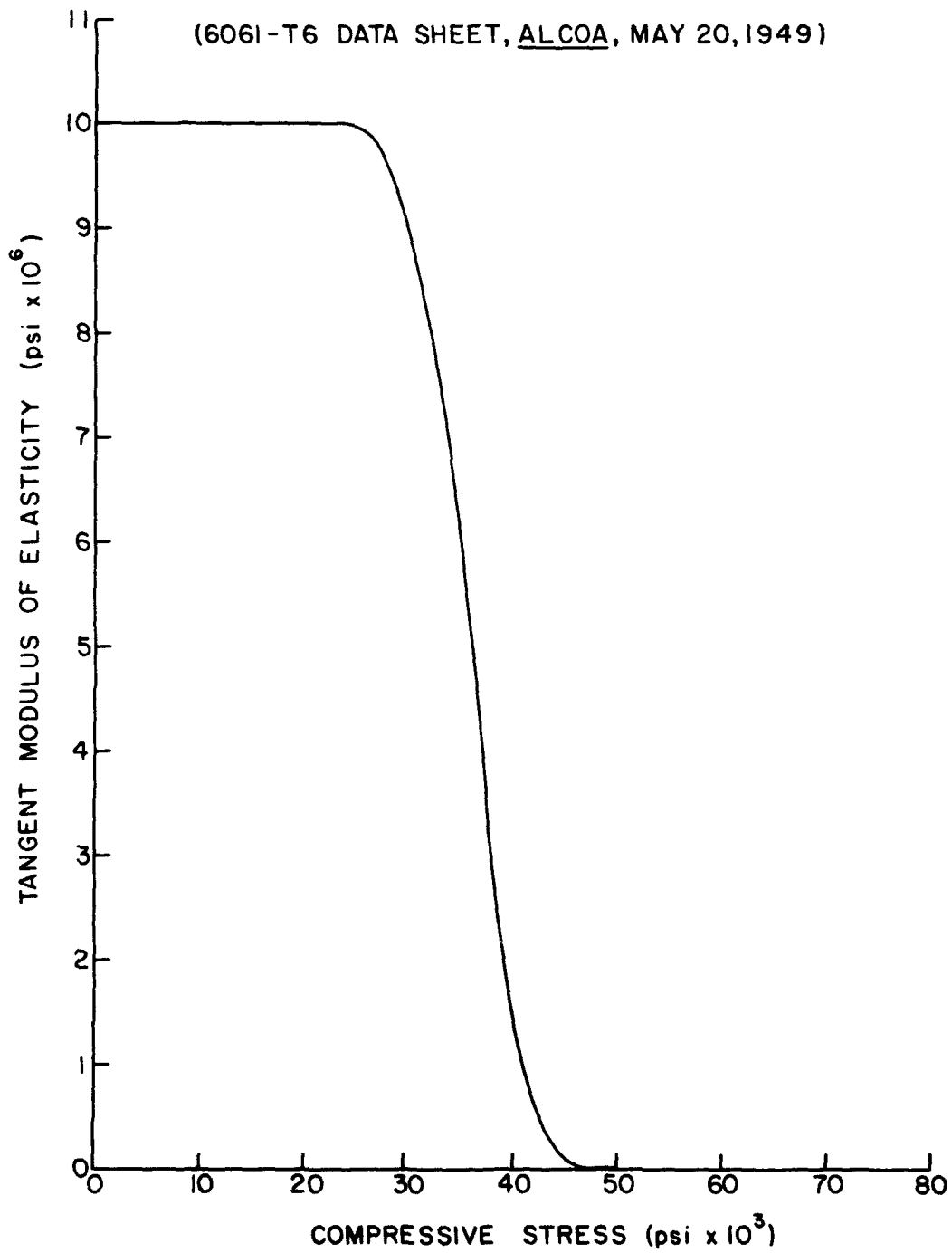


Fig. 30 - Tangent Modulus of Elasticity vs Compressive Stress for 6061-T6 Aluminum Alloy

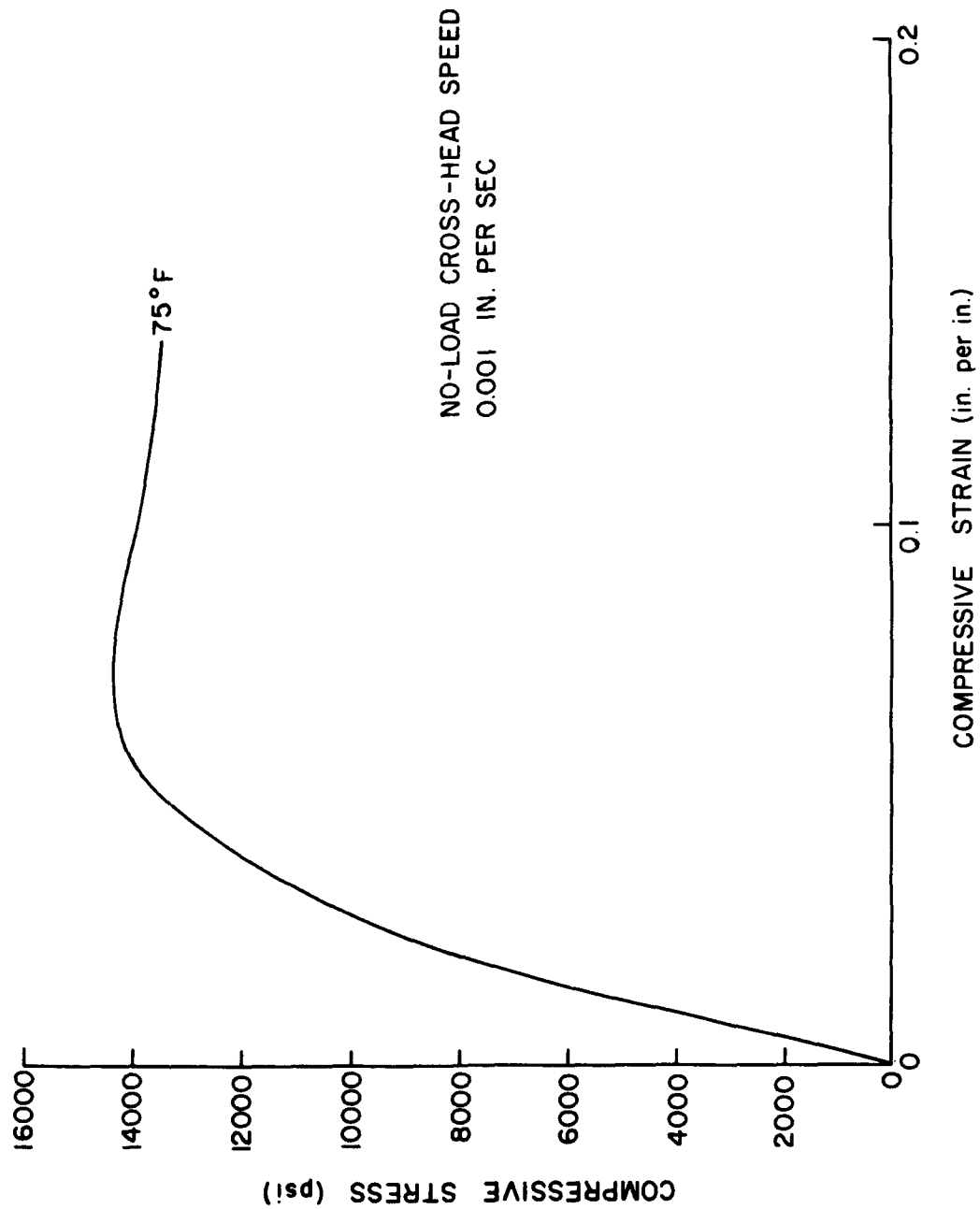


Fig. 31 - Stress-Strain Curve for Acrylic Resin Shell Material

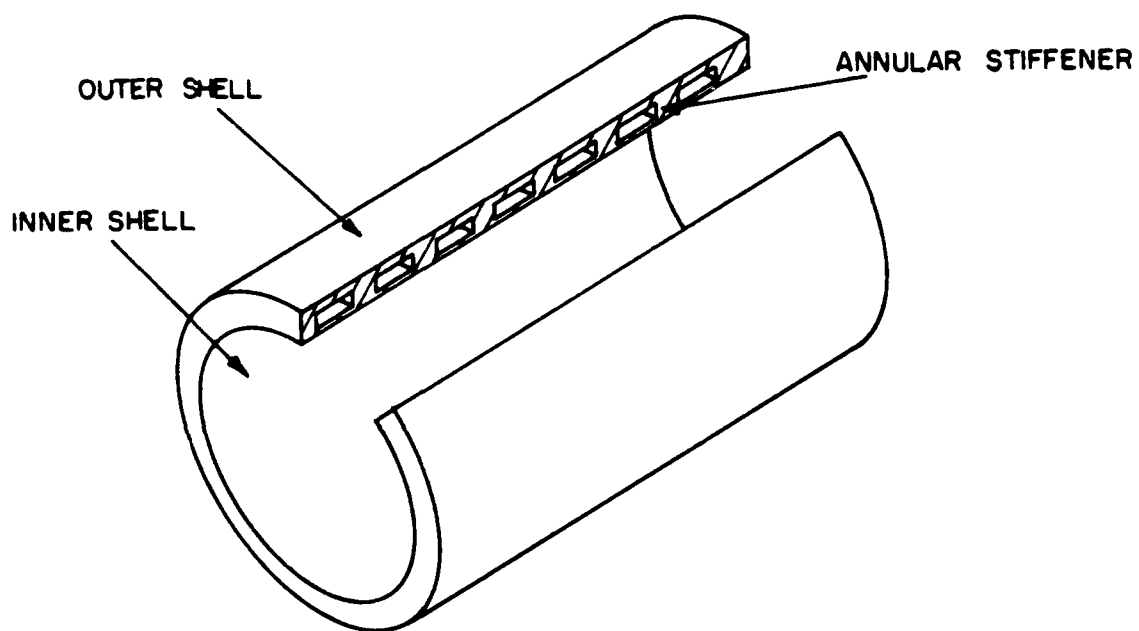


Fig. 1 - Cellular Shell

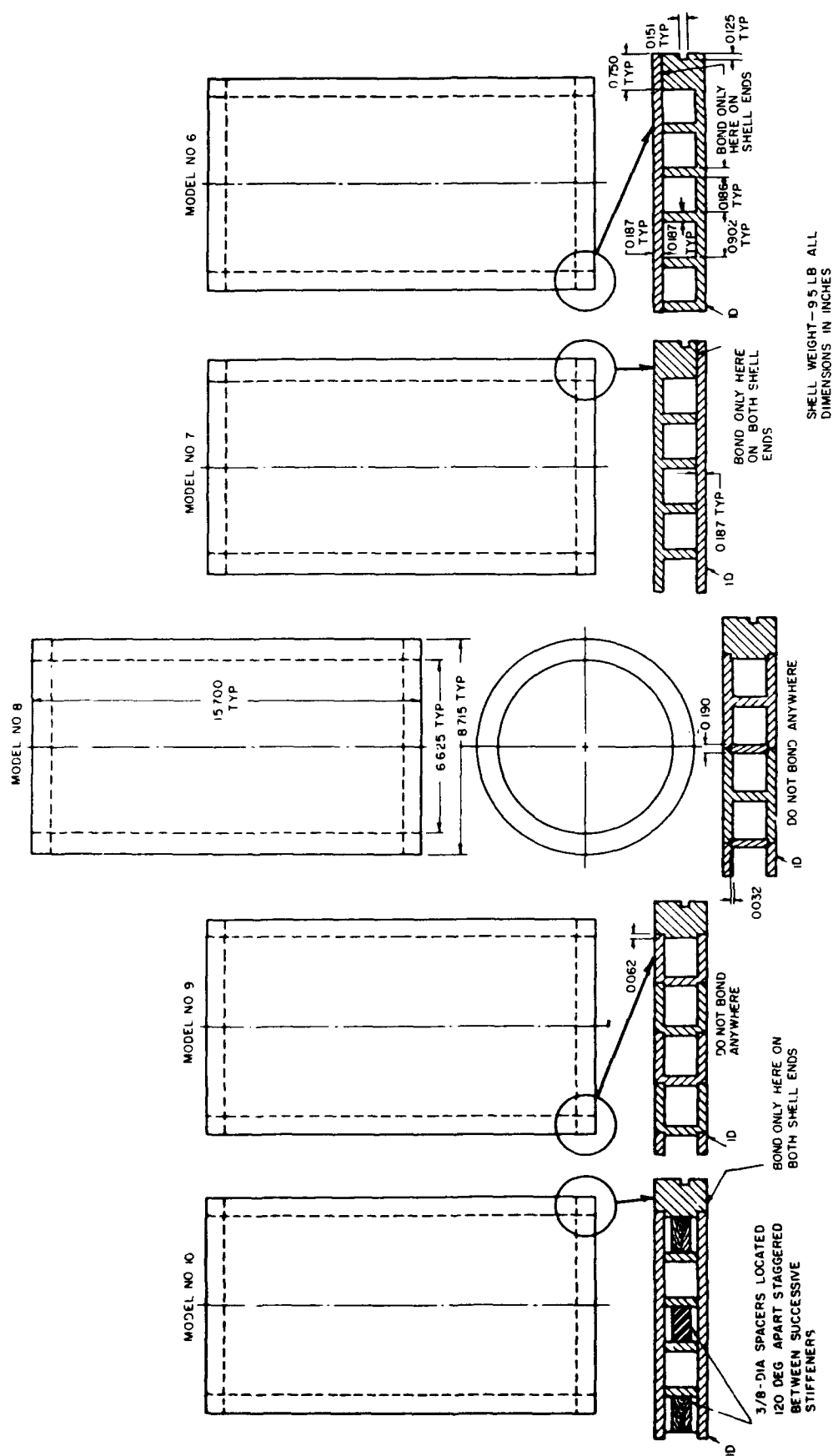
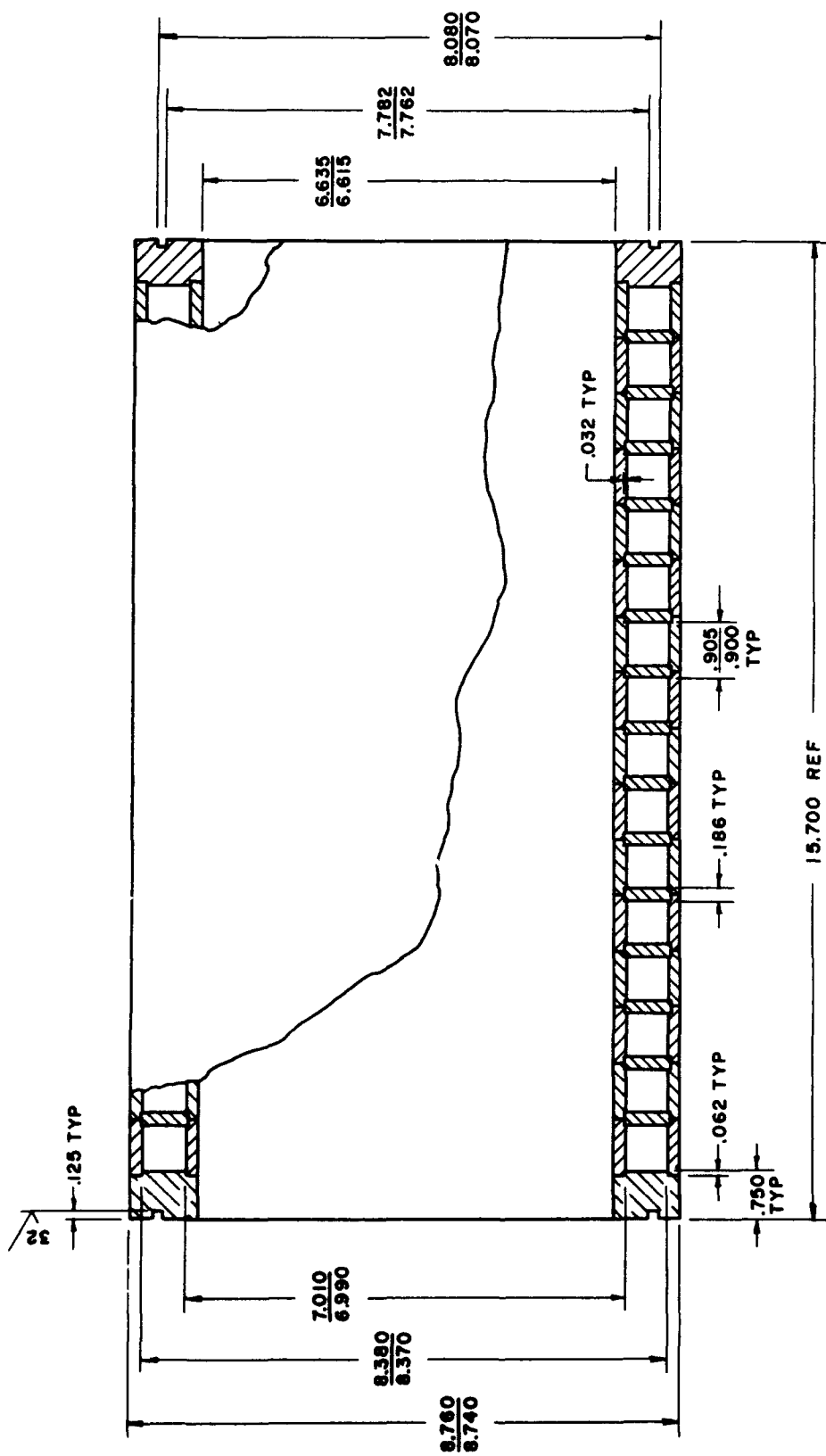


Fig. 2 - Acrylic Resin Cellular Shells (Models 6 through 10)



SHELL WEIGHT — 9.6 LB
ALL DIMENSIONS IN INCHES

Fig. 3 - Acrylic Resin Cellular Shell (Model 11)

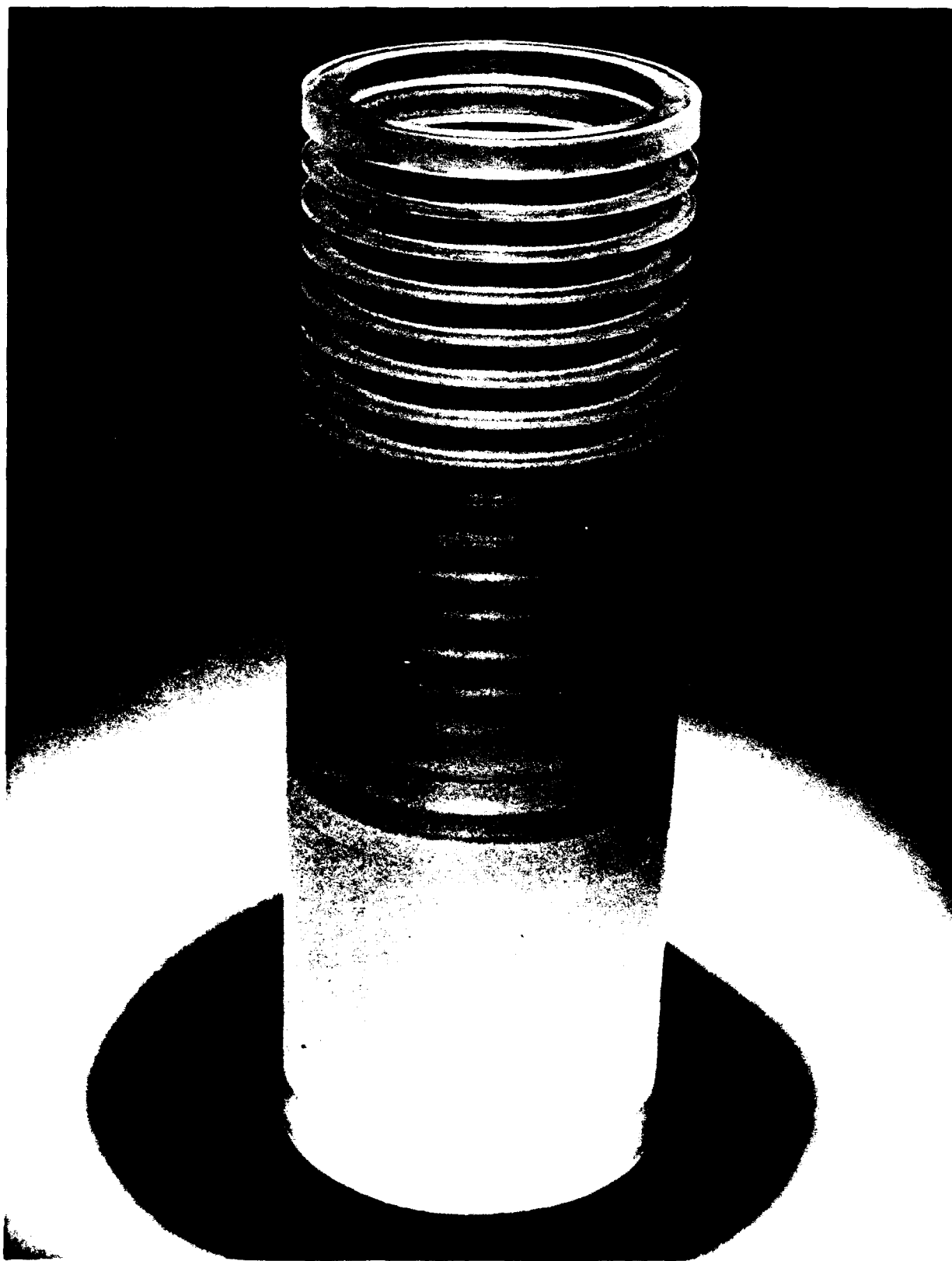


Fig. 4 - Assembly of Model 6

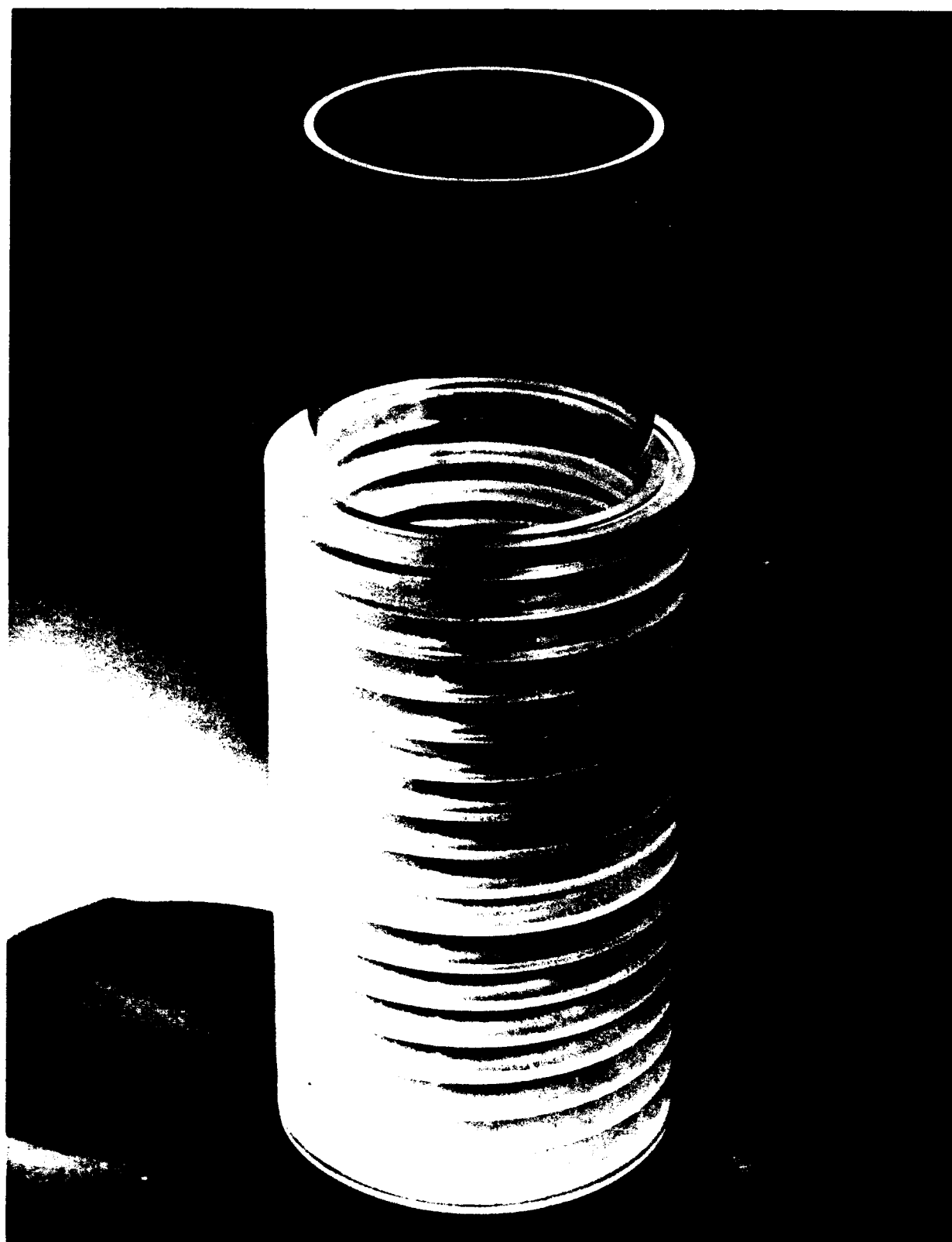


Fig. 5 - Assembly of Model 7



Fig. 6 - Assembly of Model 8



Fig. 7 - U-Ring Module Used in Assembly of Model 9

EXTERNAL PRESSURE (psi)

2800
2400
2000
1600
1200
800
400
0

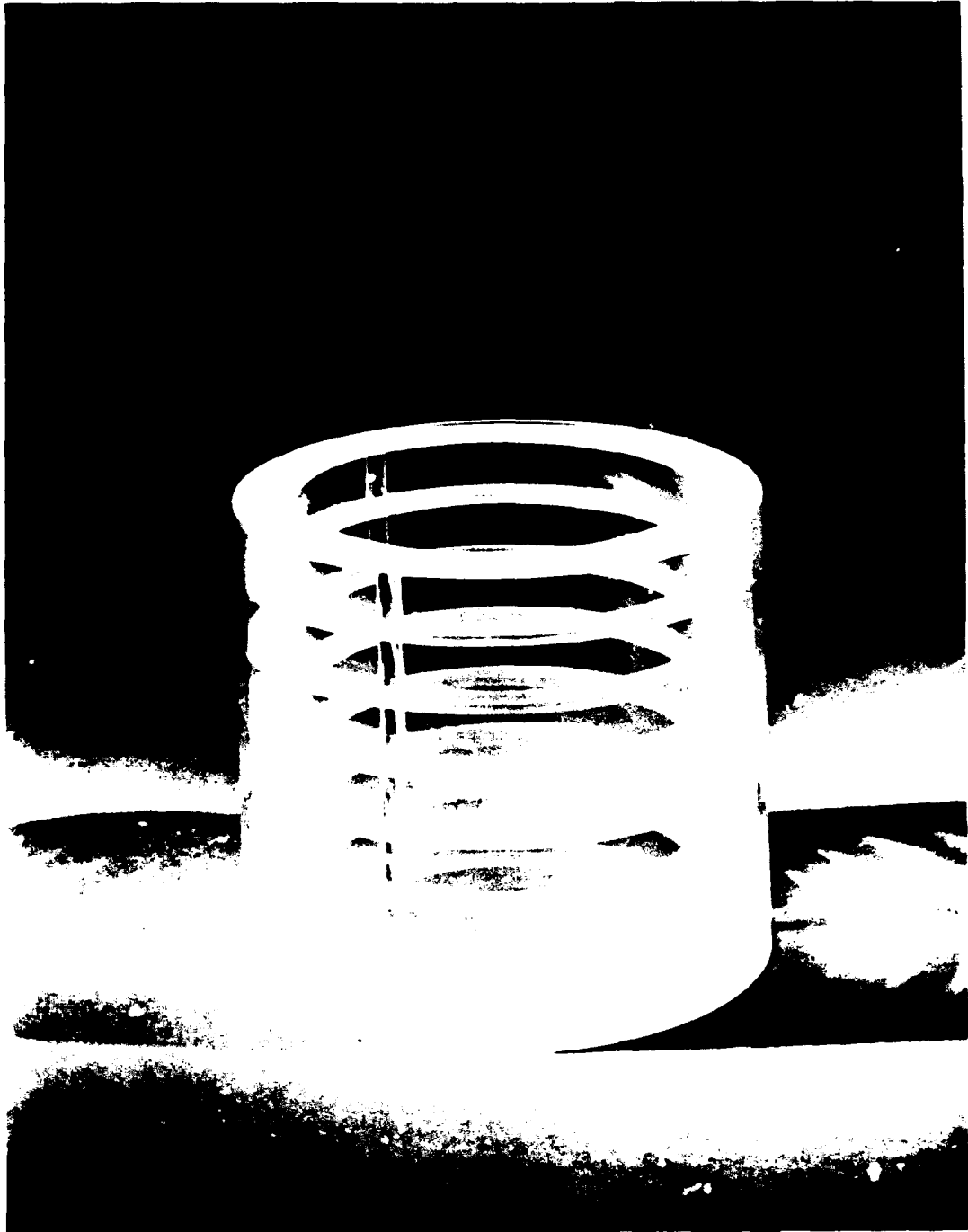


Fig. 8 - Detail of Model 10 Assembly



Fig. 9 - Structural Modules of Model 11

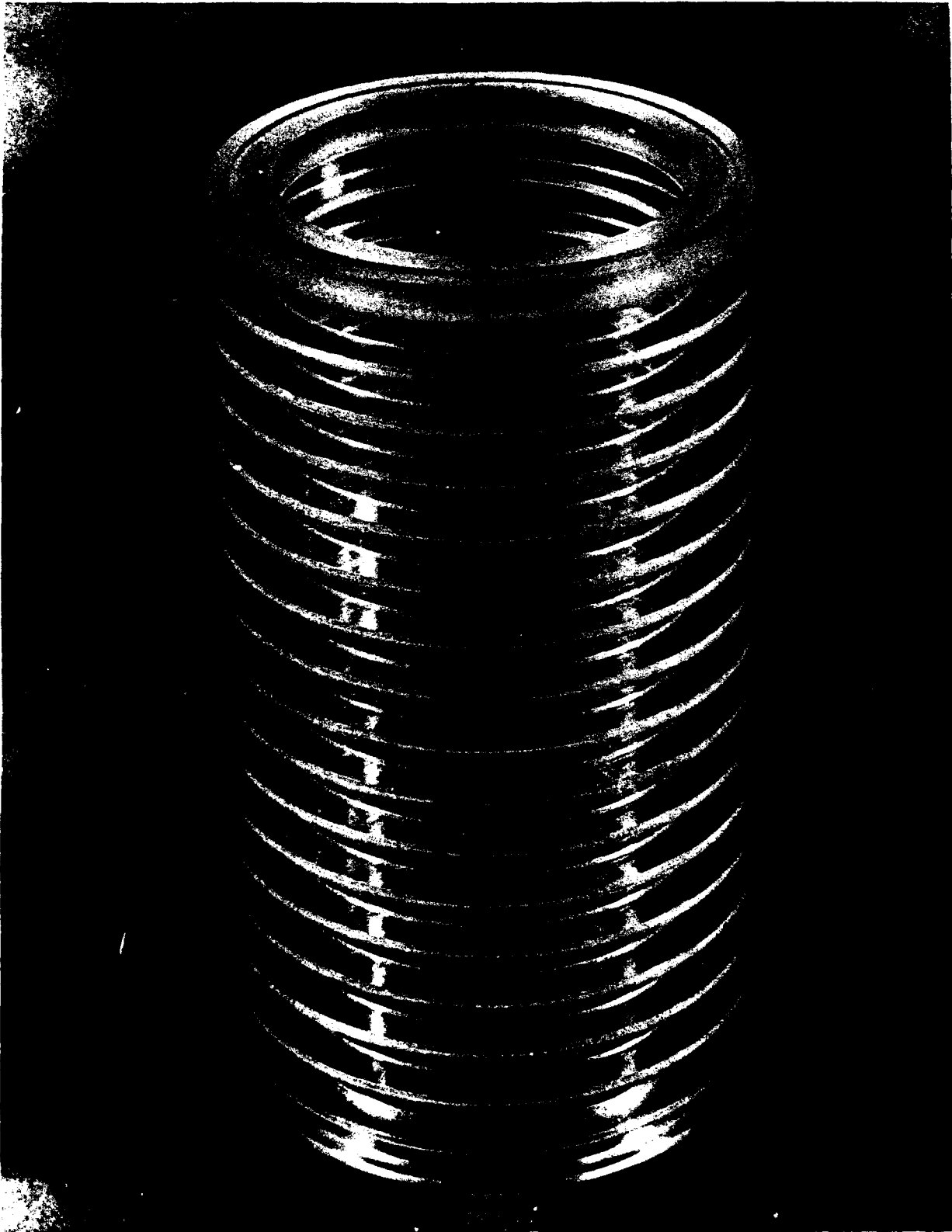


Fig. 10 - Assembly of Model 11

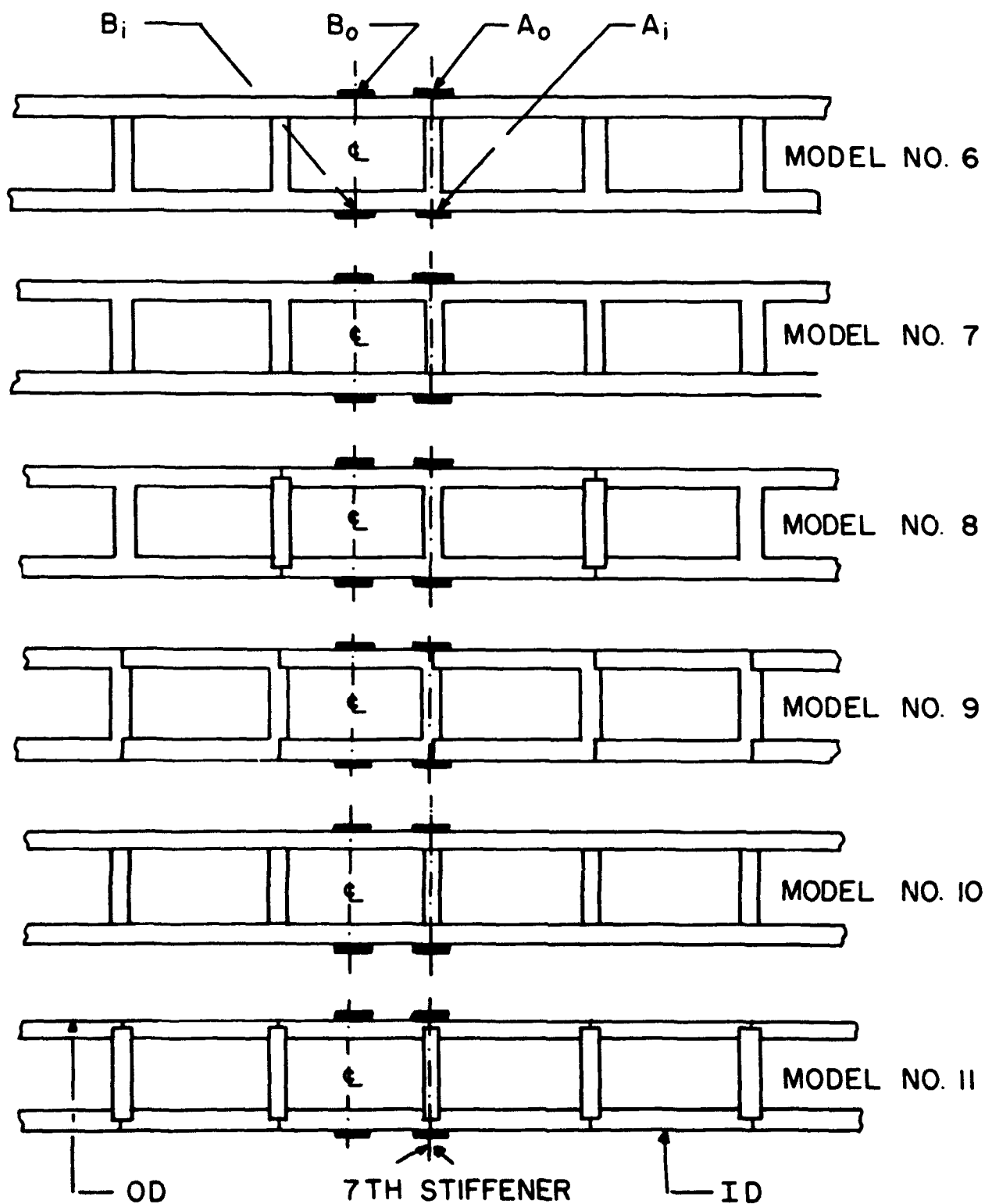


Fig. 11 - Location of Strain Gages on Acrylic Resin Cellular Shells



Fig. 12 - Equipment for Pressure Testing Acrylic Resin Shells



Fig. 13 - End Closure for Acrylic Resin Shells

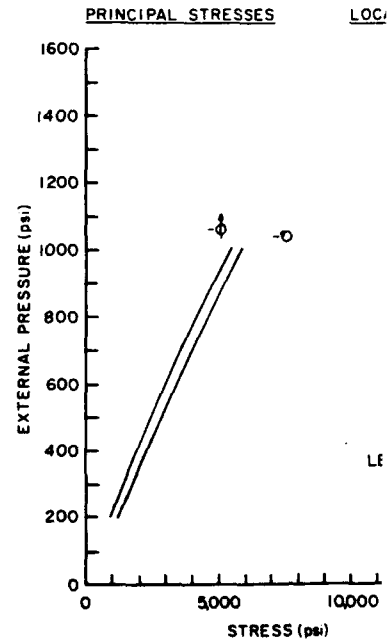
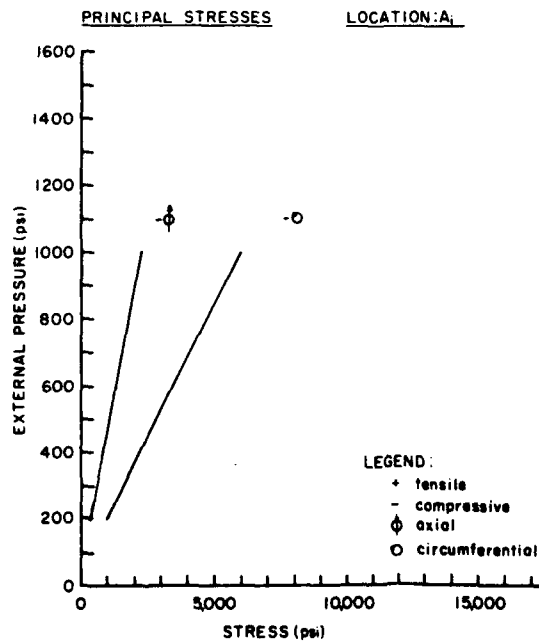
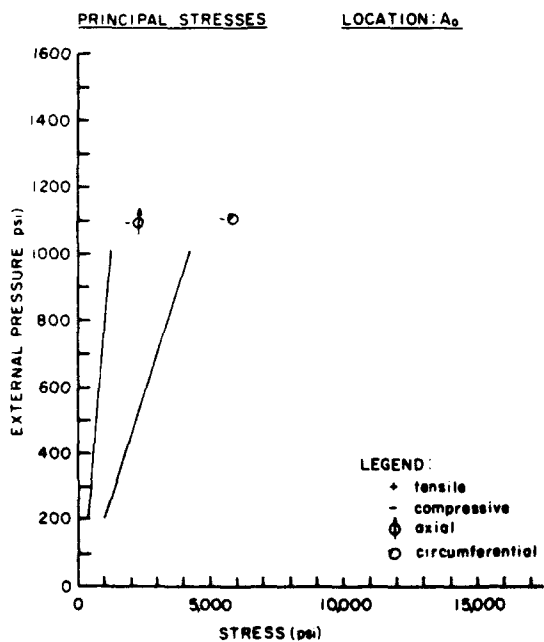
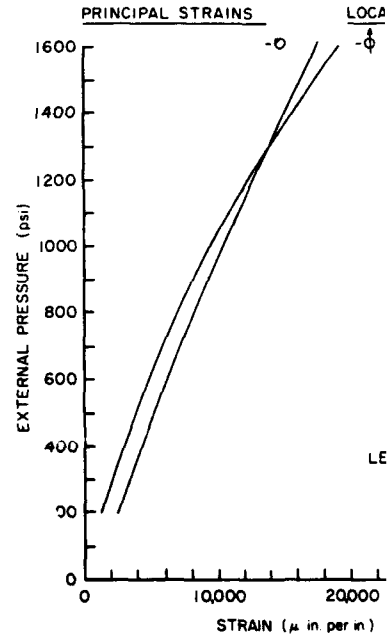
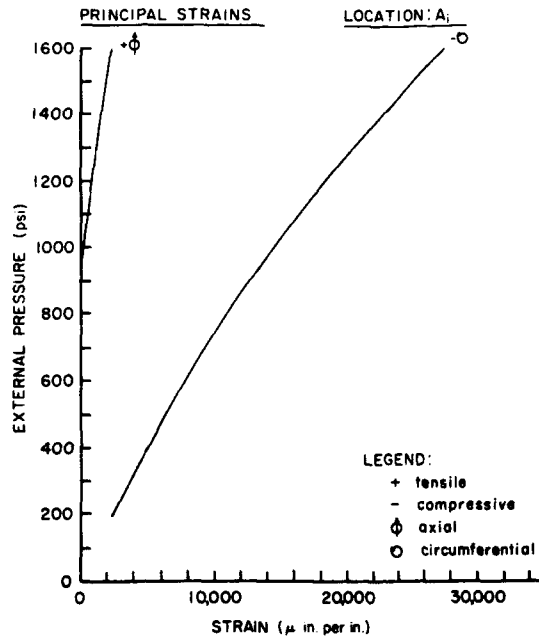
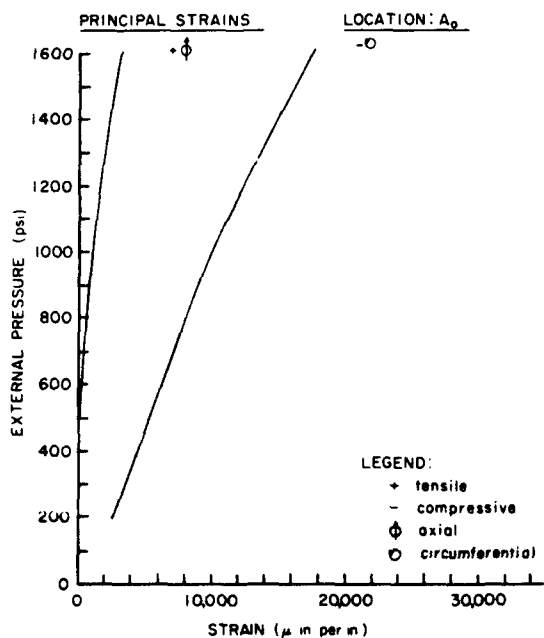
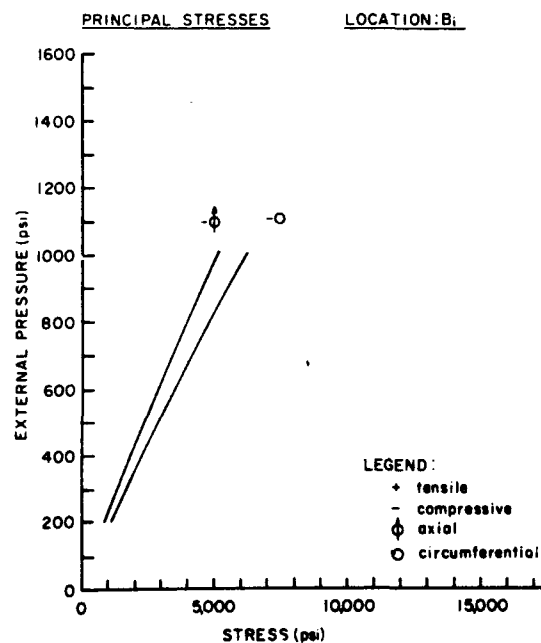
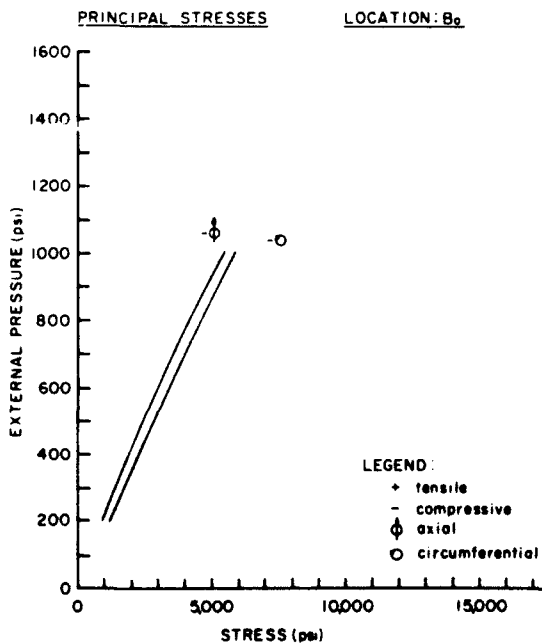
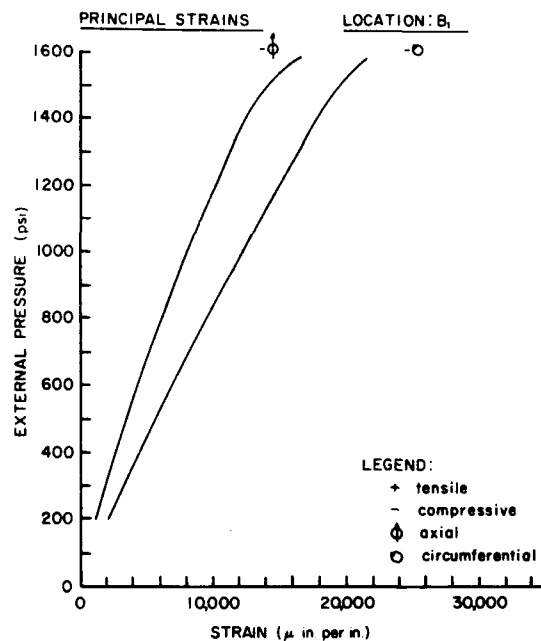
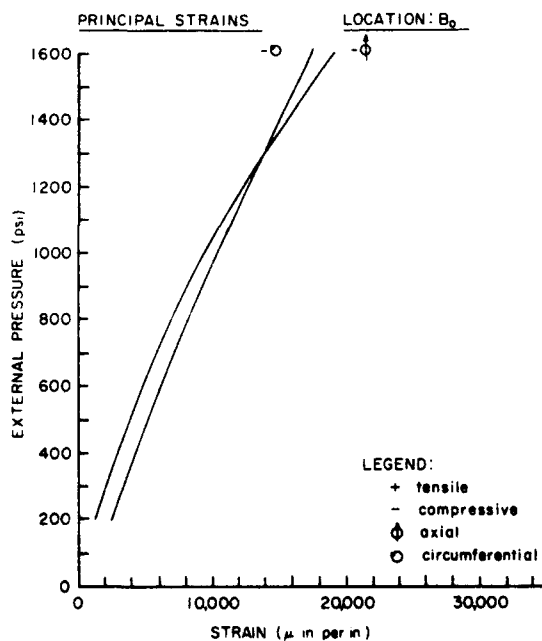


Fig. 14 - Principal Stresses and Strains in Model 6



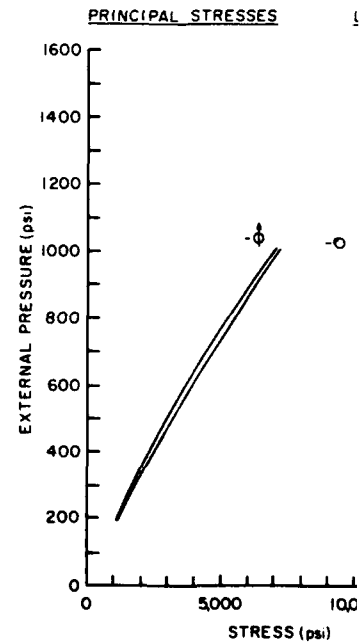
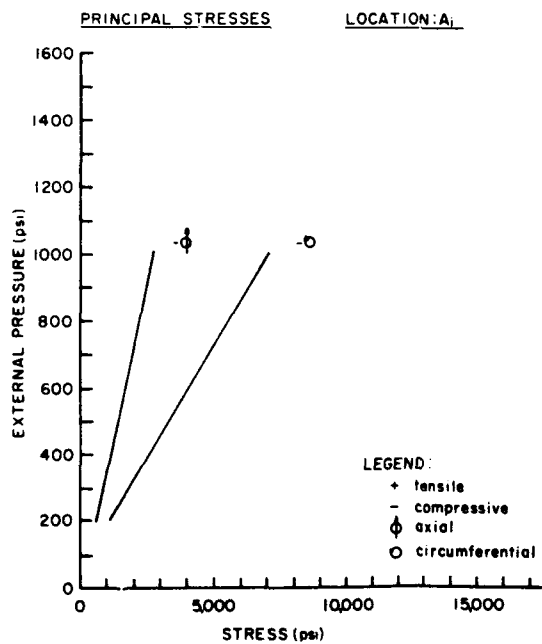
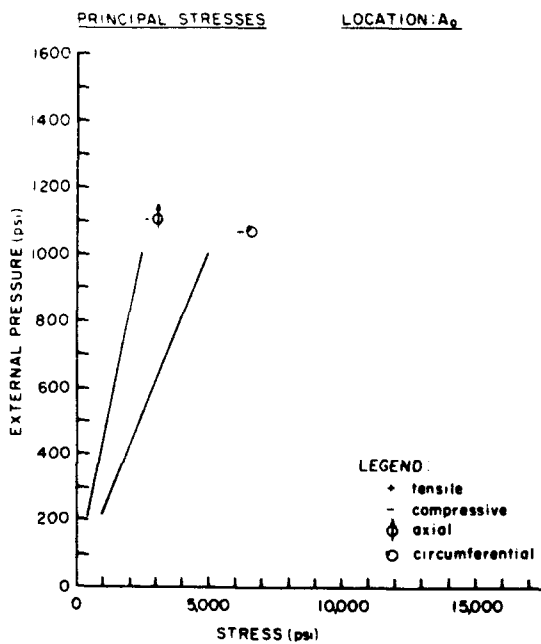
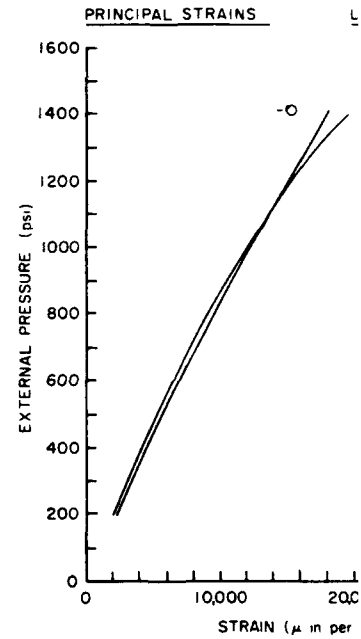
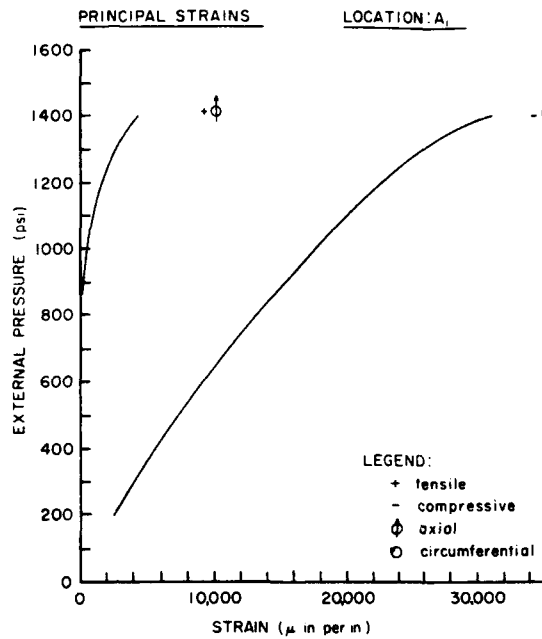
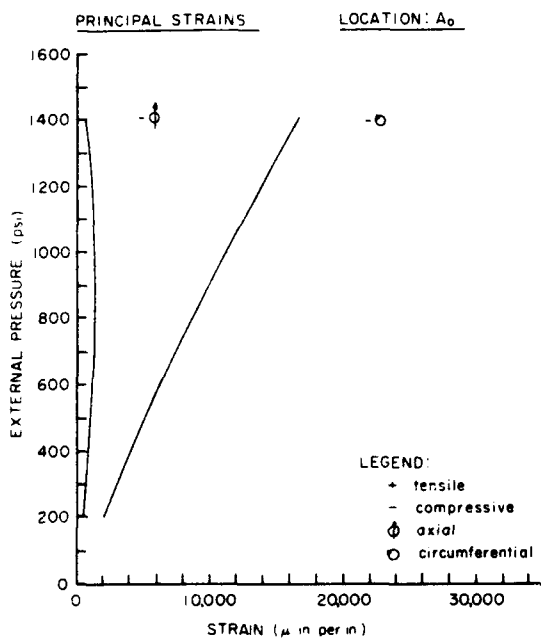


Fig. 15 - Principal Stresses and Strains in Model 7

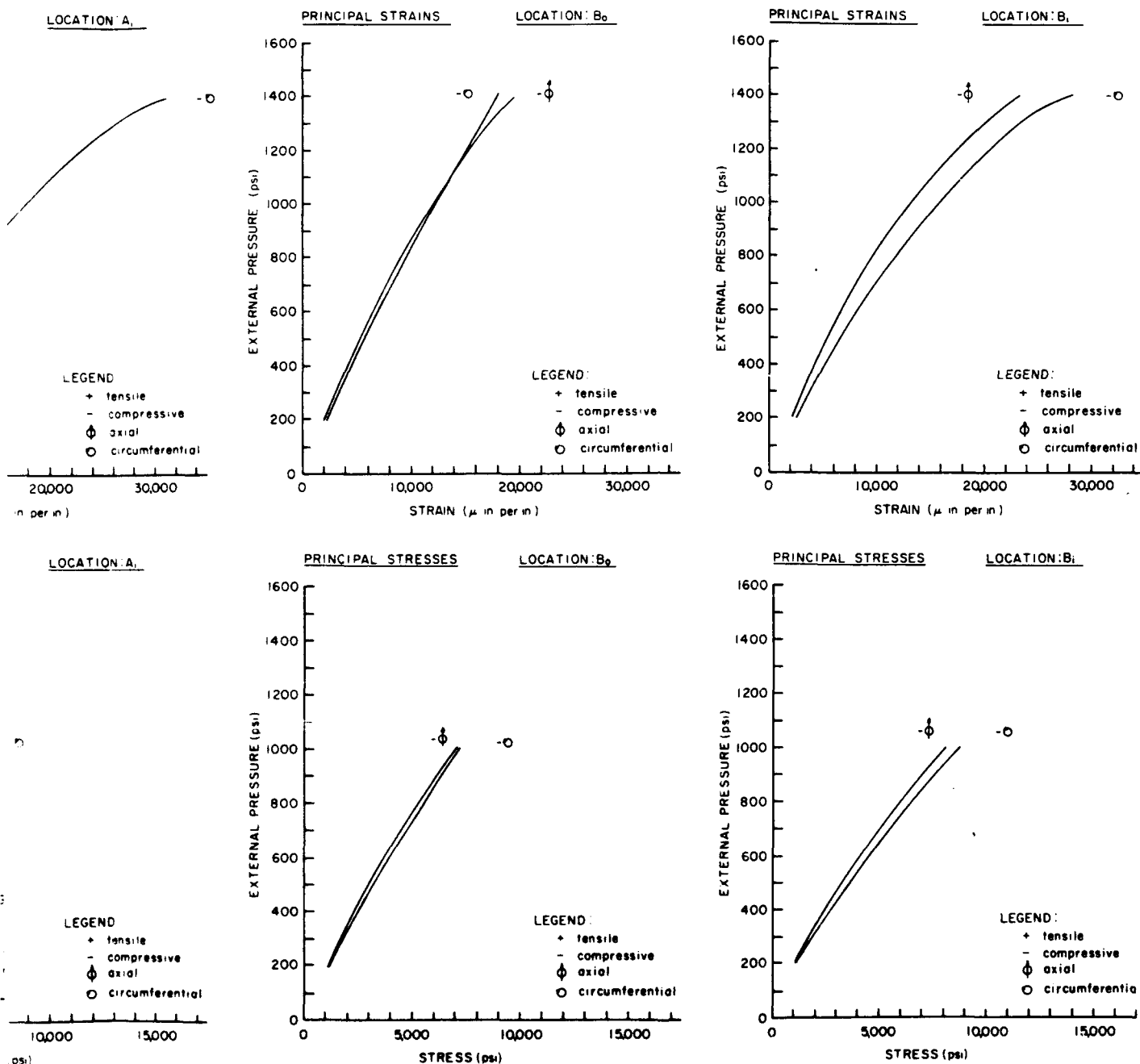


Fig. 15 - Principal Stresses and Strains in Model 7

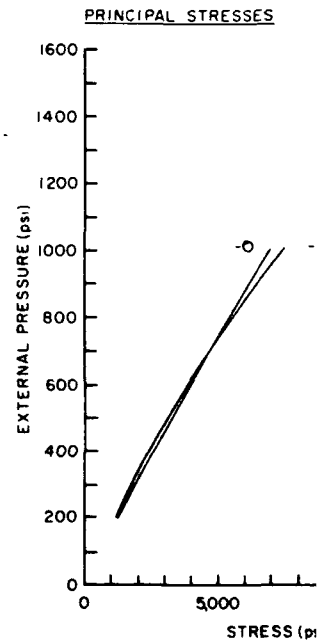
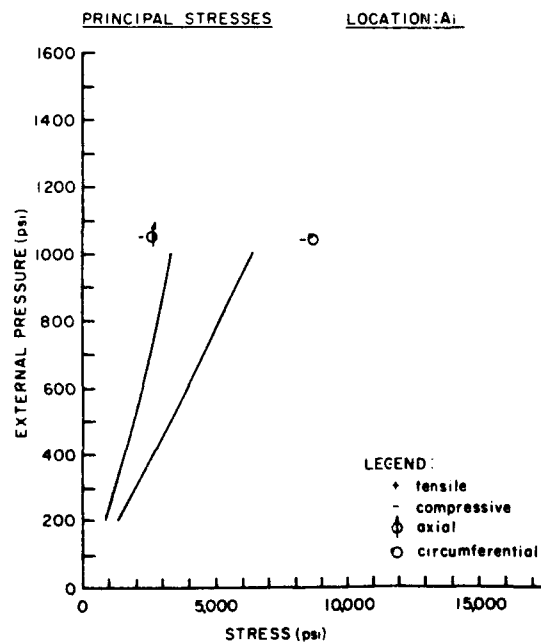
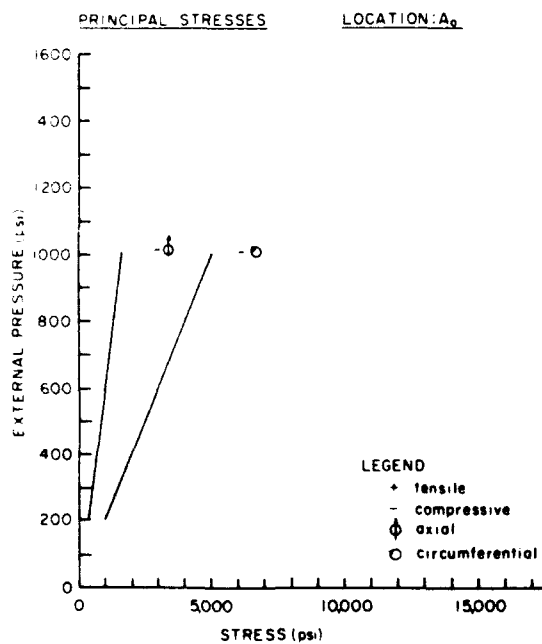
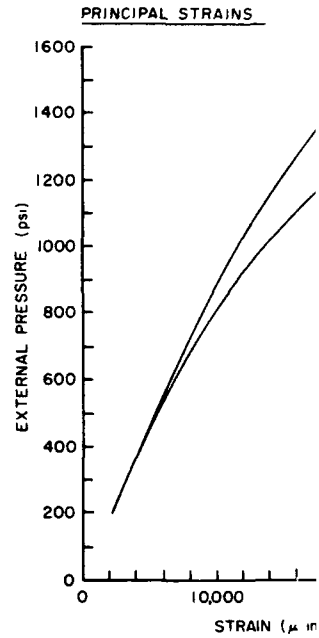
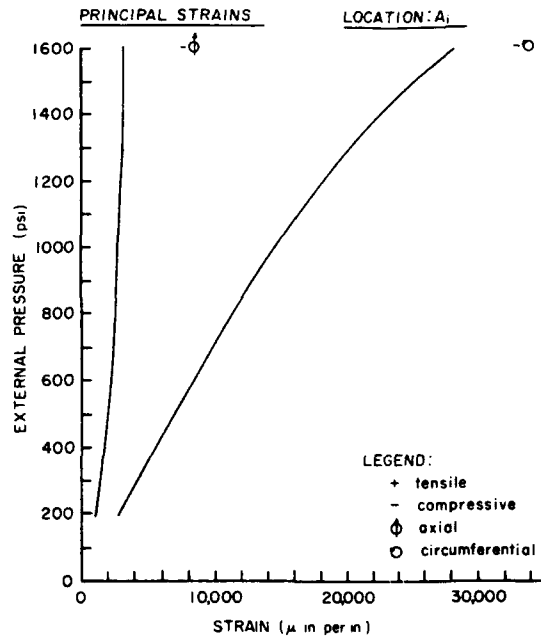
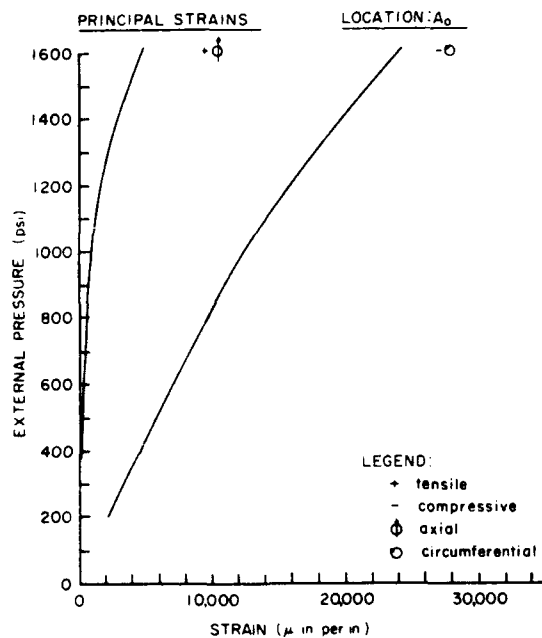
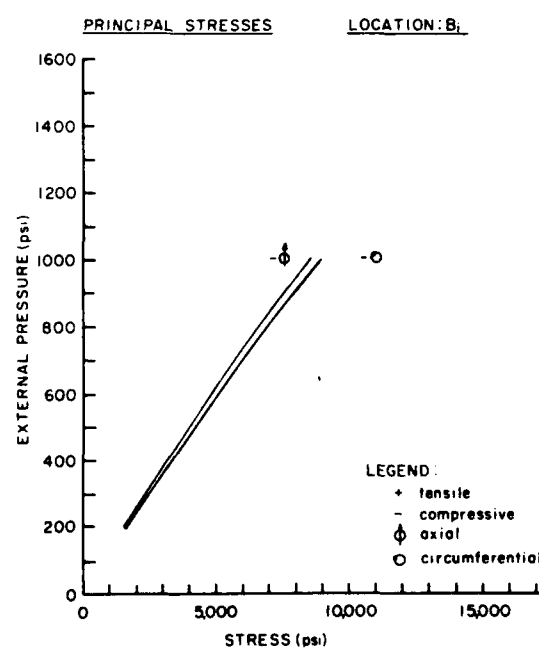
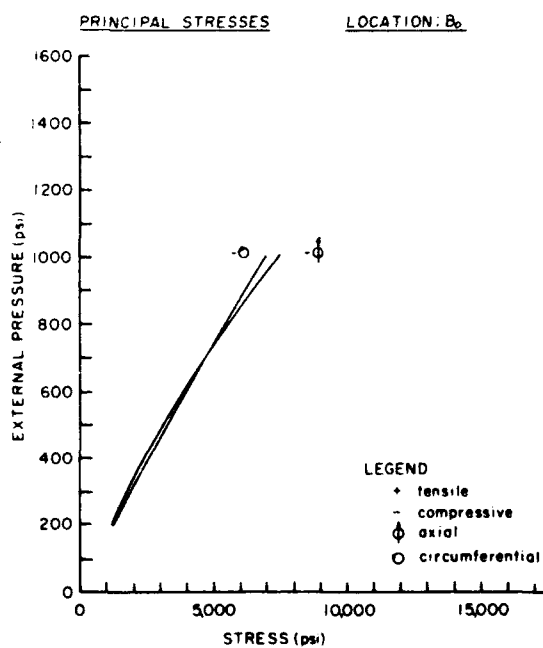
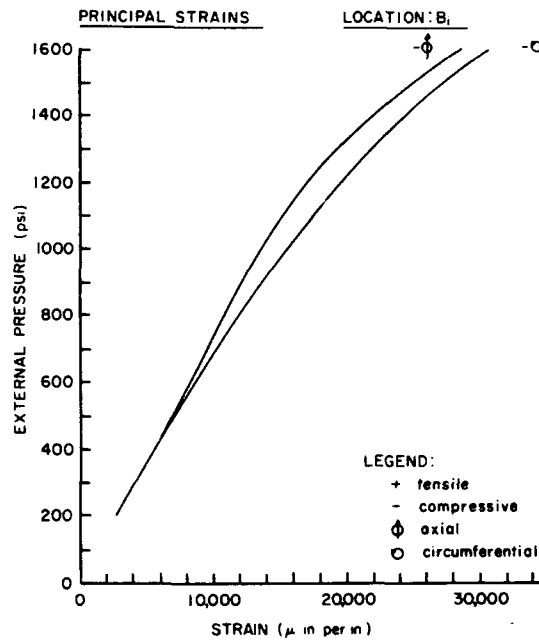
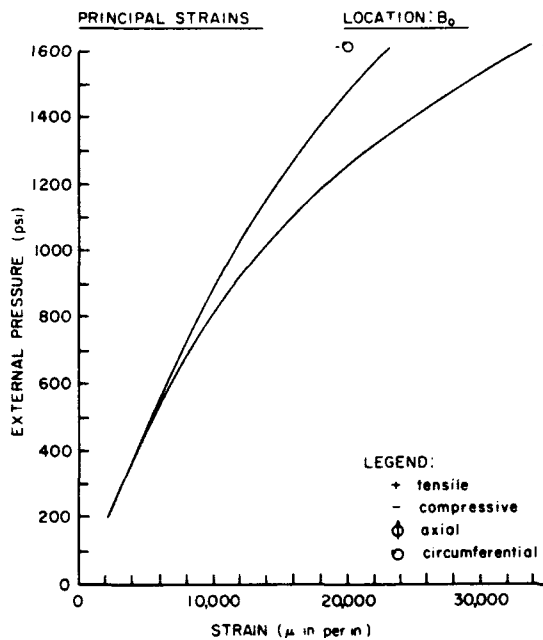
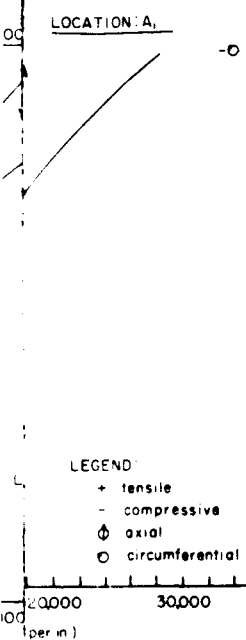


Fig. 16 - Principal Stresses and Strains in Model 8



6 - Principal Stresses and Strains in Model 8

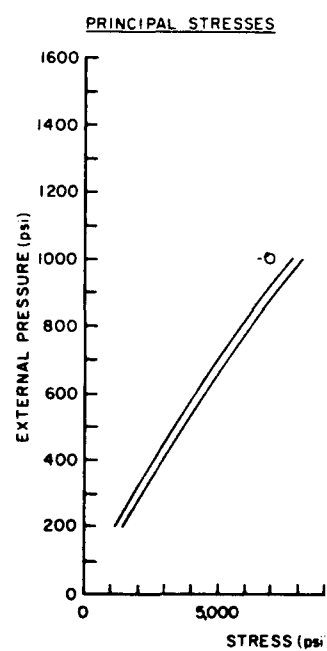
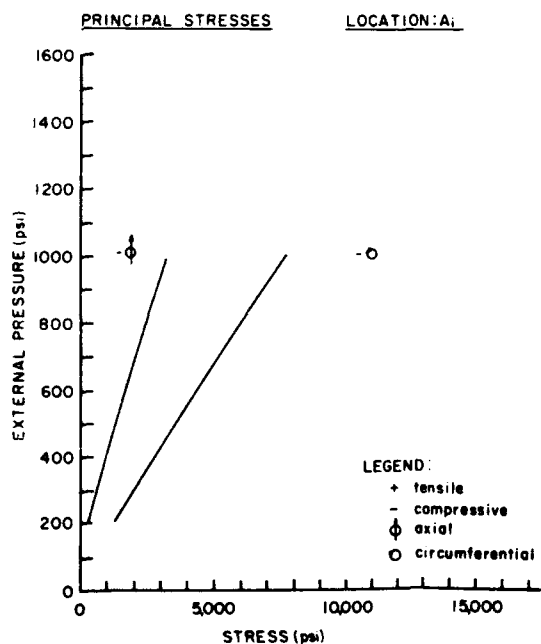
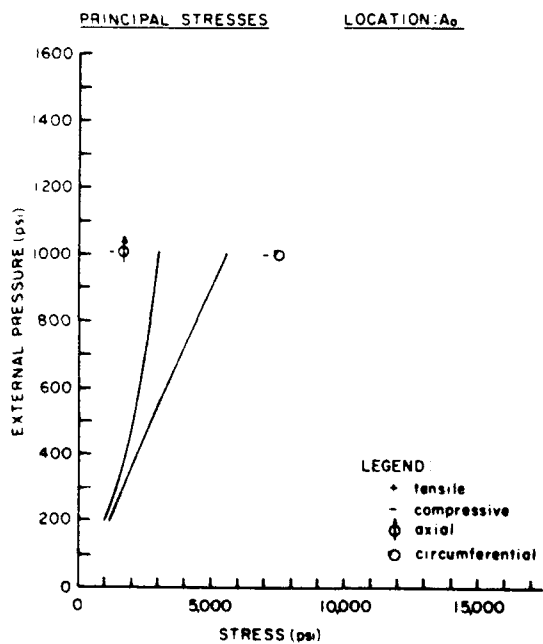
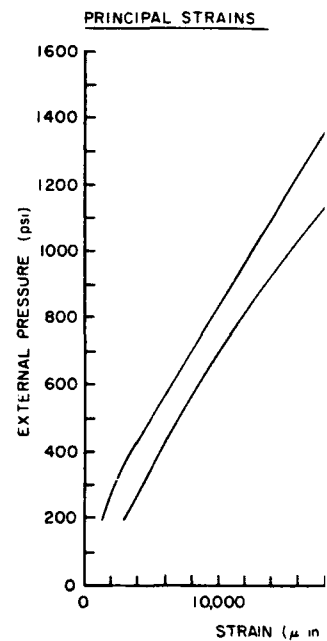
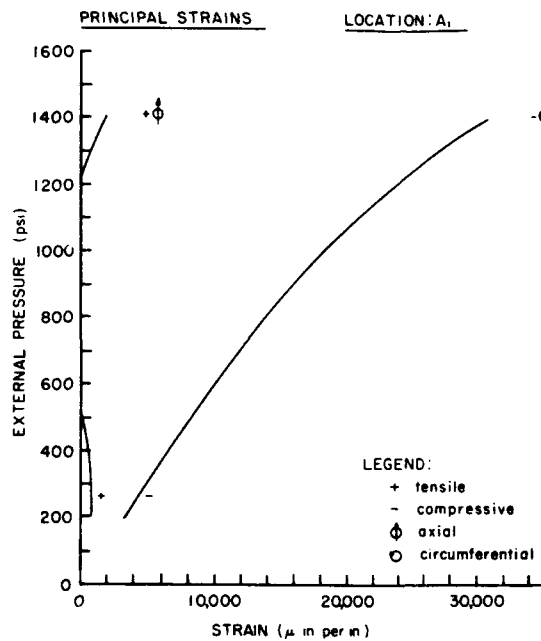
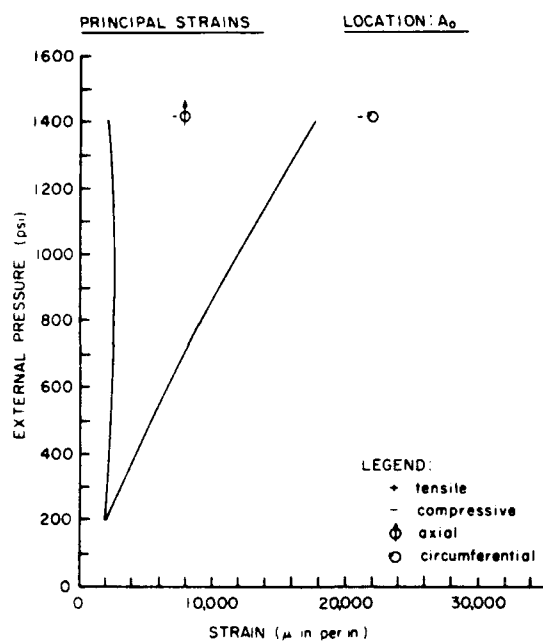
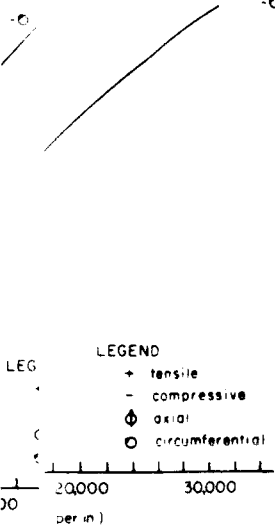
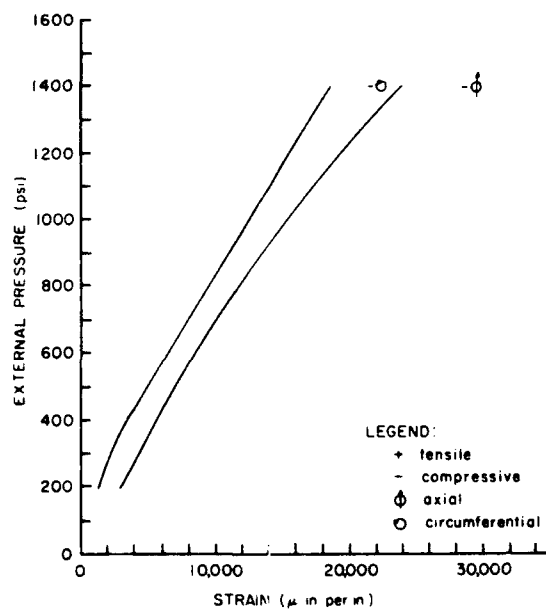


Fig. 17 - Principal Stresses and Strains in Model 9

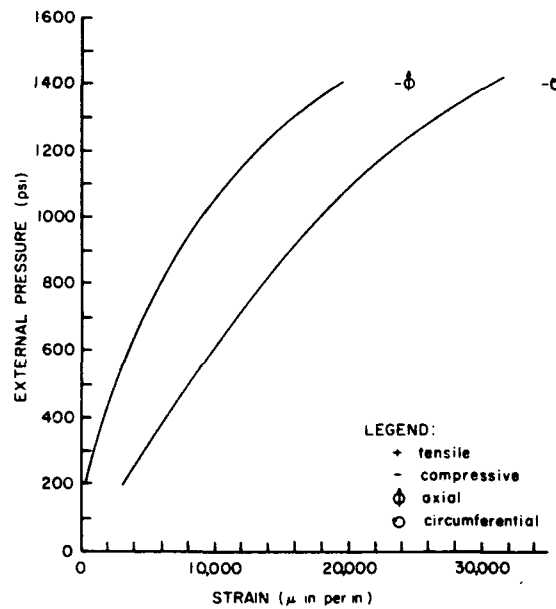
DCA1

LOCATION: A₁

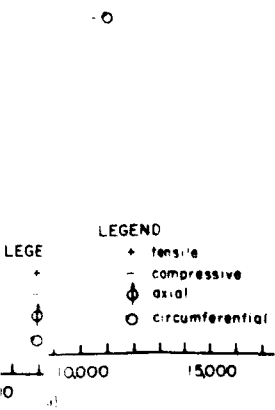
PRINCIPAL STRAINS

LOCATION: B₀

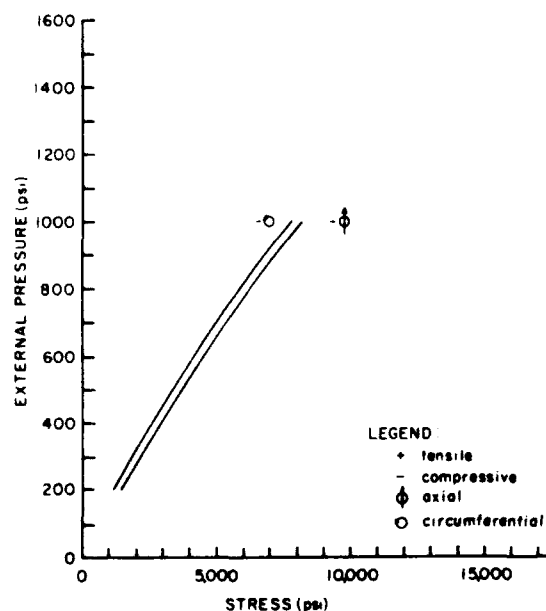
PRINCIPAL STRAINS

LOCATION: B₁

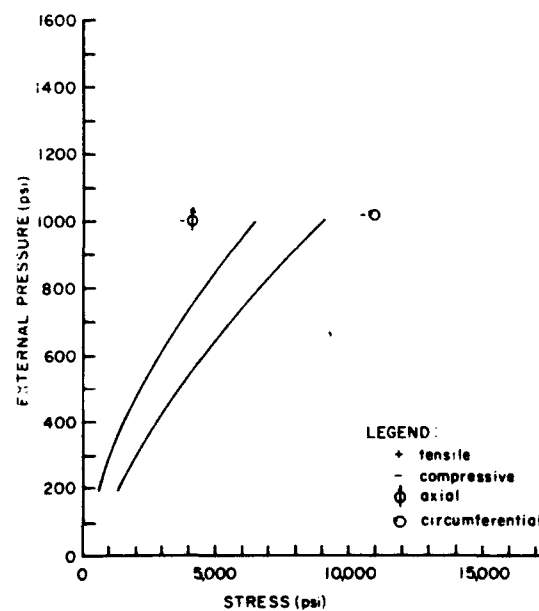
DCA1

LOCATION: A₁

PRINCIPAL STRESSES

LOCATION: B₀

PRINCIPAL STRESSES

LOCATION: B₁

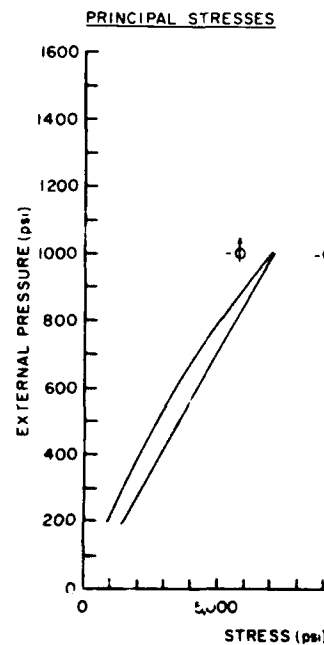
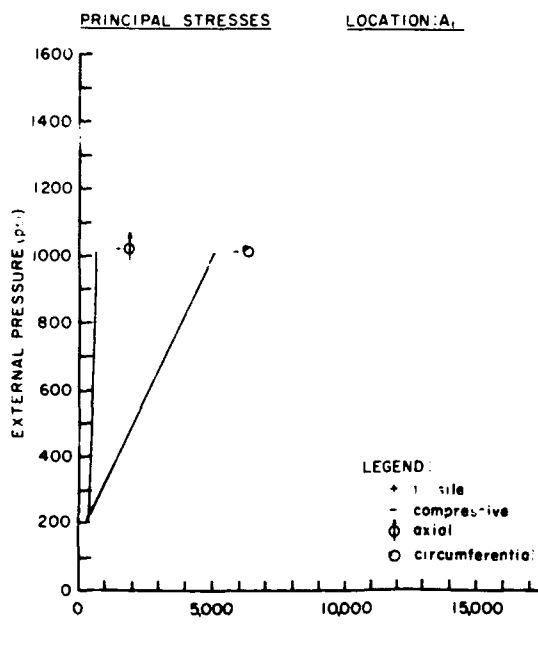
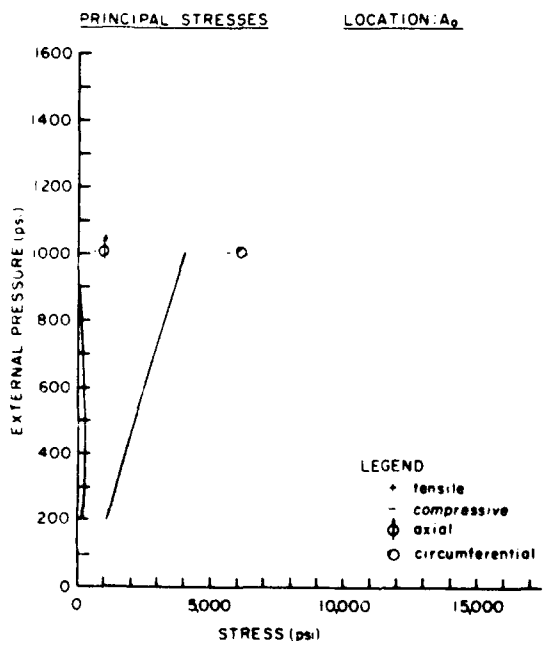
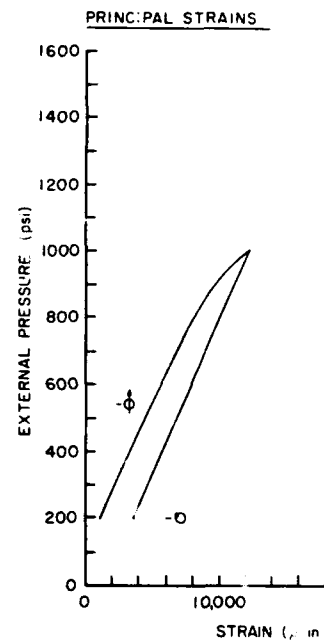
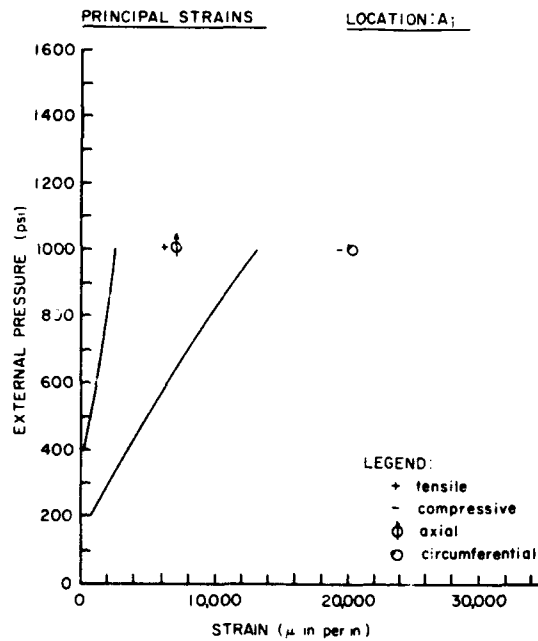
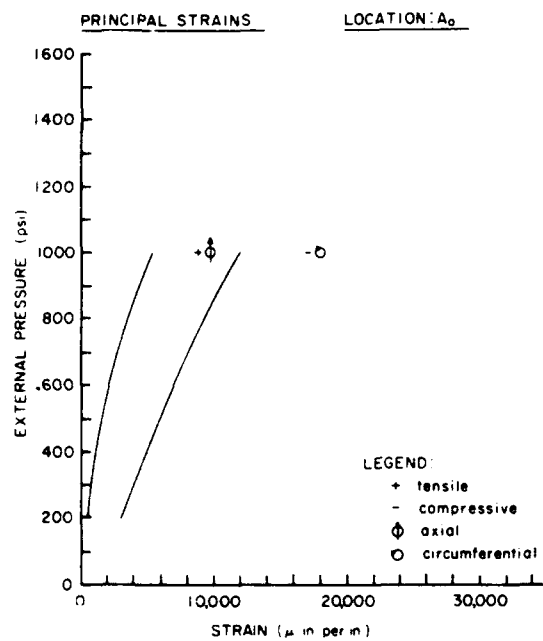
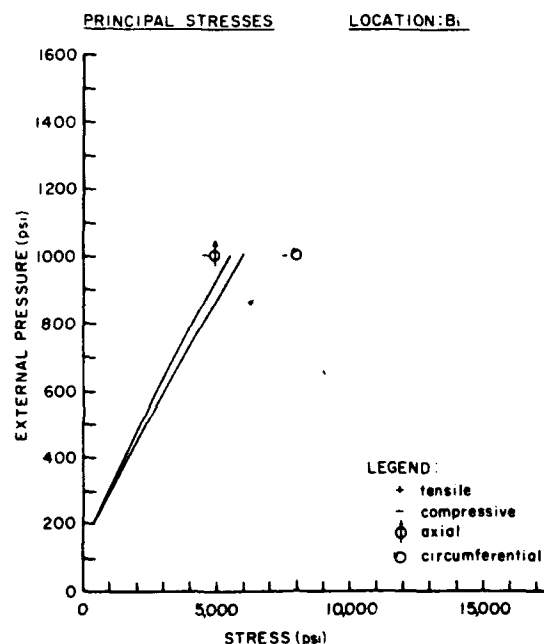
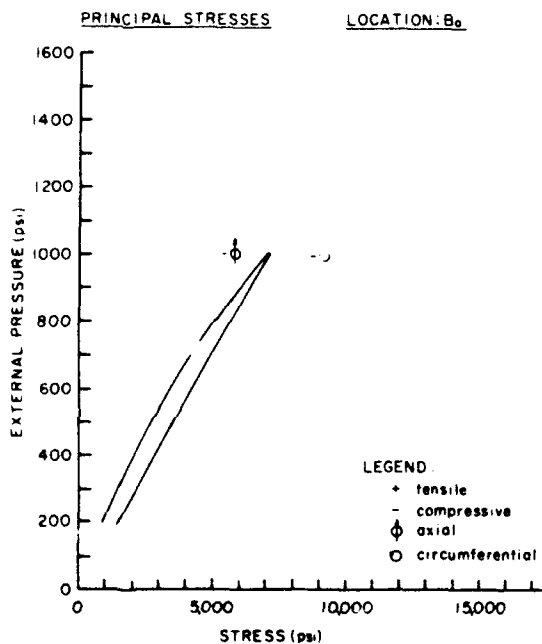
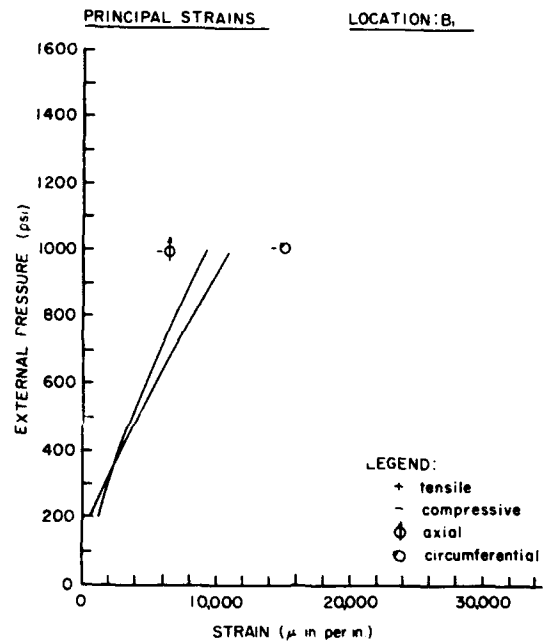
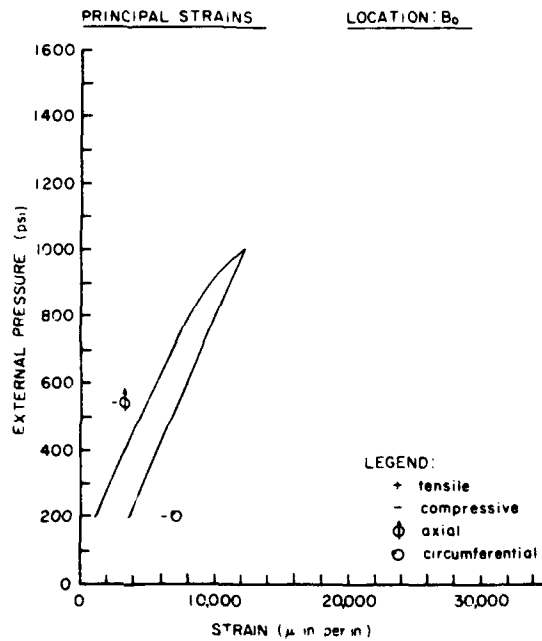
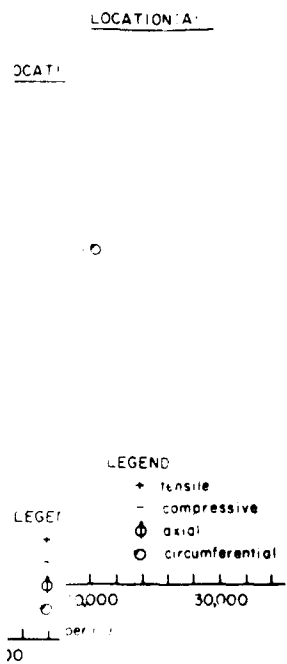


Fig. 18 - Principal Stresses and Strains in Model 10



8 - Principal Stresses and Strains in Model 10

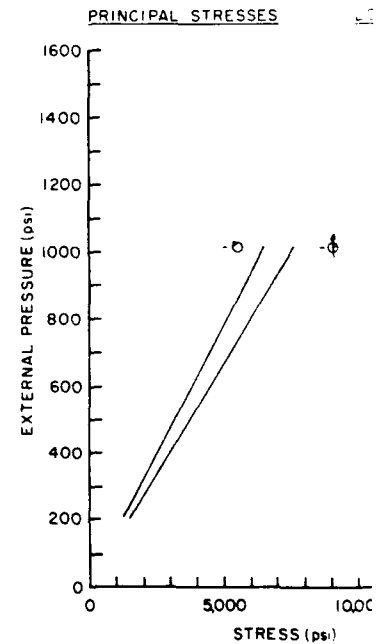
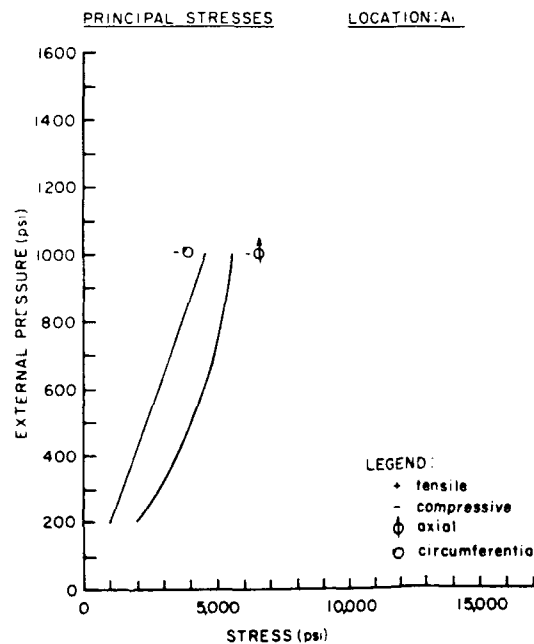
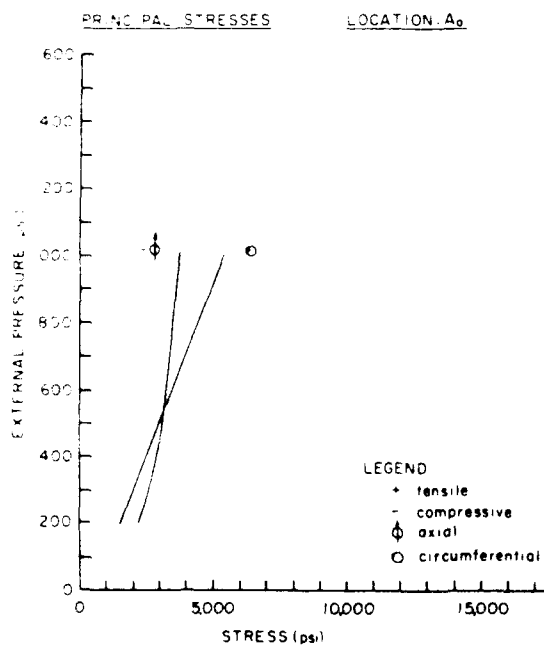
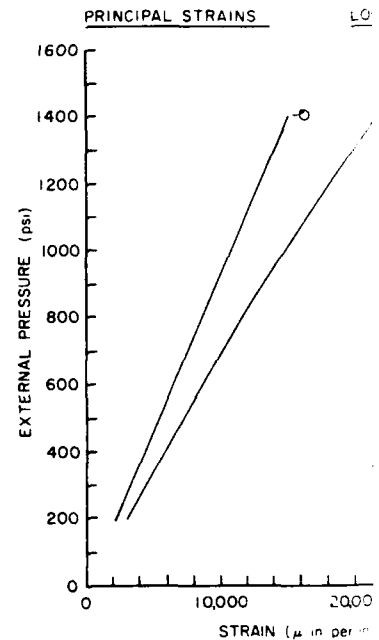
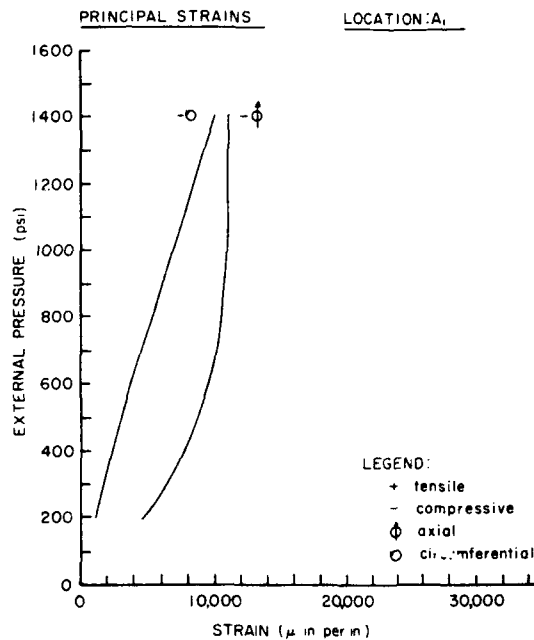
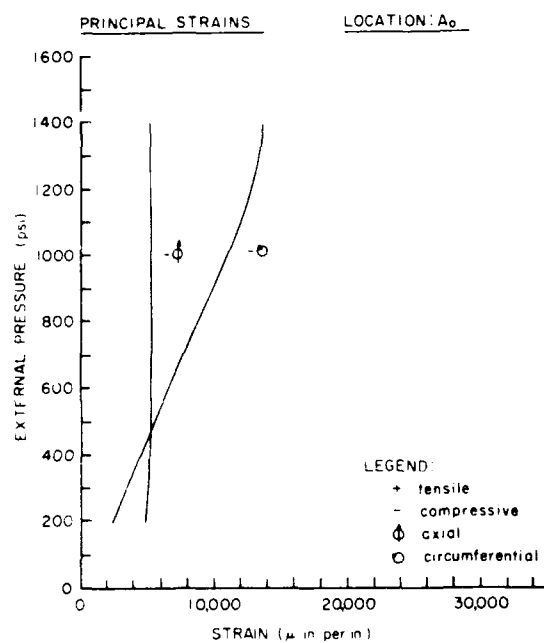


Fig. 19 - Principal Stresses and Strains in Model 11

LOCATION: A₁

PRINCIPAL STRAINS

LOCATION: B₀

PRINCIPAL STRAINS

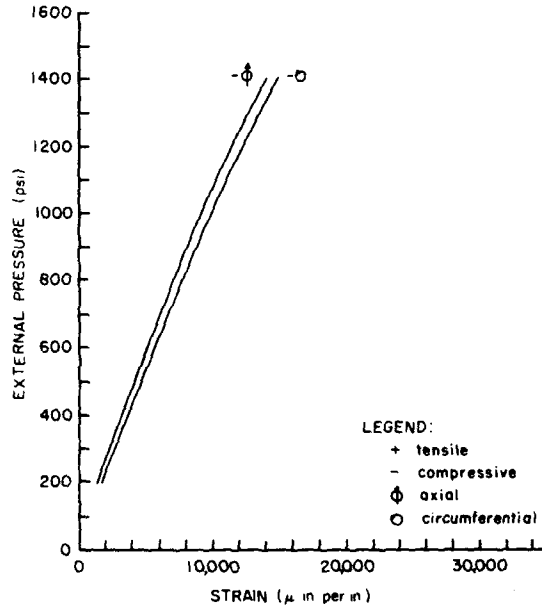
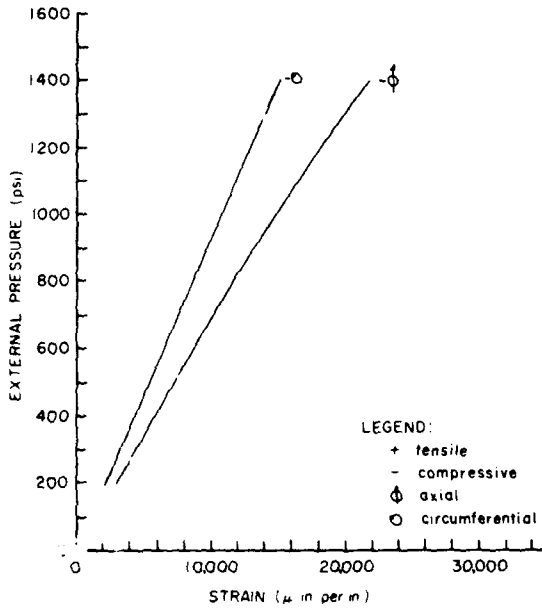
LOCATION: B₁

LEGEND:
+ tensile
- compressive
Φ axial
○ circumferential

LEGEND:
+ tensile
- compressive
Φ axial
○ circumferential

LEGEND:
+ tensile
- compressive
Φ axial
○ circumferential

0 10,000 20,000 30,000
STRAIN (μ in per in)



LOCATION: A₁

PRINCIPAL STRESSES

LOCATION: B₀

PRINCIPAL STRESSES

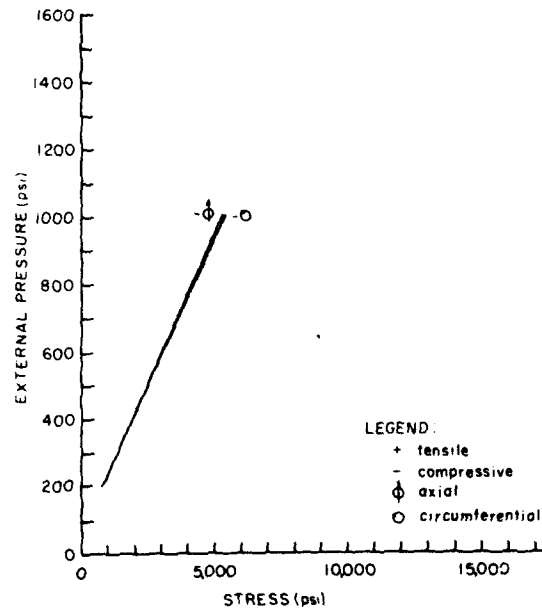
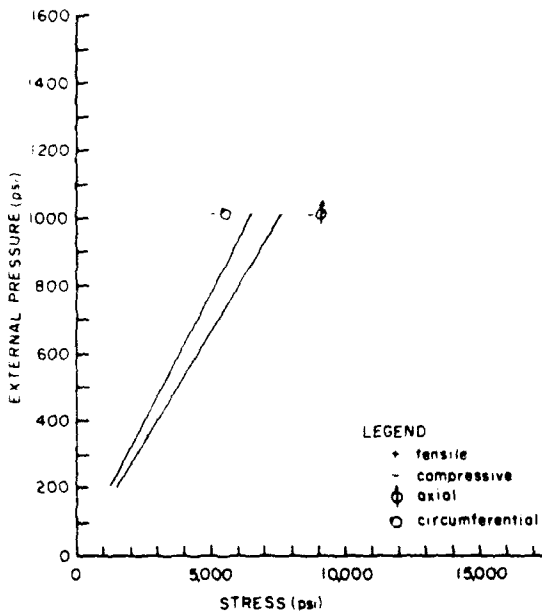
LOCATION: B₁

LEGEND:
+ tensile
- compressive
Φ axial
○ circumferential

LEGEND:
+ tensile
- compressive
Φ axial
○ circumferential

LEGEND:
+ tensile
- compressive
Φ axial
○ circumferential

0 5,000 10,000 15,000
STRESS (psi)



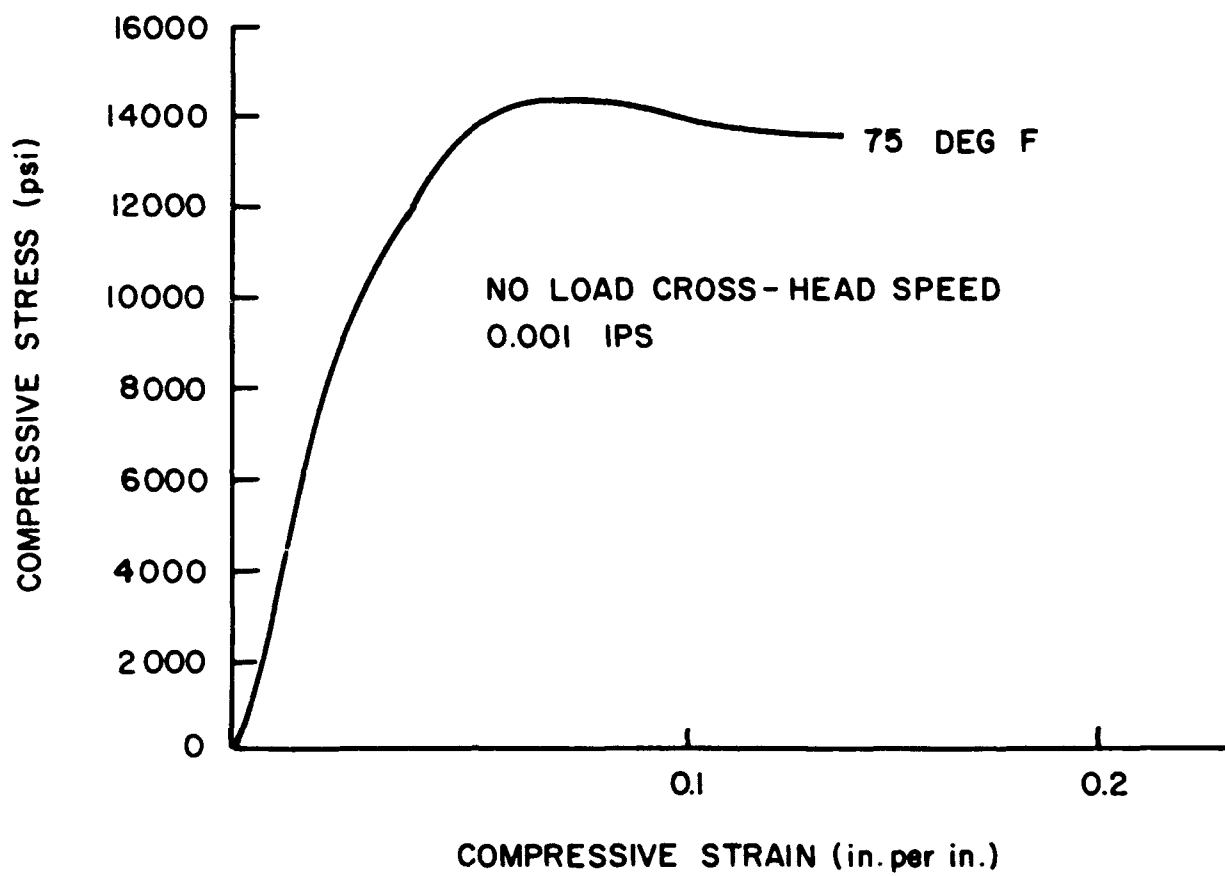


Fig. 20 - Compressive Stress-Strain Curve for Acrylic Resin Used in Cellular Shells

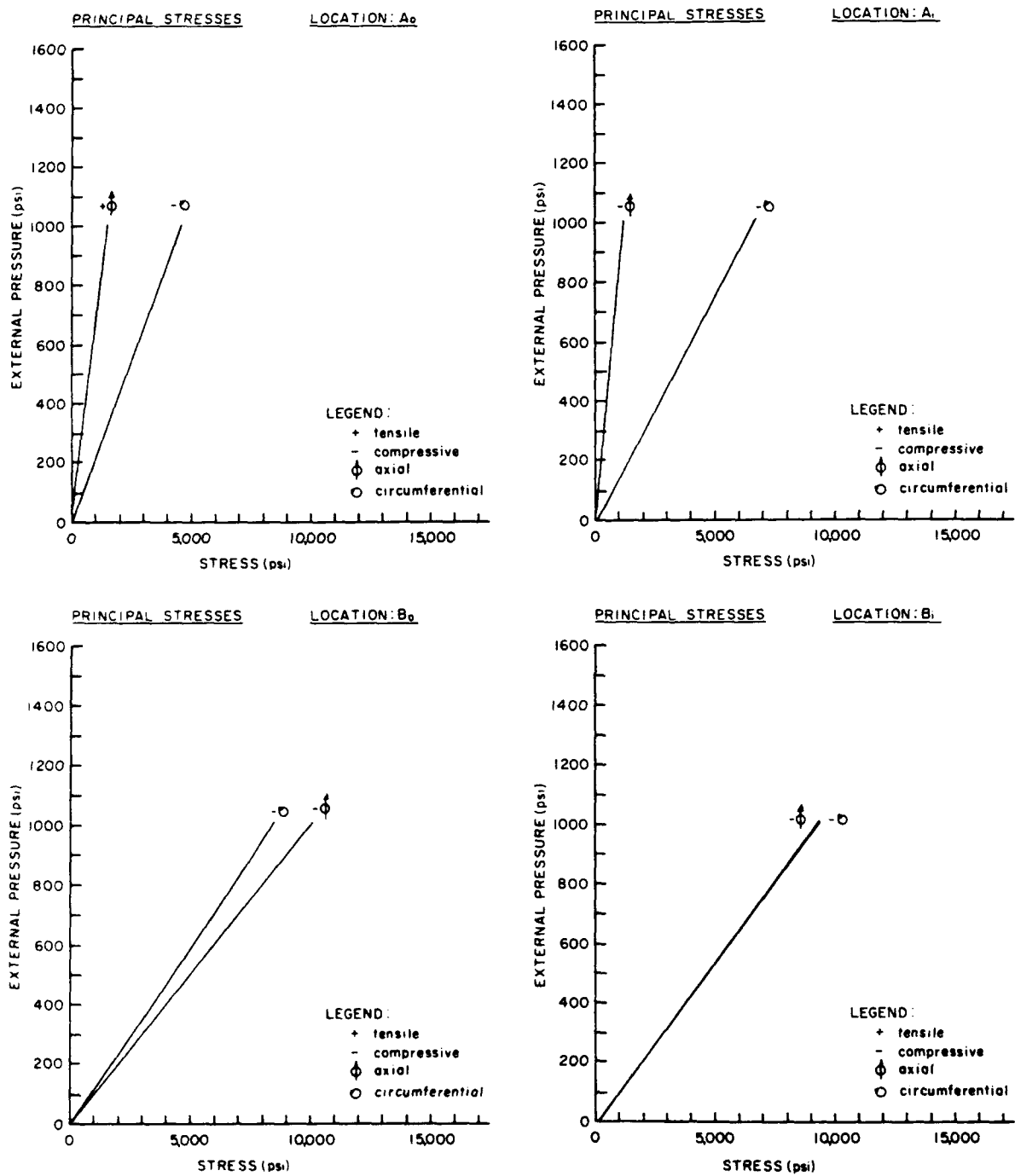


Fig. 21 - Principal Stresses at Locations A and B as Calculated by Pulos' Analysis

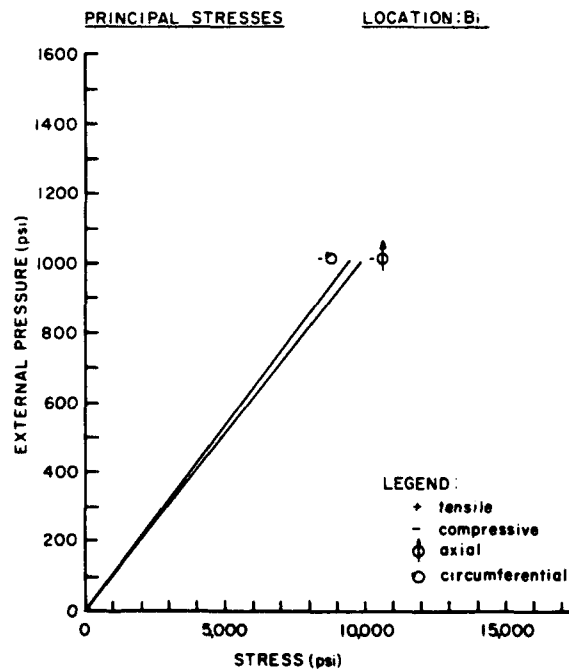
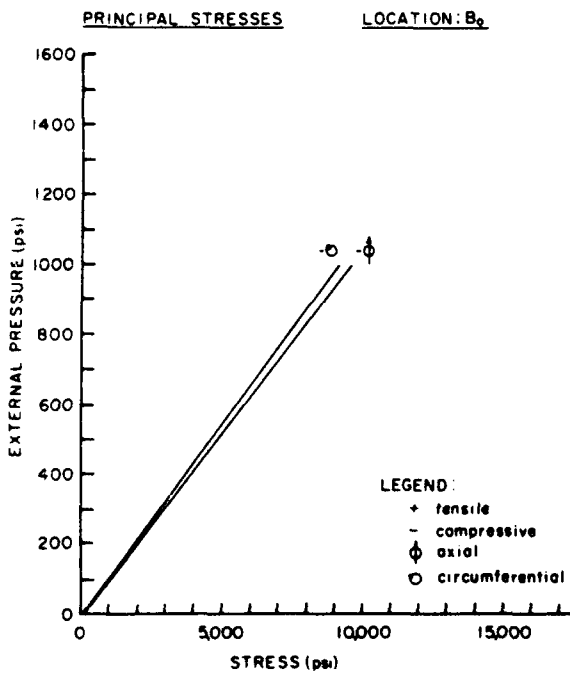
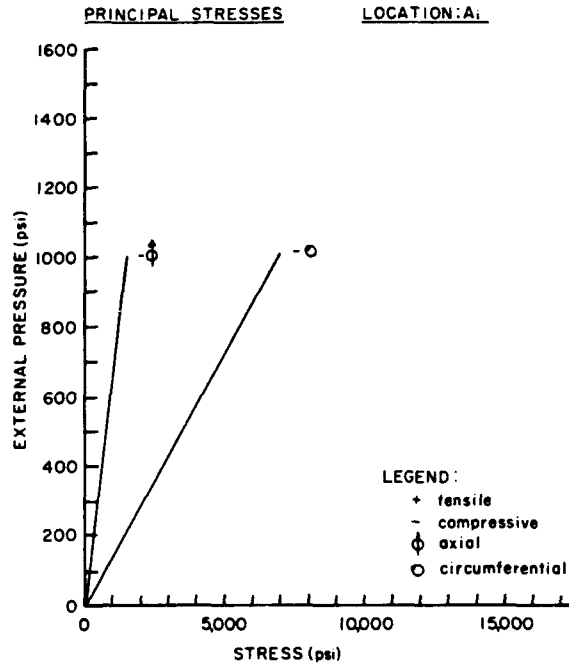
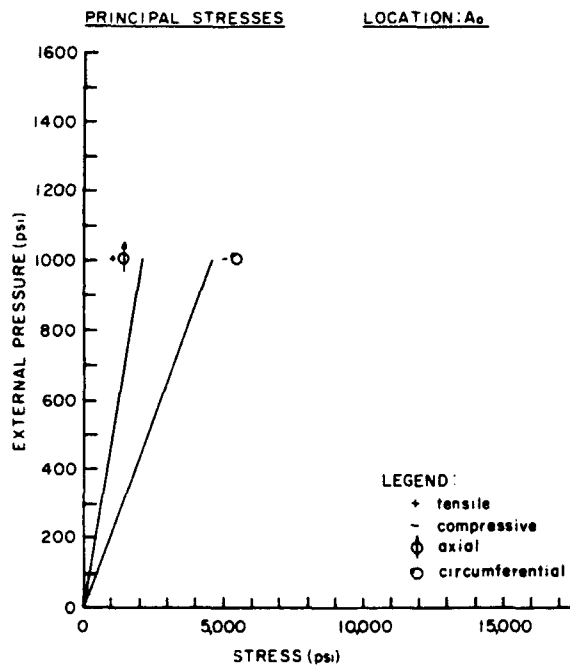


Fig. 22 - Principal Stresses at Locations A and B as Calculated by Mehta's Analysis

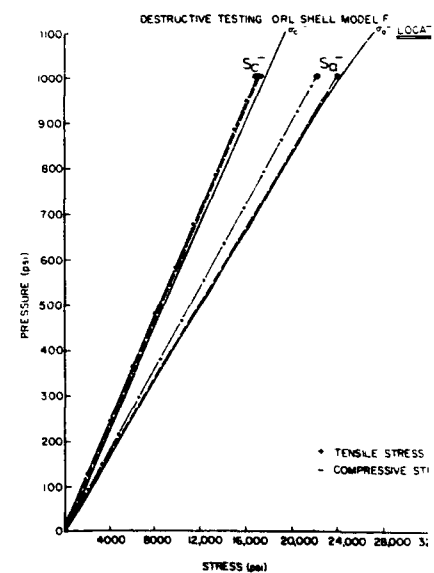
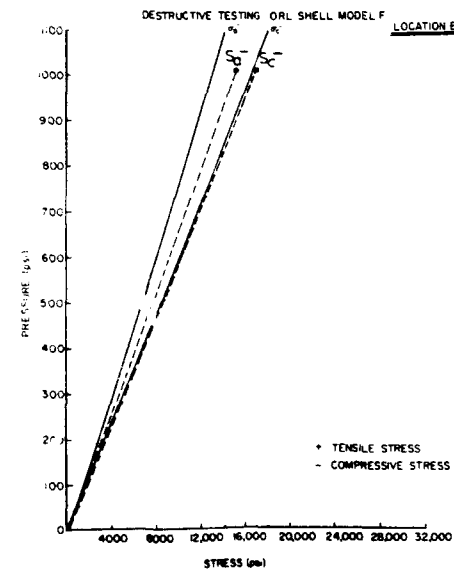
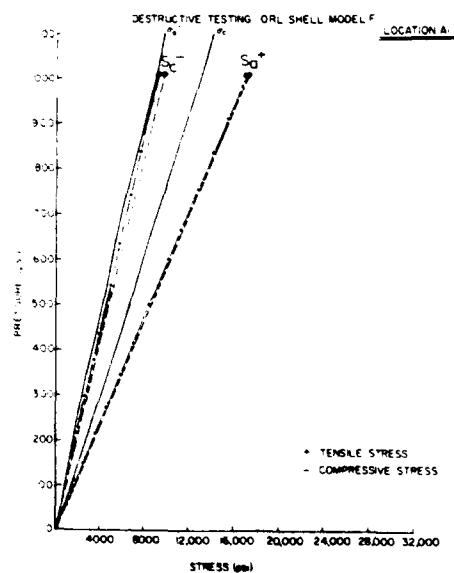
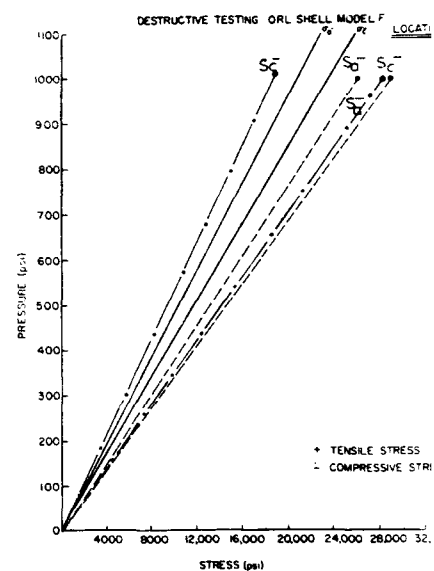
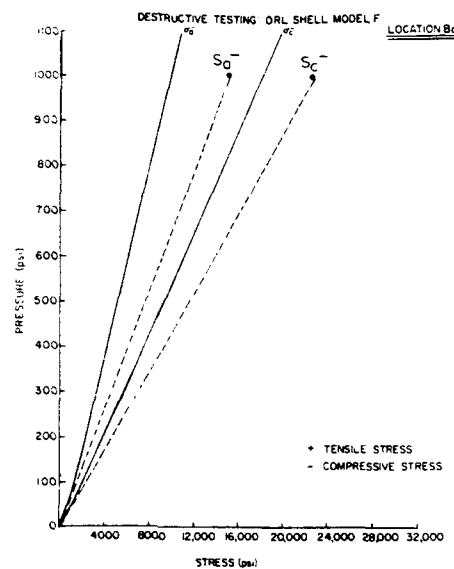
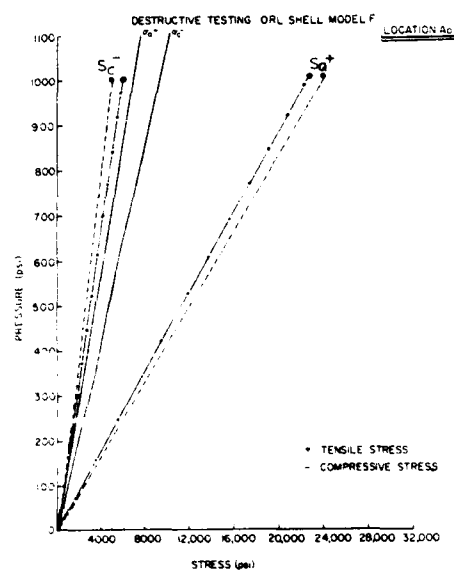
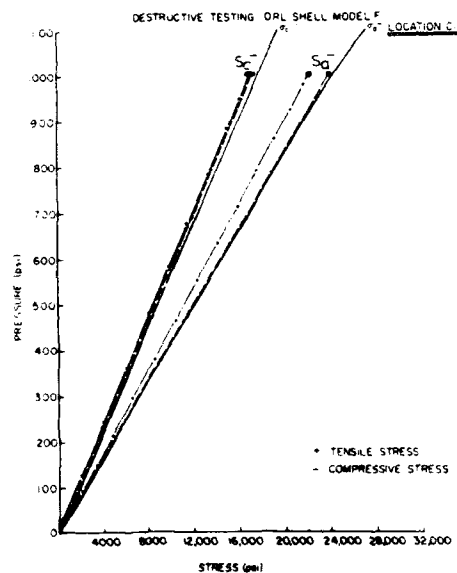
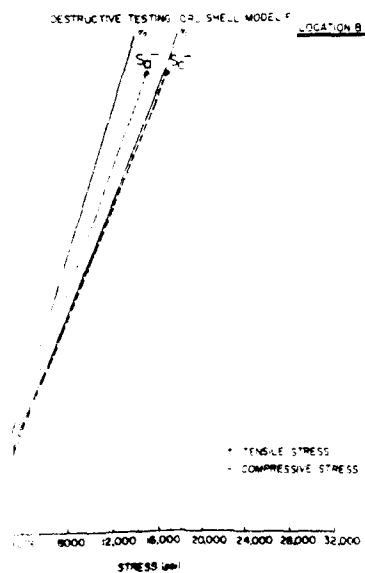
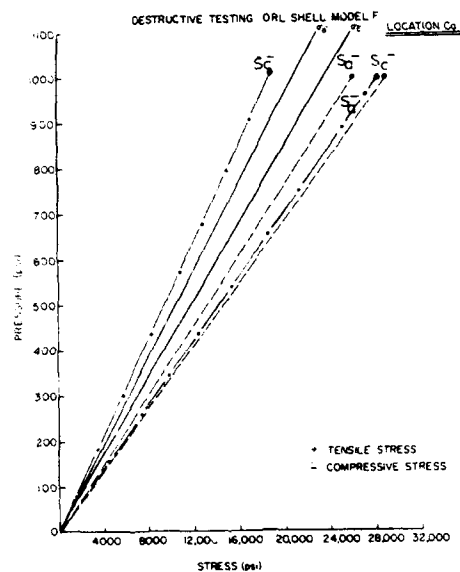
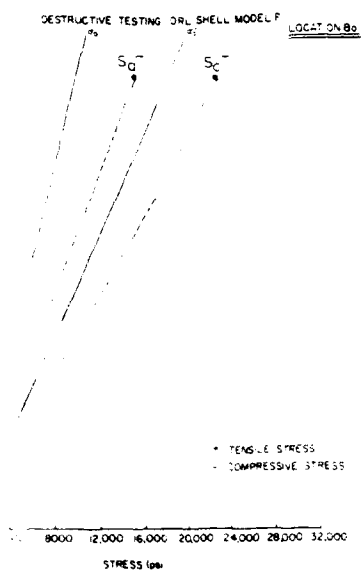
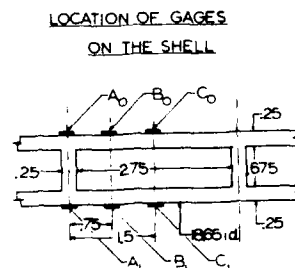


Fig. 23 - Calculated and Experimentally Determined Stresses in Model F Cellular Shell



— experimental
- - - Mehta's analysis
- - - Pulos' analysis

a - axial
c - circumferential



TYPE OF GAGES AX-7
MATERIAL: 6065-T6

ted and Experimentally Determined Stresses in Model F Cellular Shell

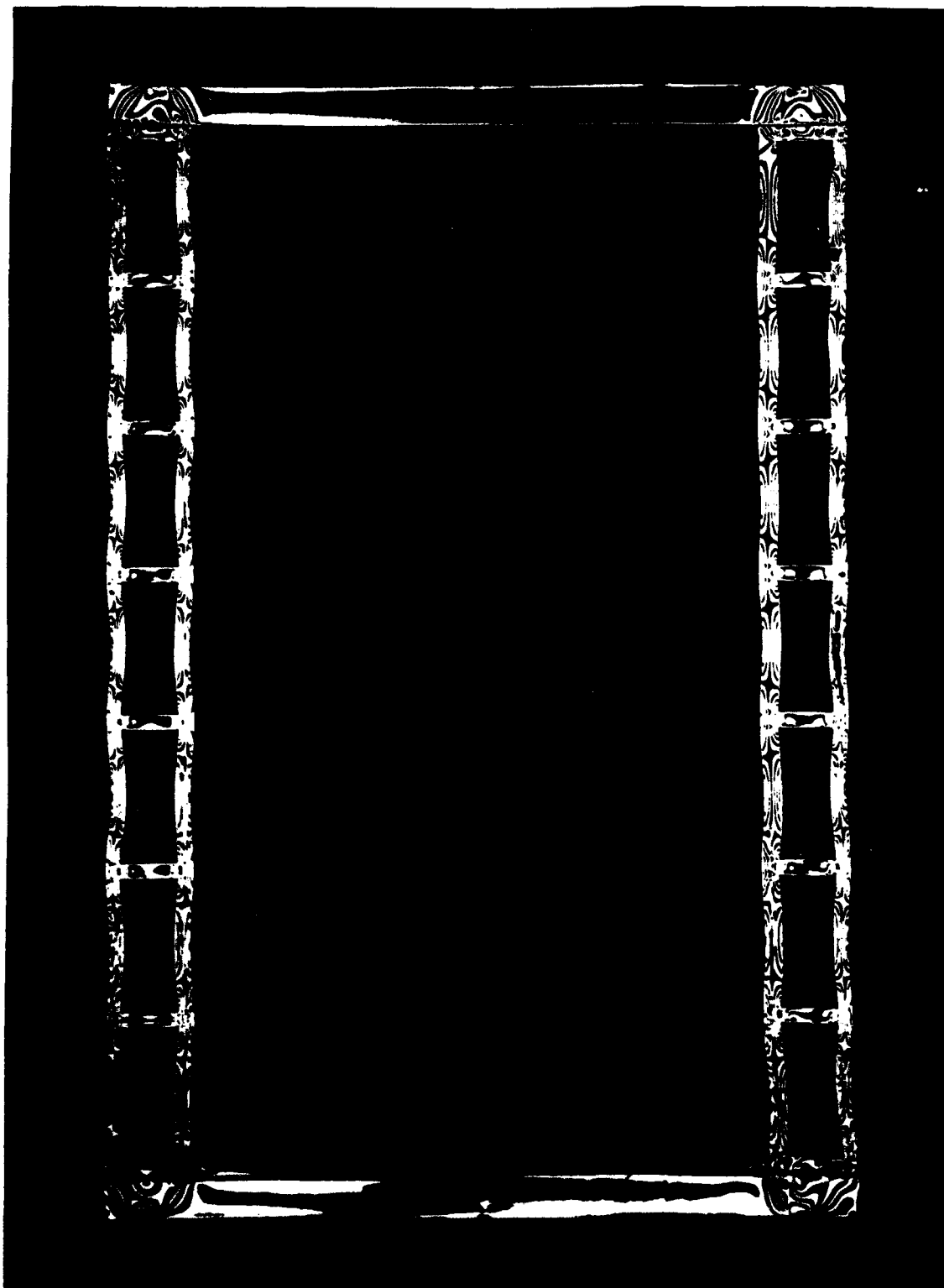


Fig. 24 - Photoelastic Fringes Obtained with Rectangular-Cell Epoxy Resin Shell

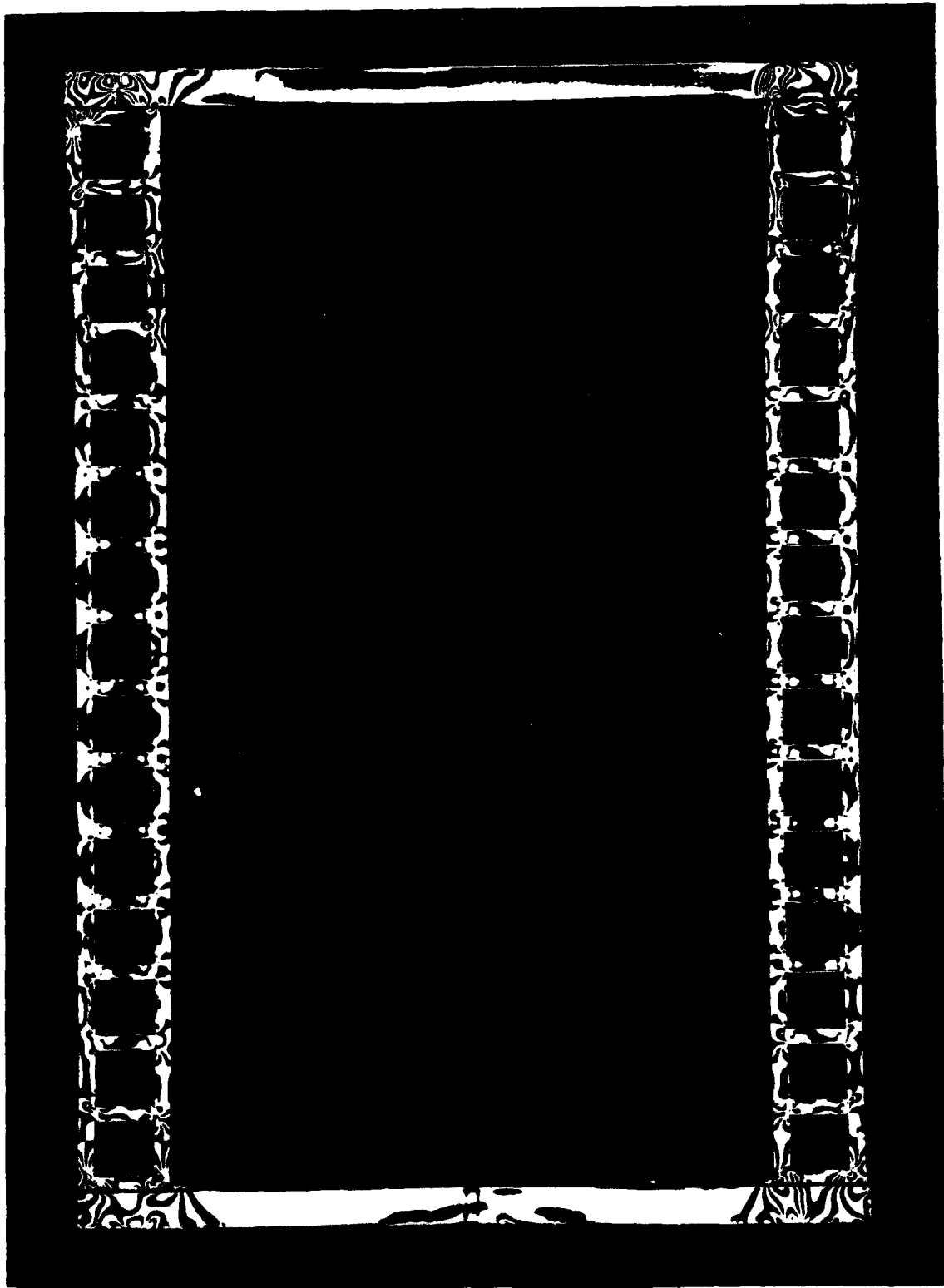


Fig. 25 - Photoelastic Fringes Obtained with Square-Cell Epoxy Resin Shell

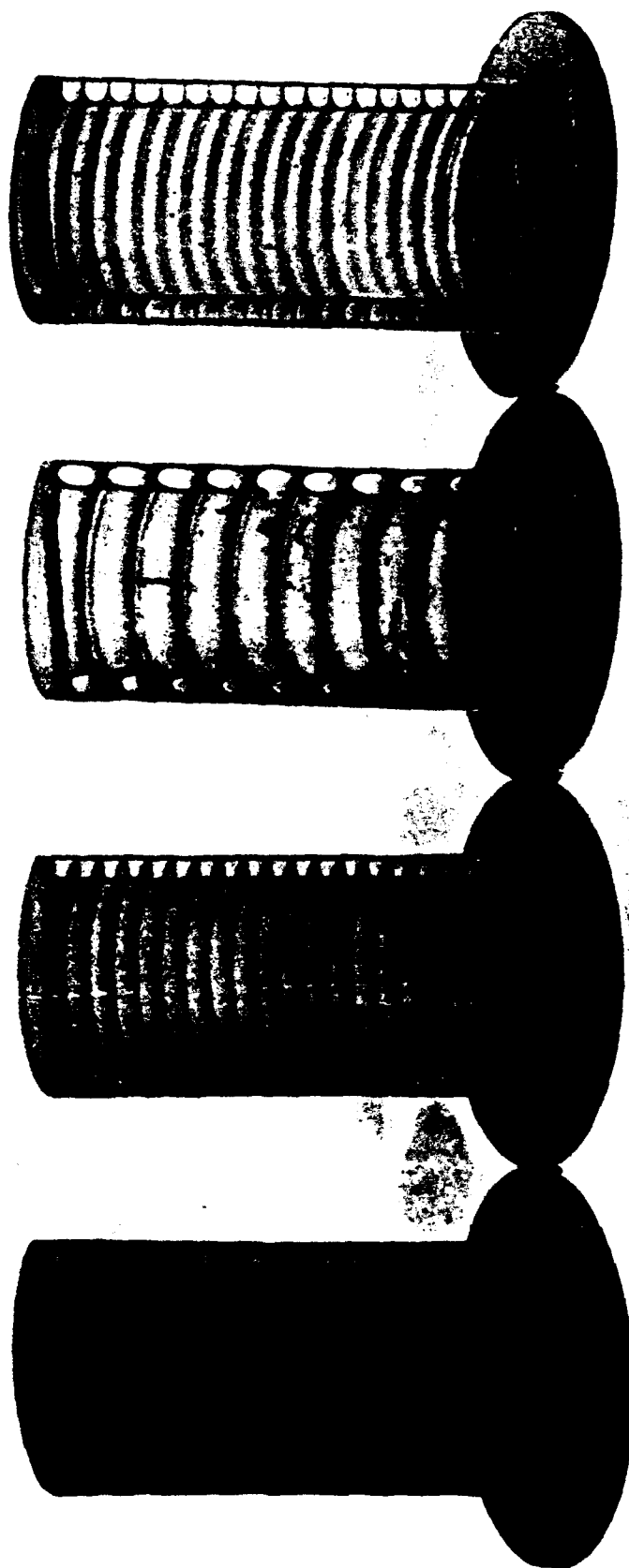


Fig. 26 - Epoxy Resin Cellular Shells

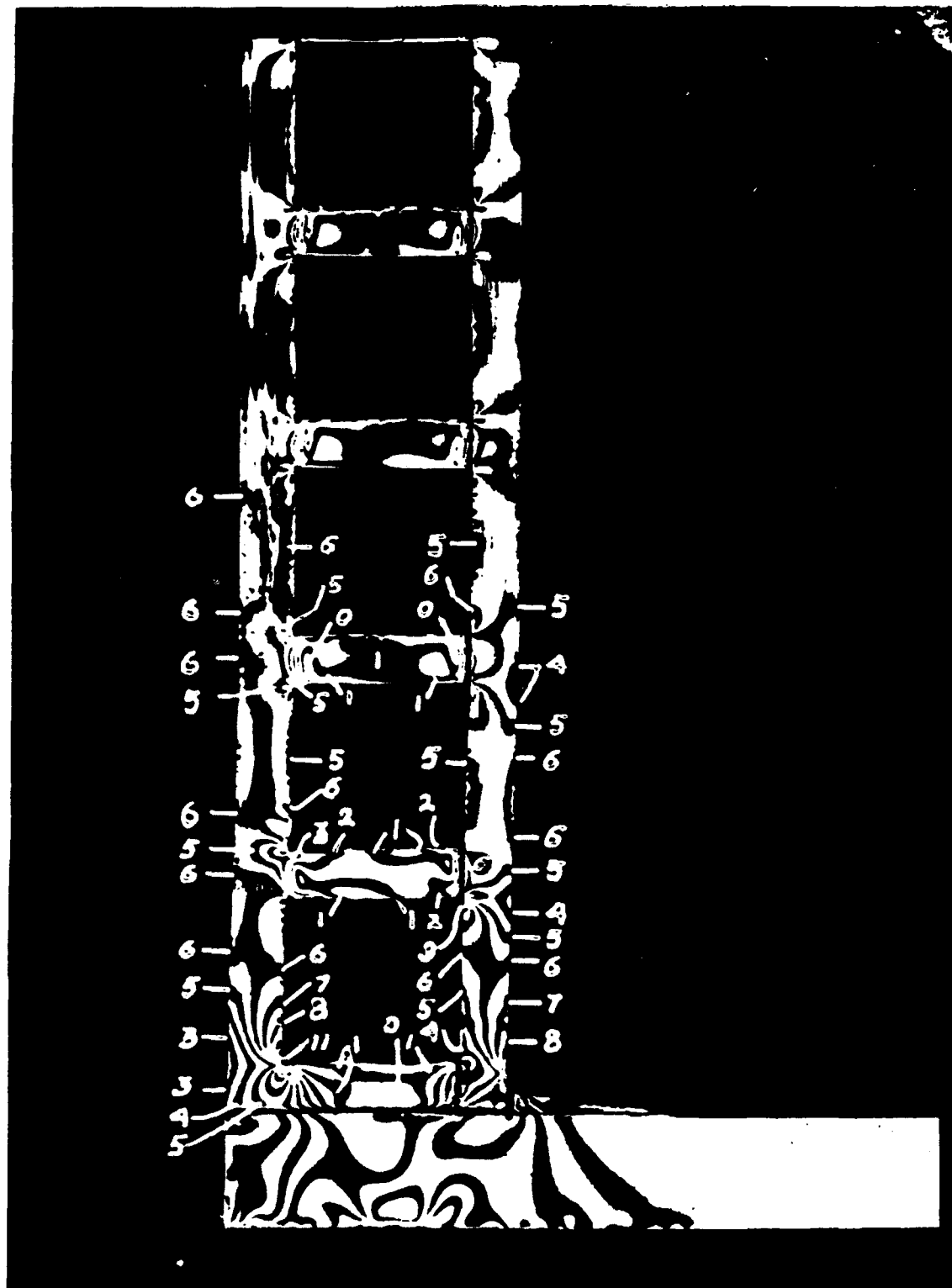


Fig. 27 - Detail of Square-Cell Epoxy Resin Shell

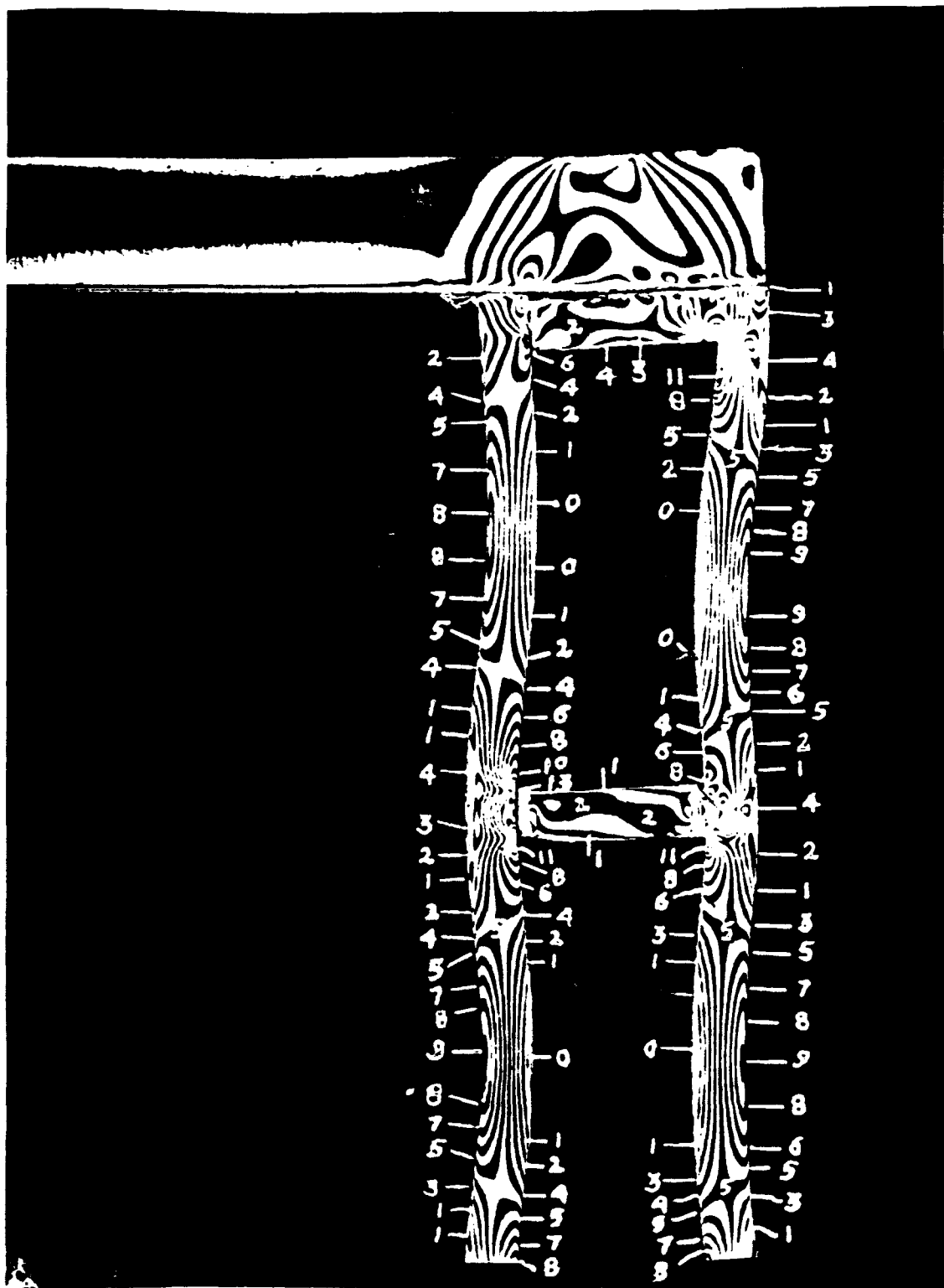


Fig. 28 - Detail of Rectangular-Cell Epoxy Resin Shell

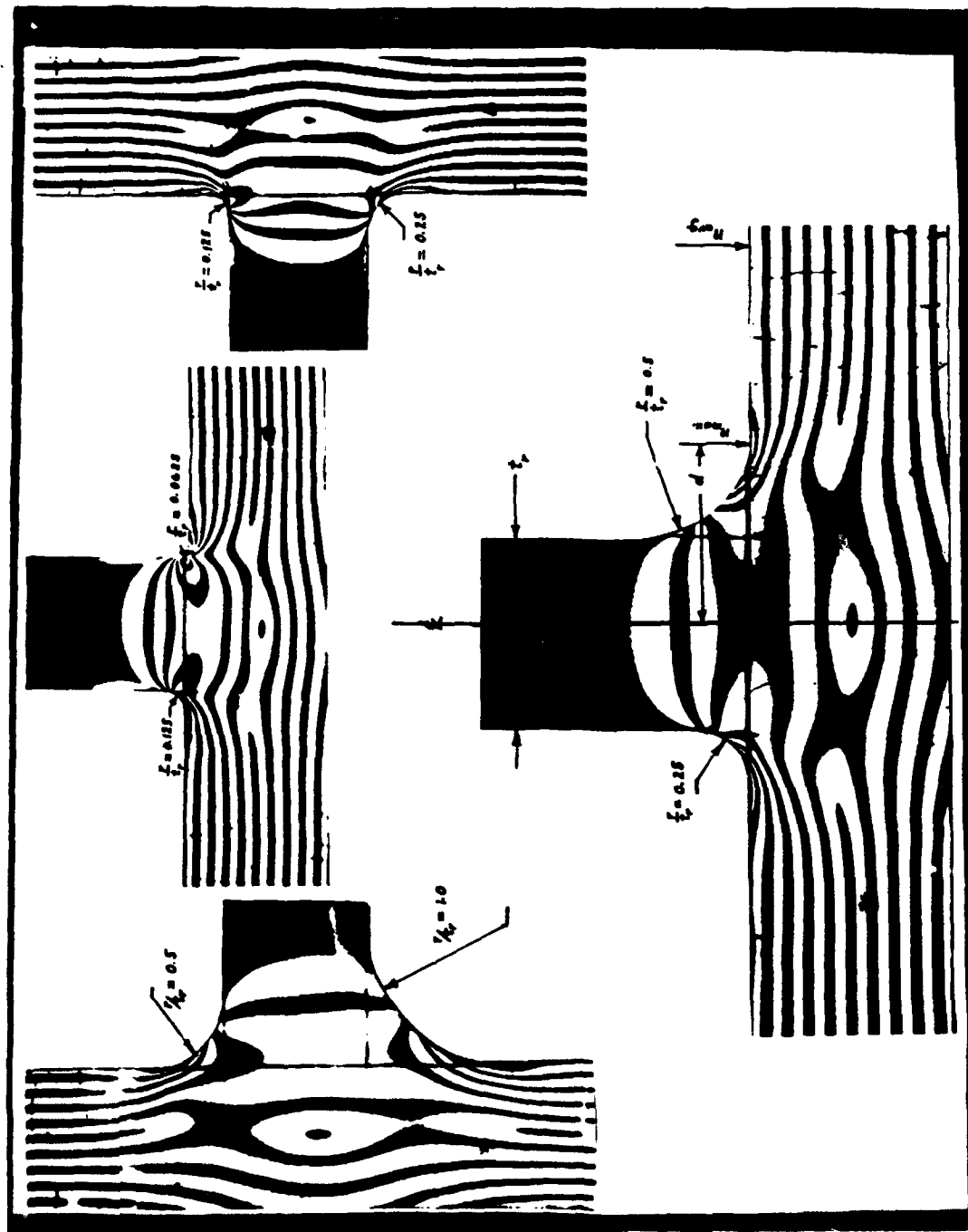
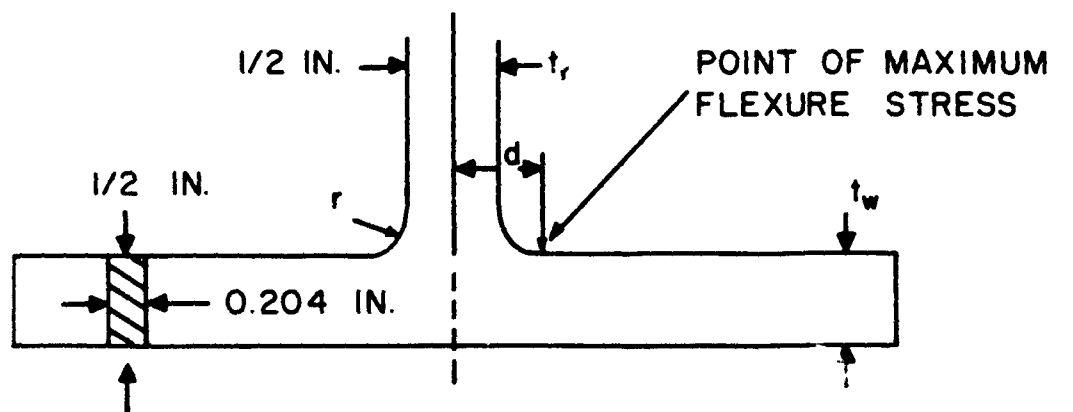
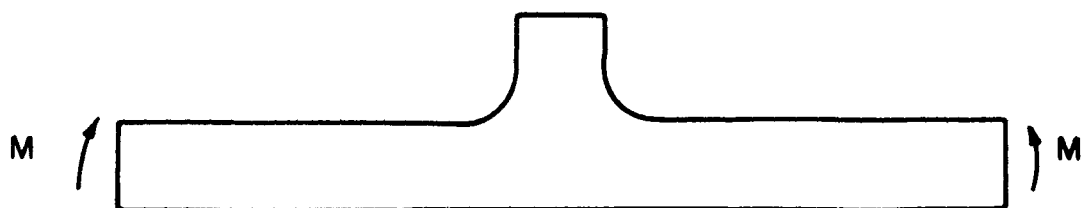


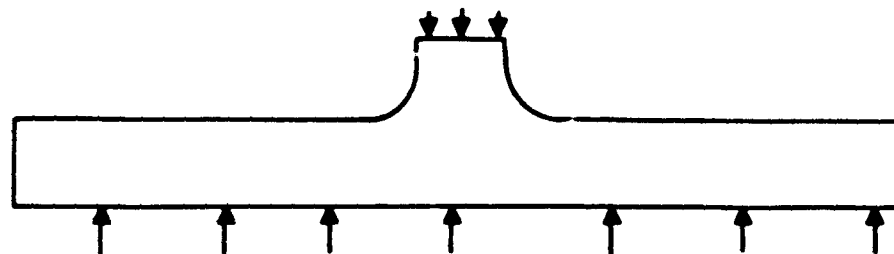
Fig. 29 - Photoelastic Fringes in Two-Dimensional T-Section Model. . in the Linear Elastic Range, during Pure Flexure of the Wall



DIMENSIONS OF TWO-DIMENSIONAL PHOTOELASTIC MODEL



GENERATION OF FLEXURE STRESS IN THE WALL



GENERATION OF RADIAL COMPRESSIVE STRESS IN THE STIFFENER



GENERATION OF AXIAL COMPRESSIVE STRESS IN THE SHELL WALL

MATERIAL: Ciba 502 Epoxy Resin

Fig. 30 - Generation of Stresses in T-Section Models

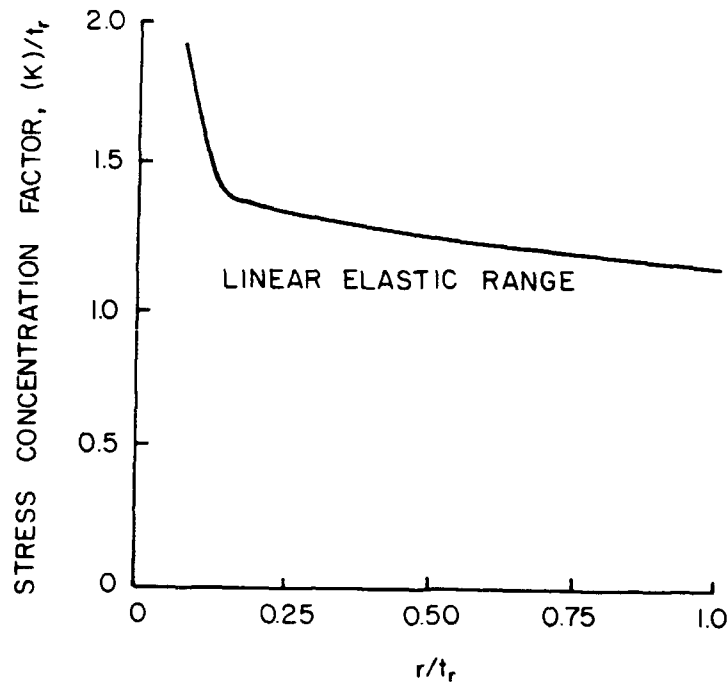


Fig. 31 - Flexural Stress Concentration Factor vs r/t_r in the Axial Plane of the Shell at the Juncture of the Stiffener and the Facing

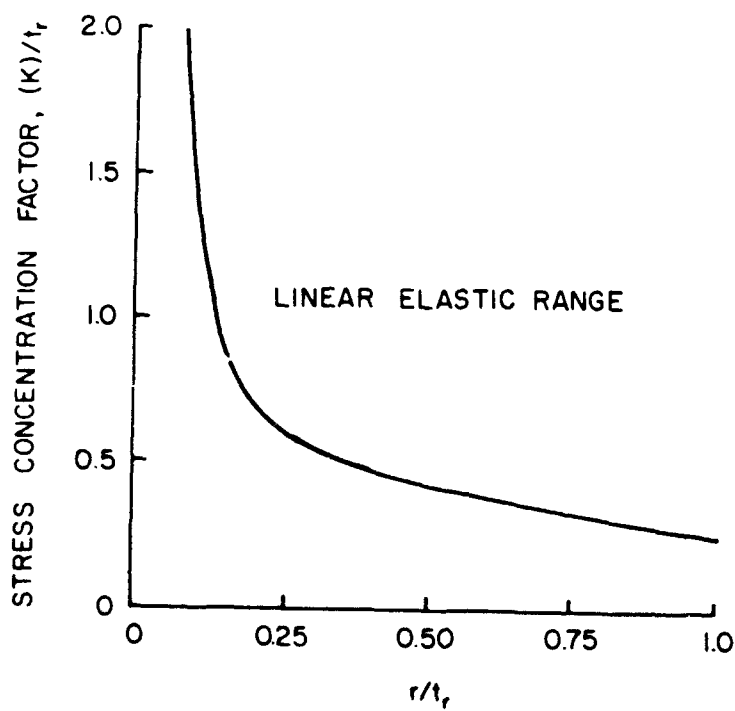


Fig. 32 - Radial Stress Concentration Factor vs r/t_r at the Point of Maximum Flexural Stress in the Facing at the Juncture of the Stiffener

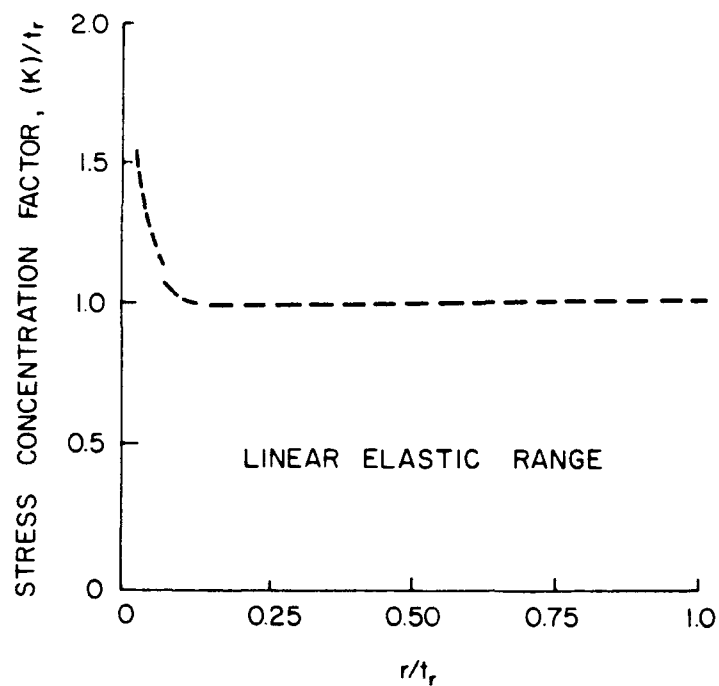


Fig. 33 - Axial Stress Concentration Factor vs r/t_r at the Point of Maximum Flexural Stress in the Facing at the Juncture of the Stiffener

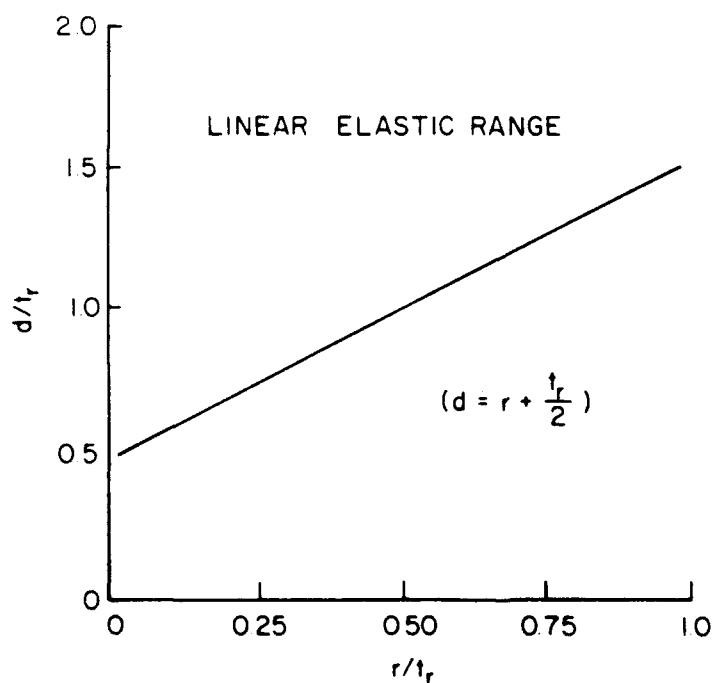
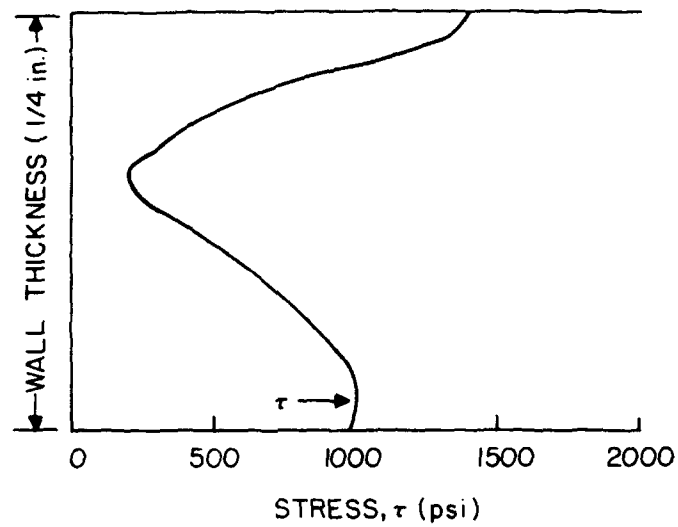
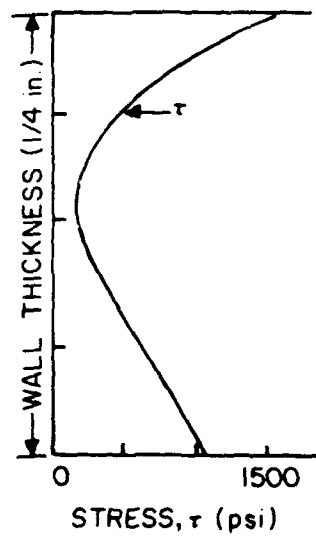


Fig. 34 - Location (d/t_r) of Maximum Flexural Stress vs r/t_r for a Shell Facing Subjected to Flexure in the Axial Plane of the Shell



(All material in the elastic strain range)



(Some of the material in the plastic strain range)

Fig. 35 - Distribution of Maximum Shear Stresses in T-Sections Subjected to Identical Flexure

<p>This card is UNCLASSIFIED</p> <p>Ordnance Research Laboratory Report No. NORD 16597-97 The Pennsylvania State University, University Park, Pa.</p> <p>THE EFFECTS OF SHELL JOINTS AND BONDING ON THE STABILITY OF ACRYLIC RESIN CELLULAR SHELLS</p> <p>This report is UNCLASSIFIED</p> <p>J. D. Stachiw</p> <p>September 25, 1963, 6 pp. & figs.</p> <p>Six acrylic resin cellular shells were tested under external hydrostatic pressure to determine the effects of joints between individual shell structure components and the effects of bonding on cellular shell stability. When the shell stiffeners were restrained from moving laterally, the location of joints and the degree of bonding did not affect the general elastic stability enough to cause failure by elastic buckling. All shells failed by material yielding except the one in which the stiffeners were not restrained from moving laterally. However, the distribution of stresses and strains on the other shell surfaces was considerably influenced by the location of joints and the degree of bonding. The shell stresses were calculated by Pulos' and Mehta's formulas and compared with the experimentally determined stresses. The calculated and experimental</p> <p>(over)</p>	<p>This card is UNCLASSIFIED</p> <p>Ordnance Research Laboratory Report No. NORD 16597-97 The Pennsylvania State University, University Park, Pa.</p> <p>THE EFFECTS OF SHELL JOINTS AND BONDING ON THE STABILITY OF ACRYLIC RESIN CELLULAR SHELLS</p> <p>This report is UNCLASSIFIED</p> <p>J. D. Stachiw</p> <p>September 25, 1963, 6 pp. & figs.</p> <p>Six acrylic resin cellular shells were tested under external hydrostatic pressure to determine the effects of joints between individual shell structure components and the effects of bonding on cellular shell stability. When the shell stiffeners were restrained from moving laterally, the location of joints and the degree of bonding did not affect the general elastic stability enough to cause failure by elastic buckling. All shells failed by material yielding except the one in which the stiffeners were not restrained from moving laterally. However, the distribution of stresses and strains on the other shell surfaces was considerably influenced by the location of joints and the degree of bonding. The shell stresses were calculated by Pulos' and Mehta's formulas and compared with the experimentally determined stresses. The calculated and experimental</p> <p>(over)</p>
<p>This card is UNCLASSIFIED</p> <p>Ordnance Research Laboratory Report No. NORD 16597-97 The Pennsylvania State University, University Park, Pa.</p> <p>THE EFFECTS OF SHELL JOINTS AND BONDING ON THE STABILITY OF ACRYLIC RESIN CELLULAR SHELLS</p> <p>This report is UNCLASSIFIED</p> <p>J. D. Stachiw</p> <p>September 25, 1963, 6 pp. & figs.</p> <p>Six acrylic resin cellular shells were tested under external hydrostatic pressure to determine the effects of joints between individual shell structure components and the effects of bonding on cellular shell stability. When the shell stiffeners were restrained from moving laterally, the location of joints and the degree of bonding did not affect the general elastic stability enough to cause failure by elastic buckling. All shells failed by material yielding except the one in which the stiffeners were not restrained from moving laterally. However, the distribution of stresses and strains on the other shell surfaces was considerably influenced by the location of joints and the degree of bonding. The shell stresses were calculated by Pulos' and Mehta's formulas and compared with the experimentally determined stresses. The calculated and experimental</p> <p>(over)</p>	<p>This card is UNCLASSIFIED</p> <p>Ordnance Research Laboratory Report No. NORD 16597-97 The Pennsylvania State University, University Park, Pa.</p> <p>THE EFFECTS OF SHELL JOINTS AND BONDING ON THE STABILITY OF ACRYLIC RESIN CELLULAR SHELLS</p> <p>This report is UNCLASSIFIED</p> <p>J. D. Stachiw</p> <p>September 25, 1963, 6 pp. & figs.</p> <p>Six acrylic resin cellular shells were tested under external hydrostatic pressure to determine the effects of joints between individual shell structure components and the effects of bonding on cellular shell stability. When the shell stiffeners were restrained from moving laterally, the location of joints and the degree of bonding did not affect the general elastic stability enough to cause failure by elastic buckling. All shells failed by material yielding except the one in which the stiffeners were not restrained from moving laterally. However, the distribution of stresses and strains on the other shell surfaces was considerably influenced by the location of joints and the degree of bonding. The shell stresses were calculated by Pulos' and Mehta's formulas and compared with the experimentally determined stresses. The calculated and experimental</p> <p>(over)</p>

values agreed within ± 5 per cent except for the principal axial stresses on the shell facings at the stiffeners. Four epoxy resin models of the cellular shells were pressure-tested and analyzed photoelastically to determine the effects of stress concentrations at the junctures of the stiffeners and the inner and outer shell facings.

values agreed within ± 5 per cent except for the principal axial stresses on the shell facings at the stiffeners. Four epoxy resin models of the cellular shells were pressure-tested and analyzed photoelastically to determine the effects of stress concentrations at the junctures of the stiffeners and the inner and outer shell facings.

values agreed within ± 5 per cent except for the principal axial stresses on the shell facings at the stiffeners. Four epoxy resin models of the cellular shells were pressure-tested and analyzed photoelastically to determine the effects of stress concentrations at the junctures of the stiffeners and the inner and outer shell facings.

values agreed within ± 5 per cent except for the principal axial stresses on the shell facings at the stiffeners. Four epoxy resin models of the cellular shells were pressure-tested and analyzed photoelastically to determine the effects of stress concentrations at the junctures of the stiffeners and the inner and outer shell facings.

STRESS ANALYSIS OF RING-STIFFENED SANDWICH SHELLS SUBJECTED TO UNIFORM EXTERNAL PRESSURE*†

G. U. OPPEL and P. K. MEHTA

The Pennsylvania State University,
Department of Engineering Mechanics, University Park, Pa., U.S.A.

(Received 28 January 1963; in revised form 25 March 1963)

Summary—This paper gives an analytical method for computing the axisymmetric elastic deformations and stresses in ring-stiffened sandwich shells subjected to uniform external pressure as shown in Fig. 1. The analysis ignores the stress concentrations

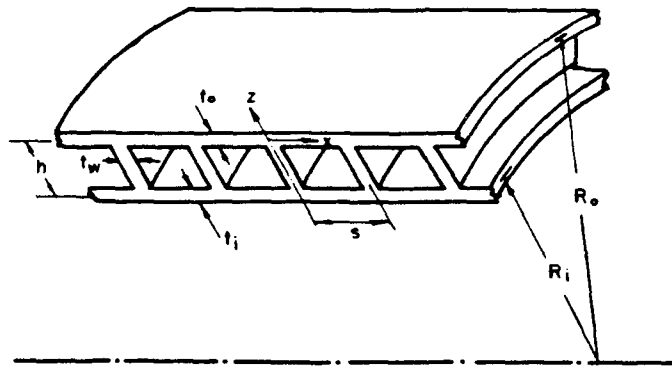


FIG. 1. Geometrical configuration of a ring-stiffened sandwich shell.

occurring at the junctures of the ring-stiffeners and the shell walls. For design calculations, the effect of the stress concentration is taken into consideration by experimentally determining the stress concentration factors. These stress concentration factors have approximately been determined by employing two-dimensional photoelastic models. A numerical example illustrating the method of computing the yield strength of a model is also included. This example shows how the analytical solution is used in conjunction with the experimentally determined stress concentration factors.

In the solution given in this paper, the stress analysis of the shell is made by considering the outer and inner cylinders and the ring-stiffeners under the applied external load and the rib reactions, as shown in Fig. 3, using known results of the usual shell theory⁴ and Lamé's solution for thick-walled cylinders.⁵ The rib reactions are determined by applying the conditions of equilibrium and structural continuity at the junctures of the shell walls and the ring stiffeners. Pulos⁴ has developed a solution for this problem by analyzing the component parts, as illustrated in Fig. 2, and using edge-coefficients for shell elements of finite length. The stress values for a model shell calculated by these two theoretical methods show an equally good agreement (Figs. 14, 15).

INTRODUCTION

THE study presented in this paper forms a part of a broader programme undertaken to develop engineering design criteria for ring-stiffened sandwich type of shell

* This work was supported by the Ordnance Research Laboratory under the Department of the Navy, Bureau of Naval Weapons, Contract NOrd 16597.

construction for pressure vessel applications. This type of shell construction seemed desirable from the viewpoint of material economy for pressure vessels designed to withstand large external pressures.

In the war and postwar years, the solid core sandwich construction became commercially feasible as a result of new developments in fabrication techniques. Theoretical and experimental studies were made in the past decade on the solid core sandwich shells and are reviewed in Refs. 1 and 2. However, very little material is available on the ring-stiffened sandwich shells. Fulton¹ and Stachiw³

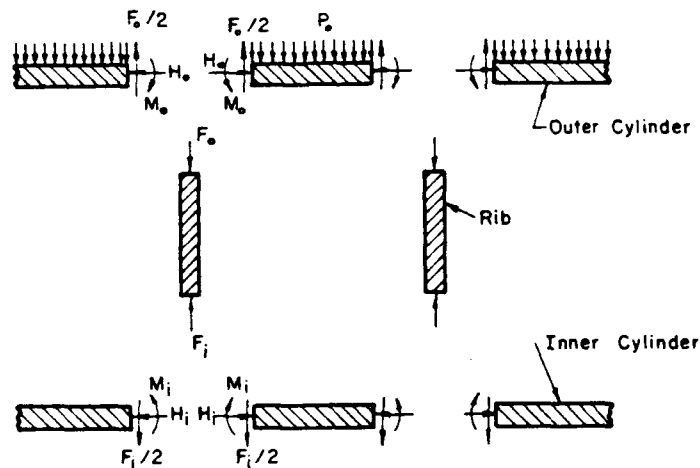


FIG. 2. Free-body diagram showing forces and moments acting on cylinder and rib elements of a ring-stiffened sandwich shell.⁴

studied the general instability strength of these shells but not the elastic yield strength behaviour. When the present study was nearly completed, the authors found a publication by Pulos⁴ which gives the theoretical solution of the same problem. Pulos' approach to the problem will now be briefly reviewed in order to see how the authors' solution differs from that of Pulos.

Pulos' solution is based on the use of edge coefficients. As shown in Fig. 2, he splits up the complex shell structure into stiffeners and short outer and inner cylindrical elements between the adjacent ribs. The displacements occurring in each of these structural elements are known from the existing theory in terms of unknown forces and moments acting at the common junctures of the elements. These forces and moments are then determined by satisfying the equilibrium and compatibility relations at the common junctures. Knowing these forces and moments, stresses and deformation in each structural element can be obtained.

The authors' solution, on the other hand, does not make use of edge coefficients. Unlike in Pulos' solution, the outer and inner cylinders are not split up into small cylindrical elements between the adjacent ring-stiffeners as shown in Fig. 3. The shell structure is broken down only into the outer and inner cylinders and the stiffeners. The unknown reactions at the common junctures

of the two cylinders and the stiffeners are determined by satisfying the equilibrium and compatibility conditions at these junctures. Knowing these reactions, the solutions for the cylinders and the stiffeners are written down from the existing results of the shell theory. This approach has led to a solution which, unlike Pulos' solution, does not involve hyperbolic trigonometric functions. A comparison of the results obtained from these two solutions is given at the end of this paper.

In what follows, a ring-stiffened sandwich shell will be referred to as a cellular shell, ring-stiffeners as ribs or webs, the outer and inner cylinders as shell walls, a single-walled cylindrical shell of constant thickness as a smooth shell and a bay of the cellular shell as a cell.

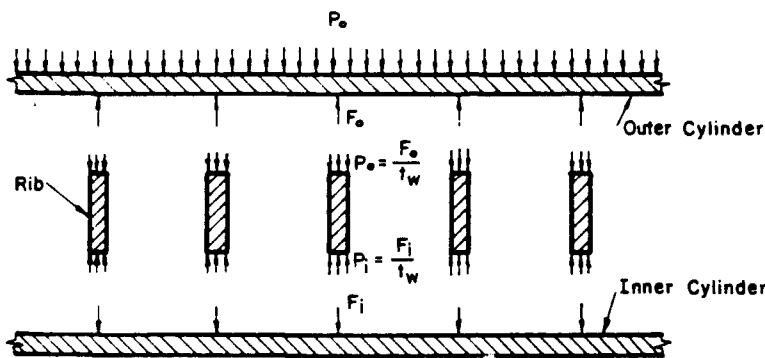


FIG. 3. Free-body diagram for radial forces acting on the outer and inner cylinders and ribs of a ring-stiffened sandwich shell.

In the following analytical solution it is assumed that the cellular shell is a long one, so that the solution is applicable to a typical cell of the shell only. It is also assumed that the ribs transmit the load from the outer wall to the inner one without buckling and that the rib reactions F_o and F_i (Fig. 3) are the same for all the ribs. Furthermore, the beam-column effect caused by the external axial pressure and the stress concentrations at the wall and rib junctures are neglected in this analysis. Finally, the external axial load is assumed to be shared by the shell walls in proportion to their thicknesses; this assumption will be in close agreement with the exact condition for practical cellular shell configurations for which the ratio of the wall spacing to the mean radius of the shell is not very large.

NOTATIONS AND ABBREVIATIONS

x, ϕ, z	longitudinal, circumferential and radial directions
w	radial displacement
p_o	external pressure
F_o, F_i	rib reactions
σ_x, σ_ϕ	longitudinal and circumferential normal stresses
τ	shearing stress
N_x, N_ϕ	normal membrane forces per unit length in x - and ϕ -directions
Q	transverse shearing force per unit length
E	modulus of elasticity in tension and compression
μ	Poisson's ratio

Subscripts

o = outer, i = inner, w = web (or rib), b = bending, m = membrane

Superscripts

c = cylinder, w = web (or rib), r = radial pressure, a = axial pressure, F = rib reaction forces

Abbreviations

$$D = \frac{Et^3}{12(1-\mu^2)} = \text{flexural rigidity of the shell plating} \quad (1)$$

$$\beta^4 = \frac{Et}{4R^2 D} = \frac{3(1-\mu^2)}{t^2 R^2} \quad (2)$$

$$\left. \begin{aligned} \phi(x) &= e^{-\beta x}(\cos \beta x + \sin \beta x) \\ \psi(x) &= e^{-\beta x}(\cos \beta x - \sin \beta x) \\ \theta(x) &= e^{-\beta x}(\cos \beta x) \\ \zeta(x) &= e^{-\beta x}(\sin \beta x) \end{aligned} \right\}^* \quad (3)$$

$$f(x) = \phi(x) + \phi(s-x) + \phi(s+x) + \phi(2s-x) + \phi(2s+x) + \dots \quad (4)$$

$$k(x) = \psi(x) + \psi(s-x) + \psi(s+x) + \psi(2s-x) + \psi(2s+x) + \dots = -\frac{1}{2\beta^2} \frac{d^2 f(x)}{dx^2} \quad (5)$$

$$m(x) = \theta(x) - \theta(s-x) + \theta(s+x) - \theta(2s-x) + \theta(2s+x) - \dots = \frac{1}{4\beta^3} \frac{d^3 f(x)}{dx^3} \quad (6)$$

$$\left. \begin{aligned} \lambda_1 &= \frac{(1-\mu^2)(R_0^2 - R_i^2)}{Et_w} = \frac{(1-\mu^2)(R_0 + R_i)h}{Et_w} \\ \lambda_2 &= \frac{\mu(R_0^2 - R_i^2)}{8} = \frac{\mu(R_0 + R_i)h}{8}, \quad \lambda_3 = \frac{f_o(0)}{R_0 D_0 \beta_0^2}, \quad \lambda_4 = \frac{f_i(0)}{R_i D_i \beta_i^2} \\ \lambda_5 &= \frac{(R_0^2 + R_i^2)}{8}, \quad \lambda_6 = \frac{2R_0^2}{E} \left[\frac{1}{t_0} - \frac{\mu}{2(t_0 + t_i)} \right], \quad \lambda_7 = \frac{\mu R_0^2 R_i}{E(t_0 + t_i)} \end{aligned} \right\} \quad (7)$$

$$\Delta_1 = \lambda_1 + \lambda_2(\lambda_3 - \lambda_4) + \lambda_5(\lambda_3 + \lambda_4) + \frac{Et_w}{8\mu} \lambda_2 \lambda_3 \lambda_4 \quad (8)$$

$$\Delta_2 = \left[8(\lambda_2 + \lambda_5) + \frac{Et_w}{\mu} \lambda_2 \lambda_4 \right] \frac{\lambda_6}{2R_0^2} + \lambda_7 \quad (9)$$

$$\Delta_3 = \left[8(\lambda_5 - \lambda_2) + \frac{Et_w}{\mu} \lambda_2 \lambda_3 \right] \frac{\lambda_7}{2R_i^2} + \lambda_6 \quad (10)$$

ELASTIC DEFORMATIONS AND STRESSES IN CELLULAR SHELLS UNDER UNIFORM EXTERNAL PRESSURE

To stress analyze the cellular shell of Fig. 1, the forces acting on its component parts will now be considered as shown in Fig. 3. Unknown rib reactions or ring-loads are introduced at the common junctures of the walls and the ribs.

The displacement of the outer wall consists of three parts: w_o^r caused by the external radial pressure, w_o^a caused by the external axial pressure and w_o^F caused by the ring-loads F_o . Then the resultant displacement w_o^c of the middle surface of the outer wall is (Fig. 4)

$$w_o^c = w_o^r + w_o^a + w_o^F \quad (11)$$

* Numerical values of these functions are given in Table 84 of Ref. 6.

Similarly, for the inner wall (Fig. 4)

$$u_i^c = u_i^a + u_i^F \quad (12)$$

The following sign convention is now introduced in order to calculate the components of the displacements: the radially outwards displacements are

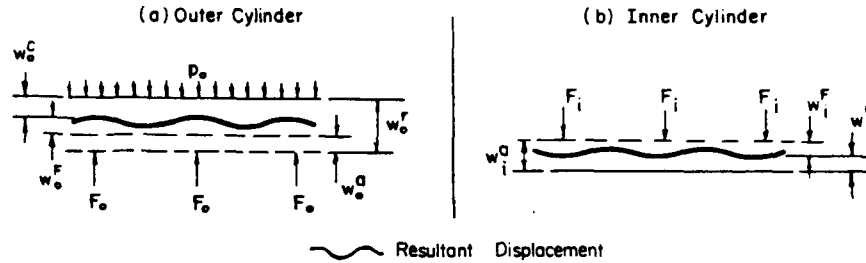


FIG. 4. Displacements of middle surfaces of the outer and inner cylinders under the imposed and reaction loads and resultant displacements.

(a) Displacements of the outer wall caused by

- (i) external radial pressure $p_o = u_o^r$
 - (ii) external axial pressure $p_o = u_o^a$
 - (iii) rib reaction forces $F_o = u_o^F$
- and the resultant displacement $= u_o^c$.

(b) Displacement of the inner wall caused by

- (i) external axial pressure $p_o = u_i^a$
 - (ii) rib reaction forces $F_i = u_i^F$
- and the resultant displacement $= u_i^c$.

positive and radially inwards displacements are negative. Then the radial contraction of the outer cylinder due to the external radial pressure is

$$u_o^r = -\frac{p_o R_o^2}{Et_o} \quad (a)$$

Assuming that the two cylinders share the external axial load in proportion to their thicknesses, the radial expansion of the outer cylinder due to the external axial pressure is

$$u_o^a = \mu \frac{p_o R_o^2}{2E(t_o + t_i)} \quad (b)$$

and the radial expansion of the inner cylinder due to the external axial pressure is

$$u_i^a = \mu \frac{p_o R_o^2}{2E(t_o + t_i)} \quad (c)$$

Now based on the small deflexion theory and neglecting the beam-column effect caused by the external axial pressure, the governing differential equation for a single-walled cylindrical shell is⁶

$$\frac{d^4 w}{dx^4} + 4\beta^4 w = \frac{Z}{D} - \frac{\mu}{R} \frac{N_x}{D} \quad (d)$$

where Z = external load normal to the cylindrical surface. Solution of equation (d) for the ring-load uniformly distributed in a plane section around

the circumference of the shell, as shown in Fig. 5, is⁶

$$u = \frac{F e^{-\beta x}}{8\beta^3 D} (\sin \beta x + \cos \beta x) = \frac{F}{8\beta^3 D} \phi(x) \quad (e)$$

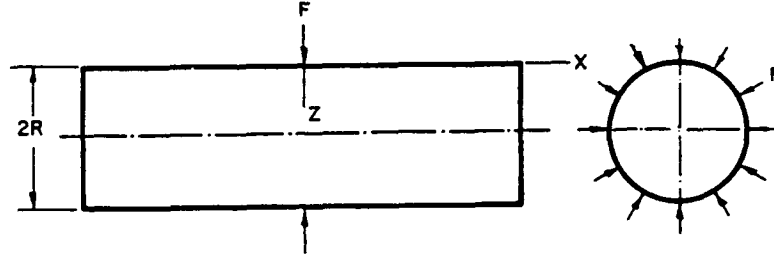


FIG. 5. A single-walled cylindrical shell of constant thickness subjected to a ring-load.

Then the deflexions w_0^F and w_i^F of the outer and inner walls caused by the rib reactions F_0 and F_i can be shown to be

$$w_0^F = \frac{F_0}{8D_0\beta_0^3} [\phi_0(x) + \phi_0(s-x) + \phi_0(s+x) + \phi_0(2s-x) + \phi_0(2s+x) + \dots] \\ = \frac{F_0}{8D_0\beta_0^3} f_0(x) \quad (f)$$

$$w_i^F = \frac{-F_i}{8D_i\beta_i^3} [\phi_i(x) + \phi_i(s-x) + \phi_i(s+x) + \phi_i(2s-x) + \phi_i(2s+x) + \dots] \\ = -\frac{F_i}{8D_i\beta_i^3} f_i(x) \quad (g)$$

Substituting values of displacements from equations (a), (b) and (f) in equation (11) and from equations (c) and (g) in equation (12), the expressions for the outer and inner wall deflexions become

$$w_0^c = -\frac{p_0 R_0^2}{E} \left[\frac{1}{t_0} - \frac{\mu}{2(t_0 + t_i)} \right] + \frac{F_0}{8D_0\beta_0^3} f_0(x) \quad (13)$$

and

$$w_i^c = \mu \frac{p_0 R_0^2}{2E(t_0 + t_i)} - \frac{F_i}{8D_i\beta_i^3} f_i(x) \quad (14)$$

The displacements of a rib due to the reactions F_0 and F_i can be calculated by considering the rib as a circular annulus subjected to external pressure $p_0 = F_0/t_w$ and internal pressure $p_i = F_i/t_w$ and using Lamé's solution of a thick-walled cylinder as given by Timoshenko⁵. For a thick-walled cylinder, the displacement equation is

$$w = \frac{(1-\mu)}{E} \left[\frac{R_i^2 P_i - R_0^2 P_0}{R_0^2 - R_i^2} \right] r + \frac{(1+\mu)}{E} \left[\frac{R_0^2 R_i^2 (P_i - P_0)}{(R_0^2 - R_i^2)} \right] \frac{1}{r} \quad (h)$$

where r is the radial co-ordinate of the point in question. The outer and inner displacements of the rib are obtained by placing $r = R_0$ and $r = R_i$, respectively,

in equation (h) and also $P_0 = F_0/t_w$ and $P_i = F_i/t_w$. Then

$$w_0^w = F_i \frac{2R_0 R_i^2}{Et_w(R_0^2 - R_i^2)} + F_0 \frac{R_0}{Et_w(R_0^2 - R_i^2)} [\mu(R_0^2 - R_i^2) - (R_0^2 + R_i^2)] \quad (15)$$

$$w_i^w = F_i \frac{R_i}{Et_w(R_0^2 - R_i^2)} [\mu(R_0^2 - R_i^2) + (R_0^2 + R_i^2)] - F_0 \frac{2R_0^2 R_i}{Et_w(R_0^2 - R_i^2)} \quad (16)$$

For structural continuity the rib displacements must be equal to the wall displacements at the rib location ($x = 0$). That is

$$(w_0^c)_{x=0} = w_0^w \quad \text{and} \quad (w_i^c)_{x=0} = w_i^w \quad (17)$$

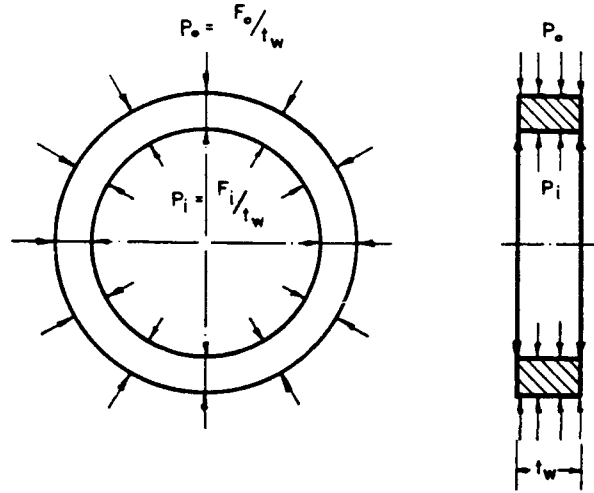


FIG. 6. Loads on a rib considered as a circular annulus.

Substituting the values of deflexions from equations (13) and (15) in the first of equations (17) and the values of deflexions from equations (14) and (16) in the second of equations (17), the following two equations for F_0 and F_i are obtained:

$$\left. \begin{aligned} F_0 R_0 \left[\frac{\mu}{Et_w} \left(\frac{\lambda_2 - \lambda_5}{\lambda_2} \right) - \frac{\lambda_3}{8} \right] + F_i R_0 \frac{\mu R_i^2}{4Et_w \lambda_2} &= -\frac{p_0 \lambda_6}{2R_0} \\ F_0 R_i \frac{\mu R_0^2}{4Et_w \lambda_2} - F_i R_i \left[\frac{\mu}{Et_w} \left(\frac{\lambda_2 + \lambda_5}{\lambda_2} \right) + \frac{\lambda_4}{8} \right] &= -\frac{p_0 \lambda_7}{2R_i} \end{aligned} \right\} \quad (18)$$

where the λ_s have been defined under the abbreviations. Solving equations (18) for F_0 and F_i and introducing Δ_s defined in equations (8), (9) and (10),

$$F_0 = \frac{\Delta_2}{\Delta_1} p_0 \quad \text{and} \quad F_i = \frac{\Delta_3}{\Delta_1} p_0 \quad (19)$$

The stress analysis of the cellular shell can now be performed. From the shell theory given in Ref. (6) and equation (5), the longitudinal bending moments for the outer and inner walls are given by

$$M_{r0} = -D_0 \frac{d^2 w_0^c}{dx^2} = \frac{F_0}{4\beta_0} k_0(x), \quad M_{ri} = -D_i \frac{d^2 w_i^c}{dx^2} = -\frac{F_i}{4\beta_i} k_i(x) \quad (20)$$

and the circumferential bending moments are given by

$$M_{\phi 0} = \mu M_{x0} \quad \text{and} \quad M_{\phi i} = \mu M_{xi} \quad (21)$$

Similarly, using equation (6), the transverse shear forces in the outer and inner walls are, respectively,

$$Q_0 = -D_0 \frac{d^3 w_0^c}{dx^3} = -\frac{F_0}{2} m_0(x) \quad \text{and} \quad Q_i = -D_i \frac{d^3 w_i^c}{dx^3} m_i(x) = \frac{F_i}{2} m_i(x) \quad (22)$$

The transverse shear stresses in the outer and inner walls are⁶

$$\tau_0 = \frac{6Q_0}{t_0^3} \left(\frac{t_0^2}{4} - t_0 z + z^2 \right) \quad \text{and} \quad \tau_i = \frac{6Q_i}{t_i^3} \left(\frac{t_i^2}{4} - t_i z + z^2 \right) \quad (23)$$

The maximum transverse shear stresses occur at $z = 0$, or

$$(\tau_0)_{\max} = -\frac{3}{4} \frac{F_0}{t_0} m_0(x) \quad \text{and} \quad (\tau_i)_{\max} = \frac{3}{4} \frac{F_i}{t_i} m_i(x) \quad (24)$$

It was assumed in the beginning that the outer and inner shell walls share the axial external load in proportion to their thicknesses. By this assumption the longitudinal normal membrane forces become

$$N_{x0} = -p_0 \frac{R_0}{2} \frac{t_0}{(t_0 + t_i)} \quad \text{and} \quad N_{xi} = -p_0 \frac{R_0^2}{2R_i} \frac{t_i}{(t_0 + t_i)} \quad (25)$$

Then the circumferential membrane forces are

$$\left. \begin{aligned} N_{\phi 0} &= -\frac{Et_0}{R_0} u_0^c + \mu N_{x0} = -\frac{Et_0}{R_0} u_0^c - \mu \frac{R_0}{2} \frac{t_0}{(t_0 + t_i)} p_0 \\ N_{\phi i} &= -\frac{Et_i}{R_i} u_i^c + \mu N_{xi} = -\frac{Et_i}{R_i} u_i^c - \mu \frac{R_0^2}{2R_i} \frac{t_i}{(t_0 + t_i)} p_0 \end{aligned} \right\} \quad (26)$$

Dividing these membrane forces by the corresponding wall thicknesses the corresponding membrane stresses are obtained, or

$$\sigma_{xm0} = -p_0 \frac{R_0}{2(t_0 + t_i)}, \quad \sigma_{xmi} = -p_0 \frac{R_0^2}{2R_i(t_0 + t_i)} \quad (27)$$

$$\sigma_{\phi m0} = -\frac{E}{R_0} u_0^c - \mu \frac{p_0 R_0}{2(t_0 + t_i)}, \quad \sigma_{\phi mi} = -\frac{E}{R_i} u_i^c - \mu \frac{p_0 R_0^2}{2R_i(t_0 + t_i)} \quad (28)$$

The resultant normal stresses are obtained by summing up the corresponding bending and membrane stresses. Then the longitudinal normal stresses are

$$\left. \begin{aligned} \sigma_{x0} &= \sigma_{xb0} + \sigma_{xm0} = \pm \frac{12M_{x0}z}{t_0^3} - \frac{p_0 R_0}{2(t_0 + t_i)} \\ \sigma_{xi} &= \sigma_{xbi} + \sigma_{xmi} = \pm \frac{12M_{xi}z}{t_i^3} - \frac{p_0 R_0^2}{2R_i(t_0 + t_i)} \end{aligned} \right\} \quad (29)$$

Similarly, the circumferential normal stresses are

$$\left. \begin{aligned} \sigma_{\phi 0} &= \sigma_{\phi b0} + \sigma_{\phi m0} = \pm \frac{12M_{\phi 0}z}{t_0^3} - \frac{E}{R_0} u_0^c - \mu \frac{p_0 R_0}{2(t_0 + t_i)} \\ \sigma_{\phi i} &= \sigma_{\phi bi} + \sigma_{\phi mi} = \pm \frac{12M_{\phi i}z}{t_i^3} - \frac{E}{R_i} u_i^c - \mu \frac{p_0 R_0^2}{2R_i(t_0 + t_i)} \end{aligned} \right\} \quad (30)$$

The normal stresses on the extreme fibers are given by placing $z = t_0/2$ or $t_i/2$, as the case may be, in equations (29) and (30). Then

$$(\sigma_{x0})_{ex} = \pm \frac{6M_{x0}}{t_0^2} - \frac{p_0 R_0}{2(t_0 + t_i)}, \quad (\sigma_{xi})_{ex} = \pm \frac{6M_{xi}}{t_i^2} - \frac{p_0 R_0^2}{2R_i(t_0 + t_i)} \quad (31)$$

and

$$\left. \begin{aligned} (\sigma_{\phi 0})_{ex} &= \pm \frac{6M_{\phi 0}}{t_0^2} - \frac{E}{R_0} \frac{w_0^c}{R_0} - \mu \frac{p_0 R_0}{2(t_0 + t_i)} \\ (\sigma_{\phi i})_{ex} &= \pm \frac{6M_{\phi i}}{t_i^2} - \frac{E}{R_i} \frac{w_i^c}{R_i} - \mu \frac{p_0 R_0^2}{2R_i(t_0 + t_i)} \end{aligned} \right\} \quad (32)$$

In equations (29) through (32), the upper sign is for the outer fiber and the lower sign is for the inner fiber.

Rib stresses

Since the rib reactions F_0 and F_i are known from equations (19), the radial and tangential rib stresses are obtained from Lamé's solution⁵ of a thick-walled cylinder by placing $P_0 = F_0/t_w$ and $P_i = F_i/t_w$, respectively, as external and internal pressures acting on the rib, considered as a circular annulus subjected to these pressure loads. Then the radial and tangential stresses are, respectively,

$$\sigma_r = \frac{R_i^2 F_i - R_0^2 F_0}{t_w(R_0^2 - R_i^2)} + \frac{(F_0 - F_i) R_0^2 R_i^2}{(R_0^2 - R_i^2) t_w r^2} \quad (33)$$

$$\sigma_t = \frac{R_i^2 F_i - R_0^2 F_0}{t_w(R_0^2 - R_i^2)} - \frac{(F_0 - F_i) R_0^2 R_i^2}{(R_0^2 - R_i^2) t_w r^2} \quad (34)$$

ILLUSTRATIVE NUMERICAL EXAMPLE

The results of the foregoing analytical solution will now be applied to compute elastic deformation and stresses in an aluminum model cellular shell. The required dimensions and the material properties for this shell are:

$$R_0 = 10.375 \text{ in.}, \quad R_i = 9.450 \text{ in.}, \quad t_0 = t_i = t_w = 0.250 \text{ in.}$$

$$h = 0.925 \text{ in.}, \quad E = 10 \times 10^6 \text{ lb/in}^2, \quad \mu = 0.333, \quad s = 2.00 \text{ in.}$$

Numerical substitution of the above values in equations (1) and (2) yields the following results:

$$D_0 = D_i = 1.465 \times 10^4 \text{ lb in.} \quad \text{and} \quad \beta_0^s = 0.3963 \text{ in}^{-4}, \quad \beta_i^s = 0.4776 \text{ in}^{-4}$$

$$\beta_0 = 0.7935 \text{ in}^{-1}, \quad \beta_i = 0.8313 \text{ in}^{-1}$$

The values of functions $f(x)$, $k(x)$ and $m(x)$ can now be calculated by using the above values of β_0 and β_i and the values of functions $\phi(x)$, $\psi(x)$ and $\theta(x)$ given in Table 84 of Ref. 6. These calculated values are given in Table 1.

Now the values of the λ coefficients defined under abbreviations can be calculated. Numerical substitution in equations (7) yields

$$\lambda_1 = 0.652 \times 10^{-5}, \quad \lambda_2 = 0.763, \quad \lambda_3 = 1.718 \times 10^{-5}, \quad \lambda_4 = 1.575 \times 10^{-5}$$

$$\lambda_5 = 24.618, \quad \lambda_6 = 81.904 \times 10^{-5}, \quad \lambda_7 = 6.78 \times 10^{-5}$$

Placing these values of the λ coefficients in equations (8), (9) and (10), the three Δ coefficients are calculated. These values are

$$\Delta_1 = 101.20 \times 10^{-5}, \quad \Delta_2 = 118.37 \times 10^{-5}, \quad \Delta_3 = 92.88 \times 10^{-5}$$

Substituting these values of Δ coefficients in equations (19), the rib reactions are obtained; that is

$$F_0 = 1.170 p_0, \quad F_i = 0.918 p_0 \quad (i)$$

TABLE 1. VALUES OF FUNCTIONS $f(x)$, $k(x)$, $m(x)$ FOR A TYPICAL CELL OF A MODEL CELLULAR SHELL

Cylinder	x (in.)	$f(x)$	$k(x)$	$m(x)$
Outer	0	1.3048	0.5238	1.0000
Inner		1.2529	0.5477	1.0000
Outer	0.4	1.2703	0.0196	0.5976
Inner		1.2143	0.0202	0.5980
Outer	0.7	1.2360	-0.1901	0.2986
Inner		1.1750	-0.1985	0.2986
Outer	1.0	1.2222	-0.2594	0
Inner		1.1589	-0.2708	0

Wall deflexions

Wall deflexions are obtained from equations (13), (14) and (i) as

$$w_0^c = -p_0[3.945 - 1.997 f_0(x)] \times 10^{-5} \text{ in.} \quad (ii)$$

and

$$w_i^c = -p_0[-0.395 + 1.363 f_i(x)] \times 10^{-5} \text{ in.} \quad (iii)$$

These deflexions can be evaluated by substituting the values of $f_0(x)$ and $f_i(x)$ from Table 1 into equations (ii) and (iii), respectively. The results are noted in Table 2. From these calculations the deflexion curves can be plotted as shown in Fig. 7.

TABLE 2. DEFLEXIONS OF THE MIDDLE SURFACES OF THE WALLS OF A TYPICAL CELL OF A MODEL CELLULAR SHELL

	Outer wall	Inner wall
x (in.)	$\frac{w_0^c}{p_0} \times 10^5 \frac{\text{in}^3}{\text{lb}}$	$\frac{w_i^c}{p_0} \times 10^5 \frac{\text{in}^3}{\text{lb}}$
0	-1.360	-1.349
0.4	-1.409	-1.296
0.7	-1.477	-1.243
1.0	-1.501	-1.221
p_0 is in lb/in ²		

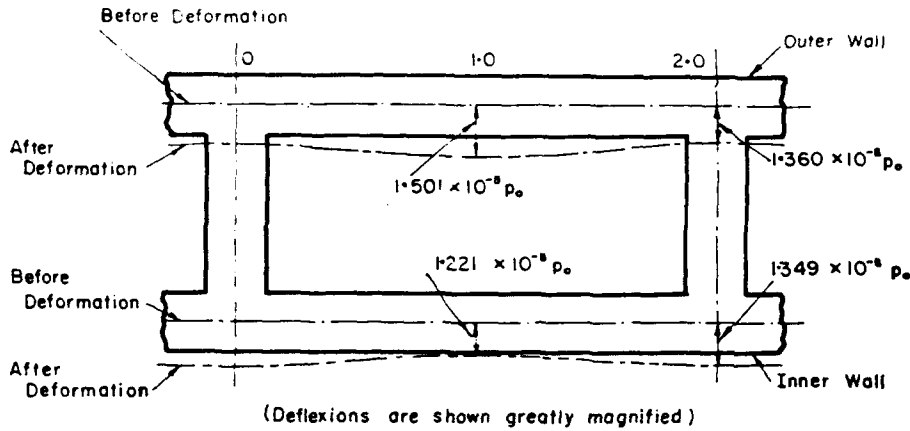


FIG. 7. Deflexion curves for the middle surfaces of the walls of a typical cell of a model cellular shell.

Transverse shear forces and stresses

From equations (22) and (i),

$$Q_0 = -0.585 m_0(x), \quad Q_i = 0.459 m_i(x) \quad (\text{iv})$$

and from equations (24) and (i),

$$(\tau_0)_{\max} = -3.510 m_0(x), \quad (\tau_i)_{\max} = 2.754 m_i(x) \quad (\text{v})$$

These shear forces and stresses are evaluated by using the values of $m(x)$ from Table 1. The results are plotted in Fig. 8.

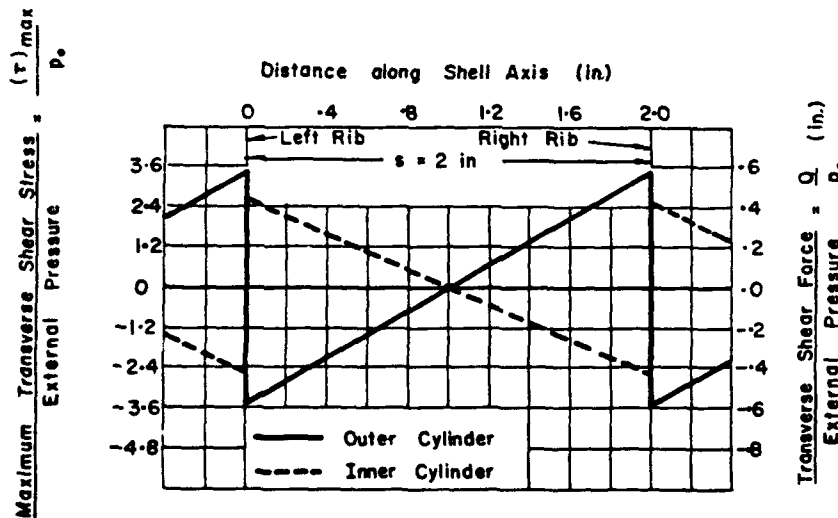


FIG. 8. Transverse shear force-pressure ratio and maximum transverse shear stress-pressure ratio distributions in the walls of a typical cell of a model cellular shell.

Bending moments and stresses

Longitudinal bending moments are obtained from equations (20) and (i) and the circumferential bending moments from equations (21) and (i).

$$M_{x0} = 0.369 p_0 k_0(x) \quad \text{and} \quad M_{xi} = -0.276 p_0 k_i(x) \quad (\text{vi})$$

$$M_{\phi 0} = 0.123 p_0 k_0(x) \quad \text{and} \quad M_{\phi i} = -0.092 p_0 k_i(x) \quad (\text{vii})$$

These bending moments are evaluated by using the values of $k(x)$ from Table 1. The results are plotted in Fig. 9. Table 3 gives values of the bending stresses in the extreme fibers of the walls, calculated from the formula $(\sigma_b)_{ex} = \pm 6M/t^2$.

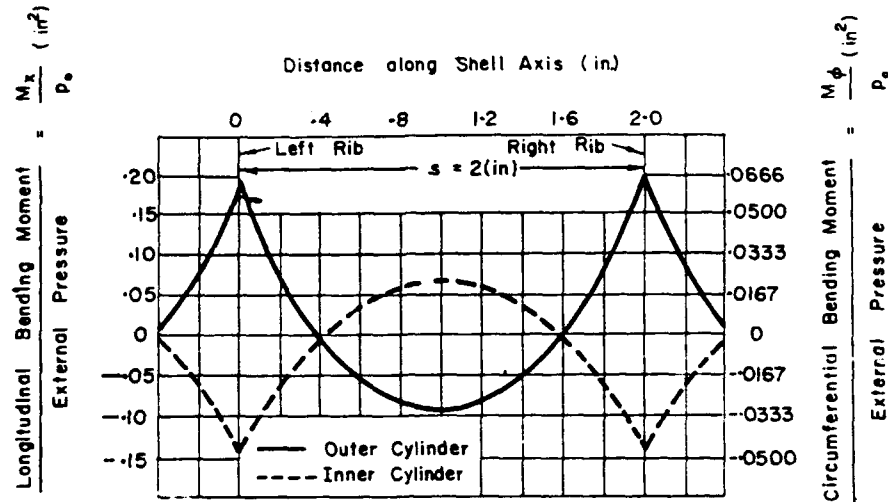


FIG. 9. Longitudinal and circumferential bending moment-pressure ratio distributions in the walls of a typical cell of a model cellular shell.

TABLE 3. MAXIMUM BENDING STRESSES-PRESSURE RATIOS FOR A TYPICAL CELL OF A MODEL CELLULAR SHELL

x (in.)	Outer cylinder		Inner cylinder	
	Longitudinal	Circumferential	Longitudinal	Circumferential
	$\frac{[\sigma_{xbo}]_{ext}}{P_0}$	$\frac{[\sigma_{\phi bo}]_{ext}}{P_0}$	$\frac{[\sigma_{xbi}]_{ext}}{P_0}$	$\frac{[\sigma_{\phi bi}]_{ext}}{P_0}$
0	± 18.53	± 6.17	∓ 14.51	∓ 4.83
0.4	± 0.69	± 0.23	∓ 0.54	∓ 0.18
0.7	∓ 6.72	∓ 2.24	± 5.26	± 1.75
1.0	∓ 9.18	∓ 3.06	± 7.17	± 2.39

p_0 is in lb/in²; the upper sign is for the outer extreme fiber and the lower for inner extreme fiber.

Normal membrane stresses

The longitudinal membrane stresses, as obtained from equation (27), are

$$\sigma_{xm0} = -10.37 p_0 \quad \text{and} \quad \sigma_{xmi} = -11.40 p_0 \quad (\text{viii})$$

The circumferential membrane stresses are obtained from equation (28) and are evaluated by using the values of the wall deflexions from Table 2. That is

$$\begin{aligned} \sigma_{m0} &= -(9.64 |w_0^c| \times 10^5 + 3.45 p_0) \\ \sigma_{mi} &= -(10.98 |w_i^c| \times 10^5 + 3.80 p_0) \end{aligned} \quad (\text{ix})$$

These calculated values are summarized in Table 4.

Resultant normal stresses

The resultant longitudinal and circumferential normal stresses are obtained from equations (29) and (30), respectively. They are evaluated for the extreme fibers of the

walls by using the values of the bending and membrane stresses given in Tables 3 and 4, respectively. The results are plotted in Fig. 10.

TABLE 4. NORMAL MEMBRANE STRESSES—PRESSURE RATIOS FOR A TYPICAL CELL OF A MODEL CELLULAR SHELL

x (in.)	Outer cylinder		Inner cylinder	
	Longitudinal	Circumferential	Longitudinal	Circumferential
	$\frac{\sigma_{xm0}}{p_0}$	$\frac{\sigma_{\phi m0}}{p_0}$	$\frac{\sigma_{xmi}}{p_0}$	$\frac{\sigma_{\phi mi}}{p_0}$
0	-10.37	-16.39	-11.40	-18.07
0.4	-10.37	-17.04	-11.40	-17.51
0.7	-10.37	-17.70	-11.40	-16.95
1.0	-10.37	-17.97	-11.40	-16.71

p_0 is in lb/in²

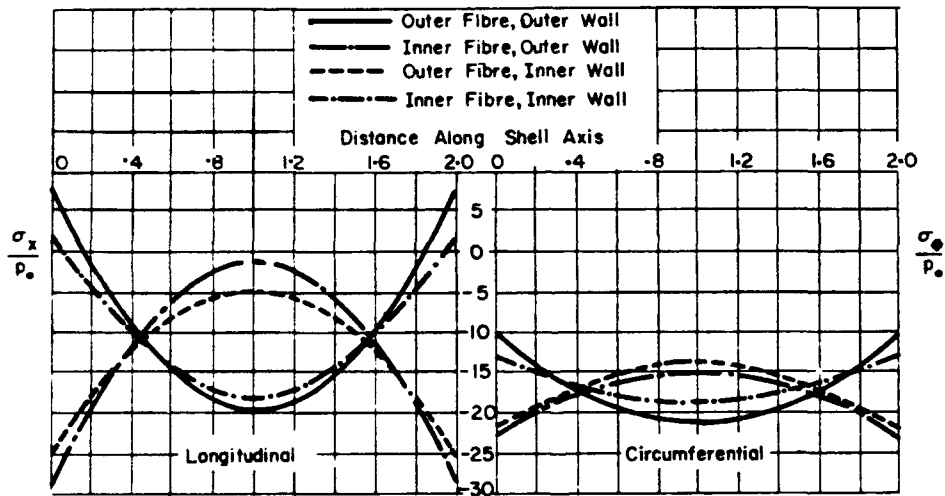


FIG. 10. Longitudinal and circumferential normal stress-pressure ratios for the extreme fibers of the two walls of a typical cell of a model cellular shell.

CONSIDERATION OF STRESS CONCENTRATION IN DESIGN

The foregoing calculations of elastic deformations and stresses in a model cellular shell were based on a theoretical solution which ignored the stress concentrations at the wall and rib junctures. For design purposes it is necessary to include the effect of these stress concentrations in evaluating the yield strength of the shell. A simple method was developed for this purpose as described below.

Two-dimensional photoelastic models shaped according to the configuration of the wall and rib junctures of cellular shells were employed for the approximate determination of the stress concentration factors. These models were subjected to moments applied to the wall in order to obtain the stress concentration factors caused by the bending of the walls. The models were further subjected to

compressive loads applied separately to the walls and the ribs for obtaining the stress concentration factors caused, respectively, by the axial compression of the walls and the compression of the ribs due to the load transmission from the outer to the inner wall. A few of the many photoelastic patterns obtained are shown in Fig. 11. The stress concentration factors thus determined for the bending and for the axial compression of the shell wall and for the compression of the ribs are plotted in Fig. 12. Fig. 12(b) shows the effect of the fillet radius on the location of the maximum bending stress in the shell wall. The use of the stress concentration factors given in Fig. 12 in the design of cellular shells is illustrated by the following numerical example.

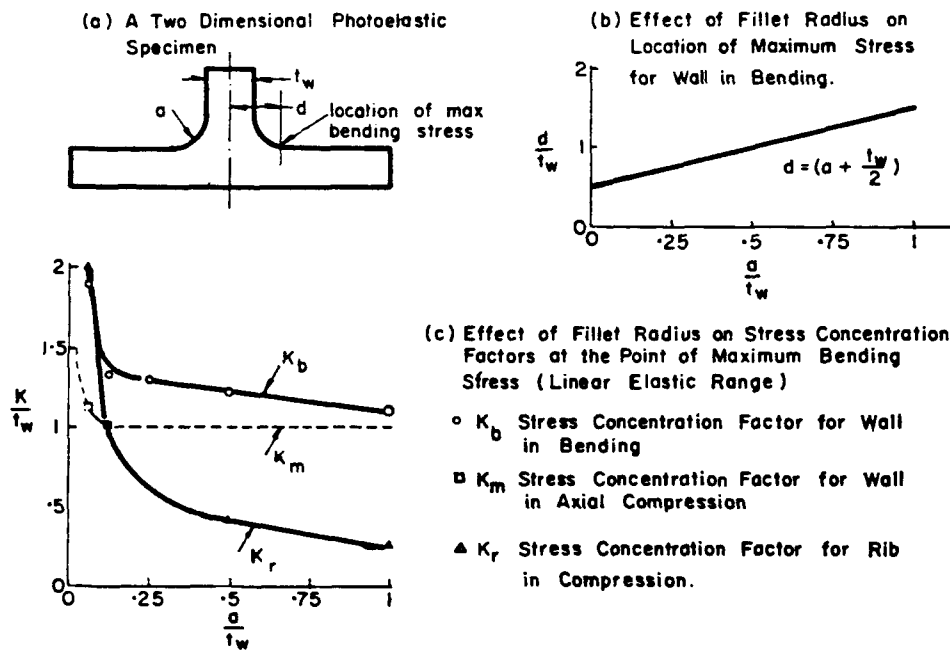


FIG. 12. Stress concentrations at wall and rib junctures.

Fig. 12(b) defines the location of maximum bending stress for a given fillet radius. For these locations the bending and membrane stresses for the model cellular shell are obtained from the preceding theoretical stress calculations. The radial rib stress at the wall and rib juncture is also known from equation (33). These stresses are multiplied by the corresponding stress concentration factors. The resulting values are then added to obtain the maximum normal stresses in the shell as a function of the fillet radius. A summary of this is given in Tables 5 and 6. The yield strength of the model shell as a function of the fillet radius is then calculated by using the distortion energy theory.⁵ A summary of the procedure and the results is given in Table 7. Fig. 13 gives a plot of the yield strength as a function of the fillet radius.

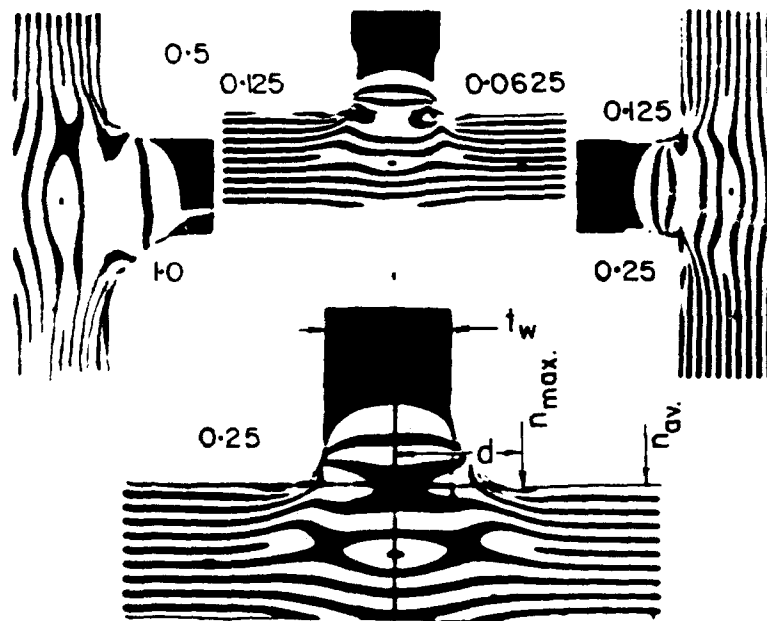


FIG. 11. Two-dimensional photoelastic fringe pattern simulating behaviour of the wall and rib of a cellular shell in pure bending in the linear elastic range for various fillet radii. Numbers near the fillets are a/t_w values, where a = fillet radius and t_w = rib thickness. Stress concentration factor = σ_{max}/σ_{av} .

TABLE 5. ELASTIC STRESSES DUE TO STRESS CONCENTRATIONS

Effect of fillet radius on maximum elastic longitudinal stress-pressure ratios for a model shell at the juncture of the outer wall and a rib.

		Without stress concentration*			With stress concentration			
a/t_w	d (in.)	σ_{x0}/p_0	σ_{xm}/p_0	σ_r/p_0	$k_b \sigma_{x0}/p_0$	$k_m \sigma_{xm}/p_0$	$k_r \sigma_r/p_0$	$[\sigma_{x0}/p_0]_{\text{resultant}}$
0	0.125	-11.85	-10.37	-4.81				
$\frac{1}{16}$	0.140	-11.12	-10.37	-4.81	-21.10	-11.17	-9.01	-41.28
$\frac{1}{8}$	0.156	-10.47	-10.37	-4.81	-14.40	-10.37	-4.81	-29.58
$\frac{1}{4}$	0.187	-9.03	-10.37	-4.81	-11.73	-10.37	-2.76	-24.86
$\frac{1}{2}$	0.250	-6.53	-10.37	-4.81	-8.00	-10.37	-2.04	-20.41
1	0.375	-1.63	-10.37	-4.81	-1.80	-10.37	-1.20	-13.37

 p_0 is in lb/in²

* These values for the model shell are obtained from the preceding stress calculations based upon authors' theoretical solution.

TABLE 6. ELASTIC STRESSES DUE TO STRESS CONCENTRATIONS

Effect of fillet radius on maximum circumferential elastic stress-pressure ratios for a model shell at the juncture of the outer wall and a rib.

		Without stress concentration*		With stress concentration		
a/t_w	d (in.)	$\sigma_{\phi 0}/p_0$	$\sigma_{\phi m}/p_0$	$k_b \sigma_{\phi 0}/p_0$	$k_m \sigma_{\phi m}/p_0$	$[\sigma_{\phi 0}/p_0]_{\text{resultant}}$
0	0.125	-3.95	-16.63			
$\frac{1}{16}$	0.140	-3.71	-16.75	-6.12	-18.97	-25.09
$\frac{1}{8}$	0.156	-3.49	-16.77	-4.88	-16.77	-21.65
$\frac{1}{4}$	0.187	-3.01	-16.78	-3.92	-16.78	-20.70
$\frac{1}{2}$	0.250	-2.18	-16.86	-2.62	-16.86	-19.48
1	0.375	-0.54	-17.20	-0.60	-17.20	-17.80

 p_0 is in lb/in²

* These values for the model shell are obtained from the preceding stress calculations based upon authors' theoretical solution.

TABLE 7. YIELD STRENGTH OF A MODEL SHELL

Effect of fillet radius on the yield strength of a model shell based on the distortion energy theory (stress concentrations included).

a/t_w	d (in.)	σ_1/p_0	σ_2/p_0	$\frac{(\sigma_1 - \sigma_2)^2}{p_0^2}$	$\frac{\sigma_1^2}{p_0^2}$	$\frac{\sigma_2^2}{p_0^2}$	$\frac{2\sigma_1\sigma_2}{p_0^2}$	$\frac{\sqrt{(2)} \sigma_{vp}}{p_0}$	$\frac{\sigma_{vp}}{p_0}$
$\frac{1}{16}$	0.140	-25.09	-41.28	262.0	629	1700	2591.0	-50.9	-36.0
$\frac{1}{8}$	0.156	-21.65	-29.58	62.9	469	875	1406.9	-37.2	-26.3
$\frac{1}{4}$	0.187	-20.70	-24.86	17.3	428	618	1063.3	-34.6	-23.0
$\frac{1}{2}$	0.250	-19.48	-20.41	0.9	379	416	795.9	-28.2	-19.9
1	0.375	-17.80	-13.37	19.6	317	179	575.6	-22.7	-16.1

Distortion energy theory (see Ref. 5, p. 454):

$$2\sigma_{vp}^2 = (\sigma_1 - \sigma_2)^2 + (\sigma_2 - \sigma_3)^2 + (\sigma_3 - \sigma_1)^2$$

where $\sigma_1 = \sigma_{\phi 0}$ (Table 7), $\sigma_2 = \sigma_{x0}$ (Table 6), $\sigma_3 = 0$.

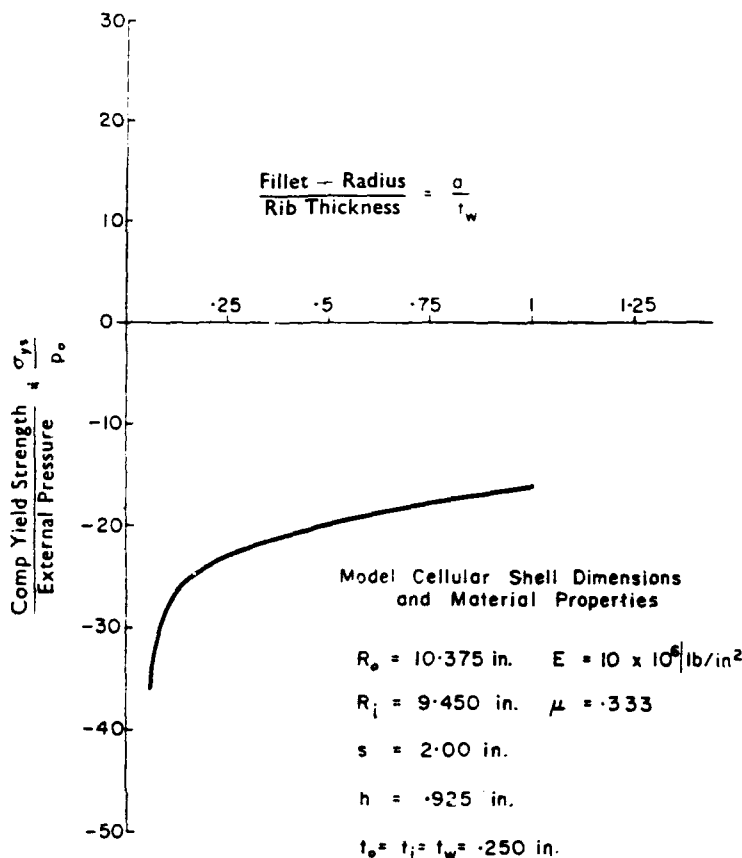


FIG. 13. Yield strength of the model shell.

DISCUSSION

An analytical solution for elastic stresses in cellular shells subjected to uniform external pressure was developed in this paper based upon certain assumptions. The first assumption made was that the beam-column effect caused by the external axial pressure is negligible. The calculations carried out for the model shell selected show that the wall deflexions are very small and, therefore, the secondary bending moments caused by the external axial pressure are indeed negligible.

Secondly, the ratio of the wall spacing to the mean radius of the shell is assumed to be small. In such cases, the assumption made regarding the distribution of the external axial load between the two shell walls will be reasonably accurate.

Thirdly, the theoretical analysis ignored the stress concentrations arising at the wall and rib junctures. The method proposed in this paper to include the effect of the stress concentrations in determining the yield strength of cellular shells is an approximate one, since two-dimensional models were employed to obtain the stress concentration factors. Further, the conditions of loading used in these experiments were different from the actual, since

separate loadings in bending and compression of the walls and in compression of the ribs were used. However, the proposed procedure is a simple one and may be quite adequate for practical purposes. The accuracy of this procedure can be determined only by future experimental work.

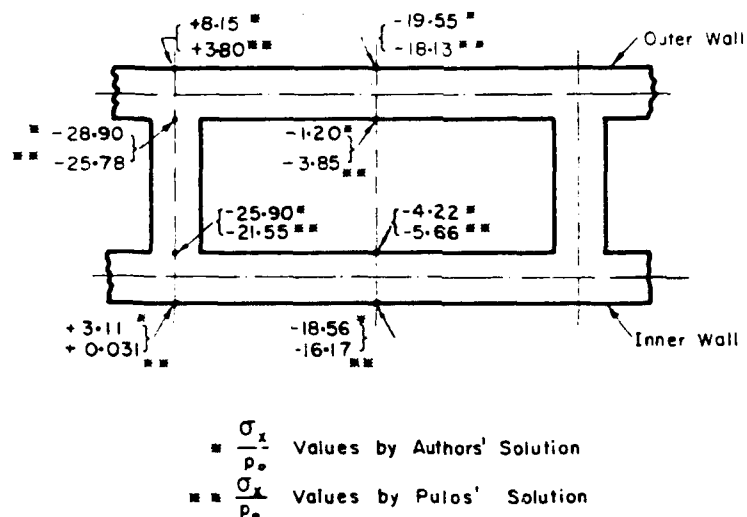


FIG. 14. Comparison of the normal longitudinal stress-pressure ratios obtained by the solution of the authors and that of Pulos.

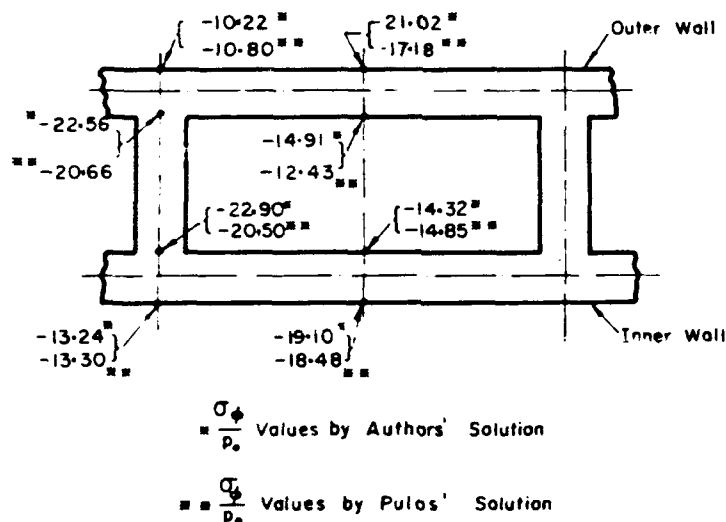


FIG. 15. Comparison of the normal circumferential stress-pressure ratios obtained by the solution of the authors and that of Pulos.

Near the completion of this study, the authors learned of another theoretical solution of the same problem developed by Pulos⁴. In this solution, a theory was developed by using the method of edge coefficients. It is of interest to compare the solution given in this paper with that made by Pulos. The results of this comparison for the model shell are summarized in Figs. 14 and 15. The

stress values obtained from these two solutions show an overall good agreement. The difference between the critical stress values calculated from the two solutions for the model shell is about 10 per cent. This difference is evidently due to the different assumptions made in the two methods of solution. Experimental investigations are necessary to determine the relative accuracy of the two theories. The solution of this paper, like that of Pulos, is applicable only to a typical bay of the cellular shell.

CONCLUSIONS

The purpose of this study was to furnish a method which would enable designers to predict the yield strength of a ring-stiffened sandwich shell subjected to uniform external pressure. The theoretical solution for elastic stresses obtained in this paper, when used in conjunction with the experimentally determined stress concentration factors, gives one such method. Experimental work will be necessary to determine the accuracy of the method. However, the theoretical solution given in this paper gives elastic stress values which are quite close to those obtained by another theory recently published by Pulos⁴. The method proposed in this paper gives a simple method for evaluating the yield strength of ring-stiffened sandwich shells.

Acknowledgements—The authors take this opportunity to thank Professors Key and Fitzgerald of the Ordnance Research Laboratory of The Pennsylvania State University under whose sponsorship the study presented in this paper was undertaken. The photo-elastic patterns and the stress concentration factors included in the paper were obtained by Mr. P. W. Hill of the Department of Engineering Mechanics of the Pennsylvania State University. The help of Dr. J. Marin, Head of the Department of Engineering Mechanics of The Pennsylvania State University, in the preparation of this paper is also acknowledged.

REFERENCES

1. R. E. FULTON, *Buckling Analysis and Optimum Proportions of Sandwich Cylindrical Shells under Hydrostatic Pressure*, Structural Research Series No. 199, University of Illinois (1960).
2. P. K. MEHTA, *Axisymmetric Elastic Stresses in Ring-Stiffened Sandwich Shells subjected to Uniform External Pressure*, Thesis in Engineering Mechanics, Department of Engineering Mechanics, The Pennsylvania State University (1962).
3. J. D. STACHIW, *General Instability of Circumferentially Stiffened Sandwich Shells subjected to Uniform External Pressure*, Thesis in Engineering Mechanics, Department of Engineering Mechanics, The Pennsylvania State University (June 1961).
4. J. G. PULOS, *Axisymmetric Elastic Deformations and Stresses in a Web-Stiffened Cylinder under External Hydrostatic Pressure*, David Taylor Model Basin Report 1543 (Nov. 1961).
5. S. TIMOSHENKO, *Strength of Materials*, II, pp. 205-210. D. Van Nostrand Co., New York (1959).
6. S. TIMOSHENKO and WOINOWSKY-KREIGER, *Theory of Plates and Shells*. McGraw-Hill, New York (1959).

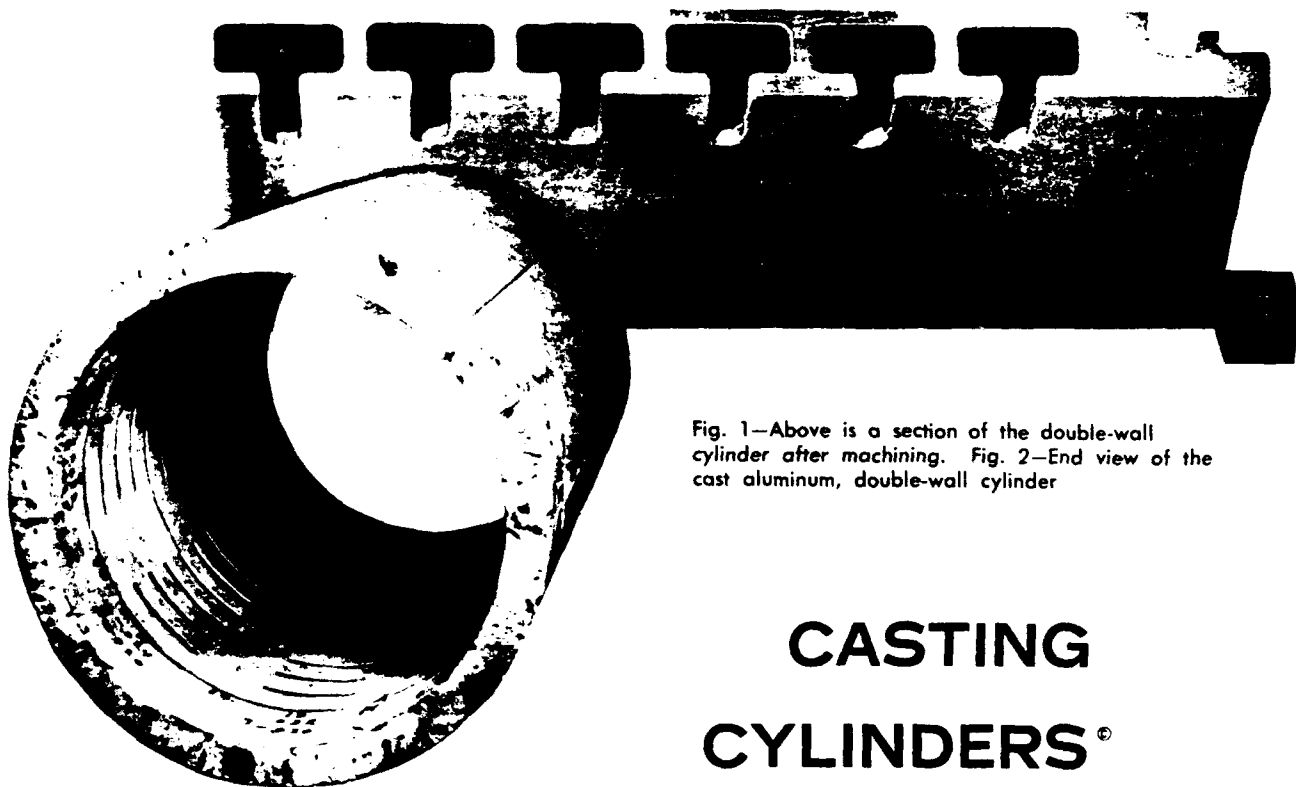


Fig. 1—Above is a section of the double-wall cylinder after machining. Fig. 2—End view of the cast aluminum, double-wall cylinder

CASTING CYLINDERS®

Subjected to External Pressure

● **CONSIDERABLE** effort has been devoted to gaining an understanding of the collapse of cylindrical vessels designed to withstand external pressure. Most of the early research was limited to simple cylinders and ring-reinforced cylinders. Despite their relative simplicity, 50 years of research were required to develop acceptable engineering formulas for ring-reinforced cylinders. Because modern technology requires vessels with high pressure-to-weight ratios, ring-reinforced cylinders no longer are adequate, despite the high-strength alloys now available.

Studies of cylinders of double-wall or sandwich-wall construction are being made in many countries. At the Ordnance Research Laboratory of Pennsylvania State University, a study¹ was made of ring-reinforced double-wall cylinders (Fig. 1 and 2).

By J. D. STACHIW

Ordnance Research Laboratory
Pennsylvania State University
State College, Pa.

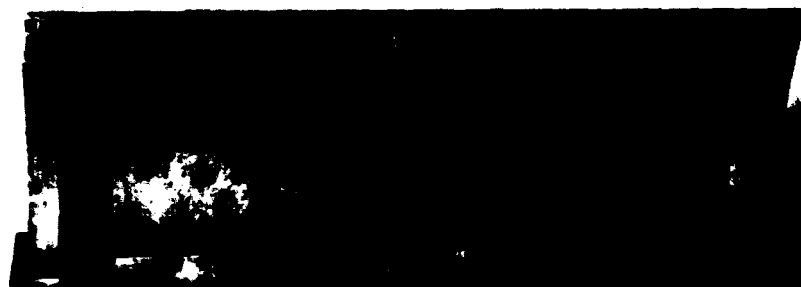
An elastic-instability formula for this type of pressure vessel was developed² first because no experimentally proved equations were available. With this design formula, the collapse pressure of the double-wall cylinder was predicted within 5 per cent.

Casting was selected as the construction method because it provided the greatest ease of including mounting bosses on the inner sur-

face of the cylinder. Aluminum alloy 356-T6 was chosen because it is light, resistant to salt-water corrosion, and can be cast in large, intricate shapes.

Design Goal—The design goal was to produce a cylindrical external-pressure vessel with a very high pressure-to-weight ratio. The final design of the cylinder represented a compromise between the desires of the designer and those of the foundry: The designer wished the cylinder facings to be free of openings, and the foundry desired as many core-support openings as possible.

Fig. 3—Sectional view of a cast aluminum, single-wall cylinder after machining. It was cast for comparison tests



In the final casting, each annular core ring was supported at eight points around its circumference (Fig. 2). Considerable skill was required to minimize distortion and shrinkage of the fragile cores during the pouring operation. Typical mechanical properties of the heat treated 356 alloy castings (supplied by Bendix Foundries) are shown in Table I.

A ring-reinforced single-wall cylinder of the same outside diameter, length, and material (Fig. 3)

TABLE I—Mechanical Properties in Cast Ring-Reinforced Cylinders

Mechanical Property	Double Wall	Single Wall
Yld str, psi	27,000	28,000
Ten str, psi	36,000	36,400
Elong, %	4	4
Hardness (Bhn)	76	74

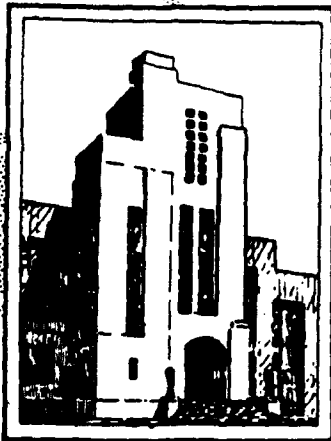
also was cast to provide an experimental comparison with the double-wall cylinder. Mechanical properties of the material in the single-wall cylinder also are shown in Table I.

The machined cylinders were implosion tested at the Southwest Research Institute, San Antonio, Tex. To seal the ends of the cylinders without appreciably affecting their elastic stability, they were placed between flat plates which were held in place only by the imposed external pressure. By use of the expression $r = p_c V/W$, the pressure-to-weight ratio of the single-wall cylinder is found to be 1.26×10^5 and that of the double-wall cylinder, 2.14×10^5 . In this expression, r is the pressure-to-weight ratio; p_c is the collapse pressure in psi; V is the displacement in cubic inches per inch of axial length; and W is the weight of the cylinder in pounds per inch of axial length. The pressure-to-weight ratio of the double-wall cylinder thus represents a 70 per cent improvement over that of the single-wall cylinder.

Engineers of the Ordnance Research Laboratory and the craftsmen of Bendix Foundries have produced a cylindrical structure that combines the best properties of cast aluminum with the most advanced theories of the elastic stability of cylindrical vessels subjected to external pressure.

REFERENCES

1. J. D. Stachiw, "Hollow Core Structures for High Pressure Hulls," *Journal of Undersea Technology*, Vol. 2, No. 2, 1961.
2. J. D. Stachiw, "General Instability of Circumferentially Stiffened Sandwich Shell Under External Hydrostatic Pressure," master's dissertation, Department of Engineering Mechanics, Pennsylvania State University, 1961.



DEPARTMENT OF THE NAVY
DAVID TAYLOR MODEL BASIN

HYDROMECHANICS

○

AERODYNAMICS

○

STRUCTURAL
MECHANICS

○

APPLIED
MATHEMATICS

AXISYMMETRIC ELASTIC DEFORMATIONS AND STRESSES
IN A WEB-STIFFENED SANDWICH CYLINDER UNDER
EXTERNAL HYDROSTATIC PRESSURE

by

John G. Pulos

STRUCTURAL MECHANICS LABORATORY
RESEARCH AND DEVELOPMENT REPORT

November 1961

Report 1543

**AXISYMMETRIC ELASTIC DEFORMATIONS AND STRESSES
IN A WEB-STIFFENED SANDWICH CYLINDER UNDER
EXTERNAL HYDROSTATIC PRESSURE**

by

John G. Pulos

November 1961

**Report 1543
S-F013 03 02**

TABLE OF CONTENTS

	Page
ABSTRACT.....	1
INTRODUCTION	1
GENERAL CONSIDERATIONS	2
COMPUTATION OF STRESSES.....	9
DETERMINATION OF EDGE SHEARS H_i AND EDGE MOMENTS M_i	12
NUMERICAL EXAMPLE.....	15
ACKNOWLEDGMENTS	18
APPENDIX A – DERIVATION OF THE FUNCTIONS $\Lambda^{[1]}$, $\Lambda^{[2]}$, $\Lambda^{[3]}$, $\Lambda^{[4]}$, $\Lambda^{[5]}$, AND $\Lambda^{[6]}$	19
APPENDIX B – DEVELOPMENT OF EDGE COEFFICIENTS AND EXPRESSIONS FOR THE RADIAL AND TANGENTIAL STRESSES OF A CIRCULAR ANNULUS	26
APPENDIX C – DEVELOPMENT OF EXPRESSIONS FOR THE SHELL STRESSES, EQUATIONS [11] THROUGH [14].....	30
APPENDIX D – DETERMINATION OF AXIAL-PRESSURE LOAD DISTRIBUTION TO THE TWO COAXIAL CYLINDERS.....	34
REFERENCES	37

LIST OF FIGURES

	Page
Figure 1 – Web-Stiffened Sandwich Cylinder Subjected to External Hydrostatic Pressure	2
Figure 2 – Free-Body Diagram Showing Forces and Moments Acting on Shell and Web Elements of Web-Stiffened Sandwich Cylinder	3
Figure 3 – Shell Element of Arbitrary Meridional Shape Subjected to Edge Moments, Shears, Forces, and Surface Loading.....	3
Figure 4 – Sign Convention for Cylindrical-Shell Element	4
Figure 5 – Sign Convention for Web Element.....	4
Figure 6 – Schematic Diagram Showing Dimensions of Model N-1	15
Figure 7 – Edge Shears, Moments, Deflections, and Rotations for a Cylindrical-Shell Element	20
Figure 8 – Distribution of Axial-Pressure Load to the Two Cylindrical Shells.....	34

LIST OF TABLES

Table 1 – Numerical Values of the Functions $\Lambda^{[1]}(\beta l)$ Through $\Lambda^{[6]}(\beta l)$ for a Range of βl from 0.40 to 2.50 in Increments of 0.02	8
--	---

NOTATION

$a_i, b_i, c_i, d_i, f_i, g_i$ $\bar{a}_i, \bar{b}_i, \bar{c}_i, \bar{d}_i, \bar{f}_i, \bar{g}_i$	Coefficients representing edge rotation and displacement per unit edge or surface load for shell elements of short length
$D_i = \frac{E^s h_i^3}{12(1-\nu^2)}$	Flexural rigidity of shells
E^A, E^s	Young's modulus of annulus and shell materials, respectively
H_i, H_j	Discontinuity shearing forces normal to axis of symmetry
h_i	Shell thickness
l	Length of shell element between stiffeners
M_i, M_j	Discontinuity bending moments in a meridional plane
P_i	Axial stress-forces due to axial portion of p
p	Hydrostatic pressure
R_i, R_j	Radial distances from axis of symmetry
r	Variable radial distance from axis of symmetry
w_i^A	Radial displacement of annulus edges
w_i^s	Radial displacement of shells
x	Axial coordinate taken along shell element
β_i	$= \frac{\sqrt[3]{3(1-\nu^2)}}{\sqrt{R_i h_i}}$
ϵ	Strain
θ_i^s	Axial rotation of shells
$\Lambda^{[1]}, \Lambda^{[2]}, \Lambda^{[3]}$ $\Lambda^{[4]}, \Lambda^{[5]}, \Lambda^{[6]}$ }	Lambda functions defining edge effects and interaction of edge effects for shell elements of short length
ν	Poisson's ratio
σ	Stress

ABSTRACT

A theoretical analysis of the axisymmetric elastic deformations and stresses in a web-stiffened sandwich cylindrical shell structure under external hydrostatic pressure is presented. The solution is based on the use of edge coefficients for plate and shell elements of finite length, and includes the computation of the edge forces and moments arising at the common junctures of these elements.

Equations are given for computing numerically the longitudinal and circumferential stresses in the two coaxial cylindrical shells and the radial and tangential stresses in the web stiffeners between the two shells.

No consideration was given to the discontinuity effects arising from rigid or elastic restraints afforded by contiguous bulkhead or adjacent shell structures. Thus, the analysis presented herein is applicable only to a typical bay of a web-stiffened sandwich cylinder of long length.

A numerical example is presented to illustrate the use of the equations developed in this report.

INTRODUCTION

The David Taylor Model Basin, under initial sponsorship by the Office of Naval Research and later continuance by the Bureau of Ships, has been investigating the feasibility of sandwich-type construction for pressure hull application. Results of exploratory experimental studies carried out under this program¹ have shown that in certain ranges of geometry strength-weight advantages on the order of 20 to 25 percent higher can be realized with sandwich designs over the conventional ring-stiffened cylindrical configuration. These results were obtained from model tests of sandwich-type cylinders having "hard" cores; i.e., the cores were capable of developing high compressive strengths in addition to transmitting the pressure loading by shear from the outer to the inner shell.

At the time these sandwich cylinders were conceived, no formulas were available on which to base an optimum design; merely intuition and engineering judgment were resorted to for proportioning the structural elements. Concurrently with the experimental program, analytical studies were initiated to develop rational formulas based on thin-shell theory for predicting the elastic deformations and stresses in the structural elements of such sandwich-type cylinders.

In this report, equations are developed for carrying out a complete stress analysis of a typical portion of a web-stiffened sandwich cylinder under external hydrostatic pressure.

¹References are listed on page 37.

The method is based on the use of edge coefficients of plate and shell elements of finite length, and satisfaction of force and moment equilibrium and compatibility of deformations at the common junctures of the elements comprising the structure. Expressions for edge coefficients of cylindrical shells of short length are developed in Appendix A.

GENERAL CONSIDERATIONS

Methods of analysis based on the use of edge coefficients have found wide application in studying stresses and deformations in complex structures composed of ring, plate, and shell elements.²⁻⁵ The underlying concept in this type of analysis is that a complex physical structure can be broken down into identifiable components for which mathematical solutions exist or can be found readily. The deformations occurring in each structural element are determined in terms of unknown forces and moments assumed to exist at the junctures common to these elements. Conditions of equilibrium and compatibility are then satisfied at each of the junctures, thus permitting determination of the redundant forces and moments. With this information, a complete stress analysis for each structural component can then be performed.

The present problem of the stresses in a web-stiffened sandwich cylinder subjected to hydrostatic pressure, shown in Figure 1, can be solved rather conveniently by the use of edge coefficients. The identifiable structural elements in this case are two coaxial cylindrical

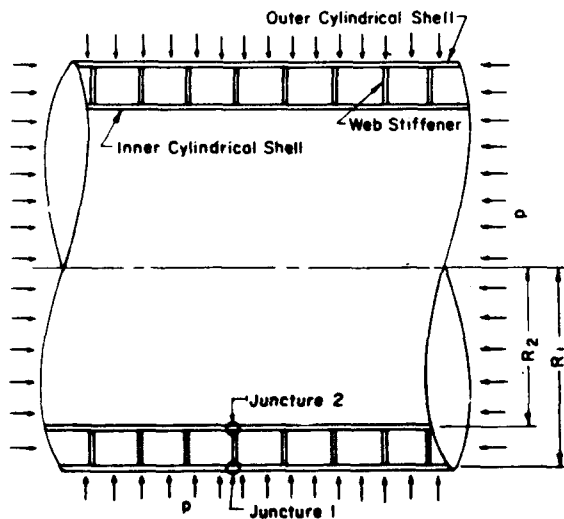
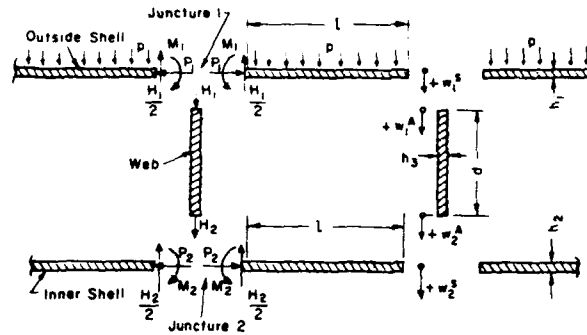


Figure 1 – Web-Stiffened Sandwich Cylinder Subjected to External Hydrostatic Pressure

shells, one subjected to radial pressure and an end load and the other to an end load only, and annular discs subjected to radial loads on the two circular boundaries. The webs or annular discs act as the connecting and stiffening members to the two shells. A free-body diagram showing the breakdown of the physical structure to its component parts, together with appropriate, but as yet unknown, edge forces and moments, is presented in Figure 2.

Figure 2 - Free-Body Diagram Showing Forces and Moments Acting on Shell and Web Elements of Web-Stiffened Sandwich Cylinder



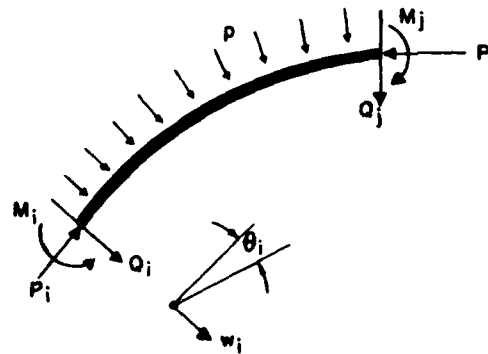
Following the method of References 2, 3, and 4, the deformations occurring at the edges of a shell element of general meridional shape can, by simple superposition, be written in terms of the unknown edge forces and edge moments and known applied loading as follows:

$$w_i = d_i M_i + g_i Q_i + f'_i P_i + f''_i p_i + f'''_i P_i + d_{ij} M_j + g_{ij} Q_j + f'_{ij} P_j \quad [1]$$

$$\theta_i = a_i M_i + b_i Q_i + c'_i P_i + c''_i p_i + c'''_i P_i + a_{ij} M_j + b_{ij} Q_j + c'_{ij} P_j \quad [2]$$

where the coefficients a_i, b_i, \dots, f'''_i are the amount of transverse deflection or meridional rotation, as the case may be, per unit bending moment, shearing force, axial force, or surface pressure loading, as shown in Figure 3. The coefficients with the double subscripts, i.e.,

Figure 3 - Shell Element of Arbitrary Meridional Shape Subjected to Edge Moments, Shears, Forces, and Surface Loading



$a_{ij}, b_{ij}, \dots, f'_{ij}$, are the interaction coefficients which reflect the deformations at edge "i" due to forces and moments at edge "j." By replacing $i \rightarrow j$ and $j \rightarrow i$ in Equations [1] and [2], expressions for the deformations w_j and θ_j can be written immediately.

Note that the effect of the end load P on the deformations w_i and θ_i has been separated into three distinct components. The components denoted by the single-primed coefficients f'_i and c'_i are those due to bending effects. The same is true of the components associated with the coefficients f'_{ij} and c'_{ij} , but these also reflect interaction influences. The components

denoted by the triple-primed coefficients f_i''' and c_i''' are essentially Poisson effects on the membrane deformations.

For the specific problem of cylindrical shell elements symmetrically loaded, as shown in Figure 4 and considered in this report, Equations [1] and [2] become:

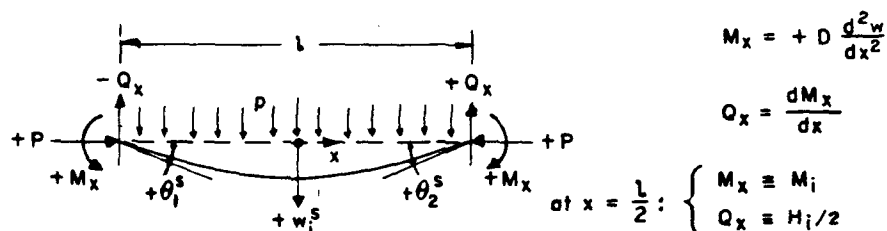


Figure 4 - Sign Convention for Cylindrical-Shell Element (Symmetric Case)

$$w_i^s = d_i M_i^s + g_i \frac{H_i^s}{2} + f_i' P_i^s + f_i'' p + f_i''' P_i^s + d_{ij} M_j^s + g_{ij} \frac{H_j^s}{2} + f_{ij}' P_j^s \quad [3]$$

$$\theta_i^s = a_i M_i^s + b_i \frac{H_i^s}{2} + c_i' P_i^s + c_i'' p + c_i''' P_i^s + a_{ij} M_j^s + b_{ij} \frac{H_j^s}{2} + c_{ij}' P_j^s \quad [4]$$

and similar expressions for w_j and θ_j , respectively. However, for the case of a cylinder some of the terms appearing in Equations [3] and [4] become zero; this will be shown later. In addition, for the pressure loading shown in Figure 1, where the inner cylindrical shell is not subjected to the radial pressure loading, those terms in Equations [3] and [4] that are multiplied by p will drop out when the deformations of the inner shell, i.e. $i = 2$, are considered.

Following the same technique employed for the shell elements, the deformations occurring at the edges of the circular annuli or web elements, as shown in Figure 5,

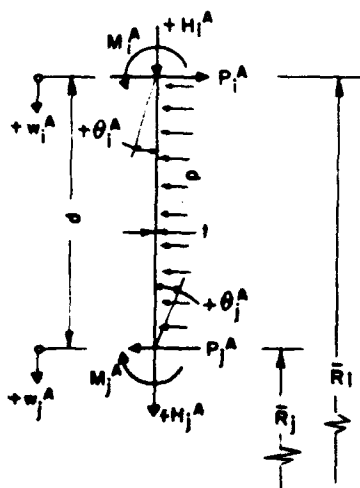


Figure 5 - Sign Convention for Web Element

can be written in terms of the unknown edge forces and moments and known applied loading as follows:

$$w_i^A = g_i^A H_i^A + g_{ij}^A H_j^A \quad [5]$$

$$\theta_i^A = a_i^A M_i^A + c_i^A P_i^A + d_i^A p + a_{ij}^A M_j^A \quad [6]$$

where it has been assumed that the edge moments M_i^A , axial thrusts P_i^A , and surface pressure p do not give rise to any radial displacement w in the plane of the circular annulus. Equations [5] and [6] give the deformations at boundary i of the circular annulus; the deformations at the other boundary, say j , can be obtained by replacing i by j and j by i in Equations [5] and [6]. The expression for the edge rotations θ_i^A and θ_j^A of the annulus are rather general to include the case in which the sandwich void between the two cylinders may become pressurized. This problem will not be considered in this report. In a later section, it will be shown that due to symmetry the edge rotations of the annulus are zero. Furthermore, for the particular case of pressure loading shown in Figure 1 and considered in detail later including a numerical example, not only are the edge rotations θ_i^A and θ_j^A equal to zero but every term in expressions [6] is zero. In such a case it is tacitly assumed that the web stiffeners act only to resist hoop compression and do not act in the sense of a circular plate to resist bending due to edge moments and edge shears.

In Reference 4, for instance, equations were developed for computing discontinuity stresses at cone-cylinder junctures, either with or without transverse reinforcement. For that problem it was tacitly assumed that the shell elements were each of semi-infinite length so that the deformations at their common juncture were not influenced by boundary effects at the others ends. This permitted the use of rather simple expressions for the edge deformations.

For the present problem of the web-stiffened sandwich cylinder, the elements comprising the structure are of such proportions that interaction of internal edge effects is very predominant. This necessitated the development of edge coefficients for cylindrical shell elements of finite length. However, it turns out that the forms of the new coefficients are exactly the same as those of Reference 4 except for multiplying factors which are functions of the shell geometry and, primarily, the length. These edge coefficients for a cylindrical shell are written in the following convenient form:

$$E^s a_i = + \frac{1}{D_i' \beta_i} \Lambda_i^{[2]}(\beta_i l)$$

$$E^s b_i = - \frac{1}{2D_i' \beta_i^2} \Lambda_i^{[1]}(\beta_i l)$$

$$E^s c_i' = E c_i'' = E c_i''' = E f_i' = 0$$

$$E^s d_i = + \frac{1}{2D_i' \beta_i^2} \Lambda_i^{[1]}(\beta_i l)$$

$$E^s f_i'' = + \frac{R_i^2}{h_i}$$

$$E^s f_i''' = - \nu \frac{R_i}{h_i}$$

[7a]

$$E^s g_i = - \frac{1}{2D_i' \beta_i^3} \Lambda_i^{[3]}(\beta_i l)$$

$$E^s a_{ij} = - \frac{1}{D_i' \beta_i} \Lambda_i^{[6]}(\beta_i l)$$

$$E^s b_{ij} = + \frac{1}{2D_i' \beta_i^2} \Lambda_i^{[4]}(\beta_i l)$$

$$E^s c_{ij} = E f_{ij}' = 0$$

$$E^s d_{ij} = - \frac{1}{2D_i' \beta_i^2} \Lambda_i^{[4]}(\beta_i l)$$

$$E^s g_{ij} = + \frac{1}{2D_i' \beta_i^3} \Lambda_i^{[5]}(\beta_i l)$$

where

$$D_i' \equiv \frac{D_i}{E} = \frac{h_i^3}{12(1-\nu^2)} ; \beta_i = \frac{\sqrt{3(1-\nu^2)}}{\sqrt{R_i h_i}} \quad [7b]$$

The "lambda" functions $\Lambda_i^{[1]}$, $\Lambda_i^{[2]}$, $\Lambda_i^{[3]}$, . . . $\Lambda_i^{[6]}$ appearing in the edge coefficients, Equations [7a], are derived in Appendix A and are defined here as follows:

$$\Lambda_i^{[1]}(\beta_i l) = \frac{\sinh^2 \beta_i l + \sin^2 \beta_i l}{\sinh^2 \beta_i l - \sin^2 \beta_i l}$$

$$\Lambda_i^{[2]}(\beta_i l) = \frac{\cosh \beta_i l \sinh \beta_i l + \cos \beta_i l \sin \beta_i l}{\sinh^2 \beta_i l - \sin^2 \beta_i l}$$

$$\begin{aligned}
\Lambda_i^{[3]}(\beta_i l) &= \frac{\cosh \beta_i l \sinh \beta_i l - \cos \beta_i l \sin \beta_i l}{\sinh^2 \beta_i l - \sin^2 \beta_i l} \\
\Lambda_i^{[4]}(\beta_i l) &= \frac{2 \sinh \beta_i l \sin \beta_i l}{\sinh^2 \beta_i l - \sin^2 \beta_i l} \\
\Lambda_i^{[5]}(\beta_i l) &= \frac{\cosh \beta_i l \sin \beta_i l - \sinh \beta_i l \cos \beta_i l}{\sinh^2 \beta_i l - \sin^2 \beta_i l} \\
\Lambda_i^{[6]}(\beta_i l) &= \frac{\cosh \beta_i l \sin \beta_i l + \sinh \beta_i l \cos \beta_i l}{\sinh^2 \beta_i l - \sin^2 \beta_i l}
\end{aligned} \tag{8}$$

For convenience and ease of calculation, numerical values of the "lambda" functions in [8] were determined with the aid of a Burroughs E-101 computer for a range of $\beta_i l$ from 0.40 to 2.50 in increments of 0.02. The results were tabulated and are given in this report as Table 1.

For the special case of a cylindrical shell of semi-infinite length, i.e., $l \rightarrow \infty$, the interaction functions given by Equations [8] simplify to

$$\begin{aligned}
\Lambda_i^{[1]} &= \Lambda_i^{[2]} = \Lambda_i^{[3]} = 1 \\
\Lambda_i^{[4]} &= \Lambda_i^{[5]} = \Lambda_i^{[6]} = 0
\end{aligned} \tag{9}$$

and the edge coefficients given by Equations [7a] reduce exactly to those given in Reference 4.

From symmetry considerations it is seen that the edges of the web stiffener, which for purposes of analysis is viewed as a circular annulus, do not undergo any rotation. This stems from the fact that a horizontal tangent or zero-slope condition is assumed to exist at the junctures of the webs with the two cylindrical shells. This assumption implies that the edge moments on each shell at the shell-web junctures balance each other, so that there are no net moments to be resisted by the web. Further, it is assumed that the web elements do not take any axial force due to the axial pressure, but that this is all resisted by the cylindrical shells. Thus, the analysis of the web stiffener is reduced to that of a circular annulus subjected to axisymmetric in-plane radial forces on both its inner and outer boundaries;⁶ see Figure 2. On the basis of these assumptions, it is necessary to derive edge coefficients for an annulus undergoing radial deflections only. Such coefficients are developed in Appendix B and are given here as follows:

TABLE 1

Numerical Values of the Functions $\Lambda^{(1)}(\beta t)$ through $\Lambda^{(6)}(\beta t)$ for a Range of βt from 0.40 to 2.50 in Increments of 0.02

(βt)	$\sin(\beta t)$	$\sinh(\beta t)$	$\cos(\beta t)$	$\cosh(\beta t)$	$\Lambda^{(1)}$	$\Lambda^{(2)}$	$\Lambda^{(3)}$	$\Lambda^{(4)}$	$\Lambda^{(5)}$	$\Lambda^{(6)}$
0.40	0.389418	0.410752	0.921060	1.08107	18.7667	47.0736	5.00122	18.7396	2.49909	46.8736
0.42	0.407760	0.432457	0.913088	1.09950	17.0750	40.6483	4.76331	16.9954	2.37989	40.4783
0.44	0.425939	0.454335	0.904751	1.09837	15.5161	35.3813	4.54707	15.4835	2.27151	35.1613
0.46	0.443948	0.476395	0.896052	1.10767	14.1998	30.9919	4.34968	14.1643	2.17752	30.7619
0.48	0.461779	0.498645	0.886994	1.11742	13.0449	27.3050	4.16877	13.0063	2.08175	27.0650
0.50	0.479425	0.521095	0.877582	1.12762	12.0261	24.1856	4.00237	11.9844	1.99821	23.9157
0.52	0.496880	0.543753	0.867819	1.13827	11.1279	21.5289	3.84882	11.0779	1.92106	21.7690
0.54	0.514135	0.566679	0.857708	1.14937	10.3186	19.2524	3.70670	10.2698	1.84910	18.9826
0.56	0.531186	0.589731	0.847255	1.16094	9.5916	17.2906	3.57477	9.54686	1.78370	17.0108
0.58	0.548023	0.613070	0.836462	1.17296	8.9317	15.5911	3.45199	8.8910	1.72135	15.3013
0.60	0.564642	0.636653	0.825335	1.18546	8.3702	14.1116	3.33744	8.3104	1.66358	13.8118
0.62	0.581035	0.660491	0.813878	1.19843	7.8460	12.8178	3.23034	7.74052	1.60950	12.5080
0.64	0.597195	0.684594	0.802095	1.21188	7.36708	11.6416	3.12998	7.79887	1.55875	11.3619
0.66	0.613116	0.708970	0.789992	1.22582	6.93763	10.6798	3.03577	6.86010	1.51105	10.3502
0.68	0.628773	0.733630	0.777752	1.24024	6.5626	9.79336	2.94715	6.45929	1.46610	9.45377
0.70	0.644217	0.758583	0.764842	1.25516	6.17371	9.00611	2.86366	6.09214	1.42368	8.65657
0.72	0.659384	0.783840	0.751805	1.27059	5.84126	8.30469	2.78487	5.75500	1.38356	7.94523
0.74	0.674287	0.809410	0.738468	1.28652	5.53571	7.67784	2.71040	5.44463	1.34557	7.30845
0.76	0.688921	0.835304	0.724836	1.30297	5.25429	7.11600	2.63992	5.15822	1.30953	6.72670
0.78	0.703279	0.861533	0.710913	1.31993	4.99456	6.61104	2.57311	4.89340	1.27529	6.22184
0.80	0.717356	0.888105	0.696706	1.33743	4.75438	6.15604	2.50972	4.64802	1.24271	5.75694
0.82	0.731145	0.915034	0.682271	1.35546	4.53188	5.74504	2.44949	4.47017	1.21166	5.33607
0.84	0.744643	0.942378	0.667467	1.37403	4.32540	5.37294	2.39220	4.20822	1.18204	4.95499
0.86	0.757842	0.969999	0.652437	1.39316	4.13348	5.03531	2.33765	4.01069	1.15374	4.60661
0.88	0.770738	0.998058	0.637151	1.41284	3.95481	4.72832	2.28565	3.87629	1.12667	4.28978
0.90	0.783326	1.02651	0.621609	1.43308	3.78823	4.44865	2.23604	3.65386	1.10075	4.00028
0.92	0.795601	1.05538	0.605870	1.45390	3.63272	4.19339	2.18867	3.49237	1.07540	3.73521
0.94	0.807558	1.08467	0.589788	1.47530	3.48734	3.95999	2.14339	3.34089	1.05704	3.49702
0.96	0.819191	1.11440	0.573519	1.49729	3.35128	3.74623	2.10008	3.19860	1.03912	3.26848
0.98	0.830497	1.14457	0.557022	1.51988	3.22377	3.55013	2.05863	3.06475	1.02070	3.06262
1.00	0.841470	1.17520	0.540302	1.54308	3.10415	3.36998	2.01891	2.93866	0.985838	2.87273
1.02	0.852108	1.20629	0.523365	1.56689	2.99181	3.20422	1.98084	2.81974	0.965374	2.69726
1.04	0.862404	1.23788	0.506270	1.59133	2.88621	3.05151	1.94433	2.70743	0.945632	2.53486
1.06	0.872355	1.26995	0.488877	1.61641	2.78683	2.91063	1.90928	2.60124	0.926568	2.38431
1.08	0.881957	1.30254	0.471328	1.64213	2.69324	2.78051	1.87562	2.50071	0.908143	2.24455
1.10	0.891207	1.33564	0.453596	1.66851	2.60502	2.66019	1.84328	2.40544	0.890318	2.11461
1.12	0.900100	1.36928	0.435682	1.69556	2.52179	2.54819	1.81219	2.31505	0.873061	1.99363
1.14	0.908633	1.40347	0.417594	1.72329	2.44322	2.44556	1.78228	2.22920	0.856338	1.88084
1.16	0.916803	1.43822	0.399339	1.75170	2.36694	2.34980	1.75350	2.14757	0.840120	1.77555
1.18	0.924606	1.47354	0.380974	1.78082	2.29879	2.26008	1.72580	2.06989	0.824379	1.67714
1.20	0.932039	1.50946	0.362357	1.81065	2.23738	2.17875	1.69912	1.99588	0.809090	1.58505
1.22	0.939099	1.54597	0.343645	1.84170	2.18077	2.10138	1.67341	1.92531	0.794227	1.49876
1.24	0.945783	1.58311	0.324796	1.87449	2.10998	2.02982	1.64844	1.85796	0.779769	1.41782
1.26	0.952090	1.62088	0.305816	1.90453	2.05355	1.96317	1.62476	1.79362	0.765694	1.34181
1.28	0.958015	1.65930	0.286715	1.93133	2.00005	1.90102	1.60172	1.73211	0.751982	1.27037
1.30	0.963558	1.69838	0.267498	1.95091	1.94930	1.84305	1.57951	1.67375	0.738615	1.20313
1.32	0.968715	1.73814	0.248125	1.97027	1.90113	1.78893	1.55807	1.61688	0.725575	1.13980
1.34	0.973484	1.77859	0.228752	2.04044	1.85539	1.73838	1.53718	1.56785	0.712895	1.08008
1.36	0.977864	1.81976	0.209238	2.07642	1.81196	1.69115	1.51741	1.51102	0.700410	1.02373
1.38	0.981853	1.86166	0.189640	2.11324	1.77069	1.64698	1.49812	1.46128	0.688257	0.970497
1.40	0.985449	1.90430	0.169967	2.15089	1.73146	1.60566	1.47950	1.41349	0.676370	0.920164
1.42	0.988651	1.94770	0.150275	2.18941	1.69417	1.56700	1.46152	1.36755	0.664737	0.877537
1.44	0.991458	1.99188	0.130423	2.22881	1.65870	1.53079	1.44414	1.32336	0.653346	0.847431
1.46	0.993866	2.03866	0.110569	2.26909	1.62496	1.49689	1.42736	1.28083	0.642185	0.818480

1.50	0.997434	2.11927	0.070737	2.18240	1.56232	1.43535	1.31145	1.19259	1.07989	0.97374
1.52	0.998705	2.11675	0.059774		1.55373	1.43434	1.31044	1.19158	1.07888	0.97273
1.54	0.999976	2.11423	0.048821		1.54011	1.43333	1.30943	1.19043	1.07773	0.97163
1.56	0.999999	2.11171	0.037868		1.52688	1.43232	1.30833	1.18933	1.07663	0.97053
1.58	0.999999	2.10919	0.026915		1.51365	1.43131	1.30723	1.18823	1.07553	0.96943
1.60	0.999999	2.10667	0.015962		1.50042	1.43030	1.30613	1.18713	1.07443	0.96833
1.62	0.999999	2.10415	0.005009		1.48719	1.42929	1.30503	1.18603	1.07333	0.96723
1.64	0.999999	2.10163	0.000000		1.47396	1.42828	1.30393	1.18493	1.07223	0.96613
1.66	0.999999	2.09911			1.46073	1.42727	1.30283	1.18383	1.07113	0.96503
1.68	0.999999	2.09659			1.44750	1.42626	1.30173	1.18273	1.07003	0.96393
1.70	0.999999	2.09407			1.43427	1.42525	1.30063	1.18163	1.06893	0.96283
1.72	0.999999	2.09155			1.42104	1.42424	1.29953	1.18053	1.06783	0.96173
1.74	0.999999	2.08903			1.40781	1.42323	1.29843	1.17943	1.06673	0.96063
1.76	0.999999	2.08651			1.39458	1.42222	1.29733	1.17833	1.06563	0.95953
1.78	0.999999	2.08399			1.38135	1.42121	1.29623	1.17723	1.06453	0.95843
1.80	0.999999	2.08147			1.36812	1.42020	1.29513	1.17613	1.06343	0.95733
1.82	0.999999	2.07895			1.35489	1.41919	1.29403	1.17503	1.06233	0.95623
1.84	0.999999	2.07643			1.34166	1.41818	1.29293	1.17393	1.06123	0.95513
1.86	0.999999	2.07391			1.32843	1.41717	1.29183	1.17283	1.06013	0.95403
1.88	0.999999	2.07139			1.31520	1.41616	1.29073	1.17173	1.05903	0.95293
1.90	0.999999	2.06887			1.30197	1.41515	1.28963	1.17063	1.05793	0.95183
1.92	0.999999	2.06635			1.28874	1.41414	1.28853	1.16953	1.05683	0.95073
1.94	0.999999	2.06383			1.27551	1.41313	1.28743	1.16843	1.05573	0.94963
1.96	0.999999	2.06131			1.26228	1.41212	1.28633	1.16733	1.05463	0.94853
1.98	0.999999	2.05879			1.24905	1.41111	1.28523	1.16623	1.05353	0.94743
2.00	0.999999	2.05627			1.23582	1.41010	1.28413	1.16513	1.05243	0.94633
2.02	0.999999	2.05375			1.22259	1.40909	1.28303	1.16403	1.05133	0.94523
2.04	0.999999	2.05123			1.20936	1.40808	1.28193	1.16293	1.05023	0.94413
2.06	0.999999	2.04871			1.19613	1.40707	1.28083	1.16183	1.04913	0.94303
2.08	0.999999	2.04619			1.18290	1.40606	1.27973	1.16073	1.04803	0.94193
2.10	0.999999	2.04367			1.16967	1.40505	1.27863	1.15963	1.04693	0.94083
2.12	0.999999	2.04115			1.15644	1.40404	1.27753	1.15853	1.04583	0.93973
2.14	0.999999	2.03863			1.14321	1.40303	1.27643	1.15743	1.04473	0.93863
2.16	0.999999	2.03611			1.12998	1.40202	1.27533	1.15633	1.04363	0.93753
2.18	0.999999	2.03359			1.11675	1.40101	1.27423	1.15523	1.04253	0.93643
2.20	0.999999	2.03107			1.10352	1.40000	1.27313	1.15413	1.04143	0.93533
2.22	0.999999	2.02855			1.09029	1.39899	1.27203	1.15303	1.04033	0.93423
2.24	0.999999	2.02603			1.07706	1.39798	1.27093	1.15193	1.03923	0.93313
2.26	0.999999	2.02351			1.06383	1.39697	1.26983	1.15083	1.03813	0.93203
2.28	0.999999	2.02099			1.05060	1.39596	1.26873	1.14973	1.03703	0.93093
2.30	0.999999	2.01847			1.03737	1.39495	1.26763	1.14863	1.03593	0.92983
2.32	0.999999	2.01595			1.02414	1.39394	1.26653	1.14753	1.03483	0.92873
2.34	0.999999	2.01343			1.01091	1.39293	1.26543	1.14643	1.03373	0.92763
2.36	0.999999	2.01091			0.99768	1.39192	1.26433	1.14533	1.03263	0.92653
2.38	0.999999	2.00839			0.98445	1.39091	1.26323	1.14423	1.03153	0.92543
2.40	0.999999	2.00587			0.97122	1.38990	1.26213	1.14313	1.03043	0.92433
2.42	0.999999	2.00335			0.95799	1.38889	1.26103	1.14203	1.02933	0.92323
2.44	0.999999	2.00083			0.94476	1.38788	1.25993	1.14093	1.02823	0.92213

$$\begin{aligned}
E^A g_1^A &= + B \left[\frac{1}{\bar{R}_1} + \left(\frac{1-\nu}{1+\nu} \right) \frac{\bar{R}_1}{\bar{R}_2^2} \right] \\
E^A g_{12}^A &= + B \left[\left(\frac{2}{1+\nu} \right) \frac{1}{\bar{R}_1} \right] \\
E^A g_2^A &= + B \left[\frac{1}{\bar{R}_2} + \left(\frac{1-\nu}{1+\nu} \right) \frac{\bar{R}_2}{\bar{R}_1^2} \right] \\
E^A g_{21}^A &= + B \left[\left(\frac{2}{1+\nu} \right) \frac{1}{\bar{R}_2} \right]
\end{aligned}
\tag{10a}$$

where

$$\begin{aligned}
\bar{R}_1 &= R_1 + \frac{h_1}{2} ; \bar{R}_2 = R_2 - \frac{h_2}{2} \\
B &= \frac{(1+\nu) \bar{R}_1^2 \bar{R}_2^2}{h_3 (\bar{R}_1^2 - \bar{R}_2^2)}
\end{aligned}
\tag{10b}$$

COMPUTATION OF STRESSES

The formulas given herein for determining the longitudinal and circumferential stresses in the shell elements of the web-stiffened sandwich cylinder are developed in Appendix C. Formulas for the radial and tangential stresses in the web elements are developed in Appendix B. The derivation follows very closely the general analysis of Reference 7 for ring-stiffened cylinders under hydrostatic pressure, the only differences arising from the elastic restraints at the shell edges and the distribution of the axial pressure loading.

The nomenclature and sign convention used in Reference 7 and in Appendix C of this report are shown in Figures 2 and 4. A longitudinal bending moment M_x is considered positive if it tends to put the outer surface of the shell in tension, and a transverse shearing force Q_x is considered positive when it acts in a direction away from the axis of symmetry but in the positive x -direction. A hydrostatic pressure p is considered positive when it is external, and negative when internal. With reference to Equations [1] and [2], the subscript i is used to distinguish the two cylinder elements.

The quantities H_i and M_i shown in Figure 2 are the edge shearing forces and bending moments arising at the junctures of the shell elements with a web stiffener. They may be determined in terms of the geometry and elasticity of the structure and the pressure loading by enforcing conditions of force and moment equilibrium and compatibility of deformations at the junctures. This determination is developed in the next section.

Once the edge forces and moments are known, the following formulas may be used for determining the critical longitudinal and circumferential shell stresses which occur at a point midbay between two adjacent webs and also at a web location, respectively:

AT MIDBAY:

$$\sigma_{Xm} = -\frac{P_i}{h_i} \mp \frac{E^s h_i \beta_i^2}{(1-\nu^2)} (w_i^p - w_i^s) \frac{\Lambda_i^{[5]}(\beta_i l/2)}{\Lambda_i^{[2]}(\beta_i l/2)} \quad [11]$$

$$\sigma_{\Phi m} = -\nu \frac{P_i}{h_i} + \frac{E^s}{R_i} (-w_i^s) \frac{\Lambda_i^{[6]}(\beta_i l/2)}{\Lambda_i^{[2]}(\beta_i l/2)} \mp \frac{\nu E h_i \beta_i^2}{(1-\nu^2)} (w_i^p - w_i^s) \frac{\Lambda_i^{[5]}(\beta_i l/2)}{\Lambda_i^{[2]}(\beta_i l/2)} \quad [12]$$

AT A WEB:

$$\sigma_{Xf} = -\frac{P_i}{h_i} \pm \frac{E^s h_i \beta_i^2}{(1-\nu^2)} (w_i^p - w_i^s) \frac{\Lambda_i^{[3]}(\beta_i l/2)}{\Lambda_i^{[2]}(\beta_i l/2)} \quad [13]$$

$$\sigma_{\Phi f} = -\nu \frac{P_i}{h_i} + \frac{E^s}{R_i} (-w_i^s) \pm \frac{\nu E^s h_i \beta_i^2}{(1-\nu^2)} (w_i^p - w_i^s) \frac{\Lambda_i^{[3]}(\beta_i l/2)}{\Lambda_i^{[2]}(\beta_i l/2)} \quad [14]$$

where in the above equations $i = 1, 2$, and the upper sign is for the outer fiber and the lower sign for the inner fiber of each shell plating. Equations [11] through [14] are developed in Appendix C.

Once the critical stresses are determined from Equations [11] through [14], the question as to how they combine to precipitate axisymmetric collapse of the cylindrical shell elements can be answered by recourse to the failure criteria discussed in References 7 and 8. This will not be discussed here.

The quantity P_i in Equations [11] through [14] is the axial load taken by each of the two cylindrical shells. On the assumption that the two shells contract the same amount longitudinally, it is shown in Appendix D that

$$P_1 = \frac{pR_1 \left[\nu(1-a_1) + \frac{1}{2} \frac{R_1 h_1}{R_2 h_2} (1-\nu^2 a_2) \right] + \frac{\nu E^s h_1}{R_1} (g_1^A H_1 + \bar{g}_1^A H_2) a_1 - \frac{\nu E^s h_1}{R_2} (g_2^A H_2 + \bar{g}_2^A H_1) a_2}{1 - \nu^2 a_1 + \frac{R_1 h_1}{R_2 h_2} (1-\nu^2 a_2)}$$

[15]

$$P_2 = \frac{pR_1 \left[-\nu(1-a_1) \frac{R_1}{R_2} + \frac{1}{2} \frac{R_1}{R_2} (1-\nu^2 a_1) \right] - \frac{\nu E^s h_1}{R_2} (g_1^A H_1 + \bar{g}_1^A H_2) a_1 + \frac{\nu E^s R_1 h_1}{R_2^2} (g_2^A H_2 + \bar{g}_2^A H_1) a_2}{1 - \nu^2 a_1 + \frac{R_1 h_1}{R_2 h_2} (1-\nu^2 a_2)}$$

The quantities a_1 and a_2 are given in Appendix D by Equations [D.13].

The quantities w_i^p in Equations [11] through [14] represent the particular integrals to the differential equations governing the axisymmetric deformations of a cylindrical shell; they are easily determined from membrane theory. For the case shown in Figures 1 and 2, where the outer cylindrical shell (but not the inner one) is loaded by lateral pressure, we find that (see Reference 7, for example)

$$w_1^p = + \frac{pR_1^2}{E^s h_1} \left(1 - \frac{\nu}{R_1} \frac{P_1}{p} \right)$$

[16]

$$w_2^p = - \frac{pR_2^2}{E^s h_2} \left(\frac{\nu}{R_2} \frac{P_2}{p} \right)$$

where the axial forces P_1 and P_2 are given by Equations [15].

The shell edge deflections w_i^s appearing in the stress formulas, Equations [11] through [14], are determined from Equation [3] once the edge shears H_i and edge moments M_i are known; i.e.,

$$w_1^s = d_1 M_1 + g_1 \frac{H_1}{2} + f_1' P_1 + f_1'' p + f_1''' P_1 + \bar{d}_1 M_1 + \bar{g}_1 \frac{H_1}{2} + \bar{f}_1' P_1$$

[17]

$$w_2 = d_2 M_2 + g_2 \frac{H_2}{2} + f_2' P_2 + f_2'' p + f_2''' P_2 + \bar{d}_2 M_2 + \bar{g}_2 \frac{H_2}{2} + \bar{f}_2' P_2$$

where the interaction coefficients have been designated by a "bar" instead of the double subscript so as not to confuse the use of the subscripts "1" and "2" to designate the two shells and their respective junctures with the web stiffeners. This notation will be used in all the equations that follow.

Expressions for the radial and tangential stresses in the web elements are developed in Appendix B. It is shown there that the maximum radial stress occurs at the intersection with the outer cylindrical shell (i.e., at $r = \bar{R}_1 = R_1 + \frac{h_1}{2}$), and the maximum tangential stress occurs at the intersection with the inner cylindrical shell (i.e., at $r = \bar{R}_2 = R_2 - \frac{h_2}{2}$). These maximum stresses are given by the following expressions:

$$\sigma_{r_{\max}} = \frac{E^A}{(1-\nu^2)} \left[A(1+\nu) - \frac{B}{\bar{R}_1^2} (1-\nu) \right] \quad [18]$$

$$\sigma_{t_{\max}} = \frac{E^A}{(1-\nu^2)} \left[A(1+\nu) + \frac{B}{\bar{R}_2^2} (1-\nu) \right] \quad [19]$$

where the constants A and B are given by

$$A = - \left(\frac{w_1^A \bar{R}_1 - w_2^A \bar{R}_2}{\bar{R}_1^2 - \bar{R}_2^2} \right) \quad [20]$$

$$B = - \bar{R}_1 \bar{R}_2 \left(\frac{w_2^A \bar{R}_1 - w_1^A \bar{R}_2}{\bar{R}_1^2 - \bar{R}_2^2} \right)$$

and the annulus edge deflections w_1^A and w_2^A by Equation [5] as

$$w_1^A = g_1^A H_1 + \bar{g}_1^A H_2 \quad [21]$$

$$w_2^A = g_2^A H_2 + \bar{g}_2^A H_1$$

In Equations [21] the edge coefficients designated by a "bar" are the interaction or double-subscript coefficients; i.e., $\bar{g}_1^A = g_{12}^A$ and $\bar{g}_2^A = g_{21}^A$. The edge coefficients appearing in Equations [21] are given by Equations [10].

DETERMINATION OF EDGE SHEARS H_i AND EDGE MOMENTS M_i

For the case of symmetry on each side of a web stiffener, the conditions of force and moment equilibrium at each of the two junctures of the web with the shells are rather obvious; these are shown in the free-body diagram of Figure 2. There remains to determine the unknown edge shears H_1 and H_2 and unknown edge moments M_1 and M_2 by enforcing conditions of compatibility of the deformations at the junctures labeled "1" and "2."

Continuity and symmetry conditions at joint "1" require that

$$w_1^s = w_1^A \quad [22]$$

$$\theta_1^s = \theta_1^A = 0 \quad [23]$$

whereas these conditions applied to joint "2" require that

$$w_2^s = w_2^A \quad [24]$$

$$\theta_2^s = \theta_2^A = 0 \quad [25]$$

Substituting Equations [3], [4], [5], and [6] into the four conditions [22] through [25], considering the zero edge coefficients by virtue of the loading shown in Figures 1 and 2 and Equations [7], and assuming that $E^s = E^A$, we must solve the following four algebraic equations simultaneously to determine H_1 , H_2 , M_1 , and M_2 :

$$M_1 [d_1 + \bar{d}_1] + H_1 \left[\frac{1}{2} (g_1 + \bar{g}_1) - g_1^A \right] + H_2 [-\bar{g}_1^A] = -f_1''p - f_1'''P_1 \quad [26]$$

$$M_1 [a_1 + \bar{a}_1] + H_1 \left[\frac{1}{2} (b_1 + \bar{b}_1) \right] = 0 \quad [27]$$

$$M_2 [d_2 + \bar{d}_2] + H_2 \left[\frac{1}{2} (g_2 + \bar{g}_2) - g_2^A \right] + H_1 [-\bar{g}_2^A] = -f_2'''P_2 \quad [28]$$

$$M_2 [a_2 + \bar{a}_2] + H_2 \left[\frac{1}{2} (b_2 + \bar{b}_2) \right] = 0 \quad [29]$$

where P_1 and P_2 are given by Equations [15] to be functions of the unknown shearing forces H_1 and H_2 . Equations [26] through [29] can be rewritten as two equations in only two unknowns as follows:

$$H_1 \left[\frac{1}{2} (g_1 + \bar{g}_1) - g_1^A - \frac{(b_1 + \bar{b}_1)(d_1 + \bar{d}_1)}{2(a_1 + \bar{a}_1)} \right] + H_2 [-\bar{g}_1^A] = -f_1''p - f_1'''P_1 \quad [30]$$

$$H_1 [-\bar{g}_2^A] + H_2 \left[\frac{1}{2} (g_2 + \bar{g}_2) - g_2^A - \frac{(b_2 + \bar{b}_2)(d_2 + \bar{d}_2)}{2(a_2 + \bar{a}_2)} \right] = -f_2'''P_2 \quad [31]$$

By the substitution of the expressions for P_1 and P_2 given by Equations [15] into Equations [30] and [31], the two simultaneous equations to be solved for H_1 and H_2 become:

$$H_1 \left[\frac{1}{2} (g_1 + \bar{g}_1) - g_1^A - \frac{(b_1 + \bar{b}_1)(d_1 + \bar{d}_1)}{2(a_1 + \bar{a}_1)} + \frac{\nu E^s h_1}{R_1} f_1''' \left(\frac{a_1 g_1^A - \frac{R_1}{R_2} a_2 \bar{g}_2^A}{1 - \nu^2 a_1 + \frac{R_1 h_1}{R_2 h_2} (1 - \nu^2 a_2)} \right) \right] +$$

$$H_2 \left[-\bar{g}_1^A + \frac{\nu E^s h_1}{R_1} f_1''' \left(\frac{a_1 \bar{g}_1^A - \frac{R_1}{R_2} a_2 g_2^A}{1 - \nu^2 a_1 + \frac{R_1 h_1}{R_2 h_2} (1 - \nu^2 a_2)} \right) \right] = -f_1''' p - f_1''' \frac{p R_1 \left[\nu(1 - a_1) + \frac{1}{2} \frac{R_1 h_1}{R_2 h_2} (1 - \nu^2 a_2) \right]}{1 - \nu^2 a_1 + \frac{R_1 h_1}{R_2 h_2} (1 - \nu^2 a_2)} \quad [32]$$

$$H_1 \left[-\bar{g}_2^A + \frac{\nu E^s h_1}{R_2} f_2''' \left(\frac{-a_1 g_1^A + \frac{R_1}{R_2} a_2 \bar{g}_2^A}{1 - \nu^2 a_1 + \frac{R_1 h_1}{R_2 h_2} (1 - \nu^2 a_2)} \right) \right] +$$

$$H_2 \left[\frac{1}{2} (g_2 + \bar{g}_2) - g_2^A - \frac{(b_2 + \bar{b}_2)(d_2 + \bar{d}_2)}{2(a_2 + \bar{a}_2)} + \frac{\nu E^s h_1}{R_2} f_2''' \left(\frac{-a_1 \bar{g}_1^A + \frac{R_1}{R_2} a_2 g_2^A}{1 - \nu^2 a_1 + \frac{R_1 h_1}{R_2 h_2} (1 - \nu^2 a_2)} \right) \right]$$

$$= -f_2''' \frac{p R_1 \left[-\nu(1 - a_1) \frac{R_1}{R_2} + \frac{1}{2} \frac{R_1}{R_2} (1 - \nu^2 a_1) \right]}{1 - \nu^2 a_1 + \frac{R_1 h_1}{R_2 h_2} (1 - \nu^2 a_2)} \quad [33]$$

After the edge shears H_1 and H_2 are determined from Equations [32] and [33], the edge moments M_1 and M_2 may be found from the following expressions as a consequence of Equations [27] and [29], respectively:

$$M_1 = -H_1 \frac{(b_1 + \bar{b}_1)}{2(a_1 + \bar{a}_1)} \quad [34]$$

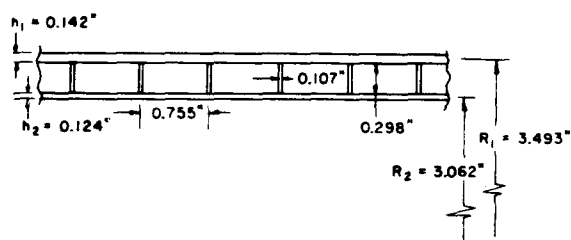
$$M_2 = -H_2 \frac{(b_2 + \bar{b}_2)}{2(a_2 + \bar{a}_2)} \quad [35]$$

NUMERICAL EXAMPLE

As part of its research and evaluation program to study the application of glass-fiber reinforced plastics for pressure vessel construction, the Model Basin in collaboration with Narmco Industries Inc., San Diego, California, is presently designing a series of web-stiffened sandwich cylinders made of these materials. The structural models are to be fabricated by Narmco and then forwarded to the Model Basin for testing.

One of the designs, Model N-1, presently being conceived will be used as a sample calculation to illustrate the use of the equations developed in this report. The detailed dimensions are shown in Figure 6, and are summarized here:

Figure 6 - Schematic Diagram Showing Dimensions of Model N-1



$$h_1 = 0.142 \text{ in.}; \quad h_2 = 0.124 \text{ in.}; \quad h_3 = 0.107 \text{ in.}$$

$$R_1 = 3.493 \text{ in.}; \quad R_2 = 3.062 \text{ in.}; \quad l = 0.648 \text{ in.}$$

$$\bar{R}_1 = 3.564 \text{ in.}; \quad \bar{R}_2 = 3.000 \text{ in.}$$

$$E^s = 6.0 \times 10^6 \text{ psi} = E^A$$

$$\nu = 0.15$$

Using Equations [7b] for each of the outer and inner cylindrical shells, respectively, we compute the values of $\beta_i l$ and D_i' to be:

$$\beta_1 l = 1.204; \quad D_1' = 24.407 \times 10^{-5} \text{ in.}^3$$

$$\beta_2 l = 1.376; \quad D_2' = 16.257 \times 10^{-5} \text{ in.}^3$$

The lambda functions are either computed by using these values of $\beta_i l$ and Equations [8] or are found by interpolation from Table 1 for each of the two shells. They are summarized here:

	$\Lambda[1]$	$\Lambda[2]$	$\Lambda[3]$	$\Lambda[4]$	$\Lambda[5]$	$\Lambda[6]$
Outer Shell	2.219	2.162	1.694	1.981	0.8061	1.567
Inner Shell	1.778	1.655	1.502	1.471	0.6906	0.9805

Next, the shell-edge coefficients $E^s a_i$, $E^s b_i$, $E^s c_i'$, . . . etc., are computed by using Equations [7a]. The numerical values thus found are summarized here:

Shell Edge Coefficient	Outer Shell ($i = 1$)	Inner Shell ($i = 2$)
$E^s a_i, \text{ in.}^{-2}$	$+ 0.4767 \times 10^4$	$+0.4795 \times 10^4$
$E^s b_i, \text{ in.}^{-1}$	$- 0.1317 \times 10^4$	-0.1213×10^4
$E^s c_i' = E^s \bar{c}_i'$	0	0
$E^s d_i, \text{ in.}^{-1}$	$+ 0.1317 \times 10^4$	$+0.1213 \times 10^4$
$E^s f_i'$	0	0
$E^s f_i'', \text{ in.}$	+85.9229	nonexistent
$E^s f_i'''$	- 3.6898	-3.7040
$E^s g_i$	$- 0.05410 \times 10^4$	-0.04822×10^4
$E^s \bar{a}_i, \text{ in.}^{-2}$	$- 0.3455 \times 10^4$	-0.2840×10^4
$E^s \bar{b}_i, \text{ in.}^{-1}$	$+ 0.1176 \times 10^4$	$+0.1003 \times 10^4$
$E^s \bar{d}_i, \text{ in.}^{-1}$	$- 0.1176 \times 10^4$	-0.1003×10^4
$E^s \bar{f}_i'$	0	0
$E^s \bar{g}_i$	$+ 0.02575 \times 10^4$	$+0.02217 \times 10^4$

The web stiffener or circular annulus edge coefficients $E^A g_1^A$, . . . etc., are computed by using Equations [10], and the numerical results found are:

$$E^A g_1^A = 190.261$$

$$E^A \bar{g}_1^A = E^A g_{12}^A = 161.949$$

$$E^A g_2^A = 168.564$$

$$E^A \bar{g}_2^A = E^A g_{21}^A = 192.396$$

The components of the end pressure loading taken by each of the outer and inner cylindrical shells, respectively, are computed to be, using Equations [15]:

$$P_1 = + 0.9843 p \text{ lb/in.}$$

$$P_2 = + 0.8695 p \text{ lb/in.}$$

With all this, the edge shear forces H_1 and H_2 are computed by solving Equations [32] and [33] simultaneously. The values thus found are then substituted into Equations [34] and [35] to determine the edge bending moments M_1 and M_2 . The numerical values thus found are:

$$H_1 = + 0.3893 p \text{ lb/in.}$$

$$H_2 = - 0.2717 p \text{ lb/in.}$$

$$M_1 = + 0.02095 p \text{ in.-lb/in.}$$

$$M_2 = - 0.01459 p \text{ in.-lb/in.}$$

When the edge shear forces and edge bending moments are known, the edge deflections of the two cylindrical shells and those of the web stiffener, at their common juncture points, are found from Equations [17] and [21] to be:

$$E^s w_1^s = + 30.072 p \text{ lb/in.}$$

$$E^A w_1^A = + 30.072 p \text{ lb/in.}$$

$$E^s w_2^s = + 29.105 p \text{ lb/in.}$$

$$E^A w_2^A = + 29.105 p \text{ lb/in.}$$

Comparison of $E^s w_1^s$ with $E^A w_1^A$, and $E^s w_2^s$ with $E^A w_2^A$ affords a check on the numerical calculations, since the boundary conditions [22] and [24] enforced at the two junctures require them to be equal in their respective cases since it was assumed that $E^s = E^A$.

The maximum radial and tangential stresses in the web stiffeners can now be computed by using Equations [18], [19], and [20]. The values found are:

$$\sigma_{r_{\max}} = - 3.638 p \text{ lb/in.}^2$$

$$\sigma_{t_{\max}} = - 10.083 p \text{ lb/in.}^2$$

Before the shell stresses can be computed, it is necessary to determine the membrane deflections of the two shells. This is done with the aid of Equations [16]. The values found are:

$$E^s w_1^p = + 82.291 p \text{ lb/in.}$$

$$E^s w_2^p = - 3.2205 p \text{ lb/in.}$$

Finally, the critical longitudinal and circumferential shell stresses at points midbay between two adjacent web stiffeners and at a web stiffener are determined by using Equations [11], [12], [13], and [14]. The numerical values are summarized as follows:

	σ_{X_m} , psi	σ_{Φ_m} , psi	σ_{X_p} , psi	σ_{Φ_p} , psi
Outer Shell	$-10.039 p$	$-10.437 p$	$-13.166 p$	$-10.584 p$
Inner Shell	$-9.843 p$	$-12.702 p$	$-12.704 p$	$-13.514 p$

For the numerical example considered, the calculations already carried out have been based on the assumption that all structural elements have the same elastic modulus E . However, in the fabrication of a shell structure such as this, it is conceivable that the elements

could have different material properties. In the case of Model N-1, which is to be made of a glass-fiber reinforced plastic, it is expected that the web stiffeners, although made of the same basic material as the cylindrical shells, will have a higher elastic modulus by virtue of the fiber distribution. Assuming that the modulus of the web material is 50 percent higher than that of the shell material, i.e., $E^A = 1.5 E^S$, we repeated the calculations and found the following results:

$$P_1 = + 0.9842 p \text{ lb/in.}$$

$$P_2 = + 0.8696 p \text{ lb/in.}$$

$$H_1 = + 0.4166 p \text{ lb/in.}$$

$$H_2 = - 0.2449 p \text{ lb/in.}$$

$$M_1 = + 0.02242 p \text{ in.-lb/in.}$$

$$M_2 = - 0.01315 p \text{ in.-lb/in.}$$

$$E^S w_1^S = + 26.406 p \text{ lb/in.}$$

$$E^A w_1^A = + 39.609 p \text{ lb/in.}$$

$$E^S w_2^S = + 25.919 p \text{ lb/in.}$$

$$E^A w_2^A = + 38.878 p \text{ lb/in.}$$

$$E^S w_1^P = + 82.291 p \text{ lb/in.}$$

$$E^S w_2^P = - 3.2211 p \text{ lb/in.}$$

$$\sigma_{r_{\max}} = - 3.894 p \text{ lb/in.}^2$$

$$\sigma_{t_{\max}} = - 13.303 p \text{ lb/in.}^2$$

	σ_{χ_m} , psi	σ_{Φ_m} , psi	σ_{χ_f} , psi	σ_{Φ_f} , psi
Outer Shell	-10.256 p	- 9.442 p	-13.603 p	- 9.600 p
Inner Shell	- 9.565 p	-11.658 p	-12.144 p	-12.390 p

ACKNOWLEDGMENTS

Mr. William E. Ball, Jr. checked all the equations in this report and also carried out the calculations for Table 1 and the numerical example. Mr. Ball has also programmed the pertinent equations of the analysis for the Model Basin IBM 7090 computer. This will permit optimization in the design of web-stiffened sandwich cylinders for prescribed material properties and weight-volume ratios.

APPENDIX A

DERIVATION OF THE FUNCTIONS $\Lambda^{[1]}$, $\Lambda^{[2]}$, $\Lambda^{[3]}$, $\Lambda^{[4]}$, $\Lambda^{[5]}$, AND $\Lambda^{[6]}$

If the beam-column effect⁷ due to the axial portion of the hydrostatic pressure is neglected, then the differential equation governing the axisymmetric elastic deformations, based on small-deflection theory, of a thin-walled circular cylinder is given by:⁷

$$D \frac{d^4 w}{dx^4} + E \frac{h}{R^2} w = P_r - \frac{\nu}{R} N_x \quad [A.1]$$

The homogeneous form of Equation [A.1] will be used to derive edge coefficients for cylindrical shells of short length in which interaction effects between the two ends of the shell prevail. Then we have

$$D \frac{d^4 w}{dx^4} + E \frac{h}{R^2} w = 0 \quad [A.2]$$

The solution⁷ of Equation [A.2], which solution describes the bending deformations, can be written in the form:

$$\begin{aligned} w_b(x) = & C_1 \cos \beta x \cdot \cosh \beta x + C_2 \sin \beta x \cdot \cosh \beta x \\ & + C_3 \cos \beta x \cdot \sinh \beta x + C_4 \sin \beta x \cdot \sinh \beta x \end{aligned} \quad [A.3]$$

and the first three derivatives of [A.3] are:

$$\begin{aligned} \frac{1}{\beta} \cdot \frac{dw_b}{dx} = & (C_2 + C_3) \cos \beta x \cdot \cosh \beta x + (C_4 - C_1) \sin \beta x \cdot \cosh \beta x \\ & + (C_4 + C_1) \cos \beta x \cdot \sinh \beta x + (C_2 - C_3) \sin \beta x \cdot \sinh \beta x \\ \frac{1}{2\beta^2} \cdot \frac{d^2 w_b}{dx^2} = & C_4 \cos \beta x \cdot \cosh \beta x - C_3 \sin \beta x \cdot \cosh \beta x \\ & + C_2 \cos \beta x \cdot \sinh \beta x - C_1 \sin \beta x \cdot \sinh \beta x \\ \frac{1}{2\beta^3} \cdot \frac{d^3 w_b}{dx^3} = & (C_2 - C_3) \cos \beta x \cdot \cosh \beta x - (C_4 + C_1) \sin \beta x \cdot \cosh \beta x \\ & + (C_4 - C_1) \cos \beta x \cdot \sinh \beta x - (C_2 + C_3) \sin \beta x \cdot \sinh \beta x \end{aligned} \quad [A.4]$$

where in Equations [A.3] and [A.4] we have $\beta = \frac{\sqrt{3(1-\nu^2)}}{\sqrt{Rh}}$.

The integration constants C_1 , C_2 , C_3 , and C_4 appearing in Equations [A.3] and [A.4] will be determined from a consideration of the load boundary conditions at the edges of the shell element; see Figure 4. The longitudinal bending moment M_x and the transverse shearing force Q_x are related to the derivatives of $w_b(x)$ by the following equations:

$$M_x = + D \frac{d^2 w_b}{dx^2}$$

$$Q_x = \frac{dM_x}{dx} = + D \frac{d^3 w_b}{dx^3}$$
[A.5]

With reference to Figures 4 and 7, let it be prescribed that the load boundary conditions are given by:

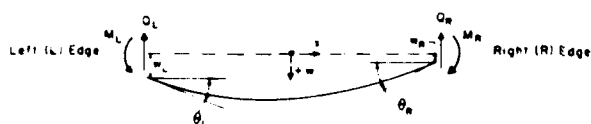


Figure 7 — Edge Shears, Moments, Deflections, and Rotations For a Cylindrical-Shell Element

$$\text{at } x = + \frac{l}{2} : M_x = M_R; \quad Q_x = Q_R$$
[A.6]

$$\text{at } x = - \frac{l}{2} : M_x = M_L; \quad -Q_x = Q_L$$
[A.7]

No considerations of symmetry with respect to the point $x=0$ have been taken in writing the solution Equation [A.3], and in formulating the boundary conditions, Equations [A.6] and [A.7]. The development to follow will be general in this sense.

The substitution of Equations [A.4] and [A.5] into the boundary conditions, Equations [A.6] and [A.7], results in the following four equations:

$$\begin{aligned} \frac{M_R}{2D\beta^2} &= C_4 \cos \frac{\beta l}{2} \cdot \cosh \frac{\beta l}{2} - C_3 \sin \frac{\beta l}{2} \cdot \cosh \frac{\beta l}{2} \\ &+ C_2 \cos \frac{\beta l}{2} \cdot \sinh \frac{\beta l}{2} - C_1 \sin \frac{\beta l}{2} \cdot \sinh \frac{\beta l}{2} \end{aligned}$$

$$\begin{aligned} \frac{Q_R}{2D\beta^3} &= (C_2 - C_3) \cos \frac{\beta l}{2} \cdot \cosh \frac{\beta l}{2} - (C_4 + C_1) \sin \frac{\beta l}{2} \cdot \cosh \frac{\beta l}{2} \\ &\quad + (C_4 - C_1) \cos \frac{\beta l}{2} \cdot \sinh \frac{\beta l}{2} - (C_2 + C_3) \sin \frac{\beta l}{2} \cdot \sinh \frac{\beta l}{2} \end{aligned} \quad [A.8]$$

$$\begin{aligned} \frac{M_L}{2D\beta^2} &= C_4 \cos \frac{\beta l}{2} \cdot \cosh \frac{\beta l}{2} + C_3 \sin \frac{\beta l}{2} \cdot \cosh \frac{\beta l}{2} \\ &\quad - C_2 \cos \frac{\beta l}{2} \cdot \sinh \frac{\beta l}{2} - C_1 \sin \frac{\beta l}{2} \cdot \sinh \frac{\beta l}{2} \end{aligned}$$

$$\begin{aligned} \frac{-Q_L}{2D\beta^3} &= (C_2 - C_3) \cos \frac{\beta l}{2} \cdot \cosh \frac{\beta l}{2} + (C_4 + C_1) \sin \frac{\beta l}{2} \cdot \cosh \frac{\beta l}{2} \\ &\quad - (C_4 - C_1) \cos \frac{\beta l}{2} \cdot \sinh \frac{\beta l}{2} - (C_2 + C_3) \sin \frac{\beta l}{2} \cdot \sinh \frac{\beta l}{2} \end{aligned}$$

Solving Equations [A.8] simultaneously gives the following expressions for the four integration constants C_1 , C_2 , C_3 , and C_4 :

$$\begin{aligned} C_1 (\sinh \beta l + \sin \beta l) &= - \frac{(Q_R + Q_L)}{2D\beta^3} \cos \frac{\beta l}{2} \cdot \cosh \frac{\beta l}{2} \\ &\quad + \frac{(M_R + M_L)}{2D\beta^2} \left(\cos \frac{\beta l}{2} \cdot \sinh \frac{\beta l}{2} - \sin \frac{\beta l}{2} \cdot \cosh \frac{\beta l}{2} \right) \\ C_4 (\sinh \beta l + \sin \beta l) &= - \frac{(Q_R + Q_L)}{2D\beta^3} \sin \frac{\beta l}{2} \cdot \sinh \frac{\beta l}{2} \\ &\quad + \frac{(M_R + M_L)}{2D\beta^2} \left(\cos \frac{\beta l}{2} \cdot \sinh \frac{\beta l}{2} + \sin \frac{\beta l}{2} \cdot \cosh \frac{\beta l}{2} \right) \end{aligned} \quad [A.9]$$

$$\begin{aligned} C_2 (\sinh \beta l - \sin \beta l) &= - \frac{(Q_R - Q_L)}{2D\beta^3} \sin \frac{\beta l}{2} \cdot \cosh \frac{\beta l}{2} \\ &\quad - \frac{(M_L - M_R)}{2D\beta^2} \left(\cos \frac{\beta l}{2} \cdot \cosh \frac{\beta l}{2} + \sin \frac{\beta l}{2} \cdot \sinh \frac{\beta l}{2} \right) \end{aligned}$$

$$\begin{aligned} C_3 (\sinh \beta l - \sin \beta l) &= - \frac{(Q_R - Q_L)}{2D\beta^3} \cos \frac{\beta l}{2} \cdot \sinh \frac{\beta l}{2} \\ &\quad - \frac{(M_L - M_R)}{2D\beta^2} \left(\cos \frac{\beta l}{2} \cdot \cosh \frac{\beta l}{2} - \sin \frac{\beta l}{2} \cdot \sinh \frac{\beta l}{2} \right) \end{aligned}$$

If Equations [A.9] for the integration constants are substituted into the deflection function, Equation [A.3], and the resulting expression is then evaluated at the two edges of the shell element, i.e., at $x = \pm \frac{l}{2}$ for the right and left edges, respectively (see Figure 7), the following equation is obtained:

$$\begin{aligned}
 (\sinh^2 \beta l - \sin^2 \beta l) [w_b]_{x = \pm \frac{l}{2}} = & - \frac{(Q_R + Q_L)}{4D\beta^3} (\cosh \beta l + \cos \beta l) (\sinh \beta l - \sin \beta l) \\
 & \mp \frac{(Q_R - Q_L)}{4D\beta^3} (\cosh \beta l - \cos \beta l) (\sinh \beta l + \sin \beta l) \\
 & + \frac{(M_R + M_L)}{4D\beta^2} (\sinh \beta l - \sin \beta l)^2 \\
 & \mp \frac{(M_L - M_R)}{4D\beta^2} (\sinh \beta l + \sin \beta l)^2
 \end{aligned} \tag{A.10}$$

The bending component of the total deflection at the right (R) edge, i.e., at $x = + \frac{l}{2}$, is then expressed in terms of the applied edge shears and edge moments by the following:

$$\begin{aligned}
 [w_b]_R = & - \frac{Q_R}{2D\beta^3} \left(\frac{\cosh \beta l \cdot \sinh \beta l - \cos \beta l \cdot \sin \beta l}{\sinh^2 \beta l - \sin^2 \beta l} \right) \\
 & + \frac{Q_L}{2D\beta^3} \left(\frac{\cosh \beta l \cdot \sin \beta l - \sinh \beta l \cdot \cos \beta l}{\sinh^2 \beta l - \sin^2 \beta l} \right) \\
 & + \frac{M_R}{2D\beta^2} \left(\frac{\sinh^2 \beta l + \sin^2 \beta l}{\sinh^2 \beta l - \sin^2 \beta l} \right) \\
 & - \frac{M_L}{2D\beta^2} \left(\frac{2 \sinh \beta l \cdot \sin \beta l}{\sinh^2 \beta l - \sin^2 \beta l} \right)
 \end{aligned} \tag{A.11}$$

The bending component of the total deflection at the left (L) edge, i.e., at $x = -\frac{l}{2}$, is then expressed in terms of the applied edge shears and edge moments by the following:

$$\begin{aligned}
 [w_b]_L = & -\frac{Q_L}{2D\beta^3} \left(\frac{\cosh \beta l \cdot \sinh \beta l - \cos \beta l \cdot \sin \beta l}{\sinh^2 \beta l - \sin^2 \beta l} \right) \\
 & + \frac{Q_R}{2D\beta^3} \left(\frac{\cosh \beta l \cdot \sin \beta l - \sinh \beta l \cdot \cos \beta l}{\sinh^2 \beta l - \sin^2 \beta l} \right) \\
 & + \frac{M_L}{2D\beta^2} \left(\frac{\sinh^2 \beta l + \sin^2 \beta l}{\sinh^2 \beta l - \sin^2 \beta l} \right) \\
 & - \frac{M_R}{2D\beta^2} \left(\frac{2 \sinh \beta l \cdot \sin \beta l}{\sinh^2 \beta l - \sin^2 \beta l} \right)
 \end{aligned} \tag{A.12}$$

Comparing the terms of Equations [A.11] and [A.12] with the corresponding terms of Equation [1] and the appropriate edge coefficients, Equations [7a], shows that

$$\begin{aligned}
 \Lambda^{[3]}(\beta l) &= \frac{\cosh \beta l \cdot \sinh \beta l - \cos \beta l \cdot \sin \beta l}{\sinh^2 \beta l - \sin^2 \beta l} \\
 \Lambda^{[5]}(\beta l) &= \frac{\cosh \beta l \cdot \sin \beta l - \sinh \beta l \cdot \cos \beta l}{\sinh^2 \beta l - \sin^2 \beta l} \\
 \Lambda^{[1]}(\beta l) &= \frac{\sinh^2 \beta l + \sin^2 \beta l}{\sinh^2 \beta l - \sin^2 \beta l} \\
 \Lambda^{[4]}(\beta l) &= \frac{2 \sinh \beta l \cdot \sin \beta l}{\sinh^2 \beta l - \sin^2 \beta l}
 \end{aligned} \tag{A.13}$$

The other two lambda functions, namely, $\Lambda^{[2]}$ and $\Lambda^{[6]}$, enter into the equations for the edge rotations of the shell element, and expressions for these two functions are derived next.

When Equations [A.9] are substituted into the first derivative or slope function, Equation [A.4], the slopes at the two edges of the shell element, i.e., at $x = \pm \frac{l}{2}$ for the right and left edges, respectively (see Figure 7), are given by:

$$\begin{aligned}
(\sinh^2 \beta l - \sin^2 \beta l) \left[\frac{dw_b}{dx} \right]_{x=\pm \frac{l}{2}} = & - \frac{(Q_R - Q_L)}{4D\beta^2} (\sinh \beta l + \sin \beta l)^2 \mp \frac{(Q_R + Q_L)}{4D\beta^2} (\sinh \beta l - \sin \beta l)^2 + \\
& - \frac{(M_L - M_R)}{2D\beta} (\cosh \beta l + \cos \beta l) (\sinh \beta l + \sin \beta l) + \quad [A.14] \\
& \pm \frac{(M_R + M_L)}{2D\beta} (\cosh \beta l - \cos \beta l) (\sinh \beta l - \sin \beta l)
\end{aligned}$$

For those terms in Equation [A.14] which have the double signs, it is intended that the upper sign apply to the right edge and the lower one to the left edge.

Thus the rotation at the right (R) edge, i.e., at $x = + \frac{l}{2}$, is expressed in terms of the applied edge shears and edge moments by the following:

$$\begin{aligned}
- \left[\frac{dw_b}{dx} \right]_{x=+\frac{l}{2}} \equiv + \theta_R = & + \frac{Q_R}{2D\beta^2} \left(\frac{\sinh^2 \beta l + \sin^2 \beta l}{\sinh^2 \beta l - \sin^2 \beta l} \right) - \frac{Q_L}{2D\beta^2} \left(\frac{2 \sinh \beta l \cdot \sin \beta l}{\sinh^2 \beta l - \sin^2 \beta l} \right) + \\
& - \frac{M_R}{D\beta} \left(\frac{\cosh \beta l \cdot \sinh \beta l + \cos \beta l \cdot \sin \beta l}{\sinh^2 \beta l - \sin^2 \beta l} \right) + \quad [A.15] \\
& + \frac{M_L}{D\beta} \left(\frac{\cosh \beta l \cdot \sin \beta l + \sinh \beta l \cdot \cos \beta l}{\sinh^2 \beta l - \sin^2 \beta l} \right)
\end{aligned}$$

and the rotation at the left (L) edge, i.e., at $x = - \frac{l}{2}$, is expressed in terms of the applied edge shears and edge moments by the following:

$$\begin{aligned}
+ \left[\frac{dw_b}{dx} \right]_{x=-\frac{l}{2}} \equiv + \theta_L = & + \frac{Q_L}{2D\beta^2} \left(\frac{\sinh^2 \beta l + \sin^2 \beta l}{\sinh^2 \beta l - \sin^2 \beta l} \right) - \frac{Q_R}{2D\beta^2} \left(\frac{2 \sinh \beta l \cdot \sin \beta l}{\sinh^2 \beta l - \sin^2 \beta l} \right) + \\
& - \frac{M_L}{D\beta} \left(\frac{\cosh \beta l \cdot \sinh \beta l + \cos \beta l \cdot \sin \beta l}{\sinh^2 \beta l - \sin^2 \beta l} \right) + \quad [A.16]
\end{aligned}$$

$$+ \frac{M_R}{D\beta} \left(\frac{\cosh \beta l \cdot \sin \beta l + \cos \beta l \cdot \sinh \beta l}{\sinh^2 \beta l - \sin^2 \beta l} \right)$$

Comparing the terms of Equations [A.15] and [A.16] with the corresponding terms of Equation [2] and the appropriate edge coefficients, Equations [7a], shows that the remaining two lambda functions, besides those defined by [A.13], are given by:

$$\Lambda^{[2]}(\beta l) = \frac{\cosh \beta l \cdot \sinh \beta l + \cos \beta l \cdot \sin \beta l}{\sinh^2 \beta l - \sin^2 \beta l} \quad [A.17]$$

$$\Lambda^{[6]}(\beta l) = \frac{\cosh \beta l \cdot \sin \beta l + \sinh \beta l \cdot \cos \beta l}{\sinh^2 \beta l - \sin^2 \beta l}$$

Consequently, the set of functions defined by Equations [A.13] and [A.17] are exactly those given as Equations [8] earlier in the report.

APPENDIX B

DEVELOPMENT OF EDGE COEFFICIENTS AND EXPRESSIONS FOR THE RADIAL AND TANGENTIAL STRESSES OF A CIRCULAR ANNULUS

With reference to Equation [5] and Figure 5, it has been assumed that the edge moments M^A , axial thrusts P^A , and surface pressure p do not give rise to any radial displacements w^A in the plane of the circular annulus. Only the inplane forces H_i^A and H_j^A acting on the outer and inner circular boundaries, respectively, of the annulus give rise to such deformations.

On Page 418 of Reference 6 the following expression is given, based on the Lamé or plane-strain solution for a thick-walled tube subjected to simultaneous internal pressure p_i and external pressure p_o :

$$\bar{w}(r) = \frac{r^2(1-\nu)(p_i r_i^2 - p_o r_o^2) + (1+\nu)(p_i - p_o)r_i^2 r_o^2}{rE(r_o^2 - r_i^2)} \quad [\text{B.1}]$$

where r_i and r_o are the radii to the inside and outside circular boundaries, respectively, of the tube, and p_i and p_o are the radial pressures acting on the inside and outside surfaces, respectively, of the tube. The variable " r " is the radial distance from the axis of the tube to a point in question through the thickness of the tube wall.

Adapting the solution, Equation [B.1], to the present problem of the circular annulus, we see that

$$\begin{aligned} r_o &= \bar{R}_i; \quad r_i = \bar{R}_j \\ p_o &= + \frac{H_i^A}{t}; \quad p_i = - \frac{H_j^A}{t} \end{aligned} \quad [\text{B.2}]$$

Substituting [B.2] into [B.1] and adapting the sign convention of Figure 5 for positive radial displacement, we obtain the following results:

$$-\bar{w}(r) = - \frac{(1-\nu)(H_j^A \bar{R}_j^2 + H_i^A \bar{R}_i^2) + (1+\nu)(H_j^A + H_i^A) \bar{R}_i^2 \bar{R}_j^2}{rE t (\bar{R}_i^2 - \bar{R}_j^2)} \quad [\text{B.3}]$$

To find the edge coefficients g_i^A , g_{ji}^A , g_j^A , and g_{ji}^A appearing in Equation [5] and its counterpart in which $i \rightarrow j$ and $j \rightarrow i$, it is only necessary to substitute the following successive four conditions into the basic solution, Equation [B.3]:

$$\text{To get } g_i^A : \text{ set } r = \bar{R}_i; H_j^A = 0; H_i^A = 1 \quad [\text{B. 4}]$$

$$g_{ij}^A : \quad r = \bar{R}_i; H_j^A = 1; H_i^A = 0 \quad [\text{B. 5}]$$

$$g_j^A : \quad r = \bar{R}_j; H_j^A = 1; H_i^A = 0 \quad [\text{B. 6}]$$

$$g_{ji}^A : \quad r = \bar{R}_j; H_j^A = 0; H_i^A = 1 \quad [\text{B. 7}]$$

Thus conditions [B.4], [B.5], [B.6], and [B.7] when substituted into Equation [B.3] lead to the following equations, respectively:

$$g_i^A = \frac{(1+\nu) \bar{R}_i^2 \bar{R}_j^2}{E^A t (\bar{R}_i^2 - \bar{R}_j^2)} \left[\frac{1}{\bar{R}_i} + \left(\frac{1-\nu}{1+\nu} \right) \frac{\bar{R}_i}{\bar{R}_j^2} \right] \quad [\text{B. 8}]$$

$$g_{ij}^A = \frac{(1+\nu) \bar{R}_i^2 \bar{R}_j^2}{E^A t (\bar{R}_i^2 - \bar{R}_j^2)} \left[\left(\frac{2}{1+\nu} \right) \frac{1}{\bar{R}_i} \right] \quad [\text{B. 9}]$$

$$g_j^A = \frac{(1+\nu) \bar{R}_i^2 \bar{R}_j^2}{E^A t (\bar{R}_i^2 - \bar{R}_j^2)} \left[\frac{1}{\bar{R}_j} + \left(\frac{1-\nu}{1+\nu} \right) \frac{\bar{R}_j}{\bar{R}_i^2} \right] \quad [\text{B.10}]$$

$$g_{ji}^A = \frac{(1+\nu) \bar{R}_i^2 \bar{R}_j^2}{E^A t (\bar{R}_i^2 - \bar{R}_j^2)} \left[\left(\frac{2}{1+\nu} \right) \frac{1}{\bar{R}_j} \right] \quad [\text{B.11}]$$

With $i \rightarrow 1$, $j \rightarrow 2$, and $t = n_3$, Equations [B.8], [B.9], [B.10], and [B.11] become exactly Equations [10a], respectively.

For expressions [6] for the edge rotations of the annulus, symmetry and loading conditions for a typical bay of the web-stiffened sandwich cylinder far removed from end effects dictate that these rotations not only total zero but each and every component is zero. The more general case shown in Figure 5 and reflected by Equations [6] will be considered in a separate report.

Equations [18] and [19] for the radial and tangential stresses, respectively, in the circular annulus are derived next by following the solution given on Pages 415 to 418 of Reference 6. The plane-strain theory applied to the axisymmetric elastic deflections of a thick-walled tube results in the following differential equation:

$$\frac{d^2 u}{dr^2} + \frac{1}{r} \frac{du}{dr} - \frac{u}{r^2} = 0 \quad [\text{B.12}]$$

where u is the radial displacement at a point in the wall of the tube at a radial distance " r " away from the axis of the tube. The solution of Equation [B.12] is given by:

$$u(r) = Ar + \frac{B}{r} \quad [\text{B.13}]$$

The integration constants " A " and " B " are determined from the following deflection boundary conditions:

$$\begin{aligned} \text{at } r = \bar{R}_j: u &= -w_j^A \\ r = \bar{R}_i: u &= -w_i^A \end{aligned} \quad [\text{B.14}]$$

Substituting the conditions [B.14] into the solution [B.13] gives:

$$\begin{aligned} A &= - \left(\frac{w_i^A \bar{R}_i - w_j^A \bar{R}_j}{\bar{R}_i^2 - \bar{R}_j^2} \right) \\ B &= - \bar{R}_i \bar{R}_j \left(\frac{w_j^A \bar{R}_i - w_i^A \bar{R}_j}{\bar{R}_i^2 - \bar{R}_j^2} \right) \end{aligned} \quad [\text{B.15}]$$

In Reference 6 the radial and tangential stresses, respectively, as a function of the distance " r ," are as follows:

$$\sigma_r = \frac{E^A}{(1-\nu^2)} \left[\frac{du}{dr} + \nu \frac{u}{r} \right] \quad [\text{B.16}]$$

$$\sigma_t = \frac{E^A}{(1-\nu^2)} \left[\frac{u}{r} + \nu \frac{du}{dr} \right] \quad [\text{B.17}]$$

Substituting the deflection $u(r)$ and its first derivative $\frac{du(r)}{dr}$ from Equation [B.13] into Equations [B.16] and [B.17] yields:

$$\sigma_r = E^A \left[\frac{A}{(1-\nu)} - \frac{B}{(1+\nu)} \cdot \frac{1}{r^2} \right] \quad [\text{B.18}]$$

$$\sigma_t = E^A \left[\frac{A}{(1-\nu)} + \frac{B}{(1+\nu)} \cdot \frac{1}{r^2} \right] \quad [\text{B.19}]$$

Note

$$\sigma_r + \sigma_t = 2E^A \frac{A}{(1-\nu)} = \text{constant} \quad [\text{B.20}]$$

which is a consequence of the plane-strain assumption, i.e.,

$$\epsilon_z = -\frac{\nu}{E} (\sigma_r + \sigma_t) = \text{constant} \quad [\text{B.21}]$$

Equation [B.21] results by putting the axial stress σ_z equal to zero in the three-dimensional Hooke's law.

The maximum radial stress σ_r occurs on the outer boundary of the annulus, i.e., at $r = \bar{R}_i$, whereas the maximum tangential stress σ_t occurs on the inner boundary, i.e., at $r = \bar{R}_j$. This together with $i \rightarrow 1$ and $j \rightarrow 2$ results in Equations [18] and [19].

APPENDIX C

DEVELOPMENT OF EXPRESSIONS FOR THE SHELL STRESSES, EQUATIONS [11] THROUGH [14]

In Reference 7 Salerno and Pulos developed a theory for the axisymmetric elastic deformations and stresses in a ring-stiffened, perfectly circular cylindrical shell subjected to uniform external hydrostatic pressure. Equations developed by these authors for the critical shell stresses are reviewed here and adapted to the present problem of the two coaxial cylinder elements comprising the web-stiffened sandwich cylinder structure; see Figure 1.

From symmetry considerations (Figure 4), the general solution for the bending deformations, i.e., Equation [A.3], simplifies to:

$$w_b(x) = C_1 \cos \beta x \cdot \cosh \beta x + C_4 \sin \beta x \cdot \sinh \beta x \quad [C.1]$$

The particular integrals to the differential Equation [A.1], which constitute the membrane deformations and which must be added to the bending component [C.1] to get the total deflection, are given by Equations [16] for the outside and inside cylindrical shells, respectively. The loading condition to which Equations [16] apply is shown in Figure 1. The total deflection can thus be written in the following form to apply to both cylinders:

$$w(x) = w_b(x) + w^p = C_1 \cos \beta x \cdot \cosh \beta x + C_4 \sin \beta x \cdot \sinh \beta x + w^p \quad [C.2]$$

The first derivative or slope expression is then given by:

$$\frac{dw(x)}{dx} = (C_1 + C_4) \beta \cos \beta x \cdot \sinh \beta x - (C_1 - C_4) \beta \sin \beta x \cdot \cosh \beta x \quad [C.3]$$

The integration constants C_1 and C_4 are determined from the following deformation boundary conditions:

$$\text{at } x = \pm \frac{l}{2} : w_i = w_i^s ; \quad \frac{dw_i}{dx} = \mp \theta_i^s = 0 \quad [C.4]$$

When the conditions [C.4] are substituted into Equations [C.2] and [C.3], the constants C_1 and C_4 are found to be:

$$C_1 = +(w^s - w^p) \left(\frac{\cos \frac{\beta l}{2} \cdot \sinh \frac{\beta l}{2} + \sin \frac{\beta l}{2} \cdot \cosh \frac{\beta l}{2}}{\cosh \frac{\beta l}{2} \cdot \sinh \frac{\beta l}{2} + \sin \frac{\beta l}{2} \cdot \cos \frac{\beta l}{2}} \right) = -(w^p - w^s) \frac{\Lambda^{[6]} \left(\frac{\beta l}{2} \right)}{\Lambda^{[2]} \left(\frac{\beta l}{2} \right)} \quad [C.5]$$

$$C_4 = -(w^s - w^p) \left(\frac{\cos \frac{\beta l}{2} \cdot \sinh \frac{\beta l}{2} - \sin \frac{\beta l}{2} \cdot \cosh \frac{\beta l}{2}}{\cosh \frac{\beta l}{2} \cdot \sinh \frac{\beta l}{2} + \sin \frac{\beta l}{2} \cdot \cos \frac{\beta l}{2}} \right) = -(w^p - w^s) \frac{\Lambda^{[5]} \left(\frac{\beta l}{2} \right)}{\Lambda^{[2]} \left(\frac{\beta l}{2} \right)}$$

where the lambda functions $\Lambda^{[2]}$, $\Lambda^{[5]}$, and $\Lambda^{[6]}$ are defined by Equations [8].

The principal stresses in the longitudinal and circumferential directions of the shell elements are given by the following expressions, respectively:

$$\sigma_X = -\frac{P}{h} + \sigma_{xb} \quad [C.6]$$

$$\sigma_\Phi = -E \frac{w}{R} - \nu \frac{P}{h} + \nu \sigma_{xb} \quad [C.7]$$

where the first term in Equation [C.6] and the first two terms in Equation [C.7] are the corresponding membrane stress components and the remaining terms are the bending components. In terms of the shell curvatures, the stress expressions [C.6] and [C.7] become (see, for example, Reference 7):

$$\sigma_X(x) = -\frac{P}{h} \pm \frac{Eh}{2(1-\nu^2)} \cdot \frac{d^2 w(x)}{dx^2} \quad [C.8]$$

$$\sigma_\Phi(x) = -E \frac{w(x)}{R} - \nu \frac{P}{h} \pm \frac{\nu Eh}{2(1-\nu^2)} \cdot \frac{d^2 w(x)}{dx^2} \quad [C.9]$$

Substituting the deflection $w(x)$ and the second derivative of $w(x)$ from Equation [C.2] into the above, gives the following equations:

$$\sigma_X(x) = -\frac{P}{h} \pm \frac{Eh\beta^2}{(1-\nu^2)} [-C_1 \sin \beta x \cdot \sinh \beta x + C_4 \cos \beta x \cdot \cosh \beta x] \quad [C.10]$$

$$\begin{aligned} \sigma_\Phi(x) = & -\frac{E}{R} w^p - \nu \frac{P}{h} + E \left[-\frac{C_1}{R} \pm \frac{\nu h \beta^2}{(1-\nu^2)} C_4 \right] \cos \beta x \cdot \cosh \beta x + \\ & -E \left[\frac{C_4}{R} \pm \frac{\nu h \beta^2}{(1-\nu^2)} C_1 \right] \sin \beta x \cdot \sinh \beta x \end{aligned} \quad [C.11]$$

Once the constants C_1 and C_4 as given by Equations [C.5] are substituted into Equations [C.10] and [C.11], the distributions of total longitudinal and total circumferential stress between adjacent supporting elements, imposing the restraint conditions defined by [C.4] on the shell "edges," can then be determined.

Of particular interest are the critical stresses that occur at a point between adjacent supporting elements, i.e., at $x = 0$, and immediately at a supporting element, i.e., at $x = \pm \frac{l}{2}$; see Figure 4. These critical stresses are found from Equations [C.10] and [C.11] to be:

AT MIDBAY ($x = 0$):

$$\sigma_{Xm} = -\frac{P}{h} \pm \frac{Eh\beta^2}{(1-\nu^2)} C_4 \quad [C.12]$$

$$\sigma_{\Phi m} = -\frac{E}{R} w^p - \nu \frac{P}{h} + E \left[-\frac{C_1}{R} \pm \frac{\nu h \beta^2}{(1-\nu^2)} C_4 \right] \quad [C.13]$$

AT A SUPPORT ($x = \pm \frac{l}{2}$):

$$\sigma_{Xf} = -\frac{P}{h} \pm \frac{Eh\beta^2}{(1-\nu^2)} \left[-C_1 \sin \frac{\beta l}{2} \cdot \sinh \frac{\beta l}{2} + C_4 \cos \frac{\beta l}{2} \cdot \cosh \frac{\beta l}{2} \right] \quad [C.14]$$

$$\sigma_{\Phi f} = -\frac{E}{R} w^p - \nu \frac{P}{h} + E \left[-\frac{C_1}{R} \pm \frac{\nu h \beta^2}{(1-\nu^2)} C_4 \right] \cos \frac{\beta l}{2} \cdot \cosh \frac{\beta l}{2} +$$

$$-E \left[\frac{C_4}{R} \pm \frac{\nu h \beta^2}{(1-\nu^2)} C_1 \right] \sin \frac{\beta l}{2} \cdot \sinh \frac{\beta l}{2}$$

[C.15]

The substitution of Equations [C.5] for the constants C_1 and C_4 into Equations [C.12] through [C.15], and the introduction of the lambda functions defined by Equations [8] into the resulting expressions lead to Equations [11] through [14], respectively, for the critical shell stresses.

The total deflections at midbay, i.e., $x = 0$, and at a web stiffener, i.e., $x = \frac{l}{2}$, can be found by using Equations [C.2] and [C.5]. These are, respectively:

$$w(0) = - (w^p - w^s) \frac{\Lambda^{[6]} \left(\frac{\beta l}{2} \right)}{\Lambda^{[2]} \left(\frac{\beta l}{2} \right)} + w^p$$

[C.16]

$$w \left(\frac{l}{2} \right) = - \frac{(w^p - w^s)}{\Lambda^{[2]} \left(\frac{\beta l}{2} \right)} \left[\Lambda^{[6]} \left(\frac{\beta l}{2} \right) \cos \frac{\beta l}{2} \cdot \cosh \frac{\beta l}{2} \right.$$

$$\left. + \Lambda^{[5]} \left(\frac{\beta l}{2} \right) \sin \frac{\beta l}{2} \cdot \sinh \frac{\beta l}{2} \right] + w^p$$

[C.17]

APPENDIX D

DETERMINATION OF AXIAL-PRESSURE LOAD DISTRIBUTION TO THE TWO COAXIAL CYLINDERS

With reference to Figure 8, if it is assumed that the web elements do not resist any axial load, then force equilibrium in the longitudinal direction requires that

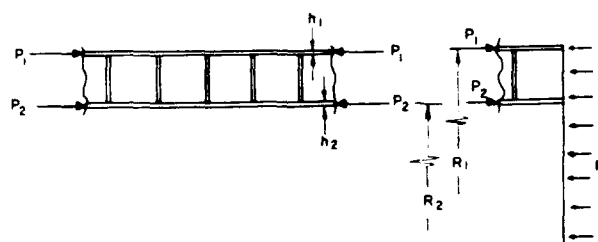


Figure 8 - Distribution of Axial-Pressure Load to the Two Cylindrical Shells

$$P_1 R_1 + P_2 R_2 = \frac{p R_1^2}{2} \quad [D.1]$$

where the axial stress forces P_1 and P_2 in the outer and inner cylindrical shells, respectively, are the unknown quantities to be determined. To find explicit expressions for P_1 and P_2 another relationship between these quantities, the applied pressure p , and the geometry of the shells is needed.

If it is assumed that both cylindrical shells displace the same amount longitudinally, i.e.,

$$u_1 = u_2 \quad [D.2]$$

then the integral of the longitudinal midthickness strains over a stiffener spacing for each of the two cylindrical shells must be equal. Therefore,

$$\int_0^{l/2} (\epsilon_{xM})_1 dx = \int_0^{l/2} (\epsilon_{xM})_2 dx \quad [D.3]$$

Equation [D.3] is a consequence of the strain-displacement relation

$$\epsilon_x = \frac{du}{dx} \quad [D.4]$$

Introducing the two-dimensional Hooke's law,

$$\epsilon_x = \frac{1}{E} (\sigma_x - \nu \sigma_\phi) \quad [D.5]$$

$$\epsilon_\phi = \frac{1}{E} (\sigma_\phi - \nu \sigma_x)$$

into Equation [D.3], we obtain

$$\int_0^{l/2} [(1-\nu^2) \sigma_{xM} - \nu E^s \epsilon_{\phi M}]_1 dx = \int_0^{l/2} [(1-\nu^2) \sigma_{xM} - \nu E^s \epsilon_{\phi M}]_2 dx \quad [D.6]$$

Since the longitudinal membrane stress and the circumferential membrane strain in each of the two shells are given, respectively, by:

$$\sigma_{xM} = \frac{P}{h} \quad [D.7]$$

$$\epsilon_{\phi M} = \frac{w}{R} \quad [D.8]$$

then Equation [D.6] becomes:

$$\int_0^{l/2} \left[\frac{(1-\nu^2) P_1}{E^s h_1} - \nu \frac{w_1(x)}{R_1} \right] dx = \int_0^{l/2} \left[\frac{(1-\nu^2) P_2}{E^s h_2} - \nu \frac{w_2(x)}{R_2} \right] dx \quad [D.9]$$

Substituting the deflection function [C.2] together with the appropriate expressions for the membrane deflections w_i^p for each of the two shells from Equations [16] into Equation [D.9], carrying out the indicated integrations, and finally introducing Equations [24], [22], and [21] into the resulting expression, we obtain

$$\begin{aligned}
& \frac{P_1}{h_1} \left[1 - \nu^2 \frac{2}{\beta_1 l} \frac{\Lambda^{[1]} \left(\frac{\beta_1 l}{2} \right)}{\Lambda^{[2]} \left(\frac{\beta_1 l}{2} \right)} \right] - \frac{\nu E^s}{R_1} \frac{2}{\beta_1 l} (g_1^A H_1 + \bar{g}_1^A H_2) \frac{\Lambda^{[1]} \left(\frac{\beta_1 l}{2} \right)}{\Lambda^{[2]} \left(\frac{\beta_1 l}{2} \right)} \\
& - \nu \frac{p R_1}{h_1} \left[1 - \frac{2}{\beta_1 l} \frac{\Lambda^{[1]} \left(\frac{\beta_1 l}{2} \right)}{\Lambda^{[2]} \left(\frac{\beta_1 l}{2} \right)} \right] \\
& = \frac{P_2}{h_2} \left[1 - \nu^2 \frac{2}{\beta_2 l} \frac{\Lambda^{[1]} \left(\frac{\beta_2 l}{2} \right)}{\Lambda^{[2]} \left(\frac{\beta_2 l}{2} \right)} \right] \\
& - \frac{\nu E^s}{R_2} \frac{2}{\beta_2 l} (g_2^A H_2 + \bar{g}_2^A H_1) \frac{\Lambda^{[1]} \left(\frac{\beta_2 l}{2} \right)}{\Lambda^{[2]} \left(\frac{\beta_2 l}{2} \right)} \quad [D.10]
\end{aligned}$$

Equations [D.1] and [D.10] constitute two equations in the two unknown forces P_1 and P_2 ; when they are solved simultaneously, the following expressions are found:

$$P_1 = \frac{p R_1 \left[\nu(1 - a_1) + \frac{1}{2} \frac{R_1 h_1}{R_2 h_2} (1 - \nu^2 a_2) \right] + \frac{\nu E^s h_1}{R_1} (g_1^A H_1 + \bar{g}_1^A H_2) a_1 - \frac{\nu E^s h_1}{R_2} (g_2^A H_2 + \bar{g}_2^A H_1) a_2}{1 - \nu^2 a_1 + \frac{R_1 h_1}{R_2 h_2} (1 - \nu^2 a_2)} \quad [D.11]$$

$$P_2 = \frac{p R_1 \left[-\nu(1 - a_1) \frac{R_1}{R_2} + \frac{1}{2} \frac{R_1}{R_2} (1 - \nu^2 a_1) \right] - \frac{\nu E^s h_1}{R_2} (g_1^A H_1 + \bar{g}_1^A H_2) a_1 + \frac{\nu E^s R_1 h_1}{R_2^2} (g_2^A H_2 + \bar{g}_2^A H_1) a_2}{1 - \nu^2 a_1 + \frac{R_1 h_1}{R_2 h_2} (1 - \nu^2 a_2)} \quad [D.12]$$

where

$$a_1 = \frac{2}{\beta_1 l} \frac{\Lambda^{[1]} \left(\frac{\beta_1 l}{2} \right)}{\Lambda^{[2]} \left(\frac{\beta_1 l}{2} \right)}; \quad a_2 = \frac{2}{\beta_2 l} \frac{\Lambda^{[1]} \left(\frac{\beta_2 l}{2} \right)}{\Lambda^{[2]} \left(\frac{\beta_2 l}{2} \right)} \quad [\text{D.13}]$$

REFERENCES

1. Buhl, J.E., Jr. and Pulos, J.G., David Taylor Model Basin Report C-1225 (May 1961)
CONFIDENTIAL.
2. Wenk, E., Jr. and Taylor, C.E., "Analysis of Stresses at the Reinforced Intersection of Conical and Cylindrical Shells," David Taylor Model Basin Report 826 (Mar 1953).
3. Taylor, C.E. and Wenk, E., Jr., "Analysis of Stress in the Conical Elements of Shell Structures," David Taylor Model Basin Report 981 (May 1956).
4. Raetz, R.V. and Pulos, J.G., "A Procedure for Computing Stresses in a Conical Shell near Ring Stiffeners or Reinforced Intersections," David Taylor Model Basin Report 1015 (Apr 1958).
5. Galletly, G.D., "Analysis of Discontinuity Stresses Adjacent to a Central Circular Opening in a Hemispherical Shell," David Taylor Model Basin Report 870, Revised Edition (May 1956).
6. Popov, E.P., "Mechanics of Materials," Prentice-Hall, Inc. (1952).
7. Pulos, J.G. and Salerno, V.L., "Axisymmetric Elastic Deformations and Stresses in a Ring-Stiffened, Perfectly Circular Cylindrical Shell under External Hydrostatic Pressure," David Taylor Model Basin Report 1497 (Sep 1961).
8. Lunchick, M.E., "Yield Failure of Stiffened Cylinders under Hydrostatic Pressure," David Taylor Model Basin Report 1291 (Jan 1959).

INITIAL DISTRIBUTION

Copies

- 17 CHBUSHIPS
 - 2 Sci and Res Sec (Code 442)
 - 1 Tech Asst (Code 106)
 - 1 Lab Mgt (Code 320)
 - 3 Tech Info Br (Code 335)
 - 1 Applied Sci Br (Code 342A)
 - 1 Prelim Des Br (Code 420)
 - 1 Hull Des Br (Code 440)
 - 1 Struc Sec (Code 443)
 - 1 Mat Dev and Appl Br (Code 634)
 - 1 Polymer, Fiber and Packaging Sec (Code 634C)
- 3 CHONR
 - 1 Res Coordinator (Code 104)
 - 1 Struc Mech Br (Code 439)
 - 1 Undersea Prog (Code 466)
- 2 CNO
 - 1 Undersea Warfare & AE Sec (Ap 702G)
 - 1 Tech Anal and Advis Gr (Ap 07TB)
- 1 CHBUWEPS (RRMA-3)
- 1 CHBUDOCKS, Attn: C-423
- 1 DIR, USNEL
- 1 DIR, USNUL
- 2 CDR, USNOL
 - 1 WM Div
- 2 DIR, USNRL
 - 1 (Code 2027)
 - 1 (Code 6210)
- 1 CDR, USNOTS, China Lake
- 1 *CO, USNOTS (R-8082) Pascagoula*
- 1 CO, USNUOS, Newport
- 10 CDR, ASTIA
 - 1 NAVSHIPYD PTSMH
 - 1 NAVSHIPYD MARE
 - 1 NAVSHIPYD CHASN
 - 1 NAVSHIPYD, Attn: NY Matl Lab (Code 948)

Copies

- 1 SUPSHIP, Groton
- 1 Elec Boat Div, Genl Dyn Corp
- 1 SUPSHIP, Newport News
- 1 NNSB & DD Co
- 1 SUPSHIP, Pascagoula
- 1 Ingalls Shipbldg Corp
- 1 Dir Def R & E, Attn: Tech Libr
- 1 CO, USNROTC & NAVADMINU, MIT
- 1 O in C, PGSCOL, Webb
- 1 Dr. E. Wenk, Jr., White House
- 1 Dr. R.C. DeHart, SW Res Inst
- 1 Prof. J. Kempner, Polytech Inst of Bklyn
- 1 Dean V.L. Salerno, Fairleigh Dickinson Univ

David Taylor Model Basin. Report 1543.

AXISYMMETRIC ELASTIC DEFORMATIONS AND STRESSES IN A WEB-STIFFENED SANDWICH CYLINDER UNDER EXTERNAL HYDROSTATIC PRESSURE, by John G. Pulos. Nov 1961. iv, 39p. illus., tables, refs. UNCLASSIFIED

A theoretical analysis of the axisymmetric elastic deformations and stresses in a web-stiffened sandwich cylindrical shell structure under external hydrostatic pressure is presented. The solution is based on the use of edge coefficients for plate and shell elements of finite length, and includes the computation of the edge forces and moments arising at the common junctures of these elements.

Equations are given for computing numerically the longitudinal and circumferential stresses in the two coaxial cylindrical shells and the radial and tangential stresses in the web stiffeners between the two shells.

1. Cylindrical shells (Stiffened)--Stresses--Mathematical analysis
 2. Cylindrical shells (Stiffened)--Deformation--Mathematical analysis
 3. Cylindrical shells (Stiffened)--Sandwich construction
- I. Pulos, John G.
II. S-F013 03 02

David Taylor Model Basin. Report 1543.

AXISYMMETRIC ELASTIC DEFORMATIONS AND STRESSES IN A WEB-STIFFENED SANDWICH CYLINDER UNDER EXTERNAL HYDROSTATIC PRESSURE, by John G. Pulos. Nov 1961. iv, 39p. illus., tables, refs. UNCLASSIFIED

A theoretical analysis of the axisymmetric elastic deformations and stresses in a web-stiffened sandwich cylindrical shell structure under external hydrostatic pressure is presented. The solution is based on the use of edge coefficients for plate and shell elements of finite length, and includes the computation of the edge forces and moments arising at the common junctures of these elements.

Equations are given for computing numerically the longitudinal and circumferential stresses in the two coaxial cylindrical shells and the radial and tangential stresses in the web stiffeners between the two shells.

1. Cylindrical shells (Stiffened)--Stresses--Mathematical analysis
 2. Cylindrical shells (Stiffened)--Deformation--Mathematical analysis
 3. Cylindrical shells (Stiffened)--Sandwich construction
- I. Pulos, John G.
II. S-F013 03 02

David Taylor Model Basin. Report 1543.

AXISYMMETRIC ELASTIC DEFORMATIONS AND STRESSES IN A WEB-STIFFENED SANDWICH CYLINDER UNDER EXTERNAL HYDROSTATIC PRESSURE, by John G. Pulos. Nov 1961. iv, 39p. illus., tables, refs. UNCLASSIFIED

A theoretical analysis of the axisymmetric elastic deformations and stresses in a web-stiffened sandwich cylindrical shell structure under external hydrostatic pressure is presented. The solution is based on the use of edge coefficients for plate and shell elements of finite length, and includes the computation of the edge forces and moments arising at the common junctures of these elements.

Equations are given for computing numerically the longitudinal and circumferential stresses in the two coaxial cylindrical shells and the radial and tangential stresses in the web stiffeners between the two shells.

1. Cylindrical shells (Stiffened)--Stresses--Mathematical analysis
 2. Cylindrical shells (Stiffened)--Deformation--Mathematical analysis
 3. Cylindrical shells (Stiffened)--Sandwich construction
- I. Pulos, John G.
II. S-F013 03 02

David Taylor Model Basin. Report 1543.

AXISYMMETRIC ELASTIC DEFORMATIONS AND STRESSES IN A WEB-STIFFENED SANDWICH CYLINDER UNDER EXTERNAL HYDROSTATIC PRESSURE, by John G. Pulos. Nov 1961. iv, 39p. illus., tables, refs. UNCLASSIFIED

A theoretical analysis of the axisymmetric elastic deformations and stresses in a web-stiffened sandwich cylindrical shell structure under external hydrostatic pressure is presented. The solution is based on the use of edge coefficients for plate and shell elements of finite length, and includes the computation of the edge forces and moments arising at the common junctures of these elements.

Equations are given for computing numerically the longitudinal and circumferential stresses in the two coaxial cylindrical shells and the radial and tangential stresses in the web stiffeners between the two shells.

1. Cylindrical shells (Stiffened)--Stresses--Mathematical analysis
 2. Cylindrical shells (Stiffened)--Deformation--Mathematical analysis
 3. Cylindrical shells (Stiffened)--Sandwich construction
- I. Pulos, John G.
II. S-F013 03 02

No consideration was given to the discontinuity effects arising from rigid or elastic restraints afforded by contiguous bulkhead or adjacent shell structures. Thus, the analysis presented herein is applicable only to a typical bay of a web-stiffened sandwich cylinder of long length.

A numerical example is presented to illustrate the use of the equations developed in this report.

No consideration was given to the discontinuity effects arising from rigid or elastic restraints afforded by contiguous bulkhead or adjacent shell structures. Thus, the analysis presented herein is applicable only to a typical bay of a web-stiffened sandwich cylinder of long length.

A numerical example is presented to illustrate the use of the equations developed in this report.

No consideration was given to the discontinuity effects arising from rigid or elastic restraints afforded by contiguous bulkhead or adjacent shell structures. Thus, the analysis presented herein is applicable only to a typical bay of a web-stiffened sandwich cylinder of long length.

A numerical example is presented to illustrate the use of the equations developed in this report.

No consideration was given to the discontinuity effects arising from rigid or elastic restraints afforded by contiguous bulkhead or adjacent shell structures. Thus, the analysis presented herein is applicable only to a typical bay of a web-stiffened sandwich cylinder of long length.

A numerical example is presented to illustrate the use of the equations developed in this report.